Cold Spray Deposition of Ni-WC Composite Coatings and Their Sliding and Erosive Wear Behaviour

Sima Ahmad Alidokht

Department of Mining and Materials Engineering McGill University, Montreal

A thesis submitted to McGill University in partial fulfillment of the requirements for the degree of Doctor of Philosophy.

Acknowledgments

This thesis work was completed with the help and support of many people, to all of whom I am deeply thankful. I first thank my supervisor, Prof. Richard Chromik, for offering me this great opportunity to work on this project at McGill University and all his generous support and help and insightful research discussion throughout this study. I also thank my co-supervisor, Prof. Steve Yue, for his expertise, vision and feedback.

I would like to thank my colleagues and friends at McGill including Praveena, Husseyin, Dina, Michael, Aroba, YinYin, Pryadarshi, Lisa, Vamsi, Sara, Nima, Yaoyao, Armin, Danae and many others who supported me during this study. I am very thankful for the technical support at McGill including Nicolas Brodusch, Liu David, Weawkamol Leelapornpisit, Florence Paray, Monique Riendeau and Robert Paquette. I would also like to acknowledge technical help form Jean-Francois Alarie at the McGill Aerospace Materials and Alloy Design Center (MAMADC). I would also like to acknowledge help from summer students and Co-ops, Hanna, Stephanie and Ata for their help with experimental work. Thanks are due to the LaRFIS (FCSE) lab group members at Polytechnique Montreal for their support to shape this project. I acknowledge Prof. Jolanta Sapieha, Jacques Lengaigne, Dr. Etienne Bousser, and Dr. Thomas Schmitt help at LaRFIS (FCSE).

I would like to thank my funding agencies without which the project would not have been possible. Acknowledgment is due to Natural Sciences and Engineering Research Council (NSERC) of Canada, Engage Grants Program, and Strategic Grants Program, Tekna Plasma Systems Inc., McGill Engineering Doctoral Award (MEDA), and Hatch Graduate Excellence Fellowships in Engineering for the financial support on my studies.

Last but not the least, I would like to thank my family, my daughter, Hannah, my husband, Hadi and my parents and my brothers, Isa and Benjamin, for their constant support and motivation during my research work.

Abstract

Ni and Ni-WC composite coatings were produced by cold spray deposition. In order to establish an optimum feedstock powders morphology and size, the Ni and WC cold spray behavior were examined. Two types of WC particles namely cast WC and agglomerated WCNi was tested. Moreover, cast WC with three size distributions was co-sprayed with Ni, where smaller WC particles retained more into coatings. A significant loss of cast WC particles during cold spraying was recorded, due to their limited ductility. Therefore, agglomerated WCNi powders were co-sprayed with Ni. The result was a significant improvement in WC retention being close to that of initial feedstock.

Reciprocating sliding wear tests were performed on Ni and Ni-10.5 and 28vol%WC coatings in dry air using a custom-built tribometer equipped with WC-Co counterspheres. WC particles reinforced matrix against significant adhesive wear at initial cycles. Moreover, they assisted in fast developing of a mechanically mixed layer (MML) to a higher coverage. MML consisted of fine WC fragments and tribochemical phases of Co/$NiWO_4$, NiO and WO_3. Subsurface microstructure examination suggested that MMLs shielded underlying materials from wear damage. MMLs on worn surfaces of composite coatings was harder and more stable and thus more protective than that for Ni coatings.

Effect of WC particles morphology i.e. cast versus agglomerated, on the sliding wear of composite coatings, was tested in two coatings with a similar fill ratio of WC particles, i.e. Ni-28WC and Ni-30WCNi. Ni-28WC was more wear resistant than Ni-30WCNi and exhibited a more stable coefficient of friction throughout the test. Lower mean free paths between WC particles in Ni-28WC effectively protected the matrix from adhesive wear in initial sliding cycles. Whereas, significant plastic deformation and adhesive wear were observed in Ni-30WCNi. Moreover, large WC particles in Ni-28WC were resistant from being pulled out from the surface, whereas in Ni-30WCNi, fine WC fragments were dislodged from the surface and caused wear on both counterparts. Both coatings developed hard and protective MML. MMLs more effectively protected underlying materials from wear damage in Ni-28WC, due to its higher coverage and stability.

Solid particle erosion (SPE) wear behavior of coatings were examined in an ambient environment using alumina erodent particles under 30 and 90° impact angles. Ni and Ni-10.5 vol.%castWC composite coatings were subjected to erosive wear. At low impact angle, erosion rates for both coatings were similar, however, Ni coatings were more erosion resistant at normal angle. At 30°, WC particles were least damaged, however, they were knocked out from the surface when the supporting effect of the Ni matrix was no longer present. Due to WC particles low content, they didn't grant a significant improvement in erosion resistance of coating at 30°. For both coatings, a higher erosion resistance was obtained at normal erosion, partly due to the embedding of erodent particles into Ni and shielding effect against further material loss.

In order to test the effect of mechanical properties of Ni matrices, cold spray coatings were prepared using two size ranges of Ni i.e. Ni(d_{50} = 7 μm) and Ni(d_{50} = 25 μm). A higher erosion resistant was obtained in Ni(7 μm) coating compared to Ni(25 μm), due to the higher hardness of Ni(7 μm) coating. Ni-WCNi coatings with WC ranging from 13 to 56vol.% were tested. The addition of below 30vol.% WC into coating didn't impart any significant effect on erosion rates, where erosion behavior was controlled by Ni matrices. Above 30vol.% WC contents, Ni-WCNi coatings erosion rates were dropped significantly and reached a similar value for both Ni(7 μm)- and Ni(25 μm)-WCNi coatings. This was associated with a transition in erosion mechanism from easy dislodgment of WC fragments in low WC content to strain accumulation and subsurface cracking in high WC content.

Résumé

Les revêtements de Ni-WC, ont été produits par dépôt de pulvérisation à froid. Afin d'obtenir des conditions de pulvérisation optimales, ainsi que la taille et la morphologie de la poudre de base, le comportement de la pulvérisation à froid des revêtements Ni et WC a été examiné. Deux types de particules de WC, à savoir le WC coulé et le WCNi aggloméré, ont été testés. Cependant, une perte significative de particules de WC coulées pendant la pulvérisation à froid. Par conséquent, les poudres de WCNi agglomérées ont été co-pulvérisées avec Ni. Le résultat fut une amélioration significative de la rétention du WC proche de l'état initial.

Des essais d'usure par frottement alternatif ont été effectués sur des revêtements composites Ni et Ni-10.5 et 28 WC dans de l'air sec à l'aide d'un tribomètre fabriqué sur mesure, équipé de contre-pointes WC-Co. Il a été constaté que les particules de WC renforçaient la matrice contre une usure importante de l'adhésif au début du frottement. En outre, elles ont aidé au développement rapide, d'une couche mécaniquement mélangée (MML), à une couverture plus élevée. L'examen de la microstructure de subsurface des pistes d'usure a suggéré que les MMLs protégeaient les matériaux sous-jacents contre les dommages dus à l'usure.

L'effet de la morphologie des particules de WC, c'est-à-dire la structure moulée par rapport à la structure agglomérée Ni-28WC et Ni-30WCNi a été. Il a été constaté que Ni-28WC était plus résistant à l'usure que Ni-30WCNi et présentait un coefficient plus stable tout au long de l'essai. Des trajets libres moyens entre les particules de WC dans Ni-28WC protégeaient efficacement la matrice de l'usure de l'adhésif lors des cycles de frottement initiaux. De plus, de grandes particules de WC dans Ni-28WC étaient résistantes à la surface. Cependant, les MMLs protégeaient plus efficacement les matériaux sous-jacents contre les dommages dus à l'usure dans le Ni-28WC, en raison de sa couverture et de sa stabilité plus élevées.

Le comportement à l'usure érosive des particules solides (SPE) du Ni et des Ni-10.5castWC composites a été examiné utilisant des particules érodantes d'alumine sous des angles d'impact de 30 et 90°. À faible angle d'impact, les taux d'érosion pour les deux revêtements étaient similaires, cependant, les revêtements de Ni étaient plus résistants à l'érosion à un angle normal. À faible

angle d'impact, les particules de WC ont été moins endommagées en raison de l'érosion. Sous un angle normal, la vue de dessus et la section transversale des surfaces usées montraient une fissuration fragile des particules de WC et une fragmentation, suivi d'un enlèvement de la surface. Pour les deux revêtements, une résistance à l'érosion plus élevée a été obtenue.

Afin de tester l'effet des propriétés mécaniques des matrices de Ni, des revêtements pulvérisés à froid ont été préparés en utilisant deux plages de taille Ni, Ni (d_{50} = 7 μm) et Ni (d_{50} = 25 μm). Une résistance à l'érosion plus élevée a été obtenue avec un revêtement de Ni (d_{50} = 7 μm) par rapport à Ni (d_{50} = 25 μm). Des revêtements Ni-WCNi avec des valeurs de WC allant de 13 à 56% en volume ont été testés. Il a été constaté que l'ajout de moins de 30vol.% de WC dans le revêtement n'a pas eu d'effet significatif sur les taux d'érosion, où le comportement de l'érosion était contrôlé par les matrices Ni. Au-dessus de 30vol.% en WC, les taux d'érosion des revêtements Ni-WCNi ont été significativement réduits, et ont atteint une valeur similaire pour les deux revêtements Ni-WCNi. Cela a été associé à une transition dans le mécanisme d'érosion du délogement rapide des fragments de WC de la surface, à faible teneur en WC à l'accumulation de contrainte et à la fissuration sous la surface dans une teneur élevée en WC.

Contribution of the authors

This thesis is manuscript-based containing three publications and two other manuscripts that are close to submission. The manuscripts are prepared in collaboration with people from different groups and universities. The detailed contribution of people is listed as below.

Chapter 4: Cold Spray Deposition of Ni and WC-Reinforced Ni Matrix Composite Coatings, Journal of Thermal Spray Technology, 2017, 26:1908–1921.
Sima Alidokht conducted cold spray deposition of the coating, sample preparation, data and image analyzing, post-test characterization and analysis, and wrote the manuscript. Phuong Vo assisted with cold spray deposition. Richard R. Chromik and Steve Yue supervised the project and edited the manuscript.

Chapter 5: Cold spray deposition of a Ni-WC composite coating and its dry sliding wear behavior, Surface & Coatings Technology, 2016, 308:424–434.
Sima Alidokht conducted cold spray deposition of the coating, sliding wear tests, post-test observation and analysis, and wrote the manuscript. Phuong Vo assisted with cold spray deposition. Praveena Manimunda assisted with sliding wear tests. Richard R. Chromik and Steve Yue supervised the project and edited the manuscript.

Chapter 6: Effect of WC morphology on dry sliding wear behavior of cold-sprayed Ni-WC composite coatings.
Sima Alidokht conducted cold spray deposition of the coating, sliding wear tests, post-test observation and analysis, and wrote the manuscript. Richard R. Chromik and Steve Yue supervised the project and edited the manuscript. This chapter is a manuscript, intended for publication.

Chapter 7: Erosive wear behavior of Cold-Sprayed Ni-WC composite coating, Wear, 2017, 376-377:566–577.
Sima Alidokht conducted cold spray deposition of the coating, erosive wear tests, post-test observation and analysis, and wrote the manuscript. Phuong Vo assisted with cold spray deposition. Richard R. Chromik and Steve Yue supervised the project and edited the manuscript.

Chapter 8: Influence of feedstock characteristics on solid particle erosion behavior of cold-sprayed Ni-WC composite coatings

Sima Alidokht conducted cold spray deposition of the coating, erosive wear tests, post-test observation and analysis, and wrote the manuscript. Jacques assisted with erosive wear tests and edited the manuscript. Richard R. Chromik and Steve Yue supervised the project and edited the manuscript. This chapter is a manuscript, intended for publication.

Table of Contents

Chapter 1

Introduction

The word “tribology” was derived from the Greek word “tribos”, meaning rubbing, and first used by Jost (1966), although friction, lubrication and wear had been studied for many years before [1]. As stated by Hutching [2], tribology is defined as “the branch of science and technology concerned with interacting surfaces in relative motion and with the associated matter, and includes the study of friction, wear, lubrication and the design of bearings”. Friction and wear are present in most mechanical systems in which surfaces slide or roll against each other, and therefore, tribology is a key enabling technology in numerous industrial applications, ranging from aerospace, transport and power generation to household appliances. Understanding the surface interactions, which lie at the heart of tribology, is very complex and requires many diverse disciplines including physics, chemistry, mechanical engineering and material science [1, 2].

According to UK government committee and Jost (1966, 1976), potential savings of £515 million per year, equivalent to about 1.36% of UK’s GDP at that time, is estimated by improving our understanding of tribological systems. Similar exercises were performed in several other countries, which arrived at same conclusions. On a recent tribology impact reports by Holmberg and Erdemir [3], a potential saving that would amount to 1.4% of the GDP annually was identified by the development of the new surface, materials, and lubrication technologies for friction reduction and wear protection. Therefore, there is a desire of tribological researches in order to gain a better understanding of surface interactions and minimization of losses resulting from friction and wear. Since the time of the Jost report, there has been a tremendous progress in evolving fundamental understanding of the mechanisms of wear and friction as well as the development of high-efficiency tribological materials and other types of technical solutions [1-6]. One general approach for minimizing the wear in a tribological system is to use metal matrix composites (MMCs) reinforced with hard ceramic particles. This group of materials combines metallic properties (ductility and toughness) with ceramic properties (high strength and high modulus), leading to improvement in tribological performance [7]. Reinforcement materials

include carbides, nitrides and oxides, among which, a considerable attention has been paid to tungsten carbide (WC) particles, due to its wear resistant properties. MMCs reinforced with WC particles using Co or Ni as matrices are well-known for their unique combination of hardness, toughness and thus superior wear performance [8-11].

Several surface engineering methods have been applied to incorporate WC particles into Co or Ni matrices, where laser cladding [12, 13] and thermal spray processes [14-17] are the most often techniques used. Laser clad Ni-WC coatings are widely used for hard-facing applications and wear protection on steel parts in oil drilling, mining and agriculture industries. Whereas, thermally sprayed WC-Co or Ni coatings have been qualified as functionally superior and cost-effective replacements for hard chromium coatings in manufacturing and maintenance operations of aerospace components [12-17]. The main issue of the above-mentioned techniques, i.e. laser cladding and thermal spray processes, is that they inevitably introduce high temperature, which causes decarburization of WC and formation of brittle phases [16, 17]. Reducing process temperature may lead to less decarburization, but it leads to increase of porosity in the coatings [18, 19]. Cold spray, however, is a relatively new thermal spray technique in which coatings are deposited using the kinetic energy of particles and the processing temperature is well below than the melting points of the particles. This makes the process ideal for heat sensitive materials such as WC [11-13]. In this technology, the particles are injected in a supersonic gas flow and accelerated to velocities ranging from 300 to 1200 m/s toward a substrate where they plastically deform upon impact and bond to build up the coating [20, 21]. With optimization of the cold spray process for deposition of Ni-WC coatings, this technique could potentially provide cost-saving replacement for laser cladding and thermal spray processes, which are energy intensive processes. These coatings can also be considered a repair method for this system, where laser clad or thermal sprayed coatings that underwent wear could be potentially refurbished by cold spray line-of-sight process.

Several researchers have deposited composite coatings containing WC by cold spray [21-27]. In most cases, pre-treatment powder processing such as cladding [21] and sintering [22-26] was utilized to overcome difficulties regarding retention of hard WC particles into coatings. Cold spray deposition of Ni-WC coatings using spherical WC particles with no additional processing routes has not been conducted in previous studies. On the other hand, as for the tribological performance of Ni-WC coatings, it was found that the structure of the coating including carbide

size and content, and morphology as well as matrix/binder microstructure must be carefully tailored to achieve the desirable wear properties for application [21-27]. The major part of the experimental studies in the field of cold-sprayed WC composite coatings have been mainly focused on microstructural characterizations including morphology of metallic matrix splats and retention, distribution, and fragmentation of ceramic particles. Micro-hardness and bond strength tests have been performed on coatings and correlated to microstructural observations in some of the studies. However, less attention has been paid to the response of cold sprayed WC composites to the conditions experienced in service such as wear, corrosion, and fatigue [21-27].

The main objective of this thesis was to develop an understanding of the role of WC particles on the cold spray deposition, dry sliding and solid particle erosive (SPE) wear behavior of Ni-WC composite coatings. To explore this, process-structure-property relationships, that is central to the field of materials science and engineering [28], was studied in cold-sprayed Ni-WC composite coating. The structure of the Ni-WC coatings is shaped by the WC particles retention into the coating, their morphology and distribution, as well as, Ni matrix microstructure, which in turn, influence coatings properties. That led to the first goal of the present thesis and that was to investigate Ni and WC cold spray deposition, with a focus on WC deposition mechanism, its retention into coatings and Ni microstructural evolution, through which the optimum spraying condition and powders characteristics were explored. The effect of WC morphology, using two WC types, i.e. cast WC and agglomerated/sintered WCNi, on deposition behavior was tested. Moreover, cast WC of various size ranges was sprayed allowing an evaluation of WC powder size effect. An optimized spraying condition including spraying material size and morphology, gas temperature, gun traverse speed, etc. was extracted based on the above observation. Mild steel plated was selected for substrates, similar to laser clad or thermal sprayed Ni-WC coatings.

The sliding and erosion performance of Ni-WC composite coatings is influenced by its structure [15, 29]. This drives the second objective and that is to investigate sliding and erosive wear of Ni-WC coatings. Sliding wear of Ni-WC coatings was investigated in terms of friction, wear, contact morphology, phase composition, and their link to subsurface microstructure, with a focus on the role of WC particles. A reciprocating ball-on-flat geometry was utilized, due to its ease of alignment of test specimens and the elimination of edge loading at the contact during testing. Moreover, this configuration is closer to some of those that are met in service such as bearing loads. The influence of WC morphology on dry sliding wear behavior was also tested

using cast and agglomerated WC particles. Erosive wear performance of Ni-WC coatings was investigated on an SPE tester using Al_2O_3 erodent particles, as recommended by the ASTM G76 standard for gas-blast erosion testing. In service, erodent particles impact surface at wide ranges of velocities. This research is focused on SPE using angular particles at relatively low velocities of 60 ± 6 m/s. The influence of WC content, as well as, matrix mechanical properties on erosion rates, worn surfaces morphologies, and subsurface microstructure were studied.

Organization of thesis

This thesis is a manuscript-based dissertation divided into ten chapters. A general background and objectives, as well as the outline of the thesis, are given in the current chapter.

Chapter 2 is a literature review of the WC-metal composites, cold spray, tribology, the tribological behavior of MMCs containing WC, and tribological behavior of cold sprayed WC composite coatings.

Chapter 3 discusses experimental procedures followed for sample preparation, testing and the characterization equipment used. This includes cold spray system, tribometers used for sliding wear, erosion tester used for SPE wear, Raman spectroscopy, optical profilometry, and nanoindentation, as well as, spraying condition selection and detailed data analysis procedure.

Chapter 4 presents microstructural characterization and nano- and micro-indentation of cold sprayed Ni and composite coatings. Electron channeling contrast imaging technique was used to reveal deformed microstructure of Ni particles and deposition mechanism. Observation of dislocation rearrangement into low energy configurations in agreement with previous studies on metallic materials subjected to high strain and high strain rate deformation. In addition to the deformed structure of Ni splats, retention, distribution, and fragmentation of WC, was performed by scanning electron microscopy (SEM). Two types of WC powders, i.e. cast WC and agglomerated WCNi, were tested. Using small cast WC particles, Ni-WC coatings with a higher WC content were obtained. Significant improvement in WC particles retention was achieved using WCNi composite powder, with the WC content in the coating being close to that of the feedstock.

Adding WC to Ni increased its hardness. The Ni-WC coatings with higher WC retained in the coatings displayed higher hardness due to lower porosity and mean free path (MFP) between WC particles. It was found that Ni-WCNi coatings can be tailored to contain 13-56vol.% WC and display a varied hardness ranging between 343-575 HV_1.

In **Chapter 5**, reciprocating dry sliding wear was conducted on a pure Ni coating and a Ni-10.5vol.% WC composite coatings. Coefficient of friction and wear rate analysis was measured and correlated to wear track morphology, phase composition, and third-bodies flow. This combined with subsurface microstructural analysis revealed role of WC particles on friction and wear. The presence of hard particles in the Ni-WC coating facilitated fast development of the mechanically mixed layer (MML), as well as stabilized the MML, characterized by less plastic flow, fewer cracking and higher hardness.

Chapter 6 explored the effect of WC morphology on the sliding wear behavior of Ni-WC composite coatings. Two cold-sprayed Ni-WC coatings with a similar fill ratio of WC but reinforced using types of WC particles, cast WC and agglomerated WCNi, were subjected to dry sliding wear. Third body morphology, microstructure and chemical composition were examined at initial cycles and at the end of sliding tests to analyze the evolution of wear tracks and its correlation to coefficient of friction and wear rates. Subsurface microstructure and chemical analysis suggested higher oxidation and more stable MMLs in Ni-28WC, with lower depths of deformation zones extended beneath the MML. Mechanical properties of the sliding-induced microstructure of coatings were examined by nanoindentation and correlated to MMLs stabilities and type of WC particles.

Chapter 7 discusses erosive wear behavior of Ni and Ni-10.5vol.% WC composite coatings as well as ceramic retention mechanisms influenced by the size of particles. In chapter 1, the mechanism of cast WC particles was discussed considering isolated impact events. In this chapter, in addition to the embedding of WC into the substrate, entrapping of these particles by later arriving particles was assumed to be an active mechanism. This necessitates interaction between particles, which is still a matter of debate in cold spray. Assuming interaction between particles near the substrate, as proposed by a few previous studies, it was found that small size WC particles,

that rebound from the surface, needed less momentum to overcome to recover them in the coating, which results in higher WC content retention. Ni coatings exhibited ductile erosion behavior, with cutting and plowing as the main wear mechanisms at 30° angle, whereas, Ni deformation localization and lip formation were observed at a normal angle. Addition of 10.5vol.% WC into Ni did not improve its erosion at 30° angle. They were dislodged from surface following severe wear of neighboring Ni. Erosion resistance of both coatings at 90° was influenced by the embedding of the Al_2O_3 particles, which was less observed at 30° attack angle. Ni-10.5vol.%WC featured a lower erosion resistance at 90° due to brittle fracture of WC particles.

Chapter 8 explored the effect of WC content and hardness of Ni matrices on erosive wear behavior of Ni-WCNi coatings. In chapter 7, erosive wear behavior of Ni and Ni-10.5vol.% WC coatings was studied. It was found that the content of WC was too low to have a significant effect on erosion behavior. As found in Chapter 4, using cast WC, WC retention into coatings was low and a maximum of 28vol.% WC was recovered into the coating. Whereas, using WCNi particles, WC content inside coatings was close to initial feedstock, and higher WC content, up to 56vol.%, in the coating was achieved. In Chapter 8, Ni-WCNi coatings with various WC contents were subjected to erosion tests to explore the influence of WC content. In addition, the effect of matrix Ni mechanical properties on SPE behavior

In **Chapter 9,** a global discussion was made in order to discuss the link between Chapters 5 and 6, where a Ni-10.5vol.%WC coating in the former and a Ni-28vol.%WC in the latter was subjected to sliding wear. Although in Chapter 6, the goal was to see the effect of WC morphology on sliding wear performance, however, testing of a Ni-28vol.%WC coating permitted further explore the role of cast WC particles during sliding, which was aimed in Chapter 5. Moreover, for cast WC particles cold spray behavior, two different mechanisms were mentioned in Chapter 4 and 7. Although, the two mechanisms could occur simultaneously, there were some points that needed to be discussed and this is covered in Chapter 9.

In **Chapter 10**, general conclusions of this thesis, contributions to original knowledge, and suggested future work were presented.

Chapter 2

Literature review

2.1 MMC coatings reinforced with WC particles

2.1.1 Definition of a MMC

A composite material consists of at least two chemically and physically distinct materials to obtain properties that would not be provided with either of individual phases. Generally, composite contain fibers or particulates that are distributed homogenously within continuous matrix of often another material. When the continuous phase is made of metallic materials, the material system is called MMC. Based on this definition, the ingredient materials remain distinct throughout the processing of the material, which draws a distinction from conventional alloys, including eutectics or alloys containing precipitates or segregated inclusions such as aluminum-silicon alloys and cast irons. Although, this definition includes in-situ composite materials in which at least one secondary phase is formed within the matrix by chemical changes during the processing but remains distinct from the matrix. Another distinction is dispersion-hardened metals, such as oxide dispersion strengthened (ODS) materials, which is excluded from consideration in the above definition. This is due to the reinforcement representing only a small fraction of the material and their role is mainly to obstruct dislocation motion in the matrix. This contrasts with MMCs where the reinforcing phase bear a significant fraction of the applied stress when physically loaded [30, 31].

2.1.2 WC as reinforcing phase

Among hard ceramic materials, the interstitial carbides including WC and TiC have been widely used to reinforce metallic matrix [12-17, 32]. This group of materials are crystalline compounds of a host metal, including the nine early-transition elements, and carbon, with a large difference in electronegativity between the two elements. Due to much smaller size of the carbon

atom than the other atom, carbon occupies specific interstitial sites in the structure. This necessitates a switch in crystal structure of the metal, which is mostly a BCC structure in early transition metals, to a close-packed structure (FCC or HCP), providing sites for the carbon atoms [33, 34]. In WC structure, as shown in Fig. 2.1, carbon nest in the trigonal prisms in the lattice to form a simple hexagonal sublattices [33, 34]. In addition to WC, W_2C is another compound existing in the W–C system with an ordered/disordered arrangement of carbon atoms and vacancies [35]. The bonding is described as partly covalent and ionic, but mostly metallic, explaining why interstitial carbides offer most of the metallic properties [33, 34]. They combine physical properties of ceramics, i.e. high hardness and strength due to covalent and ionic character of bonding and electronic properties of metals, i.e. high thermal and electrical conductivities. Also, they have high melting points and high thermal and chemical stability [22]. Combination of above-mentioned properties makes the interstitial carbides ideal materials for applications requiring rigidity and resistance to deformation, wear and corrosion. However, their main drawback, low ductility at room temperature, reduces their performance, as well as making them difficult to manufacture. Therefore, for engineering applications, the hard carbides bonded or cemented by a ductile metal binder, usually cobalt or nickel [33, 34]. Additions of binder metal cause an increase in the toughness of carbide products, improving their performance [21, 33, 34]. Among interstitial carbides, WC exhibit higher elastic modulus and smaller thermal expansion coefficient, both by a factor of 1.5–2, when compared to other transition metal carbides. Moreover, WC mechanical properties is adequately stable when temperature rises to 1200–1300 K (926–1027◦C), explaining the wide use of WC in the components of tool materials [35].

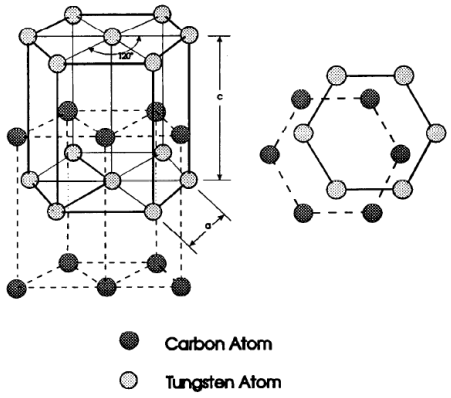

Fig. 2.1 Schematic representation of a simple hexagonal structure of WC crystal [33].

There are number of techniques to synthesize WC powder including spark plasma sintering, combustion synthesis, sol-gel and in situ carburization method, chemical vapor reaction synthesis and the spray conversion process [36]. Although some of these technologies are commercialized on a large scale, they are followed with post-processing powder densification, and/or spheroidization or sintering with binder. There are two types of WC-based powders that are often used to reinforce metallic matrix in MMCs, namely cast W_2C/WC and agglomerated WC-Co or Ni [12-17]. For the former type of WC powder, induction plasma technology is often applied to transform crushed, atomized and sponged powders into dense spherical powders. The feed particles are heated to melting point followed by cooling under controlled conditions [37]. The powder is a mix of eutectic WC and W_2C phases [37]. There are various methods for powder metallurgy of WC-Co or Ni powders, including different sintering method, liquid phase sintering (LPS), hot isostatic pressing (HIP) sintering and microwave sintering (MW) [38].

2.2 Fabrication techniques of WC-reinforced MMC coatings

As coatings, composite coating containing WC have been successfully deposited using thermal spray [14-17] and laser cladding processes [12, 13]. Laser cladding process often used cast WC powders mixed with self-fluxing alloys, whereas agglomerated WC-based powders were often deposited in thermal sprayed coating [39, 40].

Thermal spray is a generic term for a group of coating processes which use thermal energy sources to apply metallic or nonmetallic coatings. In these processes, materials in the form of powder, wire, or rod are heated to a molten or semi-molten state and then accelerated to high velocities in a gas stream. The droplets strike the substrate, flatten and rapidly solidify to form splats and a bond forms with the surface. The successive impingements of particles and inter-bonding among the splats build up a thick coating (>10 μm). The spray material may consist of a single element, but alloys and composites are often used. The temperature of thermal sources range widely from 2200 ˚C to 8300 ˚C and then, virtually any material that melts within this range can be deposited [41, 42]. However, thermal-sprayed microstructure contains of plenty of imperfections including pores, cracks, and oxides and unwanted chemical changes. The reason for these imperfections are the limited deformation of partially melted particles, low-velocity particle impact, as well as, high-temperature requirement of these processes [41, 42]. Several strategies

have been applied to increase particles velocity and reduce particle temperature in order to improve the deformability upon impact and limit the oxidation and other chemical reaction levels [43, 44]. However, there are still challenging problems associated with coating costs and chemical reactions [43, 44].

Thermal spray processes were used to deposit MMC coatings containing WC particles to enhance the surface properties [12-17]. However, high temperature during these processes often causes decarburization of WC and formation of brittle phases at interfaces [16, 17]. Stewart *et al*. [45] proposed a model for microstructural features that was observed in WC-Co thermal-sprayed coatings. Based on this model, cobalt is melted during spraying, which cause dissolution of WC into the molten cobalt. This causes loss of carbon from periphery of the particles by oxidation and forms W_2C, W and/or Co_6W_6C or Co_3W_3C η phases. The latest development in thermal spray processing is based on increasing the particles velocity and reducing particles temperature to limit the oxidation level and improve the deformability upon impact. In the high-velocity oxygen fuel (HVOF), the process is operating at increased combustion chamber pressures in order to raise particle velocities and reduce the particle dwell time in the hot flame [46]. Besides providing high density and bonding strength, and possible compressive residual stresses, there are still some degree of decarburization that is present in HVOF-sprayed coatings. Moreover, there are still problems associated with HVOF including coating costs and reactions of combustion gas jet with reactive metals such as titanium [44]. Figure 2.2 compares process temperature and particle velocities in cold spray with those of a wide range of other thermal spraying methods (Fig. 2.2), where points out that cold spray relies primarily on kinetic energy rather than thermal energy [19, 20]. Therefore, to eliminate decarburization completely, cold spray can be used to fabricate MMC coatings reinforced with WC particles [19, 20].

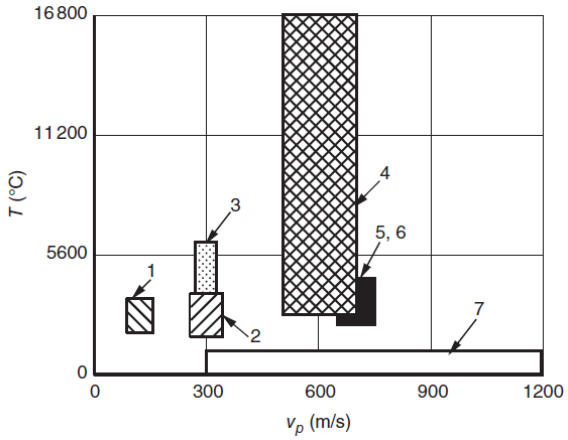

Fig. 2.2 Diagram of jet temperatures (T) and particle velocities (v_p) used in different spraying methods. 1, low-velocity gas-plasma; 2, high velocity gas-plasma; 3, electric-arc; 4, plasma; 5 and 6, detonation and high-velocity oxygen fuel; 7, cold spray [19].

2.3 Cold spray technique

2.3.1 An overview of cold spray process

Cold spray, or cold gas-dynamic spray (CGDS), is a solid-state deposition process in which a high velocity (300-1200 m/s) jet of particles impact onto a substrate. The particles are accelerated in a converging-diverging nozzle in conjunction with a preheated and pre-pressurized gas source. Upon impact, metallic particles undergo severe plastic deformation, which leads to a metallurgical bonding, and consequently coating buildup occurs [19, 20]. Cold spray was developed for the first time in the mid-1980's at the Institute of Theoretical and Applied Mechanics of the Russian Academy of Sciences in Novosibirsk. While conducting experiments of a supersonic two phases flow (gas and solid particles) in a wind tunnel, Dr. Anatolii Papyrin and his colleagues noticed that there is a transition from erosion by particles to deposition and coating formation by increasing particle velocities. The first cold spray system was then developed by the same group in 1980s [19]. Since then, the interest in cold spray process has grown significantly especially in the last two decades and a wide spectrum of research is being conducted at several research centers and universities around the world, including McGill University, for further developments and improvements of cold spray.

Figure 2.3 illustrates schematic of a cold spray setup. A compressed air or more commonly an inert gas such as nitrogen or helium, is sent through an electric heater in which it heats to high temperature of 100 to 800ºC. A typical cold spray gun is equipped with a converging/diverging or De Laval type nozzle, in which the gas and the particles achieve supersonic velocities. The high temperature compressed gas is then directed to the nozzle. Passing the narrowest portion of the nozzle (throat), the process gas reaches the speed of sound, following a rapid expansion, and continues to accelerate as it passes through the diverging part of the nozzle. A separate portion of the gas is directed through a powder feeder system, injecting powders into the converging or the diverging section of the nozzle. The powders are entrained in the high-velocity gas, accelerated and impact onto a substrate. The powder velocity ranges from 300-1200 (ms^{-1}) depending on feedstock particle size and type [19, 20, 47]. There are currently two main types of cold spray systems including high pressure cold spray (HPCS) in which particles are injected prior to the nozzle throat by a high-pressure gas jet (1-6 MPa) and low pressure cold spray (LPCS) where powders are entrained in the high-velocity gas in the diverging section of the spray nozzle from a low-pressure gas supply (0.5-1 MPa) [48, 49]. HPCS systems, using higher pressure gases and lower weight gases, such as nitrogen or helium as process gas, generate particle velocities of 600–1400 m/s, which make it favorable for depositing high melting point materials such as steel, nickel, titanium-based alloys. While, in LPCS systems, particles reach much lower velocities of 300–600, which limit its application to lighter materials such as zinc, aluminum, and tin [49]

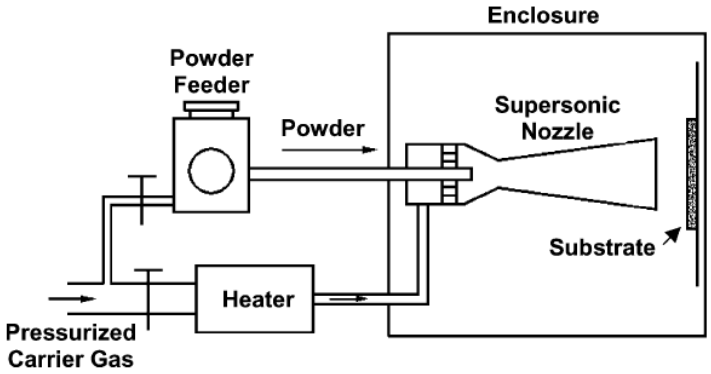

Fig. 2.3 Schematic of cold spray process [47].

2.3.2 Bonding mechanism and critical velocity

Computational modeling and experimental studies have found that only above a certain critical velocity, deposition/adhesion of particles to a substrate occurs. Adiabatic shear instability is the most acknowledged bonding mechanism in cold spray, that occurs at the particle substrate interface at or beyond the critical velocity. This is initially proposed by Assadi *et al.* [50] and later supported by numerical simulation and experimental evaluations of other researchers [50-52].

The results of impact modelling for copper as a reference material conducted by Assadi *et al.* [50] revealed a rapid increase in calculated strain and temperature at particle/substrate interface, but a significant drop in flow stress within a range of velocity between 550 and 580 m/s (see Fig. 2.4), indicating a change in the deformation mechanism from plastic flow to viscous-type resistance. Upon impact at high velocities, the particle/substrate or particle/particle interfaces experience work hardening effects due to high strains and strain rates. On the other hand, the high plastic strain at the interface can result in thermal softening due to dissipation of kinetic energy into heat. Therefore, there are two competing factors during particle impact in cold gas spraying. At high particle velocity, enough for generation sufficient kinetic energy to convert to heat, softening effect can dominate against the hardening effects. This leads to adiabatic shear instability at the interface. Under this condition, the material loses its shear strength and undergoes excessive deformation for any amount of imposed shear stress (see Fig. 2.4). According to the numerical investigation, the material deformation at the interface can reach strain rates of up to 10^9 s^{-1} and strains of 10 or even more [52]. The non-uniformities in temperature and strain distributions at the particle/substrate interface suggested that the extent of region which undergoes adiabatic shear instability, and thus bonding, is confined only to a small fraction of the overall contact area [50]. It is widely reported that a jet composed of the highly deformed particle and substrate material is formed at the interface, following accelerating thermally softened material at the interface away (see Fig. 2.5). Thus, oxide layers and other impurities are carried away, resulting in intimate contact and metallurgical bonding of the heated and clean surfaces [47, 50-52].

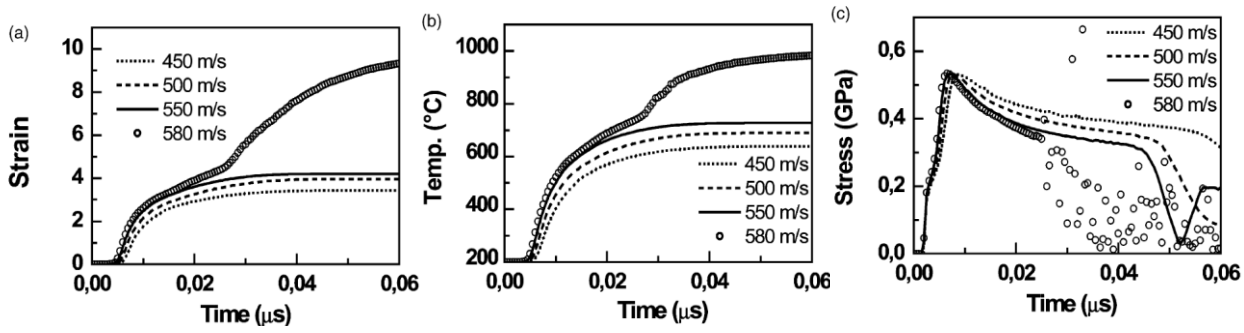

Fig. 2.4 Calculated temporal development of (a) plastic strain (b) temperature and (c) flow stress at the critical node of a sprayed copper particle for various impact velocities [50].

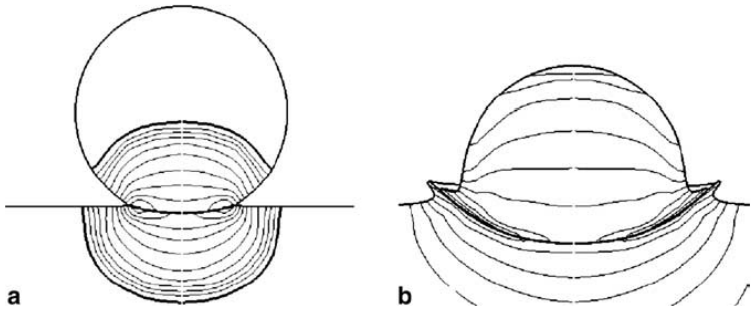

Fig. 2.5 Pressure field during impact, upon impact of a copper particle, a strong pressure field propagates into the particle and substrate (a), jetting, the pressure gradient at the contact generates a localized shear straining, leading to adiabatic shear instabilities and out-flowing material jet (b) [52].

The critical velocity, υ_{Cr}, for a given powder is the minimum velocity that an individual particle must attain in order to adhere to the substrate. When the particle velocity is lower than υ_{Cr}, then the particle hits the substrate or previously deposited layer and rebounds. However, if the particles velocity reaches or exceeds υ_{Cr}, then particle adhesion occurs, the coating process begins, and the deposition efficiency rapidly increases. When the particle velocity becomes much greater than υ_{Cr}, and reaches the erosion velocity, $\upsilon_{erosion}$, impacting particle would cause erosion of the substrate. Thus, the area between υ_{Cr} and $\upsilon_{erosion}$, there is a window of successful particle deposition, [19, 20, 50-52] as shown in Fig. 2.6.

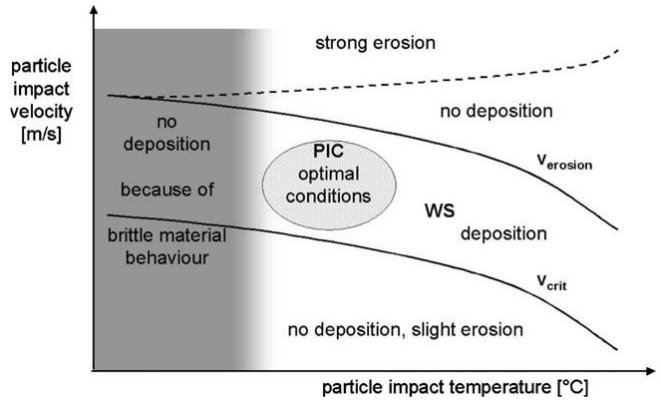

Fig. 2.6 Particle impact velocity versus particle temperature with window of spray-ability and the regime of particle impact conditions [52].

The theoretical estimation of the critical velocity is based on the particle velocity at which impact begins to cause adiabatic shear instability. Assadi *et al.* [50] developed an equation based on adiabatic shear instability to predict the critical velocity,

$$v_{cr} = 667 - 14\rho + 0.08T_m + 0.1\sigma_u - 0.4T_i \qquad (2\text{-}1)$$

, where ρ is the density, T_m melting point, σ_u ultimate strength and T_i initial particle temperature. This suggest that density and particle temperature have significant effects on the critical velocity among other factors and are thus the most influential parameters in cold spray. Schmidt *et al.*[11] improved the formula to correlate the critical velocity with materials parameters. Their results are summarized into the following equation,

$$v_{cr} = \sqrt{\left[4F_1\sigma_u\left(1 - \frac{T_i - T_{ref}}{T_m - T_{ref}}\right)\rho^{-1}\right] + (T_m - T_i)c_pF_2} \qquad (2\text{-}2)$$

, where T_{ref} is the reference temperature at which the ultimate tensile strength was determined, c_p particle specific heat capacity, and F_1 and F_2 constants representing material dependent calibration factors. Assadi *et al*. [50] do not consider the particle size to be a significant factor. However, materials deformation and heat transfer analysis imply that particle size play an important role in critical velocity. Therefore, the critical velocities predicted with equations (2-2) matches better with experimental results, since it considers the particle size effect through heat conduction and strain-rate hardening effects [52].

2.3.3 Effect of particle size and morphology on critical velocity

Small particles are accelerated to higher velocities in the gas stream. This is related to the fact that, gas/particle momentum transfer is proportional to 1/d, where d is the particle diameter. Therefore, due to higher acceleration, higher impact velocity is expected with smaller size particles [53]. However, depending on spray material and process parameters, for much smaller particles, the velocity is low due to their low mass. Figure 2.7 illustrates the relation of particle velocity and critical velocity with particle size. As mentioned before, the critical velocity increases with decreasing particle size. Considering this effect, there is an optimum powder size range for cold spray deposition of coatings, where the impact velocity is significantly higher than critical velocity. With much smaller particles, on the left side, there is no deposition due to lower particle velocity than critical. While, with larger size particles, on the right side, the impact velocity is close to critical velocity. This leads to coating with high porosity and low deposition efficiency [51]. Particle velocity can be also influenced by powder morphology. It was found that the irregular shaped particles are accelerated to higher velocities than the spherical particles, due to the aerodynamic effect. This is due to a higher drag coefficient for irregular particles, leading to higher drag force, and thus, higher velocities [53, 54].

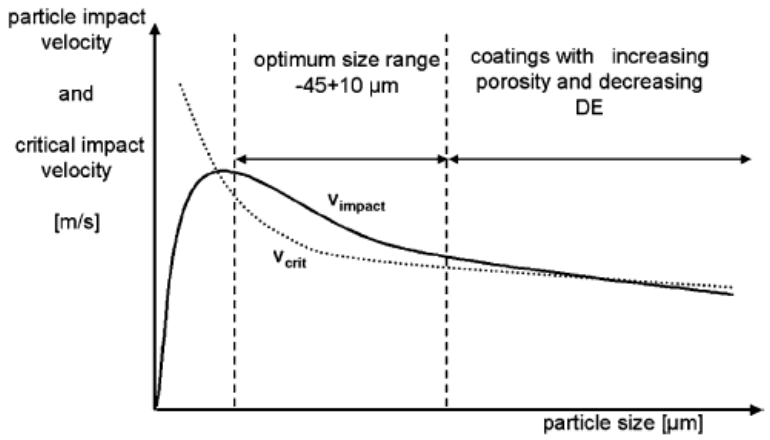

Figure 2.7 Impact velocity and critical velocity versus particle size; Optimum particle size range for deposition [52].

2.3.4 Microstructural evolution during cold spray

Typical microstructure of cold sprayed metallic coatings consists of the deposited particles known as splat-like microstructure [55] (see Fig.2.8). Figure 2.9 illustrates schematic evolution of grain refinement in a single splat. As particle hit the surface (a), the high impact pressure developed at impact region results in deformation of particle (b). with increasing particle and the substrate contact area, adiabatic shear instability occurs at the interface leading to material jetting by viscous flow (c). Dislocations are generated and entangled during the deformation (b) and then rearranged into low energy configurations such as dislocation cells, from which subgrains can develop (c). Above a critical strain and temperature, the subgrains are rotated and recrystallized (d) [56]. Zou *et al*. [57] studied the process of dynamic recrystallization in cold-sprayed Ni coatings using EBSD. They observed a non-uniform microstructure with ultrafine grains in the size of 100 – 200 nm due to dynamic recrystallization (Fig. 2.10). The operating mechanisms for dynamic recrystallization is determined through point-to-point (Fig. 2.10a) and the point-to-origin (Fig. 2.10b) misorientations analysis from the center to the edge of the deformed particle, as shown in Fig. 2.10b. The misorientation gradient in the central zone of the particle was relatively low and only a small number of LABs was observed. Whereas, towards the particle/particle interface, HABs are formed and the point-to-point and the point-to-origin misorientations was increased to 40 and 70, respectively. Moreover, deformation-induced lattice rotation in one grain was resolved using tolerance angle map (Fig. 2.10c) and the inverse pole figure (Fig. 2.10d), where lattice is gradually rotated from the center to the edge of the particle. These results show that the lattice and subgrains progressively rotated until HABs appear near the particle bonding region indicating rotational dynamic recrystallization.

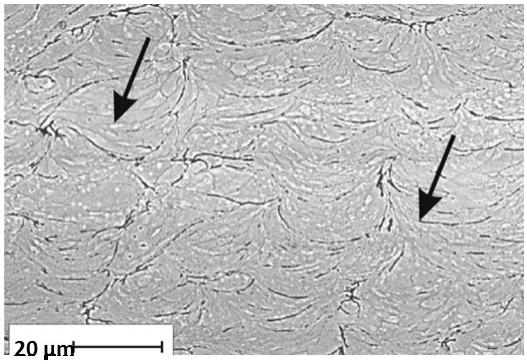

Fig. 2.8 SEM micrograph of cold-sprayed Ni coating. The left arrow in indicates a grain boundary in a Ni powder particle, the right arrow indicates an interparticle boundary [55].

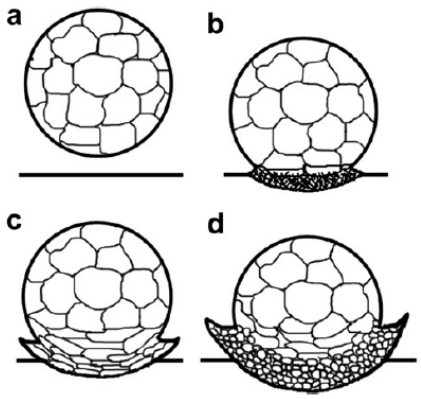

Fig. 2.9 Schematic evolution of grain refinement by dynamic recrystallization: (a) spraying titanium particle onto the substrate, (b) entanglement of dislocations, (c) formation of dislocation cells (and subgrains) and re-elongation, and (d) breaking-up, rotation and recrystallization of subgrains by thermal softening effects enough to trigger the viscous flow [56].

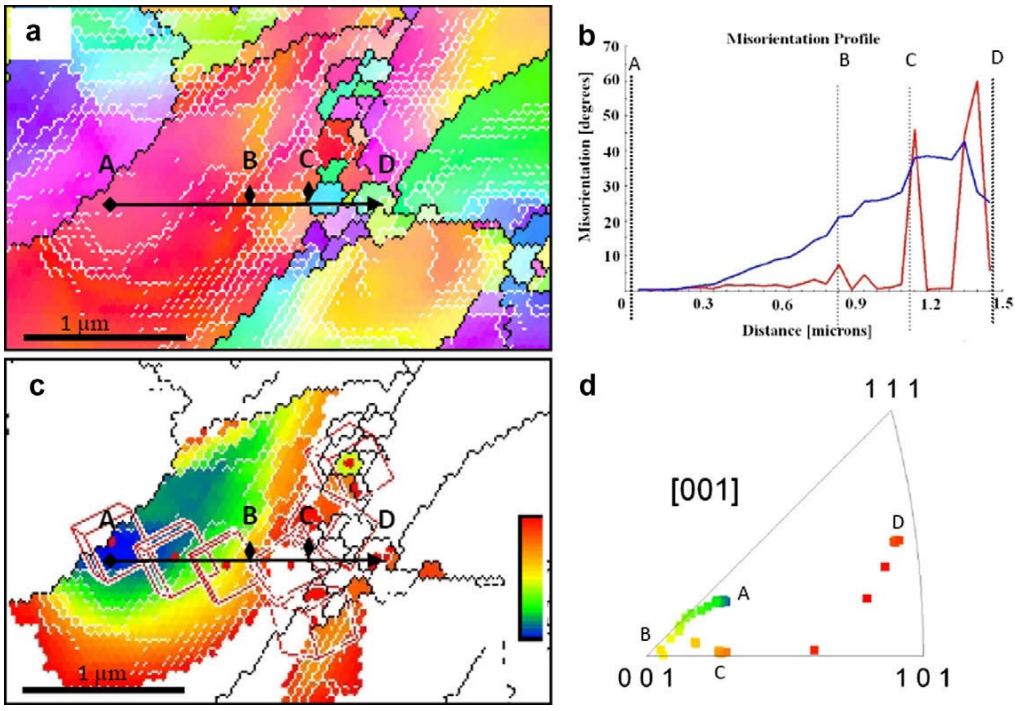

Fig. 2.10 (a) Euler angle map with four points (A, B, C and D) marked in a line from the center to the edge of the particle. (b) Misorientation profile, showing the point-to-point (the blue curve) and the point-to-origin (the red curve) along the path ABCD. (c) Tolerance angle map. The orientation of point A is selected as reference and the tolerance value is in the range of 0–25° (shown from blue to red). The cubes in the map show the local crystal orientation. (d) Inverse pole figure of the points in the line ABCD [57].

2.4 Use of cold spray technique to deposit MMC coatings

Adapted from a book chapter cited as [58]

The vast majority of research on cold spray for the first decade after its invention was devoted to metallic materials [19, 20]. The materials applicable for cold spray, is limited to those that have some degree of ductility at high strain rate, which comes from its bonding nature [50, 51]. However, by increasing demand for tribological coatings, the idea of MMCs was applied to spray brittle materials. The very first successful fabrication of MMCs coatings using cold spray were the materials that are commonly fabricated by other methods such as Al-Al_2O_3, Al-SiC and

WC-Co [15, 59-61]. Soon it spread to other materials and currently a wide range of the materials such as metals, ceramics, composites and polymers have been sprayed [19, 20, 49, 62-64]. The low temperature of cold spray was an advantageous, avoiding oxidation and carbide decomposition that commonly occurs in thermal spray [19, 20, 49, 62-64].

There are three main strategies that have been used to deposit metal matrix composite coatings. (a) sintered, crushed or otherwise manufactured metal-ceramic composite powders, (b) pretreatment of pure ceramic powders with metallic claddings, and (c) mechanical blends metal and ceramic powders. For the first two strategies, there are some reports of coating fabrication directly from composite or clad powders, although the pre-treated powders can be admixed with metal powders, as reported in previous studies [14-18]. Cold spray of mechanically blended ceramic and metallic powders is widely applied in previous studies. Co-deposition of metallic particles with oxides and carbides of different metals and especially with SiC or Al_2O_3 as reinforcement particles is reported in previous studies [65-70]. Limited deformability of ceramic particles led to lower retention of the ceramic in the coating compared to the feedstock composition. Ceramic particles are retained to coating by embedding into pre-deposited metal particles, or as reported in a few studies, entrapping by later-arriving metal particles in a so-called "burial" mechanism [71, 72].

In most of the studies, angular ceramic particles were sprayed, which led to more embedding and thus higher retention of ceramic particles than spherical of same size. However, angular morphology is not always preferred for the engineering application and there were some reports available on spherical particles [71, 72]. Particle size can also have a profound effect, where finer size ceramic particles were more prone to embed into substrate [66]. The benefit is limited because the presence of the bow shock effect at the substrate make it difficult to deposit very small particles [73]. Coatings with higher ceramic content were deposited with increasing ceramic content in the feedstock. However, above a critical content for ceramic particles, interactions between ceramic particles were more dominant, which resulted in decreased retention of ceramic particles into coating [70]. Another factor that have a profound effect on ceramic retention is the metal used at the matrix. Previous studies demonstrated that Al matrix composites have been successfully co-deposited with SiC and Al_2O_3 reinforcements using cold-spray. It was reported that above 70% of initial SiC and Al_2O_3 were recovered into coating [70, 74]. However, a much

lower fraction of feedstock Al_2O_3 particles of similar morphology into Ni (around 12-22%) was reported [73, 75]. This is linked to the deformability of the metal, where Al matrix retains significantly more ceramic compared to the Ni matrix. Figure 2.11 presents the volume fraction of Al_2O_3 retained plotted versus the volume fraction in the feedstock for both Al matrix and Ni or Ni alloy matrices [73, 75].

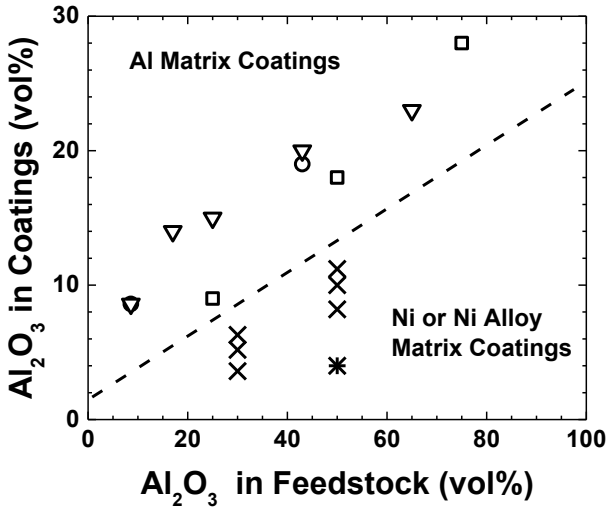

Fig. 2.11 Volume fraction of Al_2O_3 retained in cold spray coatings as a function of the volume fraction in the feedstock. Coatings with Al matrix (▽ , ○ , □) retain more alumina than a Ni or Ni alloy matrix (×, ✳) [58].

Low process temperature makes cold spray capable of depositing carbide containing materials. This has attracted considerable attention in recent years because problems inherent to the conventional thermal spray can be eliminated. Because of the unique properties of WC especially for wear resistant applications, considerable attention was given to cold spray of composite coatings containing WC. High losses of WC particles were reported with only 11-29% of WC recovered to coating from an admixed feedstock [27]. Metal-carbide type MMCs consist of a high concentration of carbide inside a harder metallic matrix such as Co, Ni or Fe. The volume fraction of carbide is much higher than the typical retention found in cold-spraying of ceramic-metal mixtures. To overcome this difficulty in cold spray, most of the studies on WC containing cold sprayed coatings have used agglomerated, sintered and crushed WC/Co and WC/Ni powders. WC composite coating with different ratios with nano and microstructures were deposited using

nitrogen and helium gasses. In this regard, several approaches were employed to overcome the low deposition efficiency and unsatisfactory bonding quality, which arises from limited deformability of WC-based powders. These strategies are including: Adequately designed porous spray powder[14-18], sufficient binder/matrix content [17], and powder preheating prior to spray [18].

Formation of a strong cohesion of impacting particle with the underlying coating is required for successive building up of a WC composite coating to a designed thickness. Upon impact at high velocity, the compaction and deformation of WC-based particles near the contact area occur through slipping and rotation of WC particle along Co/Ni binder. The creation of such cohesion is associated with certain deformation degree of both impacting particle and the underlying coating [14]. With increasing the powder porosity, the particles deform extensively. However, substrate is less influenced by particles of high porosity. On the other hand, for successive layers of coating, a certain level of porosity is needed to fulfill the deformation requirement [16]. Employing lower content WC powder resulted in higher deposition efficiency and higher quality of coating, however, lower hardness was obtained [17]. A more recent approach was used in two studies conducted by Lioma *et al.* [27] and Melendez *et al.* [76], where WC/Co powders were sprayed with Ni addition in initial feedstock. Low-pressure cold spray unit was employed to deposit mechanical blends of various WC contents ranging from 50 to 96 wt.%. Although low-pressure cold spray could recover 50-67 % of feedstock WC into the coating, it was hypothesized that higher velocities attained by particles using high-pressure cold spray may be more effective on deposition a coating with controlled WC content. Among powder pretreatment methods, using metallic coating on ceramic particles were more effective, where the obtained coatings were denser, decreased ceramics fragmentations, and recovered more hard phases compared to coatings produced from equivalent mixtures. In this regard, electroplating and chemical vapor deposition (CVD) were employed to deposit a Cu and Al metallic layer on WC particles [21] and Ni coating on hBN [63], diamond [77], and B_4C particles [78].

2.5 Selected tribology topics

Tribology is the field that studies and characterizes the interactions at surfaces in relative motion [1, 2]. Interactions at the interface transmit the forces, convert the mechanical energy, and change the physical and chemical properties of the interacting materials. The nature and consequence of these interactions determine the friction, wear and lubrication behavior of the interacting materials. Therefore, the principle of tribology is to evaluate and explore these interactions and solve the technical problems arising from interfacial phenomena [1, 2]. As noted by Bhushan, "tribology covers many diverse disciplines and topics including physics, chemistry, solid mechanics, fluid mechanics, heat transfer, materials science, lubricant rheology, reliability, and performance [1, 2]." The tribological experiments in this dissertation consisted of dry sliding wear and solid particle erosion wear, so only the tribological phenomena related to these will be discussed here.

2.5.1 Friction and wear

Friction and wear are phenomena which arise from relative movement of two solid bodies over one another. Friction is the resisting tangential force which acts in the opposite direction to the direction of motion. While, wear is the surface damage or removal of material from one or both of the contacting solid bodies. Neither friction nor wear are intrinsic material properties. They rather are the system responses to surfaces in relative motion which are strongly influenced by materials physical and chemical properties as well as by surface morphology, normal loads, sliding velocity, contaminants films or lubricants on the surface, temperature, environmental conditions, and other factors [1, 2]. Friction can be simply expressed as the coefficient of friction (COF or μ) which is the ratio of the frictional force, F, to the applied normal load, W,

$$\mu = \frac{F}{W} \tag{2-3}$$

Bowden and Tabor [79] were the first to propose a widely accepted model for friction. Based on their theory, friction includes mechanisms of energy dissipation and is attributed to adhesion and micro- and macro-scale deformations. They proposed that for two bodies in sliding contact, high pressures developed at individual asperities, cause interfacial adhesion between asperities. These interfacial adhesion contacts are sheared subsequently by relative sliding of the

surfaces. This needs frictional energy (or force) to overcome interfacial adhesion. In addition, micro-scale plastic deformation of the contacting surfaces consumes energy. In the case of plowing or grooving action of the asperities of one surface, normally the surface that is harder of the two, energy is needed for this macro-scale deformation. The particles trapped between the sliding surfaces can also cause macro-scale deformation of the contacting surfaces [1, 79]. Although too simplistic, with assuming negligible interaction between mechanisms explained above, they can be added, and the total intrinsic frictional force (F) equals the force needed to shear adhered junctions (F_a), the force needed for plastic deformation (F_d) [1]. Then, according to the Bowden and Tabor model [1, 79],

$$F = F_a + F_d \tag{2-4}$$

Therefore, using equation (1),

$$\mu = \mu_a + \mu_d \tag{2-5}$$

, where μ_a is adhesive component and μ_d is plastic deformation component of total friction coefficient (μ). It is worth noting that the dominant mechanism of energy dissipation in metals and ceramics is plastic deformation. One component of the total intrinsic friction force is adhesion. When two nominally flat surfaces come in contact under load, discrete contact spots between tips of the asperities are formed. The proximity of the asperities and physical or chemical interaction between asperities cause adhesive contacts. The sum of the areas of all the contact spots is the real area of the contact (A_r). This is only a small fraction of the apparent or nominal area of contact (A_a). During relative motion of two bodies in contact, a tangential force is needed to shear the adhesive contacts. Rupture normally occurs in the weakest regions. It can be either at the interface or in one of the two contacting bodies. After shearing the existing adhesive bonds, new contacts and bonds are developed due to the adhesion arising from molecular forces between the surfaces [1]. The force required to shear adhesive contacts is called adhesive force (F_a) and can be described as following in a dry contact:

$$F_a = A_r \tau_a \tag{2-6}$$

Therefore, the coefficient of friction for a dry contact is,

$$\mu_a = \frac{A_r \tau_a}{W} = \frac{\tau_a}{P_r} \tag{2-7}$$

Where τ_a and P_r are the average shear strength and mean contact pressure of the dry contact, respectively [1]. Therefore, one strategy to reduce the adhesive component to the friction

coefficient is to apply a hard material with a soft skin, due to reduced τ_a and increased P_r (reduced A_r) [80]. Deformation is other component of the total intrinsic friction force and can occur in two types of interaction scales: the micro-scale deformation in which asperities in very thin and interfacial regions deform locally, and the macro-scale deformation where the asperities of the harder material makes plowing or groove in the softer surface through plastic deformation. In the case of the contribution of macro-scale deformation to the total intrinsic friction force, surface roughness, relative harnesses of the two surfaces, the size, shape and hardness of any wear debris and reaction products trapped between two contacting surfaces are influential [1].

2.5.2 Classification of wear

According to Holmberg and Matthews [4], wear is defined as "the removal of material from solid surfaces as a result of one contacting surface moving over another". There are different ways of classification of wear, which is explained in the following. Blau [81] classified the wear based on contact conditions between counterparts including sliding, impact and rolling. Using this approach, abrasive, adhesive, fatigue, fretting and polishing wear mechanisms are assigned to sliding wear. in fact, he gave a greater importance to sliding wear than other types. Budinski [82] considered four different materials removal mechanisms i.e. abrasion, erosion, adhesion and surface fatigue to classify the wear. A more systematic approach toward wear classification is developed by Holmberg and Matthews [4], where three aspects of wear, i.e. (1) wear mode, (2) wear mechanisms and (3) wear failure mode, were based for classification.

2.5.2.1 Wear mode

Wear mode is a classification of wear based on the type of relative motion of surfaces, e.g. sliding, rolling, fretting, and erosion/impact wear. In the present thesis, two types of wear modes, i.e. sliding and erosion, was performed on the cold sprayed coatings. Some of these wear modes can be sub-divided further. For example, sliding wear can be categorized based on two main contact configurations, i.e. sphere on flat and flat on flat. Sliding and rolling motion can be continuous or with varying velocity, i.e. reciprocating. Erosive wear can be categorized into: 1) Solid particle erosion (SPE) (solid particles in gas stream or slurry), 2) Hot gas erosion, and 3) Liquid erosion, including droplet, slurry, liquid impingement, and cavitation [1]. SPE is the

materials loss caused by repeated impacts of solid particles entrained in a gas or liquid medium impinging on a solid at any significant velocity (greater than 1 m/s) [1, 29, 83].

2.5.2.2 Wear mechanisms and wear failure modes

A wear mechanism defines the process by which materials are detached or displaced from the surface during wear. This includes adhesive, abrasive, fatigue and chemical wear. Adhesive wear involves shearing the asperity contact, which can result in the detachment of a fragment from one surface and attach to the other surface. These transferred fragments may come off the surface and attach back to the original or form loose wear debris. Abrasive wear refers to the plastic deformation or fracture caused by hard asperities sliding on a softer surface (two-body abrasion) or hard particles trapped between two sliding surfaces (three-body abrasion). Fatigue wear occurs by surface and subsurface cracks. These cracks, observed during repeated loading and unloading cycles, cause removing of large material fragments from the surface and fatigue failure occurs after a critical number of cycles. However, prior to this critical point, negligible wear occurs compared to the wear induced by adhesive or abrasive mechanisms. Therefore, fatigue volume wear is not a useful data to report, but the number of cycles or time before fatigue failure is much more relevant and is indicative of fatigue life [1]. All four categories of wear mechanisms including adhesive, abrasive, fatigue and chemical wear are related to MMCs. However, oxidative wear, which is a subgroup of chemical wear, is highlighted and will be discussed in the following section, due to its dominating characteristics in friction and wear of MMCs. Wear failure mode is referred to the surface appearance after the tribological contact, e.g. plowing, wedge formation, cutting, gouging, grinding, indenting, surface craters, pitting, spalling, delamination, scuffing and seizure [4, 84].

2.5.2.3 Oxidative wear

Corrosive or chemical wear occurs because of the chemical or electrochemical interaction of the interface with a corrosive environment and usually is combined with the effect of mechanical contacts. One of the most common chemical wear processes is oxidative wear [1] in which oxide films are generated on the metal surfaces. This film can be removed due to mechanical contact which expose the fresh metal to oxygen and formation of new oxide films [1]. According to

Bhushan [1], friction modifies the kinetics of chemical reaction between sliding bodies. Therefore, reactions which occur at elevated temperatures could occur at moderate, even ambient, during sliding. Tribochemistry is the chemistry dealing with this modification of chemical reaction by friction or mechanical energy. The wear controlled by this reaction is referred to as tribochemical wear. In many cases, the tribological oxidation is generally a beneficial form of corrosive wear, which reduces the wear rate of metallic pairs as compared with that of the same pair under an inert atmosphere. Friction increases the rate of oxidation of surfaces due to frictional heat produced at contacting asperities. The removal of oxide scale resulting in fresh surfaces and accelerating diffusion, as well as, direct mechanochemical excitation of surface bonds are other mechanisms. Moreover, oxides are of much lower thermal conductivity than the metal. This reduces the heat flow away from wear interface and further increases the local temperature [1].

According to Stott *et al.* [85], there are three different processes for the formation of oxides, depending on the sliding and surrounding conditions including (1) "Oxidation-scrape-reoxidation", (2) "total oxidation" mechanism, and (3) "metal debris" mechanisms. In "Oxidation-scrape-reoxidation" mode, which comprises two stages, a general oxidation of apparent contract area and contact asperities occurs due to an increased interface temperature at first. Subsequent sliding removes the oxide and exposes clean metal for further oxidation. The oxide may not be completely removed by the subsequent sliding in "total oxidation", which occurs most often at elevated temperatures. So, the remaining oxide continue to thicken over time. If the oxide is adherent enough to the metal and can withstand the stress of the sliding, its formation leads to beneficial reduction in friction and wear. In "metal debris", the oxidation of fractured metal debris by the wear process itself results in the generation of load-bearing layers. Some of the oxide particles leave the sliding contact and have no further impact on wear behavior, while others can be entrained within the interface and moving along with the siding surfaces. These particles get entrapped and agglomerated to compacted layers acting as load bearing area and reducing wear. Two competitive processes then occur during subsequent sliding: (1) continuing sintering and cold welding between particles at the interface, resulting in further consolidation, (2) the compacted layers are continually broken-down, and the debris may induce wear. Previous studies indicated that above a certain transition temperature, an adherent, smooth wear-protective oxide layer is developed on the surfaces. There is no minimum temperature required for the process of forming

the wear protective oxide layers, although elevated temperatures favor compaction and sintering the wear debris. There are other factors that influence the effectiveness of an oxide layer in reducing friction and wear. Relatively more ductile oxides, such as Co_3O_4 or NiO when compared to Cr_2O_3, which resist surface and subsurface cracking, are expected to be more wear-protective during wear of the specimens. A two-phase system, consisting of brittle and a relatively ductile phase, which own an optimum ductility, may be more effective than a single-phase system. Moreover, a good oxide/substrate adhesion is necessary for retention of such oxides. Another key factor influencing the sustainability of the compacted layer is the friction force for the sliding oxide surfaces, which tend to increase with decrease in temperature. High friction force results in increases the surface tensile stresses in the region of asperity junctions, which causes brittle fracture and an increased wear rate. In addition to the factors mentioned above, load-bearing capability of the material underneath the compacted layer is important in supporting the oxide layer [85, 86].

2.5.3 Third bodies and velocity accommodation modes

Third bodies and its key role on modifying friction and wear were first introduced by in 1984 [87]. Third-bodies is defined as a zone whose composition is different from that of the bulk first bodies in a general or "material sense", or as a thickness across which the velocity difference between first bodies is accommodated in a "kinematic" sense [87]. Berthier *et al.* [88] further divided the third bodies into screens and bulk. Based on their mode, third-bodies accommodate the velocity difference at five different sites i.e S1- S5 and four different accommodation modes i.e, elastic deformation, breaking, shearing and/or rolling [88] as shown in Fig. 2.12. Third-bodies physical and chemical process such as thickening, thinning, loss of transfer films, generation of wear debris, and sliding-induced chemical changes can modify friction and wear depending how velocity between two surfaces is accommodated [80].

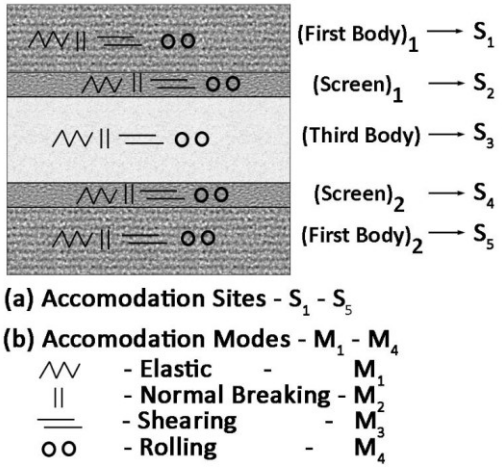

Fig. 2.1 Velocity accommodation mechanism by third bodies as proposed by Berthier *et al.* [88].

2.6 Tribology of cold spray WC-reinforced MMC coatings

Couto *et al*. [25, 89, 90] and Dosta *et al*. [91] deposited WC-Co coatings by cold spray and investigated their sliding (ASTM G99-04) and abrasive (ASTM G65-00) wear resistance. The results were benchmarked to the conventional HVOF WC-Co coatings using similar feedstock powders. The HVOF coatings was harder, but more brittle, than cold-sprayed coatings due to the decomposition of the WC/Co powder and formation of brittle phases. Cold sprayed WC-Co coatings showed higher wear resistance with an improvement of approximately 72% for WC–17Co, 60% for WC–12Co, and 80% for WC-25Co coatings. This was attributed to the absence of the detrimental phase transformation, whereas in HVOF coatings, the higher wear rate was primarily due to cracking along the preferential crack paths provided by brittle phases. For cold-sprayed WC–25Co coating, it was found that wear was occurring mainly by abrasion mechanism at the beginning of the test, pulling off some WC-Co particles from the coating. However, the carbide particles that are not extracted from coating maintain their wear resistance function. With decreasing in Co binder content, a higher hardness and improved wear resistance were obtained.

One of the advantage of the cold spray technique over thermal spray processes is to deposit coatings containing nano-structured materials without altering their original microstructure. Ji *et al.* [92] reported deposition of a WC-12Co coating, using a bimodal WC-12Co powders consisted of nano- and micro-structured WC particles. Average microhardness obtained on the coating cross

section was higher than that of HVOF multimodal WC-12Co coatings due to the dense structure. The enhanced wear resistance by multimodal distribution of WC particles was attributed to the synergetic strengthening effects of the multiscale WC particles. While nano-sized WC particles improved the abrasion resistance of the Co matrix by reducing its deformation and cutting, micro WC particles were more resistant to being pulled out and retarded retard the propagation of cracks. The abrasive wear resistance of cold-sprayed multimodal WC-12Co is greatly enhanced when comparing to the HVOF coating. The wear mechanism was mainly an initial selective removal of soft Co followed by WC removal or fracture. This was in agreement with Wang *et al.* [93] studies, where abrasive wear resistance of cold sprayed multimodal WC-12Co coatings was higher than HVOF coatings, due to the improved fracture toughness and microhardness.

Melendez *et al.* [94] studied dry abrasion wear performance of low-pressure cold-sprayed Ni and Ni-WC (WC/Co) composite coatings containing 7 to 66wt.% WC. They reported that the addition of WC to the coating minimized the wear damage to the surface. Higher wear resistance of the coatings was recorded with increasing WC percentages due to the enhanced hardness and fracture toughness. It was reported that the cold-sprayed Ni-WC coatings containing 66wt.% WC can compete with a HVOF WC-12Co coating in terms of abrasive wear resistance. Although the latter had a higher WC content (83wt.%WC), and thus, a higher hardness (~1100 HV), but hardness is not always the sole indicator of coatings ability to withstand wear. Embrittlement of the HVOF WC-Co coatings due to detrimental phases reaction decreased wear resistance. Abrasion wear resistance of low-pressure cold-sprayed coating that contained 66wt.% WC was comparable to that of the WC–25Co coatings fabricated using high-pressure cold spray suggesting that the former could be used as a low-cost alternative.

Tribological studies were conducted on cold spray WC coatings that have used agglomerated WC particles. There is no study available on cold spraying of cast WC particles and investigation of their rule in friction, sliding and SPE wear of MMCs. Moreover, the influence of WC powder morphology, i.e. cast and agglomerated, and its content on friction and wear of Ni-WC composite coatings is not studied yet. As for sliding wear, metallic materials, including MMCs, are reported to develop third bodies [87] during sliding wear. Tribological studies of MMCs have found that wear behavior is controlled by formation and structural, chemical and mechanical characteristics of the third bodies rather than correlated only with bulk strength and

hardness [22]. Incorporation of hard particles in metallic materials strongly affects the materials mixing and transfer mechanisms during sliding, which in turn influences third-bodies formation and their role in friction and sliding wear of composites [39, 95, 96]. Therefore, a careful investigation of third-bodies behavior and their link to friction and wear is required to better understand the wear mechanisms in cold spray WC coatings.

Chapter 3

Experimental procedure

3.1 Cold spray

3.1.1 Cold spray facility

All the cold spray depositions were conducted at the McGill Aerospace Materials and Alloy Design Center (MAMADC) located at NRC-CNRC Boucherville. Grit-blasted mild steel plates (thickness of 3 mm) were used as substrates. Two commercially available cold spray systems (PCS-800 and PCS-1000, Plasma Giken, Japan) were used for cold spray deposition. A de Laval nozzle FNFC-010-30S nozzle made of WC-Co was mounted in a spray gun at a standoff distance of 40 mm from the substrate. Nitrogen was used as the carrier gas. The particle velocities were measured in free-jet by a time-of-flight particle diagnostic system (DPV 2000, Tecnar, Canada) [97]. The WC and Ni powders were fed to the gun from separate hoppers. The powder feeder system was a custom installed done by the gun manufacturer, Plasma Giken. By setting feed rates of powders, various mixtures of Ni and WC were sprayed. The co-feeding system was used to avoid problems arising from the difficulty in premixing powder of differing densities and/or damage to powders due to mechanical mixing. Powder consumption was measured in situ by a digital scale mounted on the feeding system during spraying, and hence, an average feed rate throughout the spraying was obtained. Deposition efficiency was calculated as the weight gain divided by the mass of powder sprayed, which is the product of feed rate and the spray time. Scatter bar in the deposition efficiency results related to standard deviation of 10 repeat readings of feed rate throughout the spraying. Moreover, deposition efficiency of each component, e.g. WC, can be obtained by the equation below:

$$DE_{WC} = DE_{coating} \frac{WC\ Vol\%\ in\ coating}{WC\ Vol\%\ in\ feedstock} \quad (3.1)$$

where DE_{WC} is the partial deposition efficiency of WC and $DE_{coating}$ is the overall deposition efficiency of the coating.

3.1.2 Ni and WC powders

In this thesis, two types of WC particles, cast WC and agglomerated WCNi powders, were used. The original cast WC powder (TEKMAT™ WC-45, Tekna, Canada) with size distribution of -45+15 (d_{50} = 40 µm) was sieved to obtain two more finer size distributions of -38+25 (d_{50} = 30 µm), and -25+10 µm (d_{50} = 15 µm). The agglomerated WCNi (AMPERIT® 547, H.C.Starck, Germany) had a particle size range of -30+15 µm (d_{50} = 20 µm). Two size ranges of Ni powders, (4SP-10, Novamet, USA) with size distribution of -10+4 (d_{50} = 7 µm) referred to as Ni(7) and (AMPERIT® 176, H.C.Starck, Germany) -35+15 (d_{50} = 25 µm) referred to as Ni(25), were sprayed alone and mixed with WC powders. A laser scattering particle size distribution analyzer (LA-920, Horiba, Japan) was used to measure the particle sizes. Size distributions of the feedstock powders used in this thesis, as well as, their morphology and compositions are listed in Table 3.1. All the powders were in spherical morphology.

Table 3.1 The materials used in this thesis.

powders	morphology	composition	D_{10} (µm)	D_{50} (µm)	D_{90} (µm)	Chapters
Ni- Referred to as Ni(7)	Spherical	commercially pure	4	7	10	4-5-6-7-8
Ni- Referred to as Ni(25)	Spherical	commercially pure	15	25	35	8
Cast WC(40)	Spherical	W_2C/WC	15	40	45	4-5-6-7
Cast WC(30)	Spherical	W_2C/WC	25	30	38	4-5-6-7
Cast WC(15)	Spherical	W_2C/WC	10	15	25	4-5-6-7
Agglomerated WCNi	Spherical	Carbon < 2.5vol.% Ni 18-21vol.% Balance WC	15	20	30	4-6-8

Figure 3.1a shows morphology of the cast WC powders used in this study. XRD analysis of cast WC powders was performed. The spectrum showed the predominance presence of W_2C than WC (Fig. 3.2). Microstructure of cross-sectioned cast WC powders are illustrated in Fig. 3.1b. The microstructure is acicular eutectic of WC and W_2C. Figure 3.3 shows morphology and polished cross-section of a WCNi powder, with porosity revealed as dark regions. EDX

analysis of the cross-section of powders revealed the presence of regions rich in carbon. Based on the supplier data sheet, carbon content is 5.4-5.8wt.%. Considering the carbon in compound with W (5.4wt.%), there is no free-carbon or very low, 0-0.4wt.% (0-2.5vol.%). Since the powders was mounted using carbon-containing epoxy before polishing, the regions rich in carbon could be epoxy diffused into pores during mounting. XRD phase analysis of WCNi powders is given in Fig. 3.3c. The WCNi powder is made by spray drying of a suspension consisting of the WC carbides and a binder followed by a sintering process [41]. However, XRD spectrum indicated no new phase formation or less than XRD detection limit due to decarburization in partial sintering step.

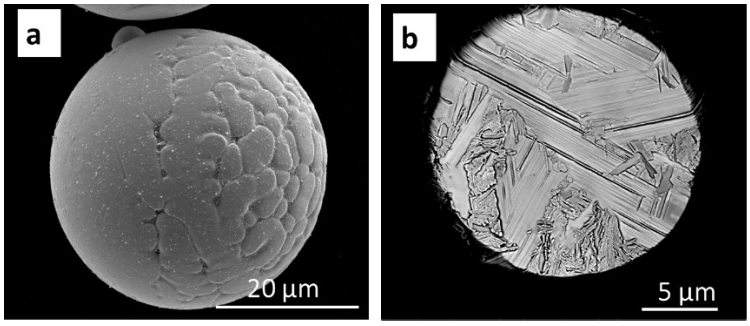

Fig. 3.1 SEM micrographs showing morphology (a) and cross-sectional microstructure (b) of as-received cast WC powders -45+15 (d_{50} = 40 µm).

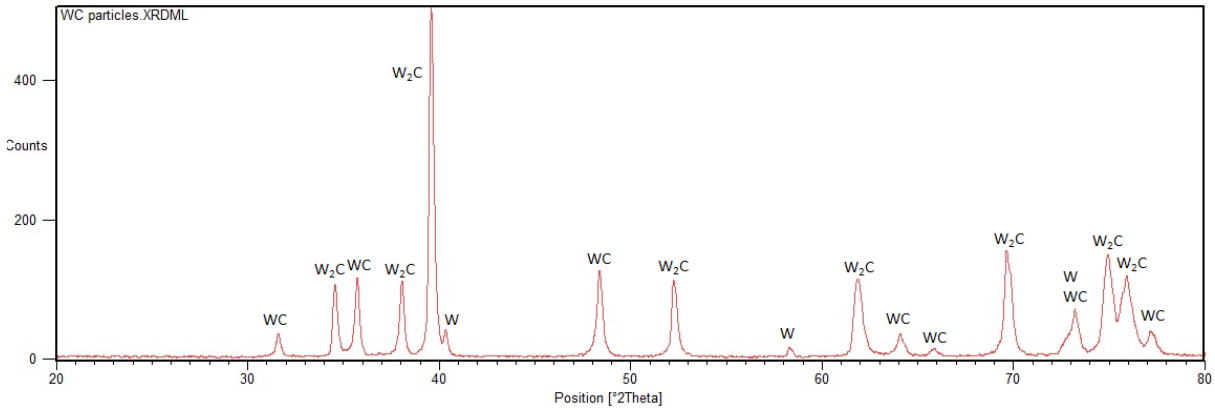

Fig. 3.2 XRD phase characterization of cast WC powder.

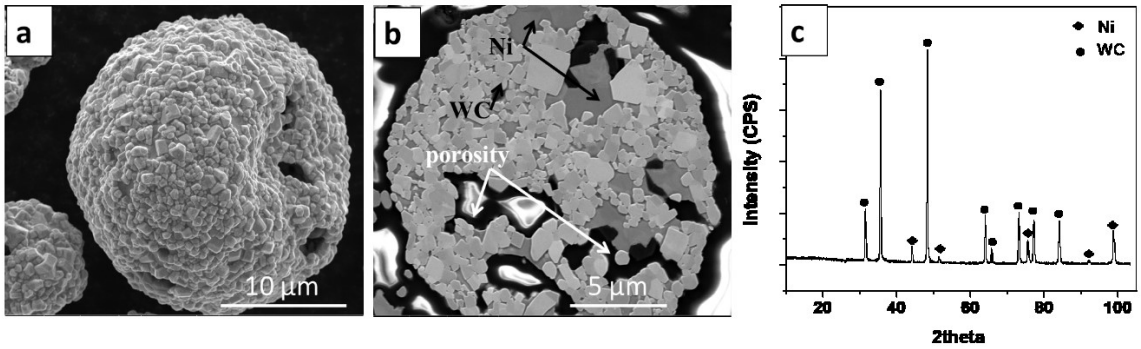

Fig. 3.3 SEM micrographs showing morphology (a) and a cross-section of WCNi powder (b) and XRD phase characterization of WCNi powder (c).

3.1.3 Selecting spraying condition and powders for cold spraying of Ni-WC

In order to obtain high deposition efficiencies and control WC content in Ni-WC composites, optimized spraying condition and powders characteristics were selected. To do this, the following research questions should be answered: 1) how does WC particle behave upon cold spray impact? 2) How this is influenced by its size? 3)How does Ni and WC influence each others deposition? 4)what is the effect of spraying condition? 5) whether porous and agglomerated structure of WCNi is beneficial in controlling the WC content?

For the first question, single particle deposition of WC was performed using original cast WC powders with a size distribution of 45+15 (d_{50} = 40 µm). A 3×1×0.125 inches of commercially pure Ni-200 plate was used as substrate. Ni substrates were polished using 1200 grit grinding papers, followed by polishing using 9, 3, and 1 µm to obtain fine polished surface. Nitrogen was used as carrying gas. Prior to entering the nozzle, the gas pressure was 4 MPa and the gas preheat temperature was varied from 700°C. The WC powder was fed to the gun at a rate of 3 gr/min. The Stand-off distance (SoD) was set at 40 mm, and the gun traverse speed at 1000 mm/s. BSE detector in SEM was used to image the WC particles on the surfaces that are subjected to single particle deposition of WC. WC particles was revealed as bright contrast. A large number of empty craters were observed on the top surface of Ni-WC coatings (Fig. 3.4a), which implies that conditions required for WC particles to embed into Ni were not entirely met for powders and spray velocities used here. The conditions may differ during co-spraying of Ni and WC. This can be due, in part, to probably a softer surface because of contact with high-temperature gas at lower gun traverse

speed. Moreover, a rougher top surface, which is developed during cold spraying, may induce inter-mechanical impacting particles. In addition, the probable interaction between particles near substrate may influence particles deposition modes. Previous studies [98] indicated that during co-deposition of metal-ceramic particles, the higher the penetration depth of a ceramic particle upon impact, the higher its chance to recover to coating. This requires higher velocity of ceramic particles and/or softer matrix. A higher impact velocity can be achieved using smaller size WC particles. The effect of WC particles size is tested in **Chapters 4 and 7.** For this, the as-received cast WC powder with size distribution of 45+15 (d_{50} = 40 µm) was sieved to obtain two more finer size distributions of -38+25 (d_{50} = 30 µm), and -25+10 µm (d_{50} = 15 µm). Moreover, fragmentation of ceramic particles upon impact, that could be observed in closer view inside craters (Fig. 3.4c), is another source of materials loss. The influence of enhanced ductility of ceramic particles was examined in **Chapters 4 and 8** with using agglomerated WCNi powders with porous structure.

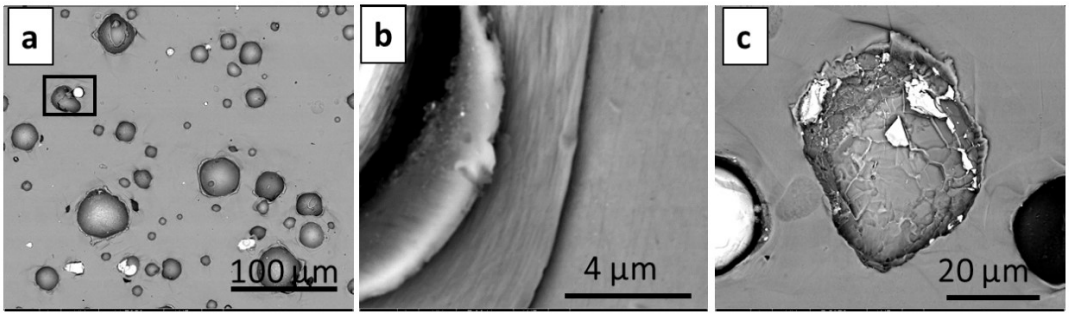

Fig. 3.4 (a) top view micrographs of the WC single particles sprayed onto Ni plate (b) close view of the rectangles in (a), WC fragments inside crater (c).

Cold spray process conditions that may have an influence on WC impact behavior can be divided into two categories. First, the factors that can change the gas stream, including gas temperature and pressure, nozzle design and type of gas. Others are spraying parameters that include substrate temperature, gun traverse speed, feeding rates and SoD. In this thesis all the factors related to the gas stream was kept fixed. Previous results [72, 99], indicated that higher velocity of impact can be achieved using high gas temperature. Using a simple isentropic gas flow model, as shown in Fig. 3.5 increasing gas temperature has a very little effect on the velocity of heavier particles [72, 99], such as WC. On the other hand, higher gas temperature can soften the Ni matrix leading to more embedding the WC particles. However, there is technical limitation to spray Ni powder, due to its tendency to clog the nozzle [73]. To avoid clogging nozzle, maximum

gas temperature of 700 and 800°C for Ni(7) and Ni(25), respectively, was used. A total feed rate of 1.75 rpm, in which the risk of nozzle clogging is lower, was used. By setting the feed rates of powders, various mixtures of Ni-WC were sprayed. SoD was fixed at 40mm. Varied gun traverse speeds of 60, 30 and 10 mm/s were tested to investigate its possible effect on increasing substrate temperature and facilitating the WC particles embedding. In a previous study [100], spraying at low gun traverse speed or with fixed gun was found to promote deposition of agglomerate WC particles with heating the previously deposited layers. In this thesis, only a slight improvement, less than 1vol.%, in WC retention was obtained as gun traverse speed was varied. A relatively low gun traverse speed of 30 mm/s was still used to ensure thickness of coatings for tribological experiments [100]. Table 3.2 summarizes the spray conditions that are used to spray coatings in this thesis.

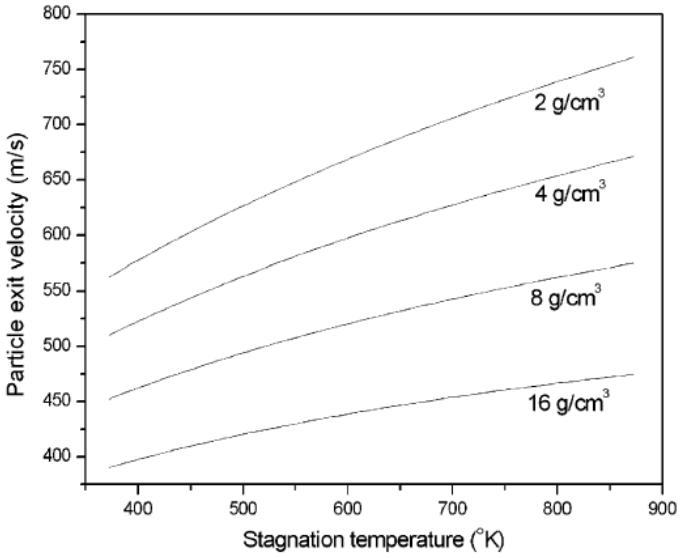

Fig. 3.5 Effect of gas temperature on particle velocity at the nozzle exit for 20 μm diameter particles of various densities [72].

Table 3.2 Spraying condition used for fabrication WC-containing composite coatings.

Total Feed rate	Gas	Gas temperature	Gas pressure	SoD	Gun speed
1.75 rpm	Nitrogen	700 and 800 °C	4 MPa	40mm	30 mm/s

3.1.4 Selecting Ni for co-spraying with WC

To examine the mutual effect of Ni and WC particles on their spraying behavior, two Ni-WC composites were sprayed using the same condition developed in the previous section and compared to the corresponding pure Ni(7) and Ni(25) coatings. A gas temperature of 700°C was used. Cast WC(30) powder was co-sprayed with Ni particles. Table 3.3 summarizes the Ni and Ni-WC properties, including overall and partial deposition efficiencies and WC vol.% in the coatings and porosities. Deposition efficiency of composite coatings was lower than that of Ni for both cases. Low deposition efficiency in cold sprayed MMCs is often due to low retention of the hard phase, WC in this case. A reduction in partial deposition efficiencies of Ni was also indicated by the fact that the feed rate of Ni particles was kept same in both Ni and Ni-WC coatings. This can be due to WC fragments which avoid close contact and bonding between Ni splats. Using Ni(25) powder, although the deposition efficiency of Ni and Ni-WC coating was improved, WC retention was not. Ni(7) particles was used for cold-spraying of coatings and subsequent tribological studies in **Chapters 4,5,6,** and **7**. The microstructure and hardness and erosive wear behavior of Ni(25) coatings were compared to that of Ni(7) coatings in **Chapter 8**.

Table 3.3 –Characteristics of cold-sprayed Ni-WC coatings.

Sample designation	DE (%)			WC in coatings (vol.%)	Porosity (%)
	Overall DE	Partial Ni DE	Partial WC DE		
Ni(7)	55 ± 3	55 ± 3	-	-	3.8 ± 0.5
Ni(25)	72 ± 5	72 ± 5	-	-	2.1 ± 0.3
Ni(7)-WC(30)	22 ± 4	31 ± 6	6 ± 1	10.5 ± 0.9	0.9 ± 0.2
Ni(25)-WC(30)	32 ± 7	60 ± 3	5 ± 2	7.0 ± 1.8	0.7 ± 0.1

3.2 Coatings characterization

3.2.1 Microstructural analysis

After cold spray, the coatings were cross-sectioned using an abrasive cutter and then cold mounted in epoxy containing conductive copper filler. Mounted samples were mechanically

ground using 240, 320, 400, 600, 800, and 1200 grit grinding papers, followed by polishing using 9 μm, 3 μm, and 1 μm diamond suspension. The samples were vibratory polished using 0.05 μm colloidal silica for 3 hours to remove residual stress induced by cutting, grinding and polishing steps. Similar procedures of grinding and polishing were used for mounted feedstock powder but subjected to vibratory polishing for 12 hours. The morphology and microstructure of the initial powders and deposited coatings were observed by scanning electron microscopy (SEM) (Quanta 600, FEI, USA). The accelerating voltage was set at 5-10 keV, working distance around 10 mm, and spot size 2-3. The concentrations of WC and porosity within the coatings were measured by image analysis. WC and porosity were revealed as bright and dark contrast, respectively, in BSE images. Ten random images of polished cross-sections were collected for each sample in a SEM, then analyzed by pixel count using an open source software ImageJ. Obtained area fractions was considered as its volume percentages. Table 3.4 presents WC content in the composite coatings that were obtained and some of them were subjected to tribology testing in this thesis. Electron channeling contrast imaging (ECCI) using a cold field emission SEM (SU-8230, Hitachi, Japan), with a photodiode backscattered electron (BSE) detector, was performed to reveal the grain and deformed structure of coatings. The source of the image contrast in the ECC images are due to the changes in channeling conditions. Incidence angle of electron beam relative to the various Bragg angles within a perfect crystal will determine the backscattered electron (BSE) yield, and thus, contrast. Any near surface defect, such as cumulative strain of a large number of dislocations can cause local variation in Bragg condition and change BSE yield [101].

Table 3.4 WC content in the composite coatings.

Chapter	Gas temperature	Coatings	WC vol.%
4	700 ˚C	Ni(7)- cast WC	0, 5.4, 9.5, 10.5
		Ni(7)- WCNi	0, 13, 30, 43,54
5	700 ˚C	Ni(7)- cast WC	0, 10.5
6	700 ˚C	Ni(7)- cast WC	28
		Ni(7)- WCNi	30
7	700 ˚C	Ni(7)- cast WC	0, 5.4, 9.5, 10.5
8	700 ˚C	Ni(7)- WCNi	0, 13, 30, 43,54
	800 ˚C	Ni(25)- WCNi	0, 18, 30,40,55

3.2.2 Vickers micro-hardness testing

Microhardness measurements were taken using a Vickers indenter on - top polished surfaces of coatings. At least 10 indentations were performed on each coatings system. Indentations were spaced at a distance of at least four times the diagonal of the previous indents, to avoid strain hardening effects and possible cracking of the ceramic particles during hardness testing. Random locations were selected for indentation to measure average hardness of the coating. A large load was used to obtain an average hardness value of the coatings. For Vickers hardness testing, the thickness of the coatings must be large enough to support the indentation. In general, the thickness should be a minimum of ten times the indentation depth. For the coatings that were subject of analysis in chapter 5 and 7, i.e. Ni(7) and Ni(25)-10.5vol.% WC(30). The load and holding time were 5kgf and 15s, respectively. For chapters 4, 6, and 7, microhardness measurements were taken using applied load of 1kgf with a hold time of 15s. This is because some of the coatings that were tested in these chapters, were thinner than ten times the indentation depth if higher load on Vickers tester would have been used.

3.3 Sliding wear tests

3.3.1 Sliding wear test setup

Sliding wear test was performed using a custom built linearly reciprocating pin-on flat disk tribometer, as schematically shown in Fig. 3.6. Normal loading was accomplished by applying dead weights on the loading arm. Reciprocating motion for tribological testing at sliding speeds between 0.1 and 50 mm/s was provided using motorized stage. The specimen holder and cantilever arm holding the counterface were enclosed in a plastic bag, in which the testing atmosphere humidity/temperature and oxygen level were monitored using a thermohygrometer and an oxygen analyzer, respectively. Friction forces were measured using a piezoelectric sensor mounted underneath the sample stage at a sampling rate between 800 and 2,800 Hz. In this thesis, spheres of WC-Co (McMaster-Carr) with a diameter of 6.25 mm was used as counterspheres. All tests were conducted in dry air (below 3% relative humidity) at room temperature of 25°C with a sliding speed of 3 mm/s and a track length of 5 mm. Prior to sliding wear tests, top surface of the coatings was mechanically ground and polished to a final step by 0.05 μm colloidal silica. In Chapter 5, the

WC-Co spheres were loaded with a normal load of 5 N onto the coatings, while two loads of 5 and 12 N were used in Chapter 6. Tests were run to short and intermediate cycles of 10, 50, 100, and 200, to evaluate the progress of wear, as well as final cycles of 1000.

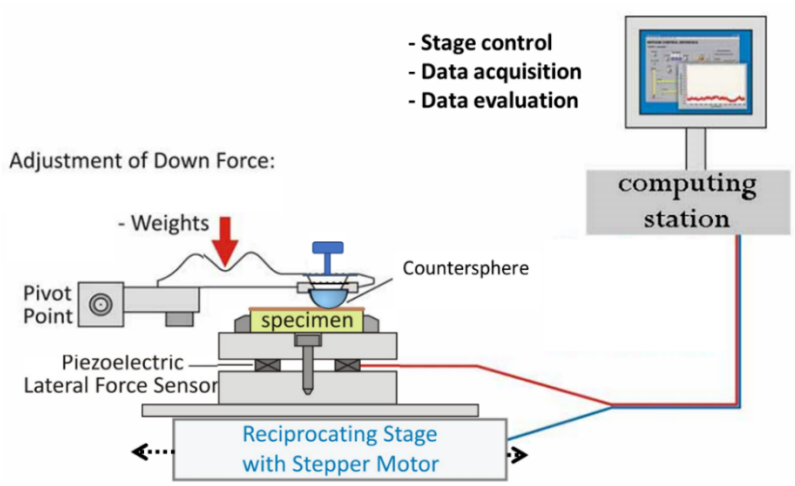

Fig. 3.6 Schematics of the tribometer setup used for this study, reproduced [80].

3.3.2 Characterization

After each sliding wear testing, morphology of wear tracks was studied using non-contact optical profilometer. Two different optical profilometers were used to measure the surface profile of the wear tracks. For the sliding tests performed in Chapter 5, surface features were measured using an optical interferometer (Wyko NT8000). While, optical surface profiler (NewView 8000, Zygo instruments, USA) was used to analyze topography of worn surfaces in Chapter6. The data was then processed using analysis software integrated with the Zygo equipment. Unworn coating surface was assumed as the reference plane and at least 10-line profiles per mm of each wear track were extracted. (see Fig. 3.7). The data was processed using an open source software Gwyddion v2.33, for data obtained from Wyko NT8000 and presented in Chapter5, which allows to extract cross-sectional profiles of the wear tracks. Cross-sectional area was determined by integrating height profiles across the wear track above and below the original surface using Origin software. The volume of material removed, v, was measured by multiplying the cross-sectional area of material removed by the track length. This, along with the total sliding distance x and applied load W, is then used to calculate wear rate $\acute{k}$ ($mm^3\ N^{-1}\ m^{-1}$) using equation (11) [1],

$$\acute{k} = \frac{v}{Wx} \tag{3.2}$$

Countersphere wear rates were measured using equation (3.2). In order to measure volume loss, the counterspheres were scanned using optical profiles (see Fig. 3.8a). Then, a sphere form of same diameter of WC-Co counterfaces was subtracted (see Fig. 3.8b), leading to a flattened surface. With setting the countersphere surface to zero, the height of different areas on the countershpere such as transfer film, as well as worn area on the sphere can be obtained. In order to reveal wear mechanisms, wear tracks and cross sections of wear track were examined using SEM (Quanta 600, FEI, USA) equipped with an energy dispersive X-ray spectroscopy (EDX). An inVia Raman microscope (Renishaw, UK) equipped with an Ar+ ion (λ = 514.5 nm) laser source was used to identify phase composition on the wear tracks and counterfaces. Subsurface regions of the wear tracks were studied by cross-sectional microstructure. In Chapter 5, they were cut transversely to the sliding direction using a lubricated slow-speed precision diamond sectioning blade, followed by cold-mounting, mechanical grinding and polishing. Electron channeling contrast imaging (ECCI) using a cold field emission SEM (SU-8230, Hitachi, Japan), with a photodiode backscattered electron (BSE) detector, was used to reveal the subsurface microstructure. An Ar+ ion milling system (IM3000 flat) was used to remove the top surface that might contain polishing-induced deformation. In Chapter 7, similar procedure and equipment were used. Moreover, subsurface morphologies of the wear tracks were observed through a cryo-STEM (Technai G2 F20, FEI, USA). TEM specimens were made using focus ion beam (FIB) lift-out equipped in an SEM (Helios NanoLab DualBeam, FEI, USA).

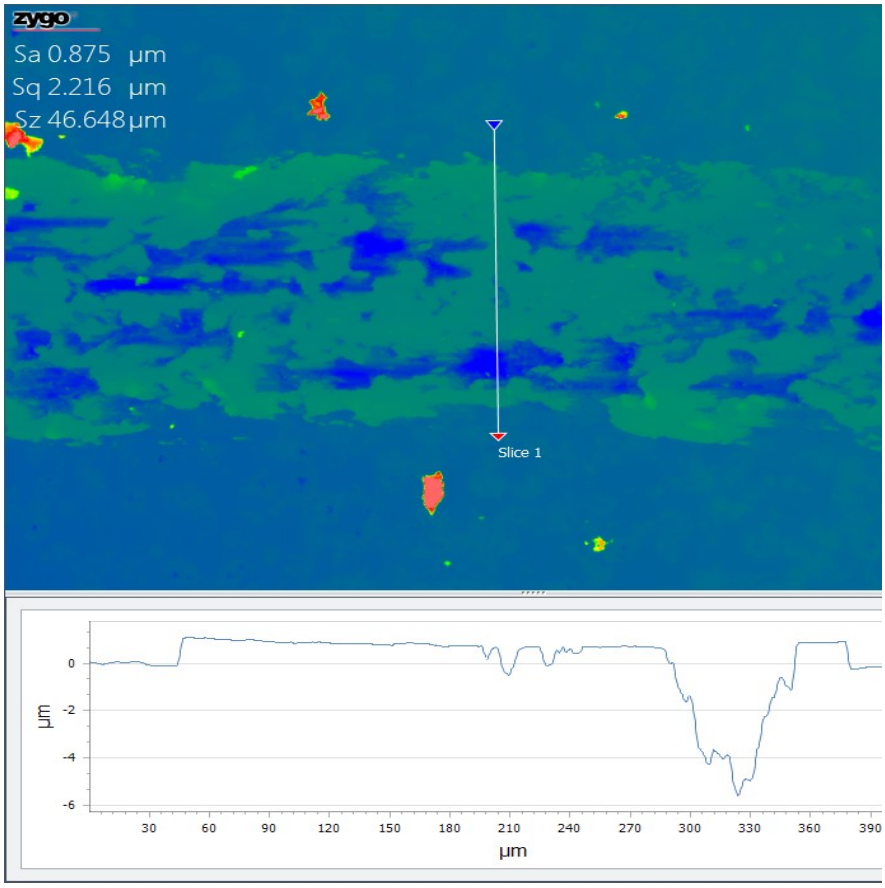

Fig. 3.7 Schematics Extraction of wear track profiles using Zygo software, after plane form removing, the profiles 100 µm apart were drawn across the wear track.

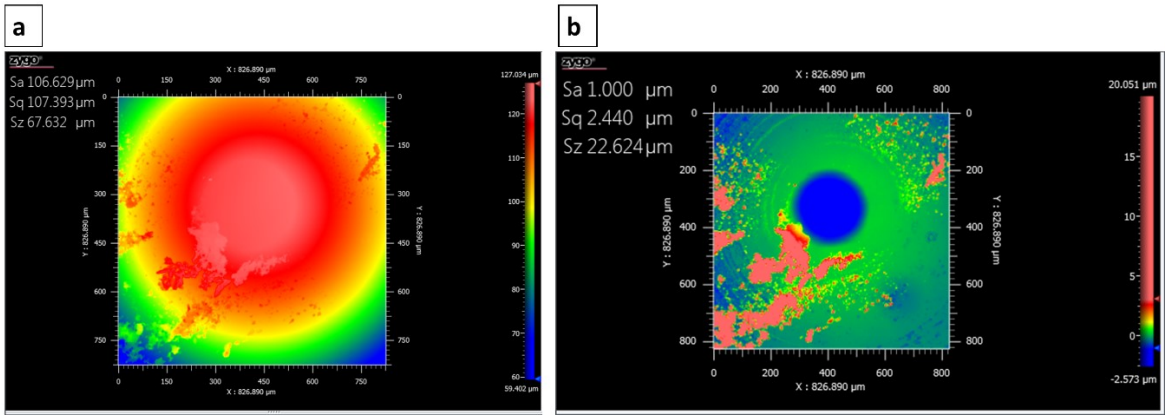

Fig. 3.8 (a) flattened height profiles of the overall features of the WC-Co countersphere, (b) after subtracting of a true sphere of 6.25 mm diameter.

3.4 Erosive wear tests

3.4.1 Erosion wear setup

SPE tests were carried out using a custom-built gas-blast erosion system tester, housed in the École Polytechnique de Montréal, based on the specifications of ASTM standard G76 [102]. The erosion tester consists of an abrasive blasting unit that adjusts the velocity and feed rate of the particles, a work chamber where the testing occurs and a combined sample and nozzle holder for accurate sample positioning with respect to the particle stream. The blasting unit is mounted on a balance with a 30kg capacity and precise to 0.1 g (Sartorius LE29000). The design of sample and nozzle holder permits for accurately controlling the angle of incidence and adjusting the working distance, distance between the nozzle exit and the sample surface, by pivoting the arm on which the nozzle is positioned (see Figure 3.9). The erodent powder was filled into the hopper and fed to a tungsten carbide nozzle with an inner diameter of 1.14 mm and a length of 36 mm. A pneumatically actuated shutter is also available on the sample holder, which can cover the sample, until the flow of particles is stabilized. In order to control particle velocity, back pressure of the abrasive blasting unit was adjusted [103]. This is calibrated using double disk time-of-flight technique [104]. The particle feed rate was controlled by adjusting the unit's shaker amplitude as well as the back pressure [103].

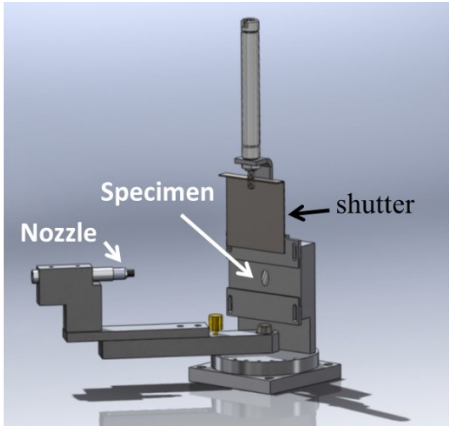

Fig. 3.9 Schematic of sample and nozzle holder for SPE testing with retractable shutter [103].

In this thesis, a particle velocity of 60 ± 6 m/s was obtained using 69 kPa air pressure in the nozzle. Working distance between the sample holder and the nozzle was kept constant at 20 mm. Angular Al_2O_3 particles of 20-70 μm size were used as erodent particles. Erosion tests was performed under two impingement angles of 30 and 90°. All erosion tests were performed at room temperature and 25% relative humidity. At least three repetitions were made per experimental condition to evaluate the experimental error of the measurement. The erosion test unit was turned on for a few minutes while the sample was shielded by a covered shutter, in order to stabilize the feed rate. Once feed rate was stabilized at 0.8 ± 0.1 g/min, the test was started. Before and after the test, samples were cleaned in acetone, dried, and weighed using an analytical weight balance (Sartorius LE225D) with a precision of 0.01 mg. Before weighing, Al_2O_3 particles were removed from the eroded surface by air blasting. Prior to testing, top surfaces of coatings were ground and polished following the similar procedure described in section. ASTM G76 standard recommends a 600s test length (without piercing the coating) to establish the steady-state erosion rate [102]. To better ensure the steady state, tests were run to 1800s (30 min). The erosion rate was calculated by normalizing the measured weight loss by the mass of erodent particles causing weight loss (i.e., testing time×particle feed rate).

3.4.2 Characterization

In a great majority of SPE studies, as proposed in the ASTM standard G76, the material loss is evaluated by weighing the sample after testing and then converting the mass loss to volume loss by dividing it by the density of the materials. In Chapter 7, this approach was used. The implement of this method can be very difficult in the case of composite coatings, due to the difficulty in acquiring the coating density, leading to inaccurate evaluation of erosion rates. Therefore, in Chapter 8, volume loss measurements were performed using a non-contact optical profilometer. Unworn coating surface was assumed as the reference plane. For measurement of volume below the wear scar, two Masks, 1 and 2, are assigned on unworn surface as reference plane and on erosion scar as the working plane, respectively. The net volume below the Mask 2 is calculated and then normalized by the mass of erodent particles. In order to reveal erosive wear mechanisms, eroded surfaces were inspected using an SEM (FEI, Quanta 600, USA). Subsurface regions of the wear scars were studied by cross-sectional microstructure. They were cut transversely to the sliding direction using a lubricated slow-speed precision diamond sectioning

blade, followed by cold-mounting, mechanical grinding and polishing. Similar procedure of grinding and polishing that were described in section 3.2.1was followed.

3.5 Raman spectroscopy

Raman spectroscopy was used to characterize phase composition and chemical changes on the contact interface. This, combined with EDX elemental analysis, was employed to gain a better understanding of tribochemical reactions that occur in wear. A inVia Raman microscope (Renishaw, UK) equipped with a 50 mW output power, Ar+ ion (λ = 514.5 nm), class 3B laser source was used to collect Raman spectra [105]. Renishaw's WiRE program installed on Renishaw system automatically references motors during instrument start-up and moves key optics to their aligned positions if the instrument configuration has been changed. Laser alignment was done by performing an auto-alignment with Renishaw's WiRE program. A low laser intensity of 5 and 10% and relatively short acquisition time of 10 s were used to avoid thermal damage on sample during Raman spectra collection. To compromise on that, 3 repeats of acquisition were used to collect data. The data were analyzed with Renishaw's WiRe program in order to get peak position and then identify tested materials by comparison with standard spectra.

3.6 Nanoindentation

Nanoindentation is a load and depth sensing indentation technique. The principal goal of this technique is to extract mechanical properties of thin films and small volumes of material [106, 107]. It permits localized measurement of mechanical properties [106, 107], making nano-indentation a useful technique to study cold-sprayed and tribologically induced microstructure, allowing a link being made to mechanical properties. Nanoindentation measurements were carried out on the sample at room temperature using Triboindenter Indenter. The Triboindenter system was equipped with a capacitive transducer, a piezoelectric scanner, and an optical microscope [108]. The piezoelectric scanner permits for "Imaging Mode" scanning probe microscopy (SPM).

The primary component of the nanoindenter, Triboindenter in this study, is the capacitive transducer. It allows the precisely controlled loading and displacement of the indenter tip into the sample, from which hardness and modulus can be obtained. As shown in Fig. 3.10, the capacitive

transducer consists of three plates. The two outer plates, also called drive plates, are stationary and driven by AC signals equal in magnitude, but 180° out of phase with each other. The middle plate, to which the indenter tip is fixed, is suspended by springs. To apply a load, a large DC signal is applied to the bottom plate. This generates an electrostatic attractive force between the bottom and central plates, which causes a movement of the center plate towards the bottom plate and hence, load is applied to the indenter [108]. The force and position of the central plate, which vary linearly with the applied voltage, are then determined [108] and used to develop a load-displacement curve as shown in Fig. 3.11. In this thesis, nanoindentations were carried out using a triboindenter system (TI 950, Hysitron, USA). A diamond indenter of Berkovich geometry was used (see Fig. 3.12).

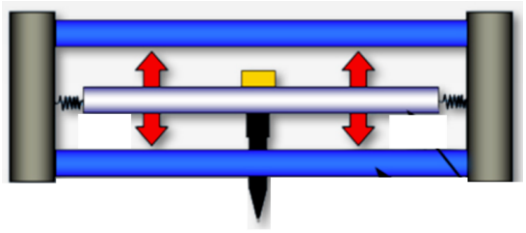

Fig. 3.10 –Schematic of a capacitive transducer used for indentation in Hysitron systems [108].

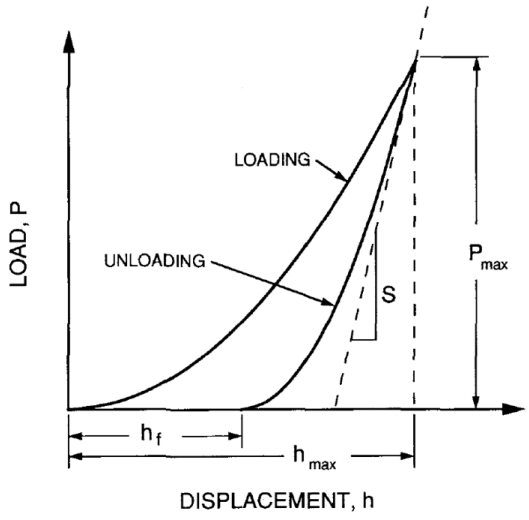

Fig. 3.11 Typical load displacement curve obtained from nanoindentation method [107].

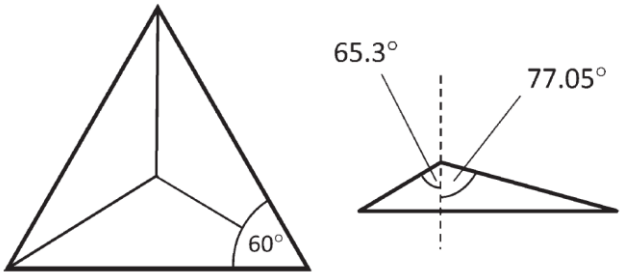

Fig. 3.12 Geometry of a Berkovich tip [106].

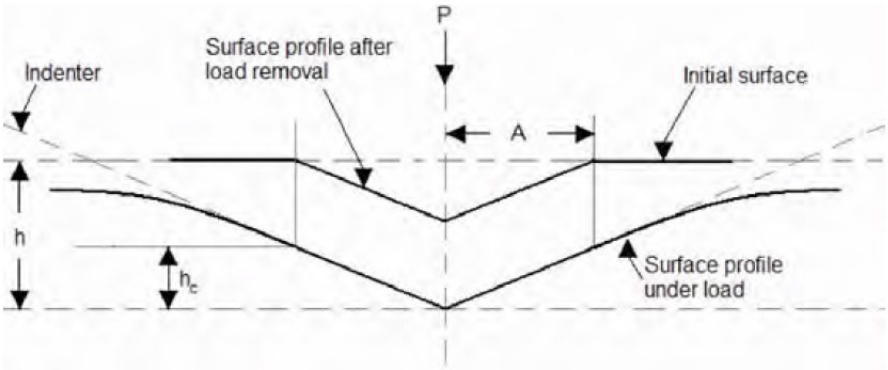

Fig. 3.13 Schematic of nanoindentation [107].

The load-displacement curve was obtained and then analyzed using Oliver-Pharr method [107] to calculate the hardness and reduced modulus, as shown in Fig. 3.11 and described as follows. A schematic of indentation is shown in Fig. 3.13. The stiffness (S) of a material, which was defined as the tangent at the maximum slope of unloading curve, was used to calculate the reduced modulus using following equations [107],

$$S = \frac{dp}{dh} = \frac{2}{\sqrt{\pi}} E_r \sqrt{A} \qquad (3.3)$$

$$\frac{1}{E_r} = \left(\frac{1-\nu^2}{E}\right)_{specimen} + \left(\frac{1-\nu^2}{E}\right)_{indenter} \qquad (3.4)$$

Where, E_r is the reduced modulus associated with elastic moduli of both indenter and tested specimen and is given by equation 3.4, and A is the projected area of contact of the indentation. The projected area A is dependent on the contact depth h_c of the indenter according to the indenter area function, for Berkovich indenter, as follows [106, 108],

$$A = c_0 {h_c}^2 + c_1 h_c + c_2 {h_c}^{\frac{1}{2}} + c_3 {h_c}^{\frac{1}{4}} + \cdots \quad (3.5)$$

where the coefficients c_n were obtained by performing area function calibration. To determine the area function, a series of indents at various contact depths (normal loads) are performed on a standard sample of a fused quartz that exhibits a well-known elastic modulus (E=72GPa). For a perfect Berkovich indenter the projected contact area is given by. $A = 24.5{h_c}^2$, i.e. c_0=24.5, whereas, the remaining coefficients account for the defect radius of the tip. The contact depth h_c is calculated as follows [106, 108],

$$h_c = h_{max} - 0.75 \frac{p_{max}}{S} \quad (3.6)$$

where h_{max} is the maximum indentation depth and P_{max} is the maximum load applied. The hardness of the coating is measured by following equation [106, 108],

$$H = \frac{p_{max}}{A} \quad (3.7)$$

For nano-indentation results to be reliable, sample preparation is a critical step since a perfectly flat surface is needed. Sample preparation was done following the grinding and polishing procedure described in section 3.2.1. Nano-indentation testing was performed on the polished cross-section and top surface of cold-sprayed coatings, on the sliding wear track cross-section, as well as, directly on the third body materials in wear track. To precisely control the location of the indents, imaging mode was used and the *in situ* scanning probe microscopy (SPM) images was matched to the previously acquired electron micrographs of the areas of interest. For all the indentations, a scheme of 5-2-5, i.e. 5 seconds loading, 2 seconds holding at peak load and 5 seconds of unloading time was used.

Chapter 4

Cold Spray Deposition of Ni and WC-Reinforced Ni Matrix Composite Coatings

Sima Alidokht, Phuong Vo, Steve Yue, Richard R. Chromik

Adapted from a paper of the same title published in *Journal of Thermal Spray Technology*, 2017. **26(8)**: p. 1908-1921

Abstract

Ni-WC composites are ideal protective coatings against wear and are often fabricated using laser cladding and thermal spray processes. High temperatures of these processes result in decarburization, which deteriorates the performance of the coating. Cold spray has the potential to deposit Ni-WC composite coatings and retain the composition of the initial WC feedstock. However, the insignificant deformation of hard WC particles makes it difficult to build up a high WC content coating by the cold spray. The effect of feedstock powders characteristics on WC retention into the coating was explored. By using three different WC powder sizes, the effect of feedstock powder size on WC retention were tested. To improve deformability of powders, a WCNi composite powder in mixture with Ni was sprayed. Microstructural characterization, including deformed structure of Ni splats, retention, distribution, and fragmentation of WC, was performed by scanning electron microscopy. An improvement in WC retention was achieved using finer WC particles. Significant improvement in WC particles retention was achieved using WCNi composite powder, with the WC content in the coating being close to that of the feedstock.

4.1 Introduction

Hard composite coatings containing WC in a metal matrix are widely used due to a unique combination of hardness, toughness and improved wear resistance [13, 39]. Coatings with Ni as

the matrix are widely applied when wear resistance combined with oxidation or hot corrosion resistance is required [9, 109]. Studies by Wang *et al* [8] and Kulu and Pihl [110] showed that the wear resistance of Ni coatings can be greatly improved by incorporation of refractory carbides such as WC, WC-Co, TiC, and CrC. These coatings are conventionally deposited using high-temperature thermal spray and laser cladding processes. However, the high temperatures of these processes cause dissolution of carbides into the molten binder phase, thermal dissociation of WC, and loss of carbon [8, 17, 110, 111]. The result is that brittle phases such as W_2C, W and/or Co_6W_6C or Co_3W_3C η phases are present in the coating, especially at carbide/metal interfaces. The presence of these defects has been found to increase the hardness of the coating. However, failure along the preferential crack paths provided by brittle phases intensifies material removal and decreases the wear properties of the coatings [13, 17, 39].

Cold spray is a solid state thermal spray process where particles are accelerated through a de Laval nozzle to supersonic velocities (500–1200 m/s) in a gas stream and impact onto a substrate. Particles remain in solid state due to a short contact time with the gas, which is at a much lower temperature than the melting points of the particles. Hence, high-temperature-induced decomposition of carbides and/or other phase transformations that could be detrimental for tribological performance can be avoided [19, 20] Continuous high-velocity impact of particles may produce a shot-peening or 'tamping' effect, which results in densification and deposition of a coating with nearly theoretical density [75]. This makes cold spray a promising replacement for traditional techniques when spraying heat sensitive materials.

There are generally two approaches for using cold spray to fabricate metal matrix composite coatings: (a) pretreatment powder processing such as cladding [21] and sintering [22-26], and (b) spraying mechanical blends of two or more powders [65, 66, 70-74, 112]. For mechanically blended ceramic and metallic powders, previous researchers reported co-deposition of metallic particles with oxides and carbides, with SiC or Al_2O_3 being frequently used as reinforcement particles [65, 66, 70, 73, 74, 112]. In most of the studies, angular ceramic particles were sprayed [65, 66, 73], although there are also some reports available on spherical particles [71, 72]. The deposition efficiency (DE) of ceramic particles in metal-ceramic mixtures strongly depends on the size and shape of ceramic particles, hardness of the metallic particles, and initial feedstock composition [65, 66, 70-74, 112]. Finer size ceramic particles were more prone to embed

into a substrate, which was related to higher velocities attained in the gas stream [65, 66, 73]. However, very small particles are difficult to deposit because the presence of the bow shock effect at the substrate [73]. Particles morphology has an effect where the retention of angular ceramic particles is higher than spherical particles of the same size [71]. Coatings with higher ceramic content were deposited with increasing ceramic content in the feedstock. However, above a critical content of ceramic particles, interactions between ceramic particles were more dominant, which resulted in decreased retention of ceramic particles into coatings. Previous studies demonstrated that Al matrix composites have been successfully co-deposited with SiC and Al_2O_3 reinforcements using cold spray. It was reported that more than 70% of the initial SiC and Al_2O_3 were recovered into coating [70, 74, 112]. However, a much lower fraction of feedstock Al_2O_3 particles of similar morphology was retained in a Ni matrix composite, with around 12-22% being reported [73], probably due to Ni being harder than Al. It is worth noting, for the studies presented above [70, 73, 74, 112], the researchers sprayed a range of conditions to find the most optimal settings. Yet, even carrying out an optimization procedure, it was always the case that the ceramic retained in the coating was less than in the feedstock.

Several researchers have deposited composite coatings containing WC by cold spray [22-26]. More recently, low-pressure cold spray deposition of mechanically blended Ni-WC with angular WC was reported by Lioma *et al.* [27]. High losses of WC particles were reported with only 11-29% of WC recovered in coatings [27]. However, in most cases, pretreatment powder processing such as cladding [21] and sintering [22-26] was utilized to overcome difficulties regarding retention of hard WC particles within coatings. Most studies on WC containing cold sprayed coatings have used agglomerated, sintered and crushed WC/Co powders [22-26]. WC/Co composite coatings with different ratios of carbide to Co and with nano- and micro-sized WC were deposited using nitrogen and helium. Several approaches were employed to overcome low DE and unsatisfactory bonding quality, which arises from limited deformability of WC/Co hard phases. These strategies include: porous feedstock powder, sufficient binder/matrix content, and powder preheating prior to spray [22-26]. A more recent approach was used in two studies conducted by Lioma *et al.* [27] and Melendez *et al.* [76], where WC/Co powders were sprayed with Ni additions in initial feedstock using low-pressure cold spray. In both studies, irregularly shaped agglomerates of a fine Ni powder that was specially designed for cold spraying as well as an agglomerated and

sintered WC–12wt.% Co powder were used as feedstock. Although low-pressure cold spray could recover 50-67% of feedstock WC into the coating, it was hypothesized that higher velocities attained by particles using high-pressure cold spray may be more effective in depositing a coating with controlled WC content [27, 76].

Using high-pressure cold spray, the effect of WC powder size and structure on cold spray behavior for Ni-WC systems was studied. Here, two types of WC-based powders, cast WC and agglomerated and sintered WCNi composite powders, were tested. The effect of WC powder sizes on WC DE and mechanical properties of the coatings were examined.

4.2 Experimental

Grit-blasted mild steel plates (thickness of 3 mm) were used as substrates. In this study, three different powders, namely, commercially pure water atomized Ni (4SP-10, Novamet, Kentucky, USA), plasma spheroidized WC (TEKMAT™ WC-45, Tekna, Quebec, Canada), and agglomerated and sintered WCNi (AMPERIT® 547, H.C.Starck, Munich, Germany) were used as feedstock powders. Laser particle size analysis (LA-920, Horiba, Kyoto, Japan) was used to measure feedstock powder size distributions. Three different particle size distributions of WC, -60+20 μm (d_{50} = 40 μm), -38+25 μm (d_{50} = 30 μm), and -25+10 μm (d_{50} = 15 μm), were tested. The designations of WC(40), WC(30), and WC(15) were used throughout this work. The Ni and WCNi powders had particle size ranges of -10+4 μm (d_{50} = 7 μm) and -30+15 μm (d_{50} = 20 μm), respectively. Figure 4.1 shows the morphology and size distribution of feedstock powders. Figure 4.1e shows the cross section of WCNi powder, with porosity revealed as dark regions.

A commercially available cold spray system (PCS-800, Plasma Giken, Saitama, Japan) was used to fabricate Ni and composite coatings. The cold spray unit utilized a de Laval nozzle made of WC-Co. Nitrogen was used as the process gas. Prior to entering the nozzle, the gas pressure was 4 MPa and the gas preheat temperature was 700 °C. The stand-off distance between the substrate and nozzle exit was set at 40 mm, and the gun traverse speed at 30 mm/s. The particle velocities were measured in free-jet by a time-of-flight particle diagnostic system (ColdSprayMeter, Tecnar, Quebec, Canada) and reported in Table 4.1. The WC and Ni powders were fed to the gun from separate hoppers. The powder feeder system was a custom installation

done by the gun manufacturer, Plasma Giken. By setting feed rates of powders, various mixtures of Ni-WC and WCNi were sprayed. The co-feeding system was used to avoid problems arising from the difficulty in premixing powder of differing densities and/or damage to powders due to mechanical mixing. Table 4.1 summarizes the cold spray tests including coatings, feedstock powders and compositions and particles velocity in gas stream. The deposition efficiency (DE) was calculated as the weight gain divided by the mass of powder sprayed, which is a product of feed rate and spray time.

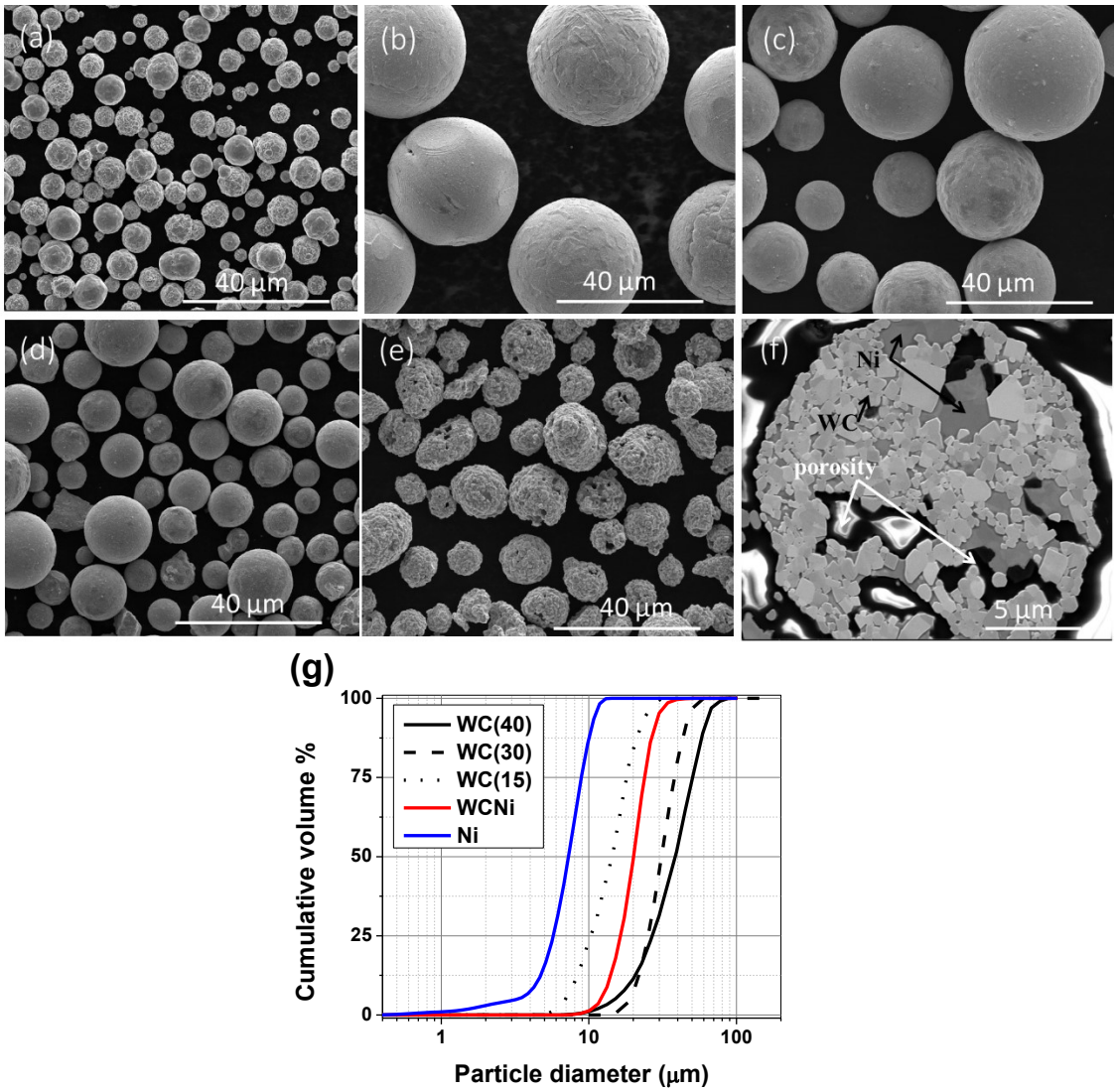

Fig. 4.1 Morphology of as-received powders: (a) Ni -10+4 (d_{50} = 7 µm), (b) WC -45+15 (d_{50} = 40 µm), (c) WC -38+25 (d_{50} = 30 µm), (d) WC -25+10 (d_{50} = 15 µm), (e) and (f) morphology and cross section of WCNi -30+15(d_{50} = 20 µm), and (g) cumulative size distribution of feedstock.

Cold-sprayed coatings were cross-sectioned perpendicular to the gun traverse direction, mechanically ground, and polished using 9, 3 and 1 μm diamond pastes followed by 0.05 μm colloidal silica. The morphology and microstructure of the initial powders and deposited coatings were observed by scanning electron microscopy (SEM) (Quanta 600, FEI, Oregon, USA). The WC and porosity concentrations within the coatings were measured by image analysis of pixel count using ten random SEM images of polished cross-sections. Electron channeling contrast imaging (ECCI) using a cold field emission SEM (SU-8230, Hitachi, Tokyo, Japan), with a photodiode backscattered electron (BSE) detector, was performed to reveal the deformed structure of coatings.

To characterize mechanical properties of Ni powder and sprayed coatings, nano-hardness and micro-hardness testing were used. Nano-hardness testing was performed using a Berkovich diamond tip with a triboindenter system (TI 950, Hysitron, Minnesota, USA). The peak load, loading and unloading rate, and hold time at peak load are fixed as 5 mN, 200 μN/s and 2 s, respectively. To calculate hardness and elastic modulus, the indentation load-displacement data during indentation was analyzed using the Oliver and Pharr method [107]. Vickers micro-indentation (Clark CM-100AT, Clarke Instruments Ltd, Salisbury, UK) was performed on top polished surfaces. To obtain an average hardness value of the composite, a large load of 1kgf with dwell time of 15s on a micro-hardness tester was used. Micro-indentation was conducted on cross-sectioned WCNi and WC(30) powders, with a load of 25 gf and dwell time of 15 s.

Table 4.1 Feedstock powders and particles average velocities in gas stream.

Sample designation	Particles average velocity (m/s)	Feedstock composition (vol.%)
Ni	650 ± 125	100% Ni
Ni-WC (d_{50} = 40 μm)- referred to as "WC(40)" Ni-WC(30) Ni-WC(15)	WC(40): 484 ± 78 WC(30): 520 ± 73 WC(15): 627 ± 135	Ni-36% WC
Ni-WC(30)	See above	Ni-36, 50, and 80% WC
Ni-WCNi	WCNi: 569 ± 108	Ni-20, 36, 50, and 76% WC

4.3 Results

4.3.1 Ni coatings

The Ni particles were accelerated to average velocities of 650 ± 125 m/s (Table 4.1) and deposited onto a mild steel substrate. A thick and relatively dense Ni coating with thickness of 1.4 ± 0.3 mm, porosity of 3.8% and DE of 55% was deposited by cold spray. Figure 4.2a shows the cumulative velocity distribution for Ni particle. According to the DE measured for Ni powder, it is possible, from this graph, to determine the critical velocity [67]. The critical velocity was found to be 650-670 m/s. A high-volume fraction (50%) of particles had velocity below the critical velocity, which reduces the measured DE. To obtain higher DE, higher velocities of powder are required. This can be achieved through increasing gas temperature, which not only increases particle velocity, but also decreases critical velocity by improving deformability. However, high gas temperatures can cause nozzle clogging with Ni particles [73]. The spray conditions selected for this study were, for our powders, the best compromise between DE and risk of nozzle clogging. Figure 4.2b and c shows micrographs of cross-section and top surface of Ni coatings. Both mechanically trapped and deformed Ni particles were found (Fig. 4.2c), which is consistent with the range of particle velocities with respect to the critical velocity (Fig. 4.2a).

Figures 4.3a and b show ECC images of cross-sectioned Ni powder and cold-sprayed Ni coating, respectively. The grain structures of Ni powder revealed relatively large grain size of 1 to 10 μm with mean grain size of 4.5 ± 0.9 μm (Fig. 4.3a). A non-uniform microstructure was observed for Ni coating (Fig. 4.3b). Near particle interfaces, microstructure is ultra-fine, while the central region of particles contains a coarser structure (Fig. 4.3c). This is related to an inhomogeneous plastic deformation field in the cold sprayed particle, where particle/particle interfaces experience ultra-high strains, strain rates and adiabatic shear instability [55]. For the Ni coating, near particle interfaces, cell structures with mean size of 340 ± 60 nm were observed, which is due to dislocation re-arrangement [55].

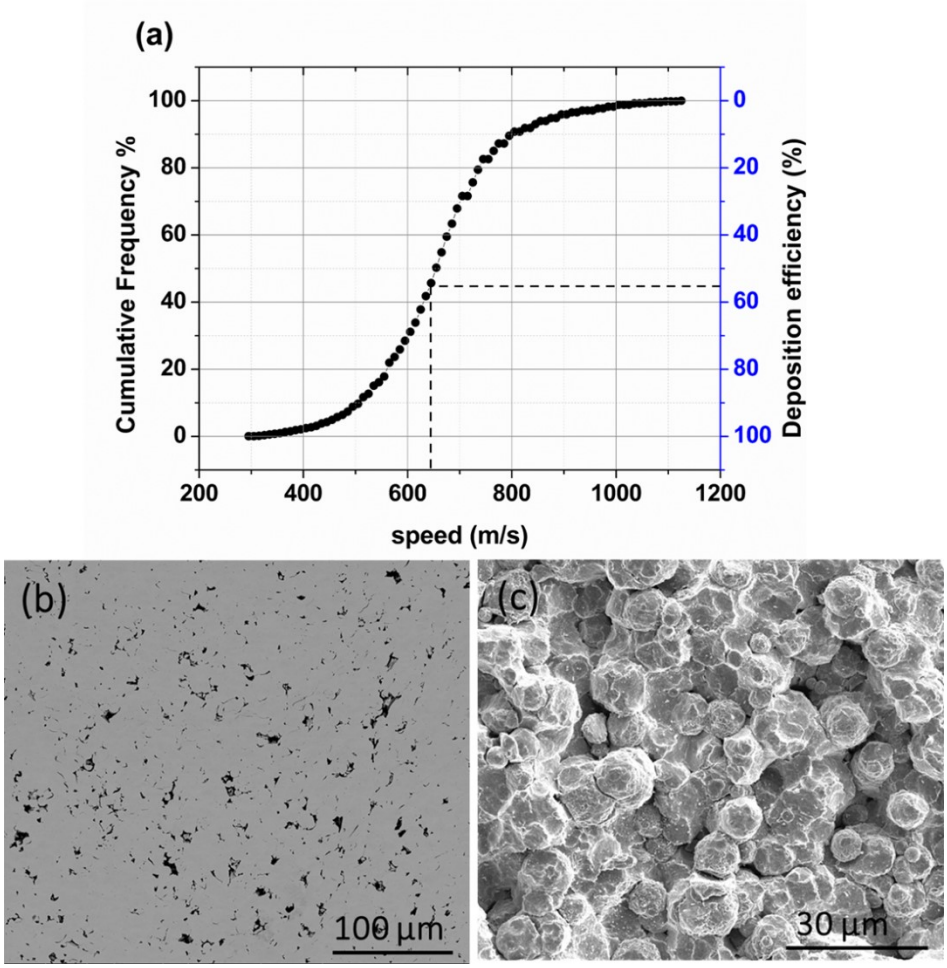

Fig. 4.2 (a) Cumulative velocity distribution for Ni particle in gas stream, (b) cross-section morphology and (c) and top-down morphology of Ni coating.

Nano-indentation was used to measure the hardness of the Ni powder and Ni coating. The average nano-hardness of the cross-section of Ni powder was 2.1 ± 0.2 GPa, while for the Ni coating, it was 4.8 ± 0.7 GPa. An increase in nano-hardness values of Ni coating compared to that of the feedstock powder was recorded. This is related to the extensive plastic deformation, increase in dislocation density, and grain refinement in cold sprayed coatings compared to Ni powders [113]. Non-uniform microstructure caused inhomogeneous distribution of hardness. Near particle interfaces regions displayed higher hardness compared to that of the central regions due to more grain refinement. The Ni coating displayed a micro-hardness of 345 ± 17 HV_1 (3.4 ± 0.2 GPa), which was significantly lower compared to nano-hardness value (4.8 ± 0.7 GPa).

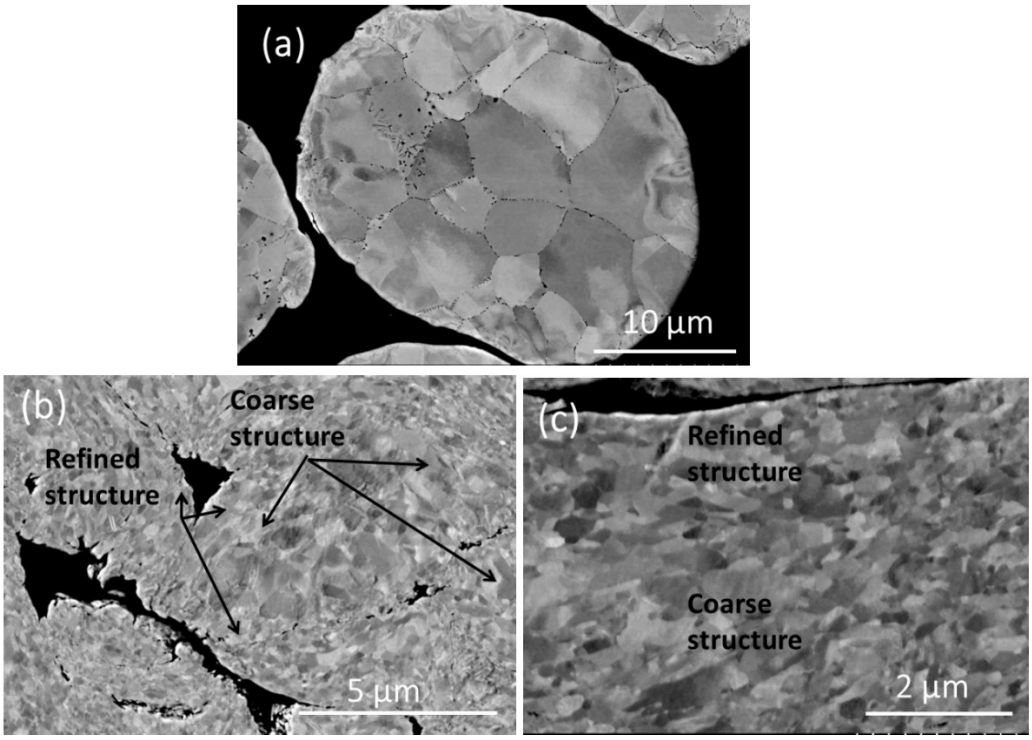

Fig. 4.3 ECC imaging of cross-section of (a) Ni powder, and (b) Ni coating, (c) high magnification view of (b).

4.3.2 Ni-WC coatings

The Ni -WC coatings were sprayed using three particle size distributions of WC with 36vol.% WC in the feedstock. WC fraction in the coatings, overall DE and partial DE of Ni and WC particles, and porosity of coatings were measured and reported in Table 4.2. Comparing WC fractions in the coatings, a higher retention of WC into the coating was achieved using the WC(30) powder. Similar results were reported in previous studies where finer size ceramic particles were more recovered into coatings [65, 66, 73]. However, with finer size WC(15), WC retention into coatings was not improved. Adding WC into the initial mixture resulted in lower DE of Ni. This can be due to WC fragments that prevent close contact between previously deposited and impacting Ni. Overall DE and partial DEs of Ni and WC particles using similar WC content in the feedstock was greater using finer size WC particles. A reduction in deposition buildup of metallic phase with adding ceramic particles to initial feedstock has been reported in previous studies [65, 66, 73]. Ni-WC(30) coatings with higher WC contents of 50 and 80vol.% in the

feedstock powders were cold-sprayed. Results showed increase in the WC content in the coatings. As the ceramic particle content in the feedstock is increased, interactions between ceramic particles during deposition are more frequent. This led to a reduction in overall DE, as well as partial DE of Ni and WC.

Table 4.2 Characteristics of cold-sprayed Ni and Ni-WC coatings.

Sample designation	DE (%)			WC in feedstock (vol.%)	WC in coatings (vol.%)	Porosity (%)
	Overall DE	Ni DE	WC DE			
Ni	55 ± 3	55 ± 3	-	-	-	3.8 ± 0.5
Ni-5.4WC(40)	12 ± 4	18 ± 6	2 ± 1	36	5.4 ± 0.7	0.9 ± 0.1
Ni-9.5WC(15)	20 ± 5	28 ± 7	5 ± 1	36	9.5 ± 0.5	1.7 ± 0.2
Ni-10.5WC(30)	22 ± 4	31 ± 6	6 ± 1	36	10.5 ± 0.9	1.1 ± 0.2
Ni-16WC(30)	15 ± 6	25	5	50	16 ± 2	0.5 ± 0.1
Ni-28WC(30)	5 ± 3	19	2	80	28 ± 4	0.3 ± 0.1

Figure 4.4 shows micrographs of cross-sectioned Ni-WC composite coatings. For all three WC sizes tested, some WC particles cracked or fragmented upon impact. To examine this further, fragmentation fraction was defined as $\frac{(\text{overall WC vol.\%} - \text{intact WC vol.\%})}{\text{overall WC vol.\%}}$. More severe fragmentation and cracking (74% ± 8) were observed in larger size WC(40), compared to WC(30) and WC(15). Using WC(30) and WC(15), fragmentation fractions were 48% ± 12 and 25% ± 5, respectively. However, at higher WC(30) contents, fragmentation fractions were higher and almost all of the WC particles were cracked/fragmented, due to higher collisions of WC particles. From the top-view images of Ni-10.5WC(30) shown in Fig. 4.4f, adding WC particles into the feedstock greatly altered the coating compared to Ni coatings (Fig. 4.2c). Interfaces between individual Ni particles were not easily visible due to improved adhesion and densification by the tamping effect of dense WC particles [75]. Most of the WC particles rebounded after impacting the surface, leaving behind empty craters, which led to low retention of WC. There were also many fine pieces of fragmented WC particles which can be observed on the top surface (Fig. 4.4f).

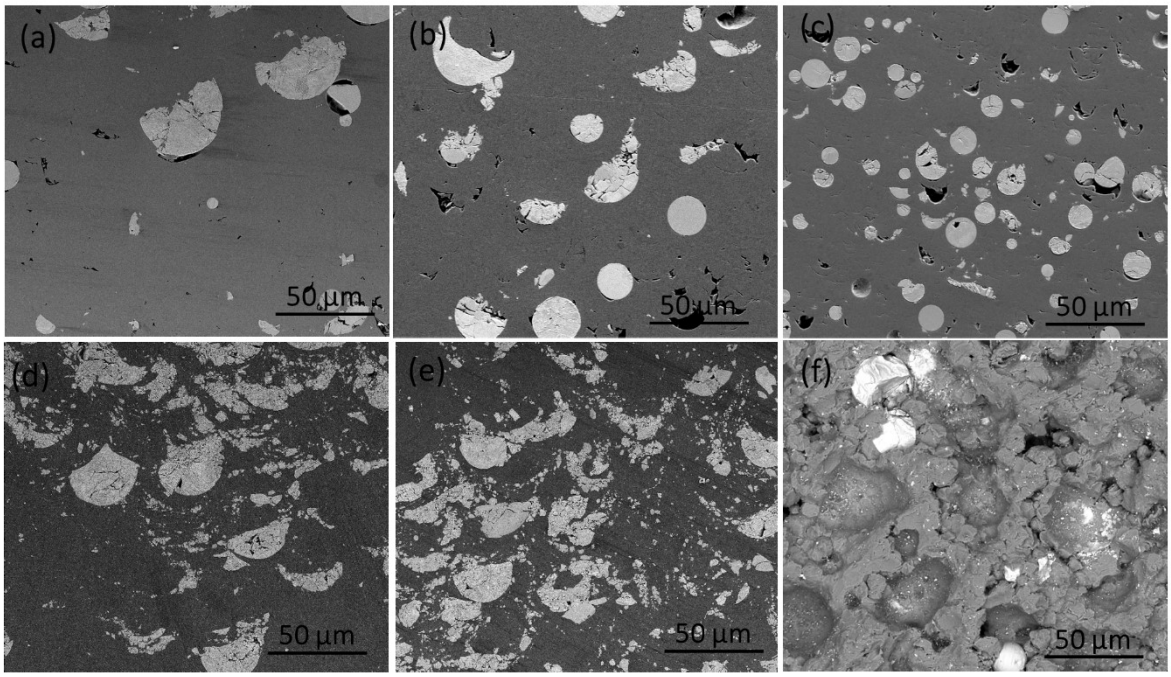

Fig. 4.4 Cross-section morphology of (a) Ni-5.4WC(40), (b) Ni-10.5WC(30), (c) Ni-9.5WC(15), (d) Ni-16WC(30), (e) Ni-28WC(30) coatings, and (f) top-down morphology of Ni-10.5WC(30) coating.

4.3.3 Ni-WCNi coatings

For the Ni-WCNi coatings, Table 4.3 summarizes the WC fraction, overall DE and partial DE of Ni and WC, and porosity of coatings. Figure 4.5 shows micrographs of cross-sectioned Ni-WCNi composite coatings sprayed using various WCNi contents in the feedstock. Using WCNi composite powder, the retention of WC into the coating was significantly improved and WC content was close to that of the initial feedstock composition. This is related to the powder porous and agglomerated structure, which allows particle densification and deformation during deposition [22-26]. Even though the WC particles in the WCNi powder were aggregated together, voids were present between WC particles. This, along with porosity inside the powders and Ni binder between WC agglomerates, provide ductility. Upon impact at high velocity, compaction and deformation of WCNi particles near the contact area occurred through slipping and rotation of WC particles along the Ni binder. This is referred to as the pseudo-deformation of the particles [22]. As the content of WCNi in initial feedstock increased, the overall DE decreased. With 95vol.% WCNi

added to initial Ni powder (76vol.% WC in total), a thin coating with lateral cracks along lamellar interfaces was obtained (Fig. 4.5d). When using WCNi powders as feedstock, with no Ni addition, the DE was very low and only a few of highly deformed and flattened particles with lateral cracks was deposited onto the substrate (Fig. 4.5e and f).

Table 4.3 Characteristics of cold-sprayed Ni-WCNi coatings.

Sample designation	DE (%)			WC in feedstock powder (vol.%)	WC in coatings (vol.%)	Porosity (%)
	Overall DE	Ni DE	WC DE			
Ni-13WCNi	75 ± 4	98 ± 5	59 ± 14	20	13 ± 3	0.9 ± 0.2
Ni-30WCNi	67 ± 5	73 ± 5	55 ± 10	36	30 ± 5	0.5 ± 0.2
Ni-43WCNi	44 ± 9	52 ± 11	36 ± 9	52	43 ± 7	0.4 ± 0.1
Ni-54WCNi	20 ± 8	38 ± 15	14 ± 6	76	54 ± 7	0.9 ± 0.2
WCNi	-	-	-	81	81	1.2 ± 0.5

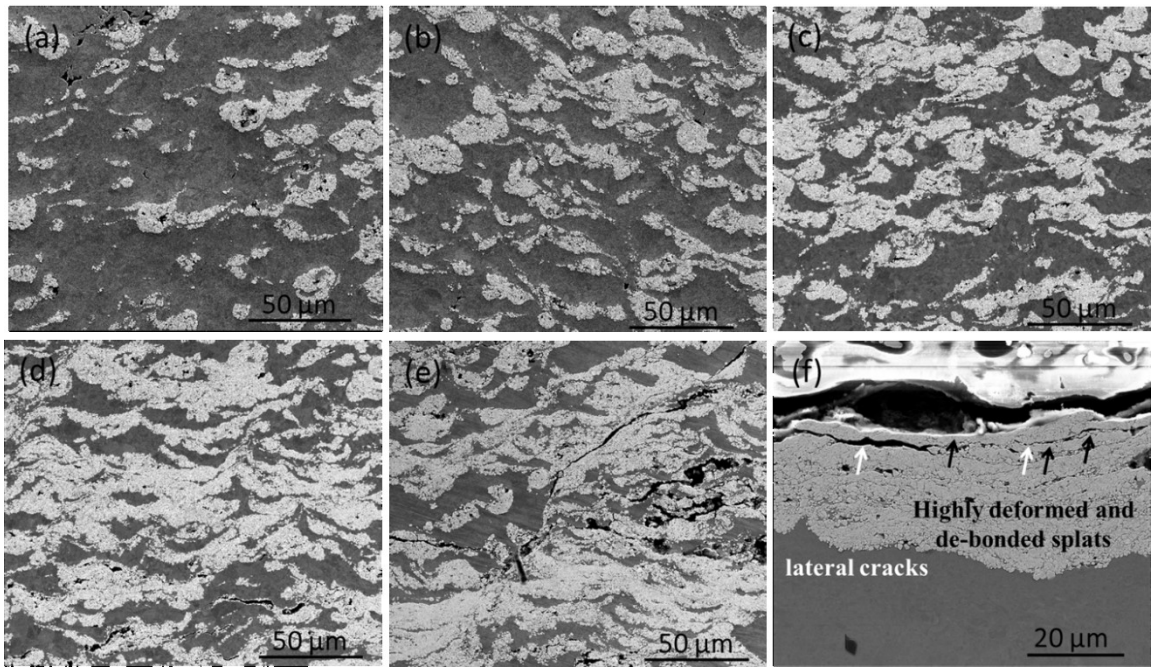

Fig. 4.5 Cross-section morphology of (a) Ni-13WCNi, (b) Ni-30WCNi, (c) Ni-43WCNi, (d) Ni-54WCNi, (e) WCNi coatings, and (f) high magnification view of (e).

The addition of WCNi to Ni not only resulted in higher retention of WC into coatings, when compared to Ni-WC coatings (see section 3.2), but also improved partial DE of Ni at 36 and 52vol.% WC in the initial feedstock. This contrasts with the negative effect of reducing DE of Ni with addition of the cast WC particles. Figure 4.6a and c shows top surface morphology of Ni-30WCNi and Ni-54WCNi coatings, respectively. Previous studies reported partial compaction of porous WC/Co particles near the interface between the particle and the underlying coating [22]. On the other hand, the compaction near the free surface of these particles is much limited [22], which provides a deformable porous surface layer for the impacting Ni particles (see Fig. 4.6a and b). However, as the WCNi content in the feedstock is increased, DE of Ni, as well as DE of WCNi particles, slightly decreased (see Fig. 4.6c). The addition of WCNi to Ni in the feedstock powders resulted in decreased coating porosity. All of the cold-sprayed Ni-WCNi coatings were dense with porosity less than 1%. The porosity in WCNi and Ni-54WCNi coatings with initial 76vol.% WC was due to cracking and debonding of splats.

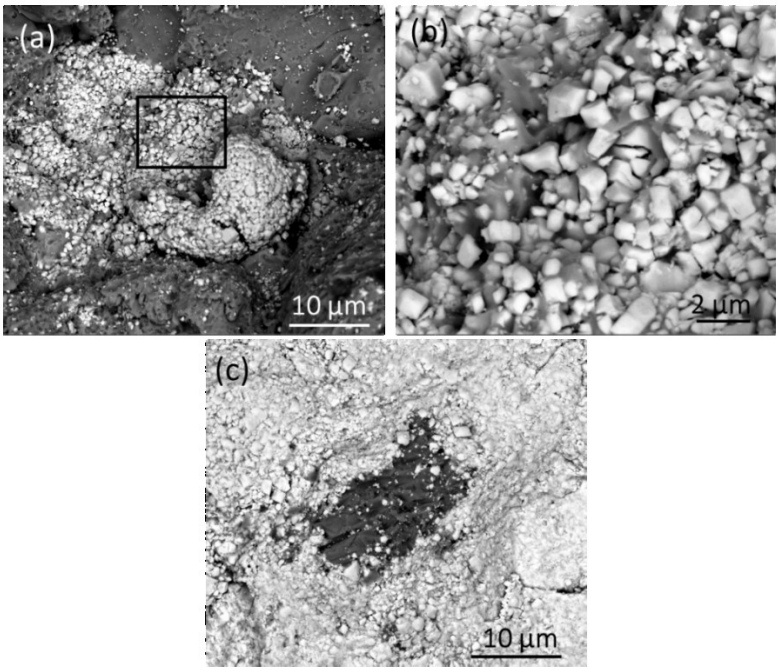

Fig. 4.6 Top-down morphology (a) and (c) of the Ni-30WCNi and Ni-54WCNi coatings, respectively, (b) high magnification view of (a).

4.3.4 Hardness of composite coatings

Micro-hardness testing was performed on the polished top surfaces of cold-sprayed Ni and composite coatings. Micro-hardness results are plotted as a function of WC content in the coatings in Fig. 4.7. There are several factors that could contribute to the hardness of composite coatings by addition of the WC particles. The possible factors are densification caused by tamping effect of impacting ceramics [75], load-bearing effect by ceramic particles [114], and increased dislocation density and work-hardening of the matrix caused by ceramic impacts [114]. To account for change in Ni matrix hardness caused by ceramic impacts, nano-hardness of the Ni matrices were measured for composite coatings and compared to that of the Ni coating. Previous studies [27, 76] showed that mean free path (MFP) between reinforcing particles directly influenced the mechanical properties of MMCs. In Fig. 4.7, MFP between reinforcing particles and nano-hardness of the Ni matrices for composite coatings versus WC content in the coatings were plotted.

For the two types of WC particles tested in this study, the decrease of the coating porosity due to the tamping effect results in the increase of the coating microhardness. The addition of WC particles to coatings play two competitive roles on the strength of bonding between Ni splats as well as Ni/WC particles. On one hand, it strengthens the Ni matrix-matrix bonding due the increased plastic deformation. On the other hand, it leads to an increasing proportion of weaker matrix-ceramic particle. Another factor that could contribute to the increase of composite coatings micro-hardness is a supporting role of WC particles to the load and a hindering role to the Ni matrix deformation. However, as mentioned above, weak interfacial bonding between Ni and WC particles limit the transferring the load to the reinforcing particles. Moreover, cracking and fragmentation of WC particles upon impact led to loose WC fragments with reduced load bearing capacity. The work-hardening effect of the matrix phase caused by impact of ceramic phase could be a possible factor influencing the hardness of composite coatings. Nano-hardness measurements of Ni matrices in composite coatings showed that addition lower contents of cast WC to the coating didn't change nano-hardness of the Ni matrices significantly. The increased nano-hardness of Ni matrix in Ni-28WC(30) coatings is due to ultra-fine (<1 μm) WC fragments. Slightly lower nano-hardness in Ni matrix of Ni-43WCNi and Ni-54WCNi compared to that of the Ni coating were recorded. Higher WC contents were more effective in increasing micro-hardness of composite

coatings. This is attributed to the lower MFP between the reinforcing particles in which the densification as well as load-bearing effect of WC particles were more effectively realized.

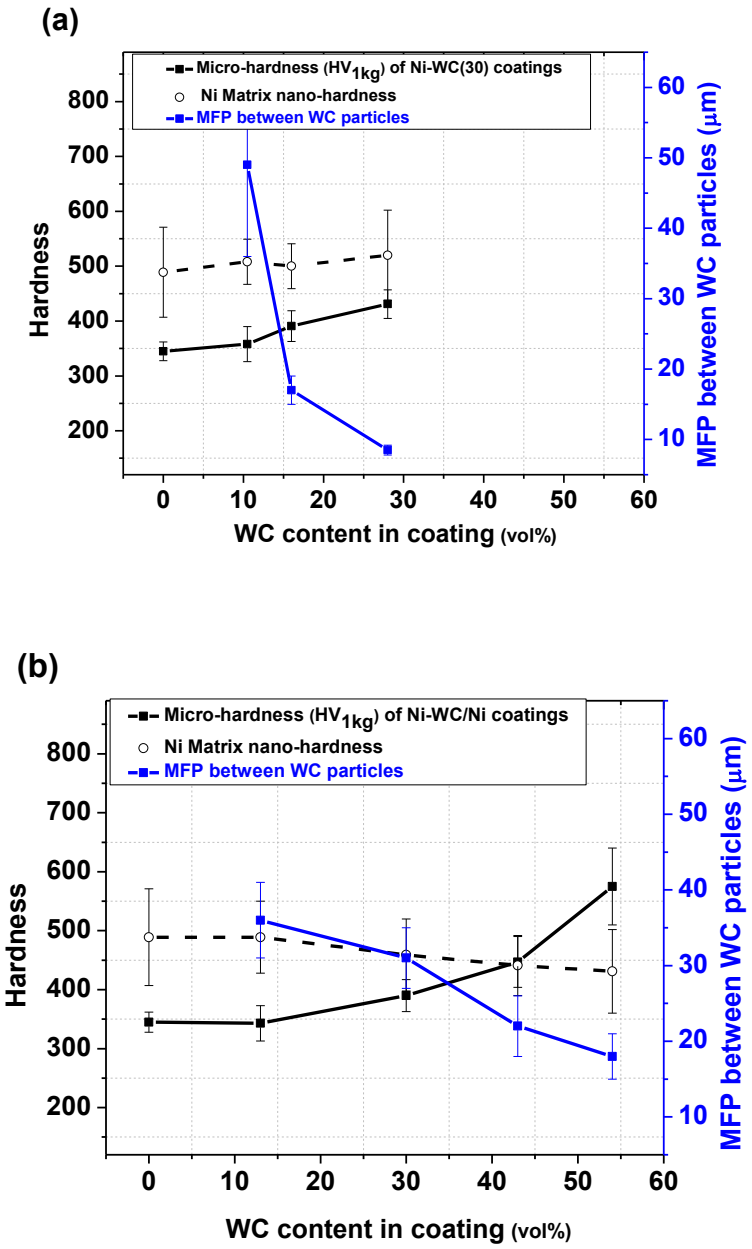

Fig. 4.7 Vickers micro-hardness of coatings, nano-hardness of Ni matrices, and mean free path between WC particles versus WC content for (a) Ni-WC(30), and (b) Ni-WCNi coatings. Scatter bars on microhardness values indicate the standard deviation of 20 repeat measurements.

4.4 Discussion

4.4.1 DE, microstructure and hardness of Ni coating

Ni particles were accelerated to an average velocity of 650 ± 125 m/s. Velocities of particles in the gas stream vary inversely with the square root of particles diameter, and thus, finer particles attain higher impact velocities [19]. According to previous studies [52, 67], critical velocity can be calculated for various materials by correlating the deposition efficiencies with particle impact velocities. Critical velocity for successful deposition of Ni was calculated to be 550-650 m/s for 25 μm powder size [52, 115]. The critical velocity for the Ni powder (d_{50} = 7 μm) tested in the present study was found to be 650-670 m/s. This range of values is higher than other reported critical velocities for Ni powder and is due to the smaller Ni particles size used in this study. Previous studies showed that shear instability in smaller metallic particles can be hindered because of higher cooling rates during impact and intensified strain-rate hardening [116]. Another probable reason could be the higher amounts of surface contaminations in smaller size particles, such as oxide shells, which can have a negative effect on bonding [52].

Significant increase in hardness value of Ni coating (4.8 ± 0.7 GPa) compared to that of the Ni feedstock powder (2.1 ± 0.2 GPa) was recorded. The increased hardness of cold-sprayed materials compared to that of the feedstock is tied to the increased dislocation density and grain refinement. Microstructure of Ni coating is non-uniform. Near particles interface, cell structure with average size of 340 ± 60 nm can be observed (Fig. 4.3b and c) which is due to the dislocation re-arrangement. High strain and high strain rate deformed microstructures are characterized with dislocation cells as most common type of low energy dislocation structure (LEDS) [117] According to previous studies, LEDS, in which dislocations are trapped into low energy configuration, minimize the energy per unit length of dislocation line [118]. Mur *et al,* [117] estimated the dislocation cells diameter (d) using following equation,

$$(\tau - \tau_0) = KGb/d \qquad (4.1)$$

Where τ is shear stress, τ_0 is friction shear stress, G is shear modulus (76 GPa for Ni), b is Burgers vector (0.3 nm for Ni), and k is a factor with a value near 10. Using Taylor factor (M), being near 2.8, term $(\tau - \tau_0)$ can be calculated from $(\sigma - \sigma_0)$, [119]

$$(\sigma - \sigma_0) = M(\tau - \tau_0) \quad (4.2)$$

Where, σ is applied stress, and σ_0 is friction stress. According to Borchers *et al*, [116] σ in cold spray is estimated by,

$$\sigma = \frac{1}{2}\rho v^2 \quad (4.3)$$

Where, ρ is density (8908 kg/m^3) and v is particle velocity (650 m/s). Assuming that for close-packed pure metals, σ_0 is about 10–30% of the applied stress value, [119] dislocation cells diameter can be calculated to be within the range of 315 - 400 nm. This is consistent with the observation from ECC images of 340 ± 60 nm.

The micro-indentation measurements showed a lower hardness value of 345 ± 17 HV_1 (3.8 ± 0.2 GPa) compared to nano-hardness of coating (4.8 ± 0.7 GPa). This is due to larger scale indentation, where porosity and poor cohesive strength between cold-sprayed Ni particles led to lower hardness. Goldbaum *et al*. [120] formulated a hardness loss parameter that helped explain the mechanical behavior at a wide length scales and its relation to the various defects within the Ti coatings, such as porosity and poor particle adhesion.

4.4.2 Effect of WC powder size on WC retention into coatings

WC is a hard ceramic phase that does not plastically deform upon impact. Rather, it becomes embedded in the substrate and is entrapped by matrix particles. Several factors, including substrate/matrix deformation properties and WC particle size and shape, affect its retention into coatings. During cold spraying, there is a stream of powder targeting the surface over a very short time. Entrapment by later-arriving Ni particles, which deform, and capture the rebounding WC into the coating, can be an active mechanism [72]. However, the interaction between particles in cold spraying has not been widely studied yet. In most studies of cold spray, isolated impacts were considered [50, 52]. During impact of WC on Ni splats, impact loading applied to Ni causes it to deform. This can lead to shear localization at the interface [51, 114] and the formation of craters and jetting around the periphery of the craters. Large number of empty craters were observed on the top surface of Ni-WC coatings (Fig. 4.4e and f), which implies that conditions required for WC particles to embed into Ni were not entirely met for powders and spray conditions used here. Getu *et al.* [121] studied the embedding behavior of hard spherical and angular erodent particles into ductile polymer substrates during solid particle erosion (SPE) by modeling and experimental work.

Embedding of spherical particles was predicted to be unlikely under normal impacts due to rebound forces being higher than the frictional forces that retain the particles [121]. Their study considers much lower particles velocity ranges (1-150 m/s) [121] compared to those attained by cold-sprayed particles (e.g. 484-627 m/s in the present study). Nevertheless, the results are consistent with the low retention of spherical WC seen here.

Coarse WC particles impact the surface with higher impact energies and are expected to cause more plastic deformation of the substrate [67]. A lower fraction of recovered WC particles as well as an increase in WC fragmentation using WC(40) particles were observed (see Fig. 4.4). Fragmentation dissipates a part of the kinetic energy of impacting particles that would otherwise be used for substrate plastic deformation and embedding [122]. Ceramic particles undergo fragmentation upon impact above a certain threshold velocity, which depends on ceramic particle properties and decreases with increasing particle radius [123]. This is due to the higher density of defects present in the coarser particles, which implies that fracture might be avoided by limiting the ceramic size. A higher fraction of recovered WC particles, as well as a reduction in WC fragmentation (see Fig. 4.4) using WC(30) and WC(15) particles, are consistent with the above explanation. However, using much smaller WC particles (15 μm) did not further improve WC retention. This can be due to much lower kinetic energy attained by these particles [122], although fragmentation is significantly avoided. Moreover, higher porosity and relatively lower micro-hardness was recorded in the Ni-WC(15) coating, where the lower kinetic energy of particles was less effective in coating densification.

The ceramic particles can fragment as they are deposited for various reasons, including ceramic-ceramic interactions, the energy of impact of the ceramic particle alone, or the energy of later arriving metal/ceramic particles striking a retained ceramic particle. Higher WC contents in the feedstock powders led to higher collisions of WC particles. This caused fragmentation of almost all of the WC particles in Ni-16 and 28WC(30) coatings and, in turn, led to reduced DE of Ni. Low Ni content in the feedstock as well as lower deposition rate of Ni in two mentioned coatings resulted in reduced DE of WC, although the WC content were higher compared to that of the Ni-10.5WC(30).

4.4.3 Effect of WC morphology on DE and WC retention into coatings

The porous and agglomerated structure of WCNi powders provided ductility during particle deformation [22-25]. Moreover, the WC particles in the powder are bonded loosely by a metallic binder. The WCNi particle deforms easily upon impact through pseudo-deformation [22], which is associated with slipping of WC fragments along the metallic binder and densification. Yet, when spraying alone, the WCNi particles did not deposit well, and coatings were thin with low DE. The addition of Ni to WCNi feedstock was found to improve coating deposition. For all the various initial WCNi contents in the Ni –WCNi tested in this study, 65-83% of WC particles were recovered in the coating compared to 24-36% achieved using cast WC(30) particles.

The deposition mechanism of WC-based particles during cold spray has not been investigated in detail. However, mechanical interlocking of WC fragments into the underlying coating and/or adhesion between metallic phases in incoming WC/Co particles and the deposited layer were reported as active mechanisms [124]. The two mechanisms, thus, have stringent conditions, that are limited by the amount of Co binder available and/or deformability of the binder phase [100]. Previous studies deposited WC-Co cermets using porous feedstock powder with sufficient binder/matrix content [22-25], powder preheating prior to spray [26], and using a fixed spray gun [100]. The deposition of a WCNi coating was not realized in the present study under tested conditions. Highly deformed and flattened particles were observed in the cross-section of a WCNi coating, at some regions of which the splats de-bonded from the surface (see Fig. 4.5e and f). The formation of a strong bond of impacting WCNi particles with the underlying coating is required for successive buildup of a WCNi coating to a designed thickness. The creation of such cohesion is associated with attaining a certain degree of deformation of both impacting particles and the underlying coating [22]. Without Ni addition, the hard WCNi underlying coating prevents significant accommodation of shear deformation. This causes impacting particles to be heavily deformed and flattened. Eventually, after a part of the kinetic energy of the impacting WCNi particle was consumed by plastic deformation in both parts and any adhesive interaction, the rest is stored as elastic energy and causes the particle to bounce off the surface.

Addition of Ni into initial feedstock was found to accommodate plastic deformation partly and prevent WCNi particle from being rebounded. As reported by previous studies, the degree of

deformation changes from the contact surface of impacting particle to its top free surface. Significant deformation is limited to the regions close to contact surfaces [57]. This leads to partial compaction of porous particles near the impact area [22]. Upon impact of particles on such a WCNi layer during coating buildup, deformation of the top surface of the underlying coating and the bottom portion of impacting particle occurs. This led to an improvement in overall DE as well as retention of WC into coatings when compared to those using cast WC particles. Figure 4.8 shows a schematic illustration of different mechanisms by which WCNi and WC particles were retained into the coatings. Partial compaction of WCNi particles, at lower ceramic contents as mentioned above, helped in deposition of Ni particles when compared to Ni coating alone. However, heavily deformed and flattened WCNi particles, using high WC content in the feedstock, were not effective in improvement of Ni DE.

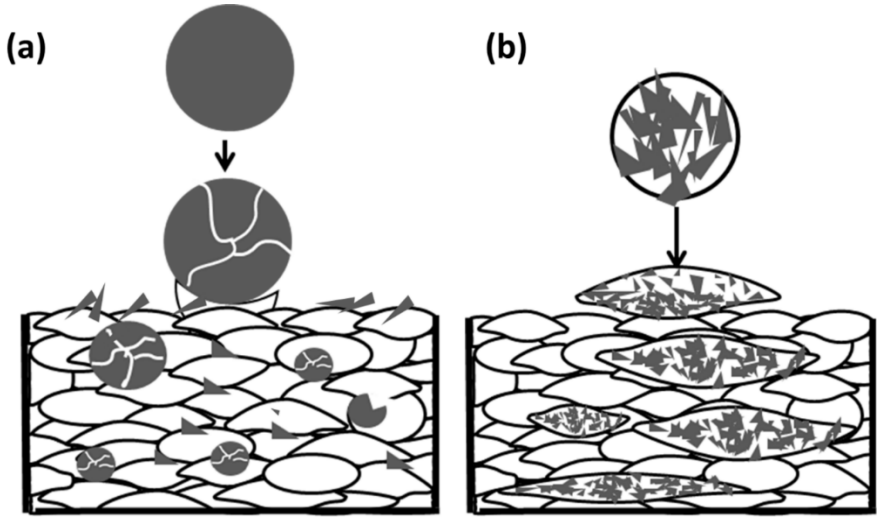

Fig. 4.8 A schematic graph showing how (a) cast WC, (b) WCNi particles were retained into coating. Gray and white represents WC and Ni particles, respectively.

The deposition of Ni-WC/Co composite coatings has been reported in previous studies by other authors, where low-pressure cold spray systems were used [27, 76]. Retention of WC into Ni-WCNi coatings in the present study was compared to those into Ni-WC/Co coatings in previous studies in Fig. 4.9. A higher retention of WC was obtained in the present study using a high-pressure cold spray system. This can be related to higher velocities attained by the WCNi particles, which causes a higher degree of plastic deformation in both Ni and WCNi particles and deposition of coatings with nearly theoretical densities. In comparison, higher porosity levels were reported

for similar coatings using the low-pressure cold spray (up to 5%), which is associated with lower velocity impact of particles [27, 76]. The higher recorded porosity for WCNi and Ni-54WCNi with 76vol.% WC in the feedstock is believed to be due to the excess of kinetic energy and de-bonding of highly deformed splats, not lack of deformation.

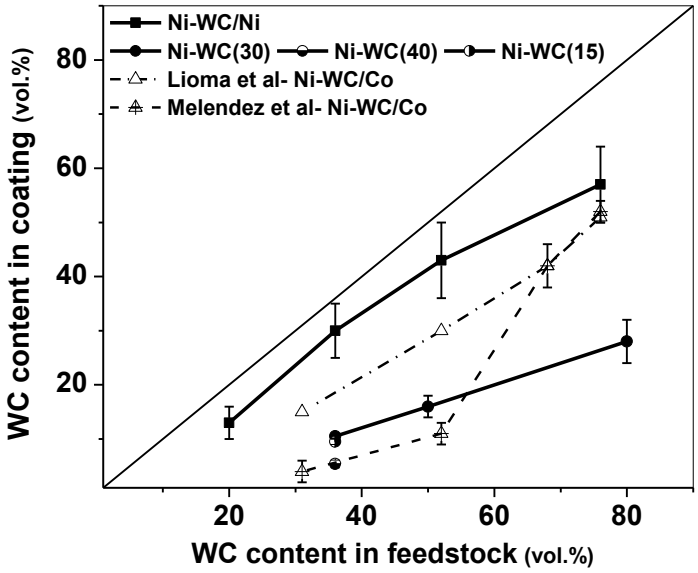

Fig. 4.9 WC content in the coating versus WC content in the feedstock powder (solid line-bold symbols). Dashed and dashed-dotted lines represent previous results [27, 76].

4.4.4 Effect of the WC particles on hardness of the composite coatings

Micro-hardness measurements of composite coatings showed that as the WC content in the coating increased, the micro-hardness increased, which is related to a reduced mean free path between WCNi particles in higher content WC coatings and densification of coatings [27, 76]. Comparing the micro-hardness values of the two composite coatings with similar WC content but different type in the coatings, 431 ± 26 HV_1 for 28 WCvol.% Ni-28WC(30) versus 390 ± 27 HV_1 for 30 WCvol.% Ni-30WCNi, cast WC particles were more effective in strengthening of the coatings. This is due to a significantly lower MFP between WC fragments (8.5 ± 0.7 μm) in Ni-28WC(30) compared to that of the Ni-30WCNi coatings (31 ± 4 μm). Another possible reason could be the harder cast WC powders (2461 ± 331 $HV_{0.25}$) when compared to WCNi powders (601

± 168 $HV_{0.25}$), although the WCNi particles hardness was significantly increased due to densification during impact.

The hardness of the composite coatings in the present study were compared to those of Ni-WC/Co obtained using low-pressure cold spray in previous studies [27, 76] in Fig. 4.10. The Ni-WCNi coatings featured a similar hardness values to those obtained by Melendez *et al.* [76]. They reported the similar porosities, but lower MFP compared to those obtained in this study, for the coatings with similar WC contents. The hardness values for the coatings obtained by Lioma *et al.* [27] were lower than those obtained by Melendez *et al.* [76] and here. This is related to higher porosity in the coatings deposited in the Lioma *et al.* study [27], due to lower velocity attained by particles. A difference in the hardness and composition of the WC-based composite powders used in these two studies may play a role. No hardness value for WC/Co powder was reported in the two previous studies.

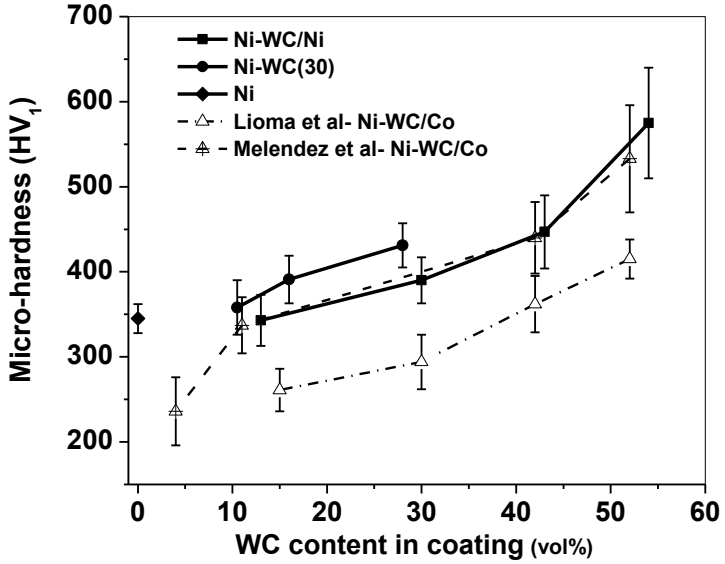

Fig. 4.10 Vickers micro-hardness versus WC content in the coating (solid line-bold symbols). Dashed and dashed-dotted lines represent previous results [27, 76]. Scatter bars on microhardness values indicate the standard deviation of 20 repeat measurements.

Significantly harder WC-Ni and WC-Co composite coatings were deposited using HVOF technology using similar feedstock powders [25, 90, 125]. The HVOF coatings was thicker and harder than cold-sprayed coatings, using similar feedstock composition, due to the decomposition of the WC-based powder and formation of hard W_2C and Ni_6/Co_6W_6C or Ni_3/Co_3W_3C (η) phases [25, 90]. HVOF coatings are characterized as more brittle when compared to cold-sprayed coatings, due to the depletion of the ductile Co matrix and the presence of fragile and hard phases such as W_2C, W and/or η phases [25, 90]. However, previous studies demonstrated that hardness is not the sole indicator of the ability of coatings to withstand wear [8, 110]. Melendez *et al* [94] studied dry abrasion wear performance of low-pressure cold-sprayed Ni and Ni- WC/Co composite coatings containing 7-66wt.% WC. They reported that that cold sprayed Ni-WC/Co coatings containing 66wt.% WC can compete with a HVOF WC-12Co coating in terms of abrasive wear resistance, although the latter had a higher hardness (~1100 versus 533 ± 63 $HV_{0.3}$) [94].

4.5 Conclusion

Cold spray was used to fabricate Ni and Ni matrix composites reinforced with WC particles. Two types of WC powders i.e. spherical cast WC and agglomerated/sintered WCNi composite powders were tested. The effect of WC powder size distributions on WC retention into coatings was studied. The concentration of WC in sprayed coatings was lower than that of the feedstock for all mixtures. The size of the WC particles was found to affect its retention into the coating. Using small WC particles, Ni-WC coatings with a higher WC content were obtained. Adding WC to the feedstock powder decreased DE of Ni. A lower DE for both Ni and WC was reported using higher WC(30) content in the feedstock powder. The Ni-WC coatings with higher WC retained to the coatings displayed higher hardness when compared to Ni and Ni-10.5WC(30) coatings, due to lower porosity and MFP. A significant improvement in WC retention into coatings was obtained using WCNi agglomerated and sintered powder in mixture with Ni. The WC content in Ni-WCNi coatings was close to that of the initial feedstock. It was found that Ni-WCNi coatings can be tailored to contain 13 to 54vol.% WC and display a varied hardness ranging between 343 to 575 HV_1. Addition of WCNi to the feedstock didn't deteriorate deposition buildup of Ni particles, with improving effect on DE of Ni at lower WCNi content in the feedstock.

Acknowledgments

The authors gratefully acknowledge the financial support from the Canadian Foundation for Innovation (CFI) project No. 8246 for the cold spray equipment, the CFI Leader's Opportunity Fund project No. 13029 for the tribometer and nanoindentation equipment, and the Natural Sciences and Engineering Research Council (NSERC) Strategic Grants Program for the operational funding of this project. Thanks, are also due to Tekna Inc for providing the Ni and spherical WC powders.

Chapter 5

Cold spray deposition of a Ni-WC composite coating and its dry sliding wear behavior

Sima Alidokht, Praveena Manimunda, Phuong Vo, Steve Yue, Richard R. Chromik

Adapted from a paper of the same title published in *Surface and Coatings Technology*, 2017. **308**: p. 424-434.

Abstract

Ni-WC composite are ideal protective coatings against wear that are often fabricated using laser cladding. However, high temperature of laser cladding and associated materials melting may result in non-homogenous distribution of WC particles, as well as decarburization and considerable residual stress and a deterioration of the wear resistance. An alternative is to use cold spray to deposit WC based composite coatings. The lower temperature allows one to retain the composition of initial WC feedstock, but the cold spray process is only recently being researched for development of composite coatings. In this study, Ni and Ni-WC coatings were fabricated by cold spray. The WC and Ni powders were fed to a de Laval nozzle from separate hoppers with independent feed rates. By adjusting federates, a blend of Ni-36vol.% WC was sprayed, which resulted in a composite coating of Ni-10.5vol.% WC. The influence of WC on Ni deposition was examined via microstructural characterization, including morphology of the coating's top surface and polished cross-sections. Mechanical properties of coatings were improved by incorporation of WC into the Ni matrix. The wear behavior of coatings was studied with reciprocating sliding wear tests using a 6.35 mm diameter WC-Co ball. All tests were conducted in dry air with a sliding speed of 3 mm/s, a track length of 5 mm, and normal load of 5 N. WC-Ni coatings were more wear resistant than cold-sprayed Ni coatings. The correlations between worn surface morphologies, subsurface microstructure induced by wear and the wear behavior of the coatings was discussed. Microstructural analyses showed a mechanically mixed layer (MML) on the top of worn surfaces

consisting of compacted oxides. It was revealed that the presence of hard particles in the Ni-WC coating facilitated fast development of the MML, as well as stabilized the MML, characterized by less plastic flow, fewer cracking and higher hardness.

5.1 Introduction

Metal matrix composites (MMCs) have long been used to enhance the wear resistance in demanding engineering applications [41]. One such system is Ni and Ni-based alloys, which exhibit high toughness and corrosion resistance that are reinforced using hard secondary phases to improve their tribological properties [126]. MMCs of WC in metal matrices, including Ni, are widespread due to a good combination of hardness and toughness, and improved wear resistance [13, 39]. One of the widely used methods for obtaining these composite coatings is laser cladding, which allows melting of high-temperature materials. Previous studies have reported very good adhesion of laser cladding MMCs to the substrate as well as low porosity [13, 39, 127-129]. However, a non-homogenous distribution of WC particles was reported. Due to higher density of WC reinforcement particles compared to molten Ni, they tend to precipitate and concentrate at the bottom of the coating [13, 39, 129]. This causes non- homogenous distribution of WC particles, whereas for wear resistance application, a high concentration of WC at the top surface is needed. Moreover, in order to obtain thicker coatings and higher concentration of hard phase inside matrix, the larger laser power is needed, which can result in unwanted chemical changes and significant residual stress [13, 39, 127-129]. Specifically, for WC containing systems, the high temperature during laser cladding causes dissolution of carbide by melted binder phase, thermal dissociation of WC, and loss of carbon [127-129]. The result is that brittle phases, such as W_2C, W and/or Ni_2W_4C intermetallic phases are present in the coating, especially at the interfaces. While the process can be optimized to minimize these effects, presence of these defects increases the wear rate, primarily due to cracking along the preferential crack paths provided by brittle phases and residual stress [13, 39]. Cold spray is a solid state thermal spray process where particles are accelerated in a de Laval nozzle to supersonic velocities (300–1200 m/s) in a gas stream and impact onto a substrate. Particles remain in solid state due to quite short contact time with the high-temperature gas. Besides, the gas temperature is often much lower than the melting points of the particles. Hence, high-temperature-induced decomposition of carbides and/or other phase

transformations that could be detrimental for tribological performance can be avoided [19, 20]. Furthermore, impact-induced high strains and the heat generated in this process may cause partial or complete recrystallization and evolution of ultra-fine microstructure [19, 20, 57]. Continuous high-velocity impact of particles may produce a shot-peening or 'tamping' effect, which results in densification and deposition of coating with nearly theoretical density [75]. This makes cold spray a promising replacement of traditional thermal spray when spraying heat sensitive materials.

Several researchers have deposited composite coatings containing WC by cold spray [8, 22-26]. However, in most cases, pretreatment powder processing such as cladding [8] and sintering [22-25] were utilized to overcome difficulties regarding retention of hard WC particles within coating. Wang *et al*. [8] used electroplating and chemical vapor deposition (CVD) to deposit a Cu and Al metallic layer on WC particles. The addition of soft metal around WC particles is reported to provide necessary ductility and make particles behave like a regular soft metal powder during cold spraying. Their investigation showed that coatings deposited using pre-coated carbide particles were denser, displayed higher hardness, and recovered more carbide phase compared to coatings produced from equivalent metal-carbide mixtures. More of the studies on WC containing cold sprayed coatings have used agglomerated, sintered and crushed WC-Co powders. In this regard, several approaches were employed to overcome low deposition efficiency and unsatisfactory bonding quality, which arises from non-deformability of hard phase. These strategies are including: Adequately designed porous spray powder [22-24], sufficient binder/matrix content [25], and powder preheating prior to spray [26]. Recent studies have been focused mostly on modifying feedstock powder [8, 22-26]. This generates extra processing steps and leads to inadequate understanding of deformation and deposition mechanisms of metallic and ceramic particles upon impact during spraying. However, more investigations are needed to clarify the micro-mechanisms involved in deposition of composite coating in order to obtain desired properties.

Metallic materials, including MMCs, will develop third bodies [87] (the materials generated from first bodies) during sliding wear. As sliding progresses, detached particles from one or both surfaces are mixed to form MMLs on top of the worn surfaces [95, 96, 130-132]. MMLs form at the interface, and hence, separate the initial contact. Thus, tribological behavior is controlled by structural, chemical and mechanical characteristics of the MML rather than

correlated only with bulk strength and hardness [95]. Gonzalez *et al*. [132] found that during dry sliding wear of NiCrBSi coating, the formation of a surface oxide layer, in which the rate of formation is higher than its destruction, can protect the surface below it. Studies of Jiang *et al*. [131] showed that oxide layers formed at 250 °C during sliding wear of a nickel-base high-temperature alloy is more wear protective, whereas at 20 °C, the real contact areas mainly consisted of loosely compacted particles. Incorporation of hard particles in metallic materials strongly affects the materials mixing and transfer mechanisms during sliding, which in turn influences the MML efficiency to protect the first bodies from wear [96]. Fernández *et al*. [39] found that incorporating 7vol.% WC into a laser cladding Ni alloy enhances sliding wear resistance, by forming a continuous oxide layers and preventing adhesive wear as the main mechanism in a matrix without reinforcement particles. Meanwhile, higher concentration of WC hinders formation of MML by the collision with hard particles and the mechanical interference with the counterbody, which promotes WC fracture into small particles and leads to instability in MML. However, there is limited literature available in the field of cold-sprayed coatings' sliding wear behavior. In the present study, cold spray deposition was utilized to fabricate Ni-WC composites. The cold spray behavior of Ni and WC were studied using unmodified powders with no additional processing routes. The effect of WC on coating formation, deposition efficiency, porosity and hardness of Ni were investigated. For the two Ni and Ni-WC coatings, dry sliding wear tests were conducted and the role of WC on friction and wear was studied.

5.2 Experimental

Mild steel plates with thickness of 3 mm were used as substrates. Plates were cleaned in acetone and then grit blasted prior to deposition. Commercial pure water atomized Ni (Novamet, Canada) and plasma spheroidized WC (Tekna, Canada) were used as feedstock powders. Laser particle size analysis (LPSA) was used to measure feedstock powder size distribution. Commercial pure Ni powders exhibited spherical morphologies and had an average powder particle size of 7 μm (Fig. 5.1a), which was confirmed by laser particle size analysis (Fig. 5.1b). Grain structure of cross-sectioned Ni powders revealed relatively large grain size of 1 to 10 μm (not shown here). WC particles with spherical morphologies and an approximate average powder particle size of 30 μm were used as reinforcing particles in Ni-WC coatings (see Fig. 5.1c and d).

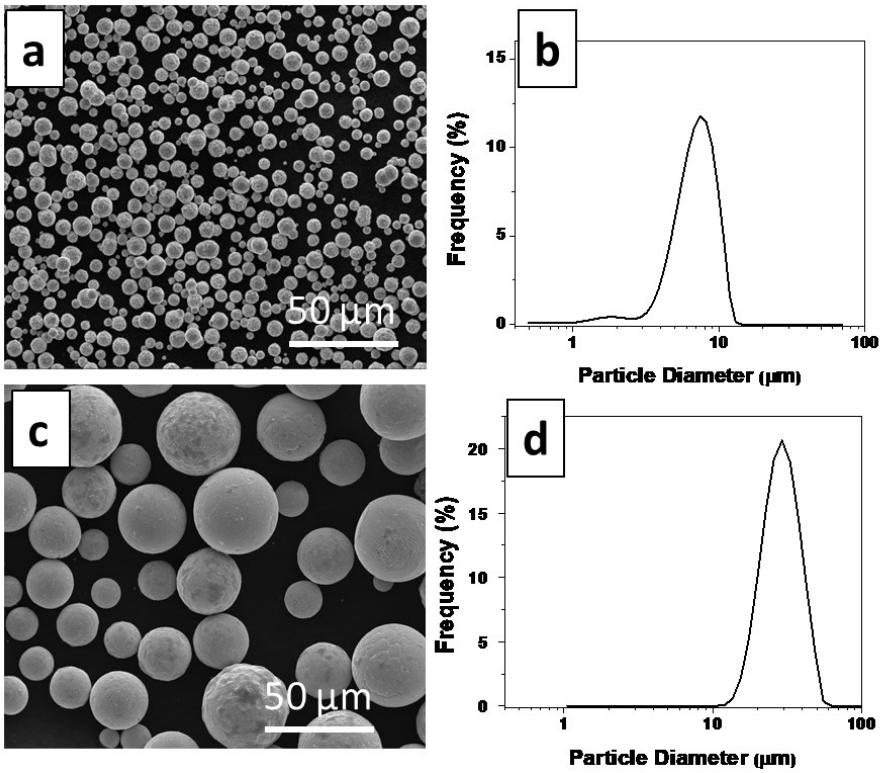

Fig. 5.1 Morphology and size distribution of the as-received powders: (a) and (b) Ni, (c) and (d) WC powder.

Cold spray was conducted using a PCS1000 system (Plasma Giken, Japan) with nitrogen as the carrier gas. Prior to entering the de Laval nozzle, the gas pressure was 4 MPa and temperature was 700°C. The stand-off distance between the substrate and nozzle exit was set to 40 mm and the gun traverse speed was fixed to 30 mm/s. The particle velocities were measured in a free-jet by a time-of-flight particle diagnostic system. The WC and Ni powders were fed to the gun from separate hoppers and, by setting feed rates, a mixture of Ni-36vol.% WC was sprayed. The co-feeding system was used to avoid problems arising from difficulty in admixing powder of differing densities and/or damage to powders due to mechanical mixing.

Cold-sprayed coatings were cross-sectioned perpendicular to the gun traverse direction, mechanically ground, and polished to a final step by 0.05 µm colloidal silica. The morphology and microstructure of the initial powders and deposited coatings were observed by scanning electron microscopy (SEM) (FEI, Quanta 600, USA). Electron channeling contrast imaging (ECCI) using a cold field emission SEM (Hitachi, SU-8230, Japan), with photodiode BSE detector was

performed to reveal the deformed structure of coatings. WC and porosity concentration within the coatings measured by image analysis by pixel count using ten random images of polished cross-sections were taken with SEM. Deposition efficiency was calculated as the weight gain divided by the mass of powder sprayed, which is the product of feed rate and the spray time. To characterize mechanical properties of initial powders and sprayed coatings, nano-hardness and micro-hardness testing were used. Nano-hardness test was performed using a Berkovich diamond tip with a triboindenter system (Hysitron, Minneapolis). The peak load, loading and unloading rate, and hold time at peak load are fixed as 5 mN, 200 μN/s and 2 s, respectively. To calculate hardness and elastic modulus, the indentation load-displacement data during indentation was analyzed using the Oliver and Pharr method [107]. Micro-hardness testing was performed using a Vickers diamond indenter. The load and holding time were 49 N and 15 s, respectively. In order to obtain an average hardness value of the composite, a large load on micro-hardness tester was used. With 49 N, the diagonal of indent was 150-160 micron and many WC particles were encountered with indents.

Sliding wear tests on the coatings were performed in dry air (below 3% relative humidity) using a custom-built ball on flat reciprocating tribometer. Prior to wear test, coatings were polished to a final step by 0.05 μm colloidal silica. Spheres of WC-Co with a diameter of 6.25 mm were used as counterfaces. All tests were also conducted with normal load of 5 N, sliding speed of 3 mm/s, and track length of 5 mm. Wear tests were run to 10, 50, 100, 500, and 1000 cycles. Friction forces were measured with a sampling rate of 800 Hz using a piezoelectric sensor mounted underneath the sample stage. Along each cycle, CoF was averaged across a central portion of the track and then graphed versus number of cycles. Worn samples were examined using a non-contact optical profilometer (Veeco Instruments, USA) to obtain profiles of the wear tracks. The volume of material removed, v, was measured by multiplying the cross-sectional area of material removed, measured by profilometry, by the track length. Cross-sectional area was determined by integrating height profiles across the wear track above and below the original surface, where a total number of 50 - 60 surface profile measurements per wear track were used. This, along with the total sliding distance x and applied load W, was then used to calculate wear rate, $\acute{k}$ (mm^3 /Nm) using the equation (1) [1],

$$\acute{k} = \frac{v}{Wx} \qquad (5\text{-}1)$$

In order to reveal wear mechanisms, worn surfaces and cross sections of wear tracks were examined using an SEM (Hitachi, SU-8230, Japan) equipped with energy dispersive X-ray spectroscopy (EDS). Nano-indentation was performed on worn surfaces to measure mechanical properties of third-bodies.

5.3 Results and Discussion

5.3.1 Coating deposition and characterization

Table 5.1 summarizes coatings deposition efficiencies and thicknesses, WC in initial feedstock and in the coating, and porosity and micro-hardness of coatings. A thick and relatively dense Ni coating with 1.4 ± 0.3 mm thickness and porosity of 3.8% was deposited by cold spray (see Fig. 5.2). Deposition efficiency was 55%. Ni particles have been accelerated to an average velocity of 650 ± 125 m/s. Velocities of particles in the gas stream vary inversely with the square root of particles diameter, and thus, finer particles attain higher impact velocities [19]. According to Schmidt *et al*. [52], critical velocity can be calculated for various materials by correlating the deposition efficiencies with particle impact velocities. Critical velocity for successful deposition of Ni was calculated to be 620-680 m/s for 25 μm powder size [52]. Average powder velocity in the present study fell into this range. However, materials deformation and heat transfer analysis imply that particle size plays an important role in critical velocity. The critical velocity is higher for smaller size particles due to these effects: (1) Occurrence of shear instability in smaller particles can be hindered because of higher cooling rate and intensified strain-rate hardening, (2) Smaller size particle usually contains higher amounts of surface contaminations such as oxide shells which can have negative effect on bonding, and (3) Smaller size particles may exhibit intrinsically higher strength since they are exposed to higher quench rates during powder production [52]. In order to obtain higher deposition efficiency, higher velocities of powder are required. This can be achieved through increasing gas temperature, which not only increase particle velocity, but also decrease critical velocity by improving deformability [99]. However, due to the fact that high gas temperatures can cause nozzle clogging with Ni particles, there are technical limitations to spray Ni powder [73]. Figure 5.2c and d represent top surface of a cold-sprayed Ni coating. Mechanically trapped particles as well as well-deformed and highly flattened particles were observed.

Table 5.1- Characteristics of tested coatings.

Sample designation	DE (%)	Thickness (mm)	Porosity (%)	Micro-hardness (HV_5)	WC in initial feedstock (vol.%)	WC in deposited coatings (vol.%)
Ni	55 ± 3	1.40 ± 0.03	3.8%	368 ± 8	-	-
Ni-WC	22 ± 4	1.01 ± 0.01	1.1%	378 ± 18	36	10.5 ± 0.9

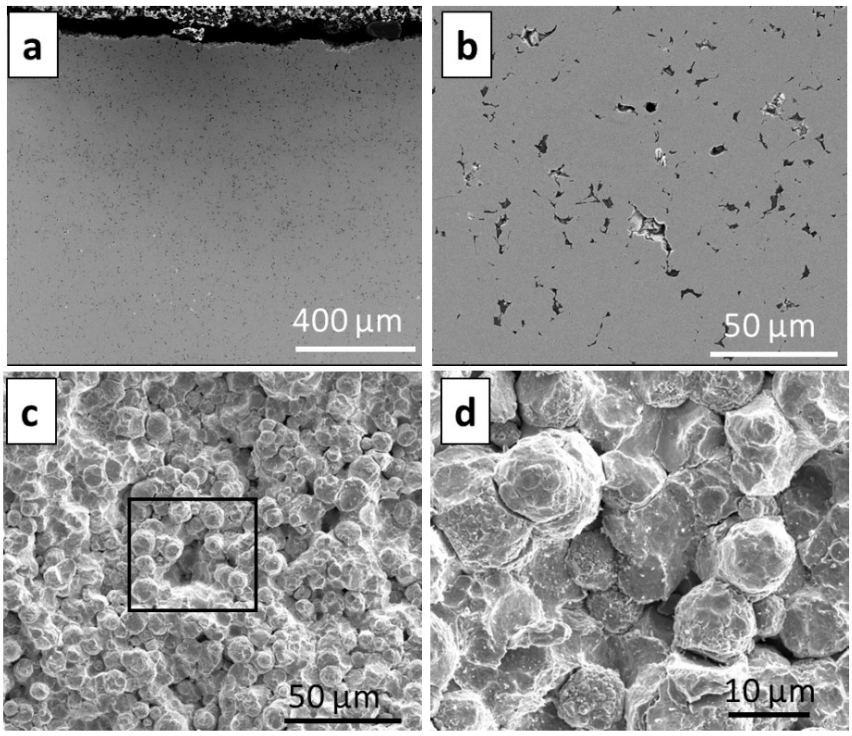

Fig. 5.2 – Cross-section morphology (a) and top-down morphology (b) of the Ni coating, (c) high magnification view of (b).

Figure 5.3 shows micrographs of a cross-sectioned Ni-WC composite coating. The particles in bright contrast correspond to carbide particles and regions in dark contrast correspond to porosities. With 36vol.% WC in initial feedstock, only around 28% of WC particles were recovered in the coating and it yielded a WC content of 10.5vol.%. Low deposition efficiency and WC retention was achieved using the WC and Ni powders under the sprayed condition. More investigation is needed to explore the effect of various powders characteristics and spray parameters in order to optimize deposition condition. However, even with low deposition rate, it

is believed that cold spray can be used to repair and restore a wide range of damaged components and result in life cycle improvement and major cost savings [133, 134].

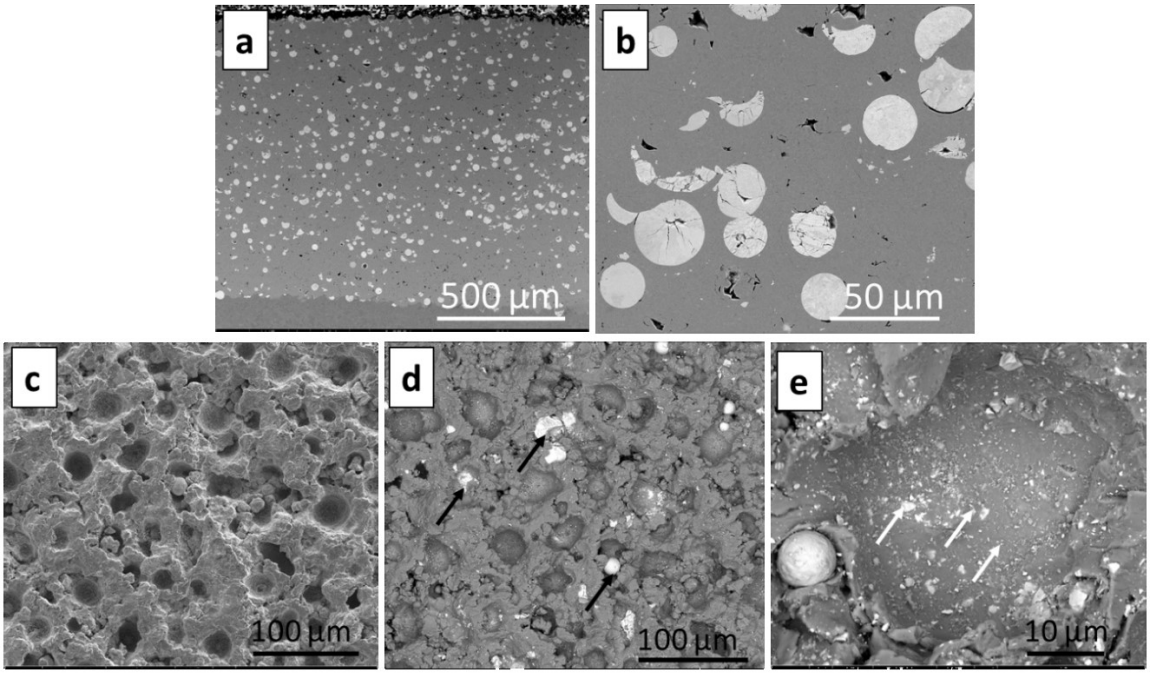

Fig. 5.3 Cross-section morphology (a) and top-down morphology (c), (d) of the Ni-10.5vol.% WC coatings, (b) and (e) high magnification view of (a) and (d), respectively. Black arrows indicate adhered WC particles to surface. White arrows indicate WC fragments.

As can be seen from the top-view image of the sprayed composite shown in Fig. 5.3c and d, adding WC particles into feedstock, the top surface of the coating was greatly altered compared to Fig. 5.2. Interfaces between individual Ni particles were not easily visible due to improved adhesion by the tamping effect, where most of the WC particles bounced back after impacting the surface, leaving behind empty craters. A few particles penetrated deeply to the surface (see Fig. 5.3d). The ratio of adhered embedded particle to empty craters was significantly lower than actual WC concentration recovered to coating (measured from polished cross-sections). This was probably because of high hardness of Ni and low velocity of dense and relatively large size WC particles [135]. Therefore, during Ni-WC composite coating build up, WC particles were mainly entrapped to the coating by later-arriving Ni and WC particles, in which Ni particles deformed and surrounded WC particles [72]. There was also a large number of fine fragmented WC particles which can be observed on the top surface at some regions (Fig. 5.3e). As can be seen in a higher

magnification view of the cross-section (Fig. 5.3b), some of the WC particles were cracked or fragmented upon impact.

The deposition efficiency of Ni-WC was 20%. Low DE in cold sprayed MMCs is often due to low retention of the hard phase, WC in this case. A reduction in deposition efficiency of Ni was also indicated by the fact that the feed rate of Ni particles was kept same in both Ni and Ni-WC coatings, yet WC added to Ni led to a thickness reduction. This can be due to WC fragments which avoid close contact and bonding between Ni splats.

Lower porosity of cold-sprayed Ni-WC composite coating compared to Ni coating (1.1% versus 3.8%) was due to continuous high-velocity impact of dense WC particles, which produced the tamping effect, and results in densification of deposited coating [75]. Micro-hardness tests were done on top surface of cold-sprayed Ni and Ni-WC coatings and the results were reported in Table 5.1. Micro-hardness results were inhomogeneous which is due to a non-uniform microstructure. Relatively uniform dispersion of the WC particles, which have an extremely high hardness, and densification due to tamping effect of impacting dense WC particles are the possible contributions to the higher hardness in the Ni-WC composite coating (see Table 5.1). However, hardness improvement due to incorporation of WC particles into Ni matrix is not significant, probably due to decreased bonding between Ni particles and fragmented/cracked WC particles.

5.3.2 Coatings sliding wear behavior

5.3.3.1 Friction and Wear

The coefficient of friction (CoF) was plotted versus number of cycles for Ni and Ni-WC coatings in Fig. 5.4. The two friction plots showed that Ni and Ni-WC coatings exhibited similar behavior; COF curves increased rapidly and reached steady state. The initial spike in CoF at the beginning of the sliding (see inset in Fig. 5.4) was linked to a localized adhering of two surfaces in contact as reported in previous studies. The rupture of the adhered asperities and occupying the mating surface led to a steady value of CoF [136]. The Ni-WC coating showed a very short run-in period followed by steady state friction coefficient value of 0.71. CoF curve for Ni coating reached steady state at longer distance (150-200 cycles) and its steady-state value was 0.70.

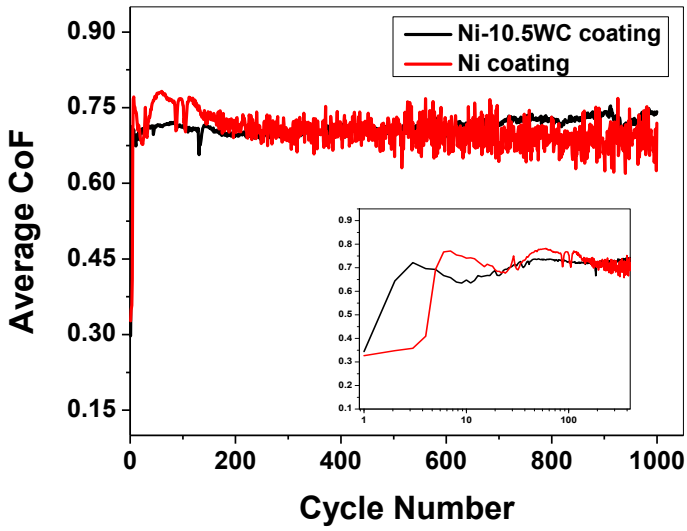

Fig 5.4 Average friction coefficient plotted versus number of cycles for tests run to 1000 cycles on cold sprayed Ni and Ni-10.5vol.%WC coatings.

The wear rates at the end of the 10, 50, 100, 500, and 1000 cycles' tests were calculated using Eq. 5.1 and plotted as a function of cycle number in Fig. 5.5. The wear rate for both coatings was high during the initial cycles, due to adhesive wear, after which it decreased. A slight improvement in wear rate at 10 cycles for the Ni-WC composite coating may be due to decreased porosity compared to the Ni coating and load-bearing effect of WC particles which reinforce materials against plastic deformation. While the wear rate of composite approached a steady state at 50 cycles, the curve of the Ni coating appeared to increase again after an initial decrease at 50 cycles. A close comparison of the graphs in Fig. 5.5 revealed that except for initial cycles of tests, which displayed similar wear rates for both coatings, wear rate of the composite coating was approximately seven times lower as compared to the Ni coating.

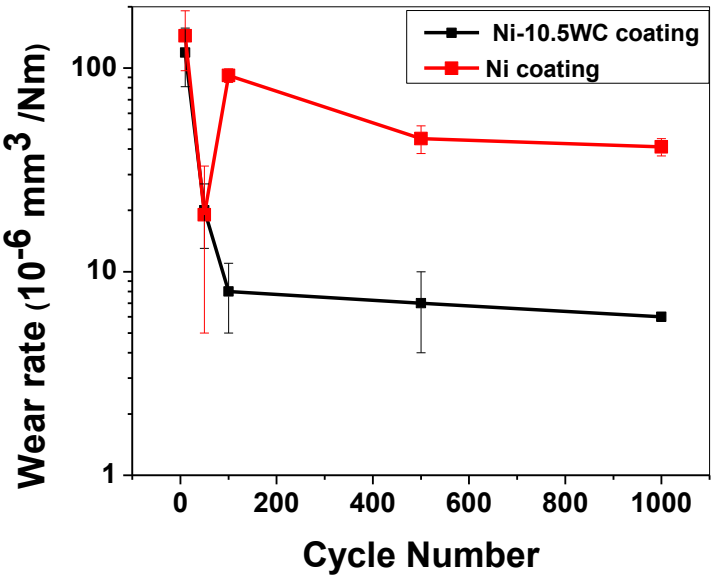

Fig 5.5 Volumetric wear rate plotted versus number of cycles. Scatter bars indicate the standard deviation of 5 repeat measurements.

5.3.3.2 Worn surfaces morphologies

SEM micrographs of worn surfaces were used to study the materials removal mechanisms of cold-sprayed Ni and Ni-WC coatings. Short and intermediate cycles were used to evaluate the formation of tribolayers. Figure 5.6 shows the morphology of the wear track for Ni and Ni-WC coatings after 10 cycles. Significant plastic flow and adhesive wear, as evidenced by tongue-shaped structures and removal of patches of material (Fig. 5.6 indicated by white arrows), were observed for both coatings. This was consistent with the initial spike in CoF and wear rate at the beginning of the test. Extensive scoring of the surface in the sliding direction was observed on Ni coating worn surface (see Fig. 5.6c black arrows) as an indication of plowing wear that were not observed in the Ni-WC coating. Load bearing effect of relatively uniformly distributed WC particles in Ni-WC composite coating improved resistance to plastic deformation. As can be seen in Fig. 5.6b, Ni was preferentially worn away and squeezed up against WC particles. This led to earlier formation of tribolayers (see Fig. 5.6a black arrows) compared to the Ni coating.

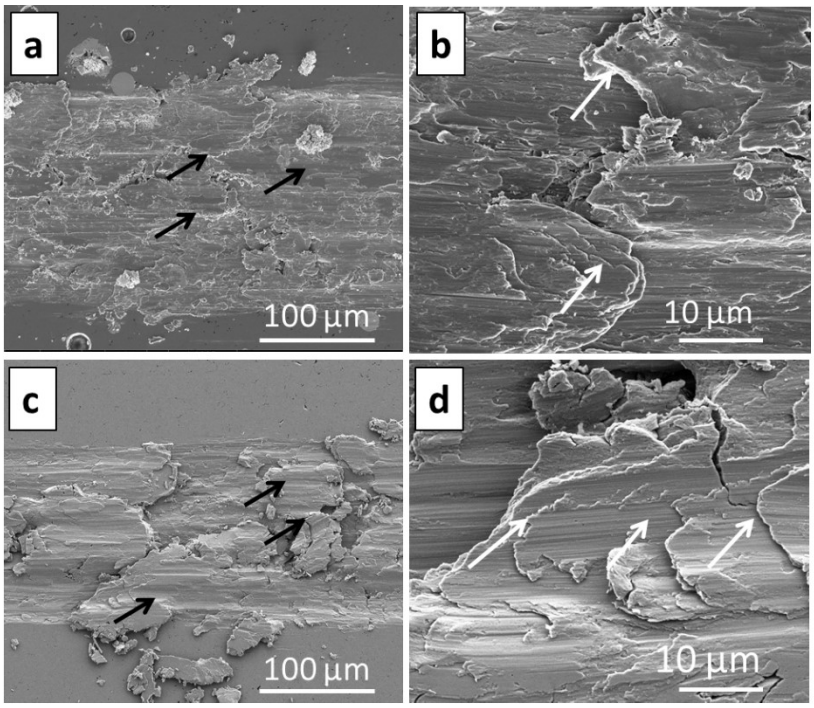

Fig 5.6 Morphology of (a) Ni-10.5vol.%WC, where black arrows indicate early formation of tribolayers and (c) Ni wear track after 10 sliding cycles, where black arrows indicate scoring of surface (b) and (d) high magnification view of (a) and (c), respectively. White arrows indicate tongue-shaped features.

As the tests progressed to further sliding cycles, the formation of MMLs became more evident (Fig .5.7). Detached particles within the wear track underwent repeated plastic deformation and oxidation. Wear particles with promoted work-hardening and oxidation were comminuted to fine size fragments. Because of adhesion forces existing between small size debris due to surface energy, fine debris were agglomerated at some regions and formed compact layers [95, 130, 131, 137]. For the Ni-WC coating, fragmentation of wear debris and formation of relatively compact layer was observed as early as 10 cycles (see Fig. 5.6a, black arrows). For the Ni coating, comminution of wear debris started later as observed for wear track morphology after 50 and 100 cycles (see Fig. 5.7c and d). However, the compactness of MML for the Ni coating was clearly less than that of the composite coating after 50 and 100 cycles (Fig. 5.7 a and b). Compact MML, in the case of Ni coating, formed at longer cycles (Fig. 5.7d,), but its coverage on the worn surface was lower than that of the composite coating. Likewise, 150-200 sliding cycles were needed for the Ni coating to reach steady-state COF value. However, loose wear debris on the worn surface

of the Ni coating acted as obstacles against the sliding and led to fluctuation in CoF for the Ni coating after reaching an initial steady state.

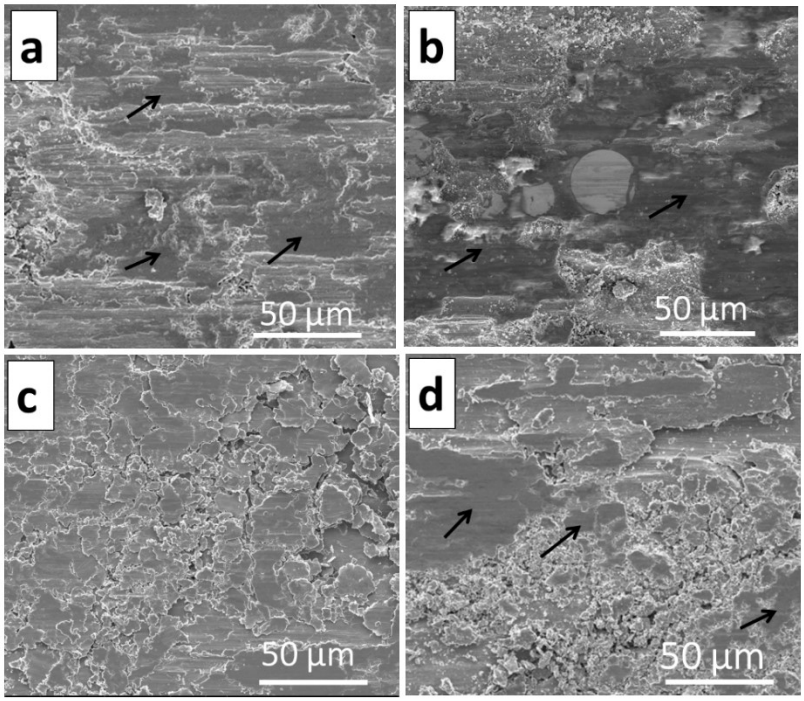

Fig 5.7 Morphology of (a), (b) Ni-10.5vol.%WC and (c), (d) Ni wear track after (a),(c) 50 and (b),(d) 100 sliding cycles. Black arrows indicate tribolayers.

The wear track of the Ni-WC composite coating after 1000 cycles consisted of three main features, the elevated compact MML rich in oxygen (see Fig. 5.8a and c, black arrows), and low oxygen content zone in which Ni and oxygen intensity remaining roughly the same as unworn coating from the results of EDX (see Fig. 5.8a and c, white arrows) and wear debris, which covered the wear track. Part of the wear debris was ejected outside the wear track. Cracks on MML were also visible at higher magnification. The wear track of the Ni coating displayed similar morphology, but with less coverage of the MML and less wear debris compared to that of the Ni-WC coating. Abrasive grooves were observed in the Ni coating worn surface using higher magnification view of tribolayers (see Fig. 5.6d, white arrows). With adding WC into Ni, the worn surface was covered with MML to a larger extent and the amount of wear debris was significantly reduced.

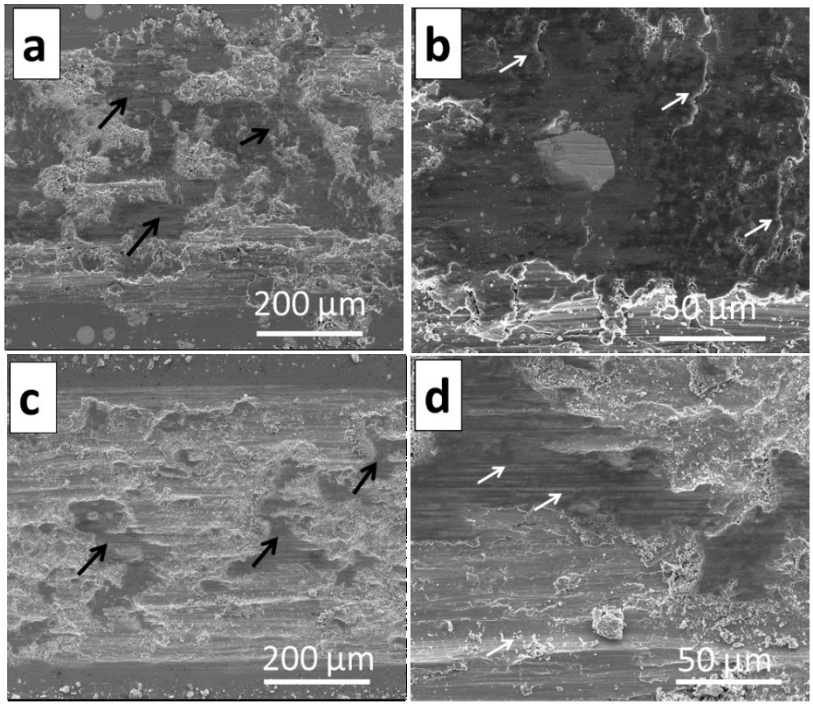

Fig 5.8 Morphology of (a) Ni-10.5vol.%WC and (c) Ni wear track after 1000 sliding cycles, (b) and (d) high magnification view of (a) and (c), respectively. Black arrows indicate tribolayers. White arrows indicate abrasive grooves and cracks.

Greater contrast between the Ni and WC was achieved from backscattered electrons (BSE) imaging in Fig. 5.9, representing worn surfaces of the Ni-WC composite coating at 10 and 1000 cycles. As can be seen, there was no pulled out WC detected on the worn surfaces, indicative of good cohesion between the Ni matrix and the WC particles [138]. However, surfaces were covered by fine fragmented WC particles, which were pulled out during sliding and redistributed on the surfaces as early as 10 cycles. These fine particles were retained between the two contacting surfaces and directly incorporated in the fast development of the compact layers. As demonstrated by worn surface features of the Ni-WC coating at 10 cycles (see Fig. 5.7c, black arrows), some regions of the wear track showed an early stage of MML development evidenced by the smoother surface compared to the smeared and layered structure around it. The fine redistributed WC particles not only facilitated fast development of the tribolayer, but also improved its stability and increased hardness and contributed to superior sliding wear resistance of the Ni-WC coating compared to the Ni coating.

Significant improvement in sliding wear resistance with only small concentration of WC in Ni matrix was also reported in a previous study on laser clad Ni-WC with 10vol.% WC tested at similar wear conditions [13]. The reported wear rate of 10×10^{-6} mm^3/Nm [13] is in good agreement with that of the present study. Adhesion and oxidation were reported to be dominant wear mechanisms for laser cladding Ni and Ni-WC coatings with WC concentrations lower than 25-30vol.% [39, 129]. Although, adhesive wear was found to remain more pronounced for Ni coating, which is consistent with this study [39].

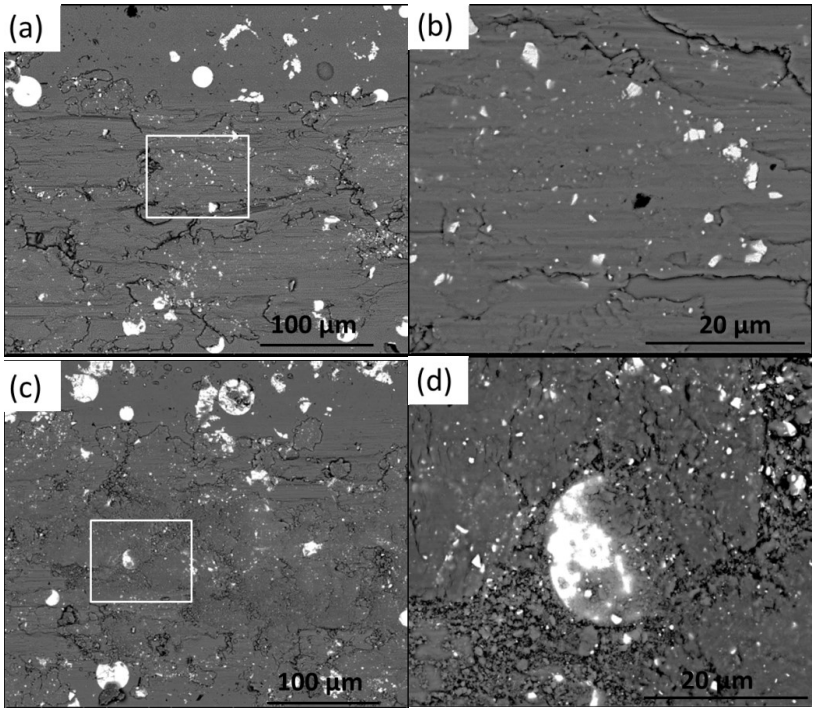

Fig 5.9 Backscattered image of cross-section of Ni-10.5vol.%WC coatings after (a) 10 and (c) 1000 sliding cycles, (b) and (d) high magnification view of (a) and (c), respectively.

A transition to three-body abrasive wear was found at higher WC concentrations, where WC particles can be easily dislodged from surface and trapped in contact due to cracking at interfaces [39, 129]. These cracks are originated from brittle phases at interface and also significant residual stress at higher concentration of WC in coating [13, 39]. However, these defects can be avoided using cold spray. While previous findings show that a significant decrease in wear does not occur above approximately 25-30vol.% WC in laser cladding composite coatings, retention of high content WC to cold sprayed coating is challenging. Although higher WC concentration wasn't

achieved in this study using cold spray at applied conditions, testing of processing parameters and initial feedstock are currently in progress to improve the efficiency of the process.

Figure 5.10 shows morphology of the wear debris outside the wear tracks for Ni and Ni-WC composite coatings. In the Ni-WC worn surface, compacted fine wear debris of 1 - 5 μm in size was observed, while plate-like wear debris up to 100 μm in size was found in the Ni coating. The scale of the wear debris also correlated to tribological behavior, where the Ni coating, with larger wear debris, exhibited a higher wear rate than the Ni-WC coating, with smaller wear debris.

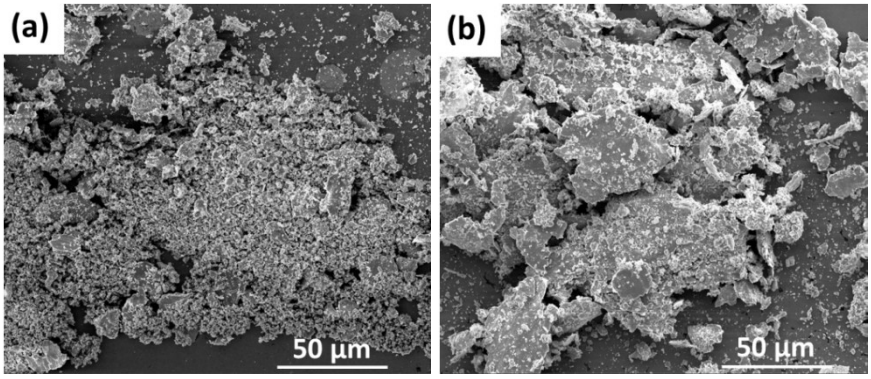

Fig 5.10 Morphology of wear debris outside the wear track of (a) Ni-10.5vol.%WC and (b) Ni coatings.

During initial contact of the WC-Co ball on the coatings surface, high contact stress is expected to occur. The initial mean Hertzian contact stress [139, 140] for Ni and Ni-WC coatings were estimated to be 718-723 MPa and 794-805 MPa, respectively. The predicted contact stress is only valid during initial contact of two mating surfaces. As sliding progresses, plastic deformation, materials transfer, wear debris generation and etc occur, contact stresses become far more complicated. In the present study, both coatings caused wear of counterparts and contributed to a drop-in contact pressure. The morphologies of worn surface of the WC-Co ball after 1000 cycles sliding against Ni and Ni-WC coatings are shown in Fig. 5.11. The apparent contact stresses after 1000 cycles sliding for Ni and Ni-WC coatings were estimated to be 36 and 41 MPa, respectively. WC–Co ball mating with Ni coating underwent more severe wear under lower contact stress, which may come from the bigger wear debris generated during the wear process, as plate-like debris can be also observed (Fig. 5.11b indicated by arrow).

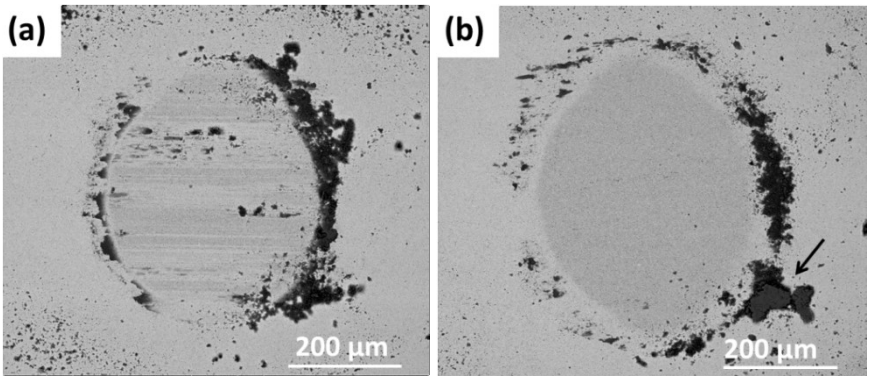

Fig 5.11 Morphology of the worn surfaces of the WC-Co ball mating with the (a) Ni-10.5vol.%WC and (b) Ni coatings. Black arrow indicates plate-like debris.

5.3.3.3 Subsurface microstructure

Figure 5.12 shows BSE micrographs of wear track cross sections taken perpendicular to the sliding direction for Ni and Ni-WC composite coatings at 1000 cycles. In both cases, a layer of mixed material with a thickness of about 5 µm was found at the surface. The layer consisted of Ni fragments detached from surfaces and nano-crystalline Ni-rich in oxygen, covered the top of worn surfaces. For cross-section of the wear track of the Ni coating (Fig. 5.12a), subsurface micro-cracking was observed. This was attributed to the shear stresses transferred to the bulk surface material underneath the MML due to low load-bearing capacity of Ni which resulted in a larger tendency for plastic deformation of asperity junctions [141]. The intersection of these cracks led to detachment of wear particles. The hard particles detached from MML acted as third-bodies abrasive particles which induced wear on sliding surfaces and resulted in increased wear rate and made CoF fluctuate. However, in the case of the Ni-WC composite coating, the development of a coherent and stable MML, which is evident from Fig. 5.12b, contributed to superior wear resistance of the Ni-WC coating compared to the Ni coating. The presence of fine redistributed WC particles in the MML improved friction stability as evidenced by stable CoF.

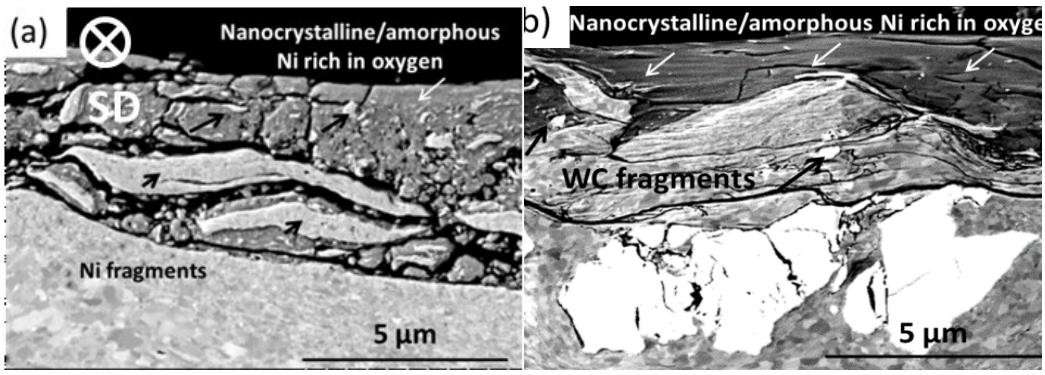

Fig 5.12 Cross-sections of the near-surface microstructures after 1000 sliding cycles for (a) Ni, where black arrows indicate Ni fragments and white arrows indicate oxygen-rich regions, and (b) Ni-10.5vol.%WC coatings, where black arrows indicate WC fragments and white arrows indicate oxygen-rich regions. SD indicates sliding direction.

5.3.3.4 Hardness and elemental composition of third bodies

The hardness of the MML of cold-sprayed Ni and Ni-WC composite coatings were measured using nanoindentation. In the unworn Ni and Ni-WC coatings, the average hardness of the pure Ni was 4.6 ± 1.0 and 5.2 ± 1.0 GPa, respectively, which showed significant increase in hardness value compared to that of the Ni feedstock powder (2.1 ± 0.2 GPa). This is due to extensive plastic deformation, grain refinement, and increased local dislocation density [57]. The MML of the Ni coating had a hardness of 6.2 ± 0.7 GPa which was 1.4 times higher than that of the underlying Ni. This is similar to the degree of hardening in the tribolayer of micro and nano-crystalline Ni subjected to dry wear sliding test, which was 1.3-1.5 times, reported in a previous study [142]. The strain hardening due to grain refinement and surface oxidation are the possible contributions to the increased hardness of MML [142]. The hardness of the Ni-WC coating's MML was 11.2 ± 3.6 GPa which was 2.2 times harder than the bulk of the tested material. Several previous studies have reported increases in MML's hardness for metal matrix composites compared to the underlying materials. A large value of hardness of the worn surface was due to the redistributed fine WC particles and strain hardening.

Elemental microanalysis of the unworn and the wear tracks of coatings revealed increased oxygen in the worn surfaces. Representative EDX spectra were collected from the regions of interests. In the EDX spectra, the relative intensities of Kα peaks of oxygen and Ni are centered at

0.53 and 0.85 keV, respectively. In the unworn Ni, the Ni peak was dominant with a small oxygen peak; whereas in the Ni coating's MML, the Ni peak intensity remained roughly the same as the unworn coating, but oxygen peak intensity increased. The Ni-WC coating MML showed roughly equal intensity of Ni, however, a larger presence of oxygen was measured. There are several possible reasons for increased oxygen content in the worn surfaces. One is materials mixing during sliding where clean metal is exposed to oxygen [143]. This can be promoted by deformation heat and an increased energy level of particles due to sliding induced defects and surface energy [130, 131]. The higher oxygen content in the load-bearing areas of Ni-WC composite coating and fine debris around these areas compared to those of the Ni coating can be attributed to more localized plastic deformation of MML due to its higher hardness.

5.4 Conclusion

Using the cold spray process, Ni and Ni-WC coatings were deposited and their tribological behavior during dry sliding wear was studied and compared. Inclusion of WC resulted in a reduction in coating porosity. However, the presence of WC particles decreased deposition efficiency and also reduced bonding between Ni particles. Much less WC particles were retained (10.5vol.%) than in feedstock (36vol.%). For the sliding wear, the presence of WC particles in the coating stabilized CoF and decreased wear rate by a factor of seven. This improvement was linked to the formation of a stable and cohesive MML on top of the wear track of Ni-WC coating which protected first bodies from wear. This, in turn, was attributed to the fine fragmented WC particles which were redistributed during sliding and enhanced resistance to plastic flow of Ni matrix. Fine fragmented WC particles facilitated the fast development of MML, as well as, improved its stability and increased its hardness which contributed to superior wear resistance of composite.

Acknowledgments

The authors gratefully acknowledge the financial support from the Canadian Foundation for Innovation (CFI) project No. 8246 for the cold spray equipment, the CFI Leader's Opportunity Fund project No. 13029 for the tribometer and nanoindentation equipment, and the Natural Sciences and Engineering Research Council (NSERC) Strategic Grants Program for the

operational funding of this project. Thanks are also due to Tekna Inc. of Sherbrooke, QC for providing the Ni and WC powders.

Chapter 6

Effect of WC morphology on dry sliding wear behavior of cold-sprayed Ni-WC composite coatings

Sima Alidokht, Steve Yue, Richard R. Chromik

This is a manuscript, intended to submit to a journal. In Chapter 5, the Ni and Ni-10.5vol.% WC were subjected to sliding wear studies. In the present chapter, the effect of a higher WC volume fraction, i.e. 28vol.%, on the friction and wear behavior was tested. Moreover, since a better control of WC content was achieved using agglomerated WCNi powders, the influence of WC morphology on the friction and wear response of composite coatings was investigated.

Abstract

Cold spray is a relatively new method to deposit WC reinforced composite coatings, where its low temperature is an advantageous, avoiding oxidation and carbide decomposition. Previous studies demonstrated that using agglomerated and porous WC powders allowed particle densification and elongation during deposition, resulting in higher WC retention within the Ni matrix, as compared to that of cast WC powders. However, the influence of starting powders morphology on coatings wear properties is not well understood yet. Here we report cold spray deposition of Ni with nearly 30vol% WC, using two types of WC particles, i.e. cast and agglomerated, and labeled as Ni-28WC and Ni-30WCNi, respectively. Ni-28WC featured a multimodal distribution of WC particles ranging from 0.2 to 20 μm with significantly lower mean free path between them, as compared to Ni-30WCNi with WC size ranging from 0.3 to 1.3 μm. The wear behavior of coatings was studied with reciprocating sliding wear tests under normal loads of 5 and 12 N. Ni-28WC coatings were found to be resistance against materials removal at the two tested loads, while they were causing damage on the counterspheres. Whereas, wear rates of 6×10^{-6} and 36×10^{-6} mm^3/Nm were determined for Ni-30WCNi at 5 and 12 N, respectively. Multi-modal size distribution of cast WC with significantly lower mean free paths between them

minimized adhesive wear and helped to develop protective mechanically mixed layers more rapidly. Subsurface microstructure and chemical analysis suggested higher oxidation and more stable mechanically mixed layers in Ni-castWC, with lower depths of deformation zones extended beneath the mechanically mixed layer. Mechanical properties of sliding-induced microstructure of coatings was examined by nanoindentation and correlated to mechanically mixed layers stabilities and morphology of WC particles.

6.1 Introduction

Metal matrix composites (MMCs) reinforced with WC have long been used in demanding engineering applications due to their exceptional wear resistance [13, 39, 41, 126]. There are various methods to prepare MMCs of WC with metal matrices based on Co or Ni, including liquid phase sintering (LPS), hot isostatic pressing (HIP) and microwave sintering (MW). These wear resistant MMCs may also be prepared as coatings by various thermal spray methods, including HVOF, plasma spray, cold spray and others. For all of these processes, the feedstock powders play a role in optimizing the process and the properties of the MMCs [38, 39]. Several types of WC powder are used for the surface coating process, among which cast WC and agglomerated WC-Co or Ni powders are most often the materials of choice [13, 39, 41, 126]. For the former type of WC powder, induction plasma technology is often applied to transform crushed, atomized and sponged powders into dense spherical powders. The feed particles are heated to melting point followed by cooling under controlled conditions [37]. The powder is a mix of eutectic WC and W_2C phases [37].

Cold spray is a relatively new method to deposit WC reinforced composite coatings. The low temperature of cold spray is advantageous, avoiding oxidation and carbide decomposition that commonly occurs in thermal spray and laser cladding processes [19, 20]. Previous studies found that the recovery of WC particles to coatings during cold spraying are influenced by their morphology [27, 76, 144-146] . Dense morphology of cast WC and their limited deformability causes fracture of WC particles during deposition and their loss. Whereas, porous structure of agglomerated WC particles along with Co/Ni binder between WC agglomerates provide ductility. This allows for deformation, densification and elongation of agglomerated particles through slipping and rotation of WC particles along the Ni binder, leading to a significantly higher WC

retention within the matrix. Previous studies reported high losses of cast WC particles with only 11-29% of WC were retained into coatings [27, 145]. A significant improvement in WC retention into coatings was obtained using WC agglomerated and sintered powder in mixture with Ni. The WC content in coatings was reported to be close to that of the initial feedstock [27, 76, 145]. It is important to note that, although there is a desire for higher recovery of ceramic particles into cold sprayed coatings in the past recent studies, however, higher retention of the ceramic particles may not necessarily lead to best tribological performance. The wear properties of WC composite coatings are influenced by their structure, which is shaped by the WC particles fraction, their morphology and distribution, metallic matrix microstructure, as well as, WC/Ni interfacial bonding [29]. Therefore, for future tribological applications of cold sprayed MMCs, both process optimization and characterization of the tribological performance is required.

During the sliding of metallic materials and MMCs, plastic deformation, material mixing, and wear debris generation take place between the specimen and the counterpart. This is often accompanied by a chemical reaction with the environment, most commonly oxidation. After some time, the imposed load, shearing stresses, mechanical mixing and chemical reactions results in a surface oxide layer, which is often referred to as a mechanically mixed layer (MML) [95, 96, 130, 131]. The formation and stability of MMLs are closely associated with the wear performance of MMCs in sliding systems. Hard, stable and continuous MMLs are often beneficial to reduce friction and wear [95, 96, 130, 131]. Pure metals and alloys also form MMLs, but the hard phase present in MMCS is found to play a role in the oxidative wear mechanisms of MMCs [147, 148]. The size and the interfacial bonding strength of the hard reinforcement particles to the matrix have a relationship to the “critical oxide thickness”, which determines the possibility for the reinforcement particles to provide protection against oxidational wear of the matrix [148, 149].

In an unreinforced material during sliding cycles, oxide grows progressively to its critical thickness, before it becomes unstable and is subsequently removed from the surface. Then, fresh metal contact is established, leading to rapid wear. However, in the presence of hard particles, this mechanism can be significantly altered. Larger particle can offer load support, which will delay removal of the oxide layer, making it stable to greater thicknesses. Smaller particles can be incorporated into the MML and enhance the properties, again leading to greater stability. When the MML is eventually broken down, the reinforcing particles underneath the MML become

exposed and reduce metal contacts to the counterbody. At this stage, the load supporting nature of the particles as well as their cohesion strength with the metallic matrix determines their effectiveness on protecting the metallic matrix from wear [147, 148]. The "critical oxide thickness" is reported to vary enormously and, depending on oxide load bearing capability, can be in the range of 1-5 μm for metallic materials. Compressive stress within the oxide is caused by the expansion of the lattice, to accommodate the oxide growth. Beyond "critical oxide thickness" the stress would be sufficient for adhesion loss and formation of wear debris [148, 149]. Although this term is established for the metallic materials when "total oxide mechanism" is concerned, in which oxide grows progressively to its critical thickness and then it's removed. However, it is reported that this could be the case for the oxide layer developed by the debris compaction [147].

Wear properties of cold-sprayed WC coatings were reported in the previous studies. In the work of Alidokht *et al*. [145], room temperature sliding wear of a cold-sprayed Ni-10.5 vol% WC coating using cast WC was analyzed. A significantly lower wear rate compared to a cold-sprayed pure nickel coating was reported, due to formation of a stable oxide film or mechanically mixed layer (MML) on worn surfaces. WC particles promoted the formation of MML composed of Ni and W oxides and WC fragments. As reported in **Chapter 4** [146], using agglomerated WC, deposition and retention of WC can be significantly improved. Although there is a desire for higher recovery of ceramic particles into cold sprayed coatings in the past recent studies, however, it is not still clear that higher retention of the ceramic particles leads to best tribological performance. Moreover, there is no systematic study where the two morphologies of WC particles and their role in the friction and wear of Ni-based composite coatings were compared. In the present study, two Ni-WC coatings with similar fill ratio of cast and agglomerated WC were cold-sprayed. For the two composite coatings, dry sliding wear tests were conducted and the effect of WC particles morphology in the friction and wear was studied.

6.2 Experimental

Feedstock powders for cold spray were commercially pure water atomized Ni (4SP-10, Novamet, Kentucky, USA), plasma spheroidized WC (TEKMAT™ WC-45, Tekna, Quebec, Canada), and agglomerated and sintered WCNi (AMPERIT® 547, H.C.Starck, Munich, Germany). A co-feeding system with two powder hoppers was used to spray composite coatings

with various contents of WC, where the feed rate of WC or WCNi powder was varied. The structure and properties of these coatings are reported on in **Chapter 4**. Here two composite coatings (one using cast WC and one using agglomerated WCNi) of roughly 30 vol% WC were selected for extensive side-by-side comparison of their tribological properties. Coatings were deposited onto steel plates using a commercially available cold spray system (PCS-800, Plasma Giken, Saitama, Japan). The cold spray unit utilized a de Laval nozzle made of WC-Co. Nitrogen was used as the process gas. Prior to entering the nozzle, the gas pressure was 4 MPa and the gas preheat temperature was 700°C. The stand-off distance between the substrate and nozzle exit was set at 40 mm, and the gun traverse speed at 30 mm/s. Cold-sprayed coatings were cross-sectioned perpendicular to the gun traverse direction, mechanically ground, and polished using 9, 3 and 1 μm diamond pastes followed by 0.05 μm colloidal silica. The morphology and microstructure of the initial powders and deposited coatings were observed by scanning electron microscopy (SEM) (FEI Quanta 600, Thermo Fisher Scientific, USA). The WC and porosity concentrations within the coatings were measured by image analysis of pixel count using ten random SEM images of polished cross-sections. The two coatings selected for the present study contained 28 vol% cast WC and 30 vol% WC in the form of agglomerated WCNi, with assigned designations of Ni-28WC and Ni-30WCNi, respectively, used throughout this work.

Sliding wear tests on the coatings were performed in dry air (below 3% relative humidity) using a custom-built ball on flat reciprocating tribometer. Prior to wear test, coatings were polished to a final step by 0.05 μm colloidal silica. Spheres of WC-Co (McMaster Carr, USA) with a diameter of 6.25 mm were used as counterfaces. The Voigt and Reuss bounds were used to predict the upper and lower bounds of elastic modulus of composite coatings, and then used to calculate the corresponding upper and lower bounds of Hertzian contact pressure. The initial mean Hertzian contact stress [139] for composite coatings were estimated to be 821-827 MPa and 1082-1198 MPa, for 5 and 12 N, respectively. All wear tests were also conducted with normal load of 5 and 12 N, sliding speed of 3 mm/sec, and track length of 5 mm. Tests were run to 10, 50, 100, 500, and 1000 cycles. Friction forces were measured with a sampling rate of 800 Hz using a piezoelectric sensor mounted underneath the sample stage. Along each cycle, CoF was averaged across a central portion of the track and then graphed versus number of cycles. Worn samples were examined using a non-contact optical profilometer (NewView, Zygo instruments, USA) to obtain

profiles of the wear tracks. The volume of material removed, v, was measured by multiplying the cross-sectional area of material removed, measured by profilometry, by the track length. Cross-sectional area was determined by integrating height profiles across the wear track above and below the original surface, where a total number of 50 - 60 surface profile measurements per wear track were used. This, along with the total sliding distance x and applied load W, was then used to calculate wear rate, ḱ (mm^3 /Nm) using the equation (1) [1],

$$\acute{k} = \frac{v}{Wx} \quad (1)$$

In order to study wear mechanisms, worn surfaces and cross sections of wear tracks were examined using an SEM (Hitachi, SU-8230, Japan) equipped with energy dispersive X-ray spectroscopy (EDS). Nano-indentation using a Berkovich diamond tip with a triboindenter system (TI 950, Hysitron, USA) was performed on wear tracks and on the cross section of worn surfaces to measure mechanical properties of third-bodies. The peak load, loading and unloading rate, and hold time at peak load are fixed as 1 mN, 200 μN/s and 2 s, respectively. To calculate hardness and elastic modulus, the indentation unloading-displacement data was analyzed using the Oliver and Pharr method [107]. Subsurface morphologies of the wear tracks were observed with a Cryo-STEM (FEI Tecnai G2 F20, Thermo Fisher Scientific, USA). TEM specimens were made with focus ion beam (FIB) lift-out performed using a DualBeam SEM (FEI Helios Nanolab 660, Thermo Fisher Scientific, USA) .

6.3 Results

6.3.1 Coatings

For the Ni-28WC and Ni-30WCNi coatings, Table 6.1 summarizes the WC fraction, porosity and micro-hardness of coatings, nano-hardness of Ni matrices, and MFP between WC particles. Figure 6.1 shows micrographs of cross-sectioned Ni-28WC and Ni-30WCNi composite coatings. Using WCNi composite powder, the retention of WC in the coating was significantly improved and WC content was close to that of the initial feedstock. Particles retention mechanisms and WC fill ratios for various mixtures were discussed in detail in an earlier work [146]. No significant fracture of WC particles was observed in Ni-30WCNi coating. However, most of the

cast WC particles were cracked/fragmented, leading to WC fragments consisting of particles size ranges from 0.2 to 20 μm. The addition of WC particles enhanced the hardness of coatings. Comparing the micro-hardness values of the two composite coatings, cast WC particles were more effective in strengthening the coatings. This is due to significantly lower MFPs between WC particles in Ni-castWC compared to that of the Ni-30WCNi coatings (see Table 6.1). A difference in the hardness and composition of the WC powders used in feedstock may also play a role. Cast WC was a eutectic mixture of WC and harder phase of W_2C with a "feather" microstructure (not shown). The higher nano-hardness of Ni matrix in Ni-28WC coatings is due to ultra-fine (<1 μm) WC fragments caused by severe fragmentation upon impact.

Table 6.1 Characteristics of cold-sprayed Ni-28WC and Ni-30WCNi coatings. Scatter bars on microhardness values indicate the standard deviation of 20 repeat measurements. Scatter bars on nanohardness values indicate the standard deviation of 100 repeat measurements.

Sample designation	WC in feedstock (vol.%)	WC in coatings (vol.%)	Porosity (%)	Hardness (HV_1)	Ni matrices hardness (GPa)	MFP (μm)
Ni	-	-	3.8 ± 0.5	345 ± 17	4.8 ± 0.9	-
Ni-28WC	80	28 ± 4	0.3 ± 0.1	431 ± 26	5.1 ± 0.8	8.5 ± 0.7
Ni-30WCNi	36	30 ± 5	0.5 ± 0.2	390 ± 27	4.5 ± 0.6	31 ± 4

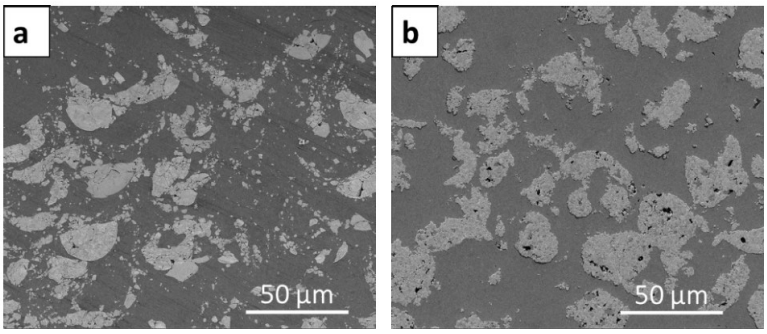

Fig. 6.1 Secondary electron (SE) images of unworn microstructures of (a) Ni-28WC and (b)Ni-30WCNi viewed in the cross-section.

6.3.2 Friction and Wear

For sliding wear tests at two loads of 5 and 12 N, both coatings, Ni-28WC and Ni-30WCNi, showed similar CoF behavior (Fig. 6.2), developing higher CoF values during run-in period, before reaching steady-state values. The Ni-28WC coating sliding under 5 N load showed a run-in period until 190 cycles followed by steady state friction coefficient value of 0.67. CoF curve at 12 N reached steady state at slightly longer distance (230-250 cycles) and its steady-state value was 0.75. Run-in periods for Ni-30WCNi coatings tested under the two loads lasted up to longer cycles (250 cycles), compared for those observed for Ni-30WCNi coatings. Similar to Ni-28WC coating, higher steady-state value was recorded at 12 N (0.75) compared to that at 5 N(0.61). This is attributed to an increase in contact area and hence frictional contact at higher load. Under 5 N applied load, Ni-28WC coatings exhibited higher CoF compared to that of Ni-30WCNi coatings, however for 12 N, the steady-state values for both coatings was around the same value of 0.75. The friction behavior of Ni-30WCNi was considerably less stable than that of Ni-30WC. Higher fluctuation in CoF was observed at lower load of 5 N for Ni-30WCNi coating, where CoF fluctuated between 0.57 and 0.68, with many temporary drops and shifts to plateau values. Large fluctuations in CoF for Ni-30WCNi coating at 5 N is attributed to formation of wear debris and its recirculation throughout the contact interfaces. Sliding tests were repeated at least 5 times for each condition. For both coatings, friction trends were repeatable. For Ni-28WC coatings, steady state was much more stable in each instance when compared to friction behavior of Ni-30WCNi coatings. Friction curves shown in Fig. 6.2 were close to mean value per cycle for each instance. Steady-state CoF values, averaged from all tests, were 0.70 ± 0.07 and 0.73 ± 0.04 for Ni-28WC, and 0.63 ± 0.03 and 0.73 ± 0.02 for Ni-30WCNi, at 5 and 12 N, respectively.

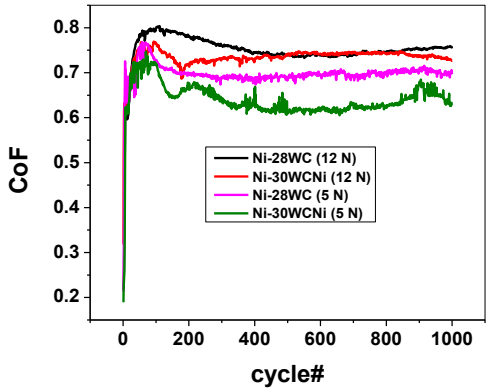

Fig. 6.2 Representative coefficient of friction versus sliding distance at 5 and 12 N of cold sprayed Ni-28WC and Ni-30WCNi coatings.

Surface profiles of the wear tracks for the two coatings tested under two loads of 5 and 12 N are shown in Fig. 6.3. For Ni-28WC coating tested at 5 and 12 N, the worn surface exhibited an elevated MML, which has greater height relative to its surrounding surface and unworn surfaces. Wear track topography (see Fig. 6.3c and d) of Ni-30WCNi reveals sharp contrast when compared to Ni-28WC coatings. The MML appeared as islands. Moreover, areas having lower depth, around 4-6 µm, were continuous. For Ni-30WCNi, at 5 N, elevated MML was observed, whereas, at 12 N, MML were at lower height as compared to unworn surfaces yet elevated compared to regions inside wear track with mostly 4-6 µm depth.

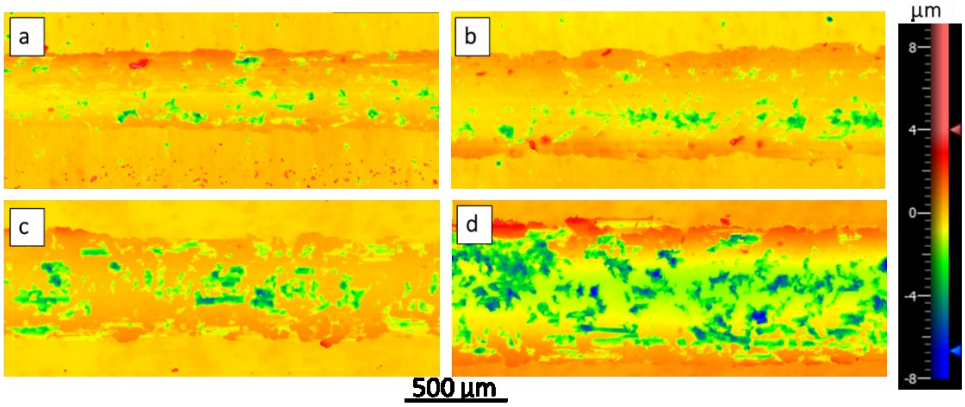

Fig. 6.3 Wear track topography of Ni-28WC at 5 N(a) and 12 N(b), and Ni-30WCNi at 5 N(c) and 12 N(d).

The wear rates at the end of the 50 and 1000 cycles tests were calculated using equation (1) and presented in Fig. 6.4. Ni-28WC coatings were found to be more wear resistance when compared to Ni-30WCNi coatings. The wear rate measurement on Ni-28WC coatings was indicative of volume gain by these coatings after 1000 cycles. Whereas, for some tests, very low material loss was recorded after 50 cycles, reflected as higher standard deviations in the wear rates (Fig. 6. 6.4). However, for Ni-30WCNi, mild wear rate values of 7 and 36 × 10^{-6} mm^3 /Nm for 5 and 12 N were measured after 1000 cycles, respectively. Increasing the load from 5 to 12 N, mean wear rates of Ni-30WCNi increased by a factor of 5.

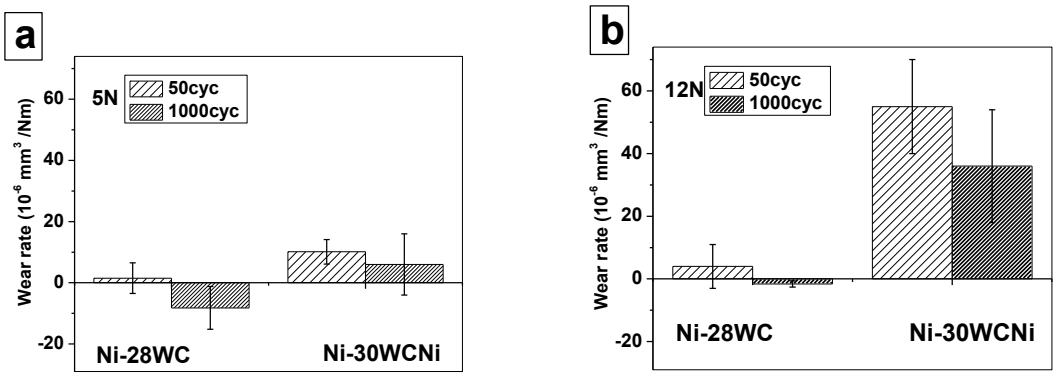

Fig. 6.4 Volumetric wear rate for Ni-28WC and Ni-30WCNi tested at (a) 5 N and (b)12 N.

Wear rates of the WC-12Co counter-spheres after 1000 cycles sliding tests are given in Fig. 6.5. Both coatings caused wear of counterparts. Wear of counterparts during sliding contributed to a drop in the contact pressure. The apparent contact stresses after 1000 cycles sliding for Ni-28WC coatings were estimated to be 94 and 168 MPa, tested at 5 and 12 N, respectively. While WC–Co ball mating with Ni-30WCNi coating underwent more severe wear, which may come from the higher amount of abrasive wear debris generated during the wear process. This led to the lower contact stresses after 1000 cycles, 62 and 139 MPa, under 5 and 12 N, respectively, when compared to Ni-28WC coatings. For both coatings, higher load led to higher wear on counter-spheres, increasing sliding contact areas. However, despite significant ball wear for both cases, overall the Ni-cast WC sample remained more wear resistant than the Ni-30WCNi sample.

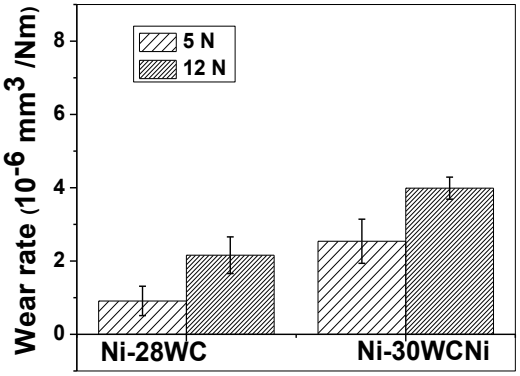

Fig. 6.5 Volumetric wear rate at 1000 cycles plotted for counter-spheres mating with Ni-28WC and Ni-30WCNi coatings at 5 and 12 N.

6.3.3 Worn surfaces morphologies

Figures 6 shows worn surface morphologies of Ni-30WC during initial sliding cycles (i.e. 10 and 50). Tongue-shaped features, indicative of adhesion of Ni to the countersphere, were observed in areas where less WC was present at surface. However, these features were less frequently observed here compared to a pure Ni coatings tested in **Chapter 5** [145], which indicates some effectiveness of WC at reducing adhesive wear. Evidence was also found that Ni adhering to the countersphere was sometimes transferred back on the WC particles (Fig. 6.6a).

Evidence of abrasive wear was also observed. Pulled out WC fragments and oxidized or work-hardened metallic debris can act as abrasive particles. Fine scratching marks in the direction of sliding were also observed and indicative of abrasive wear caused by hard particles (Fig. 6.6a). From the size of scratching marks on the center and sides of the wear tracks, it appears that only small WC particles were dislodged from surface and moved along sliding. As sliding continued, the wear debris were compacted between the sliding surfaces and developed areas of wear-protective oxide, MML (Fig. 6.6b and d). EDX analysis (not shown) showed oxidation of the surface, especially in the area of the MML, and of the debris.

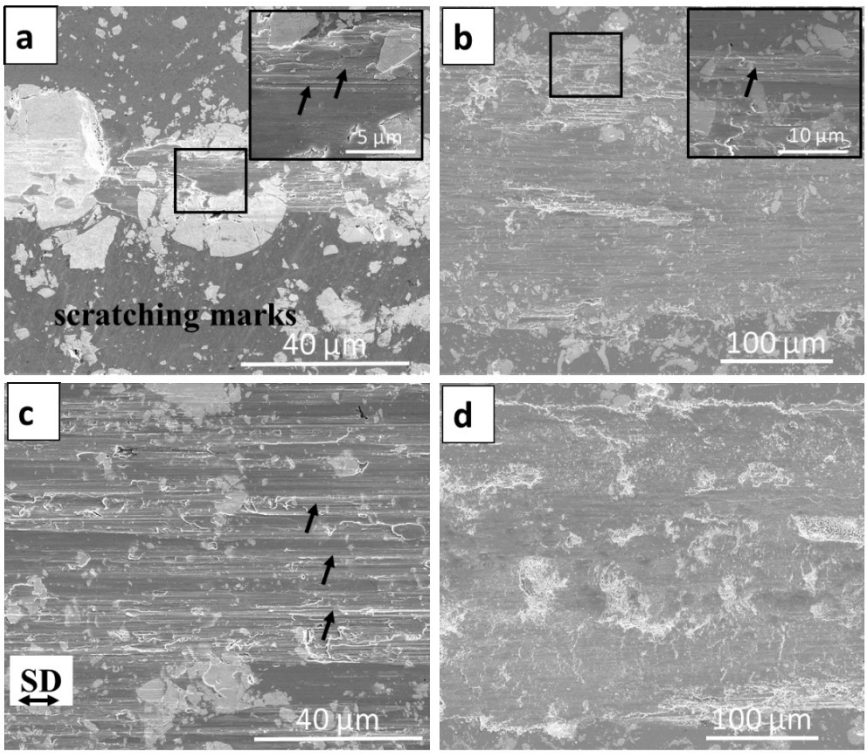

Fig. 6.6 Wear track topography of Ni-28WC after 10cycles (a) and (c), 50 cycles (b) and (d) at 5 and 12 N, respectively. Black arrows show scratching marks.

Worn surface morphologies of Ni-30WCNi developed during initial sliding cycles (Fig. 6. 7) were different from those for Ni-28WC coatings (Fig. 6. 6). This indicated different effect of the two WC particles types due to their different structures. Adhesive wear was much more intense in Ni-30WCNi coatings, despite having similar fill ratio of WC particles as Ni-28WC coating (Fig. 6. 7a and c). Formation of large metallic debris as well as decohesion of WCNi particles and re-distribution of WC fragments over the wear track occurred (see inset in Fig. 6. 7a and d). Extensive scoring of the surface in the sliding direction was observed on Ni-30WCNi coating worn surface (see Fig. 6. 7a and c). As the tests progressed, the formation of MMLs became more evident (Fig. 6. 7 b and d), but MML coverage was significantly lower than that of the Ni-28WC composite coating. In addition, at some regions on the wear track, MML became damaged and partially escaped from the contact area (Fig. 6. 7b). This exposed clean metal beneath for further oxidation and wear. Adhesive wear can be seen even at longer cycles of 50, as indicated by tongue shape features. A close comparison of the worn surfaces tested at two loads revealed that the extent of

wear was significantly higher in Ni-30WCNi tested at 12 N as compared to that at 5 N. EDX analysis (not shown) of the initial cycles worn surfaces were indicative of oxidation of the surface.

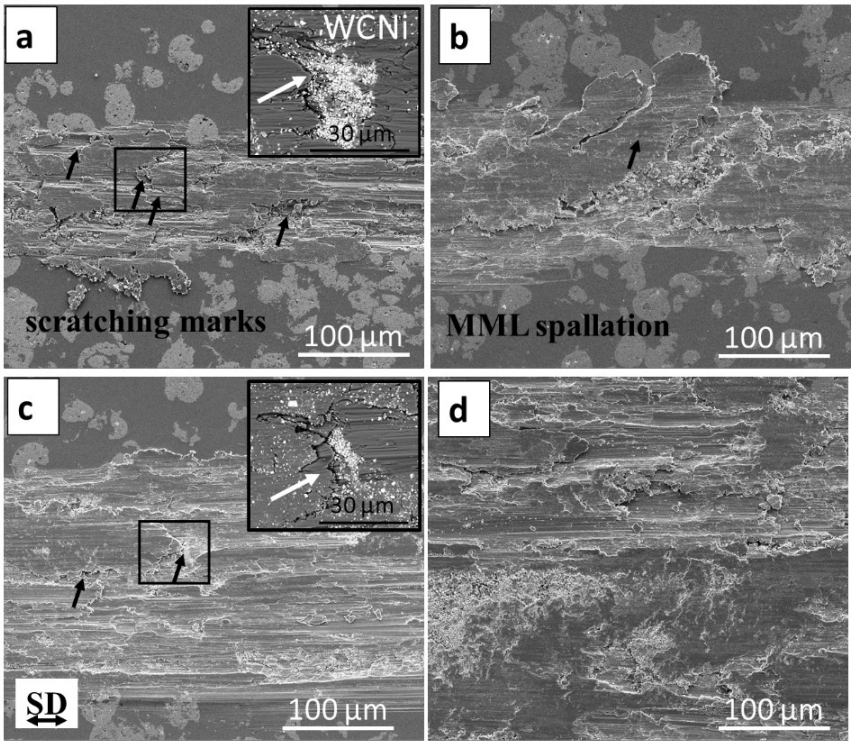

Fig. 6.7 Wear track topography of Ni-30WCNi after 10cycles (a) and (c), 50 cycles (b) and (d) at 5 and 12 N, respectively. Black arrows show adhesive wear. White arrows indicate WC dislodgments.

Figures 8 shows worn surface morphologies of mating surfaces at the end of 1000 cycles sliding tests for Ni-28WC coatings tested under 5 and 12 N. Image analysis through pixel count was used to measure the coverage ratio of MML on the worn surfaces, which has greater height relative to its surrounding region. Wear tracks were covered by MML with relatively high coverage of 85% and 89% at 5 and 12 N, respectively (Fig. 6.8a and d). MMLs were smooth (Fig. 6.8b and e) with very few scratch marks. However, some fatigue cracks were observed on MMLs (inset in Fig. 6.8c). BSE images with greater contrast between the Ni and WC showed distribution of WC fragments on the worn surfaces (Fig. 6.8b and d). Previous study showed that the presence of WC fragments provided MML with resistance against plastic deformation and contributed to its

stability [145]. No distinct change was observed by increasing the load from 5 to 12 N, except slightly higher MML coverage at 12 N.

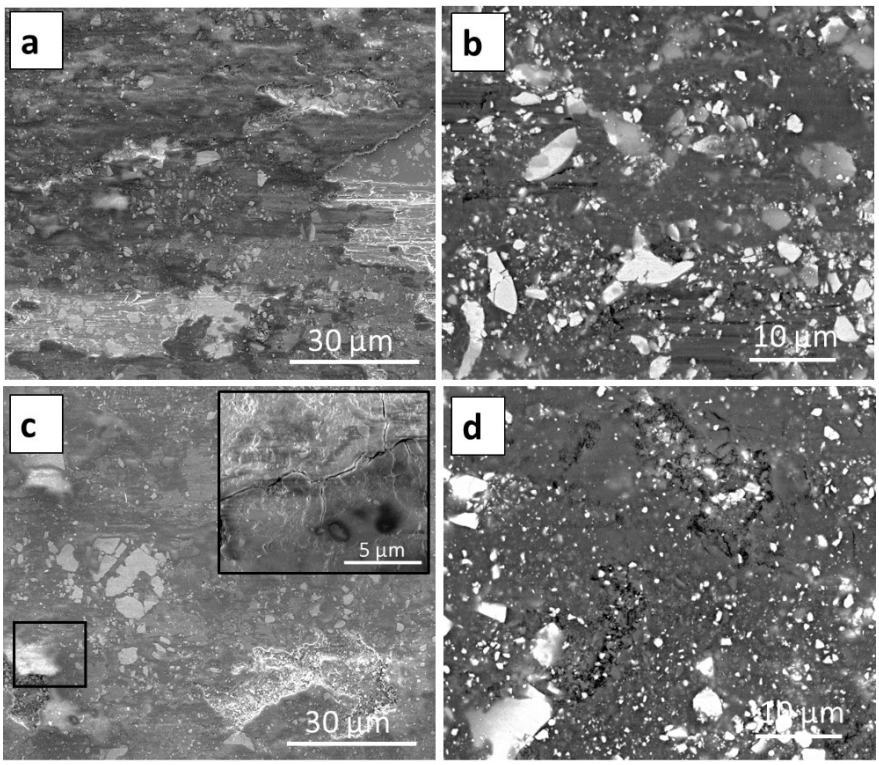

Fig. 6.8 Wear track topography of Ni-28WC after 1000cycles (a) at 5 N, (c) at 12 N, (b) and (d) higher magnification BSE images of (a) and (c), respectively.

Worn surface morphologies of Ni-30WCNi coatings at the end of 1000 cycles sliding tests under 5 and 12 N are shown in Fig. 6. 9, which showed different features compared to the Ni-28WC coatings (Figure 8). Features that were observed on the surface of Ni-30WCNi coatings indicated higher damage, as compared to those on Ni-28WC coatings. MML coverage on the surface was around 50% for the tested loads (Fig. 6. 9a and d), which was significantly lower compared to Ni-28WC coatings. Higher magnification view of the MMLs revealed cracking of the oxide layer, leading to plate-like debris detachments (inset in Fig. 6. 9a and b). BSE images of worn surfaces for Ni-30WCNi coatings showed that WC particles distribution was modified during sliding, however, in this case, it was quite non-uniform (see Fig. 6. 9b and d). The wear track of the Ni-30WCNi coatings at 12 N displayed similar morphology to that at 5 N, except the amount of wear debris on the wear track which was significantly decreased (see Fig. 6. 9a and c).

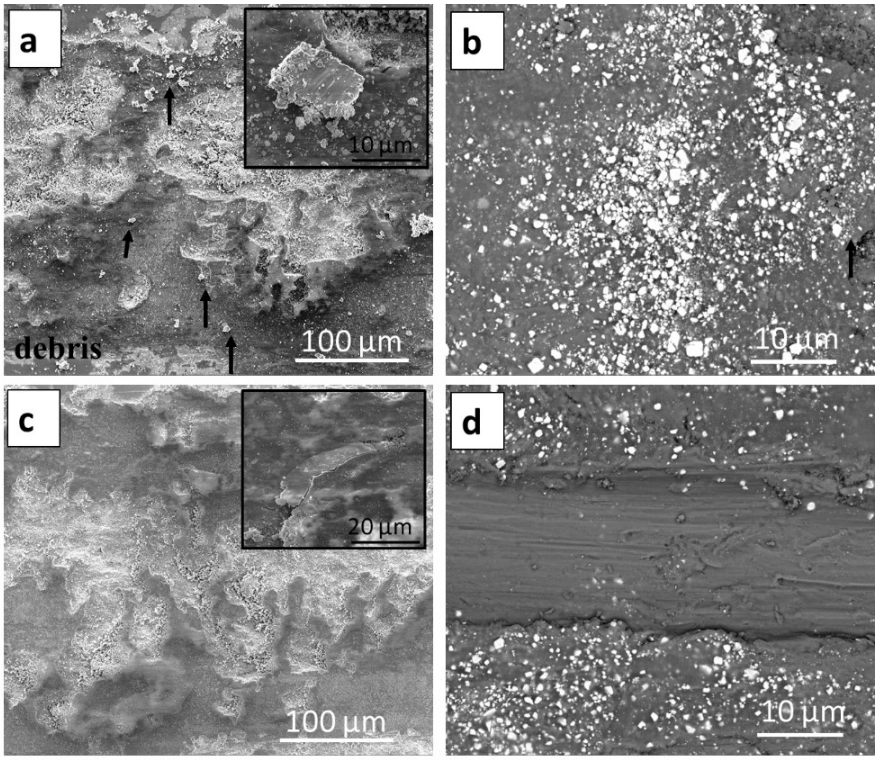

Fig. 6.9 Wear track topography of Ni-30WCNi after 1000cycles (a) at 5 N, (c) at 12 N, (b) and (d) high magnification BSE images of (a) and (c), respectively. Black arrows show wear debris. Inset in (a) and (c) shows cracking and plate-like debris formation.

The scale of the wear debris was also correlated to tribological behavior. Figure 10 shows morphology of the wear debris outside the wear tracks for Ni-28WC composite coatings. The Ni-28WC coating, with smaller wear debris, exhibited a lower wear rate than the Ni-WC coating, with larger wear debris (see Fig. 6. 10a and b). Large plate-like debris can be observed (Fig. 6. 10b indicated by arrow) were observed for Ni-30WCNi coatings. Whereas, in the Ni-28WC worn surfaces, under both loads, compacted fine wear debris of 0.1 - 2 µm in size was observed.

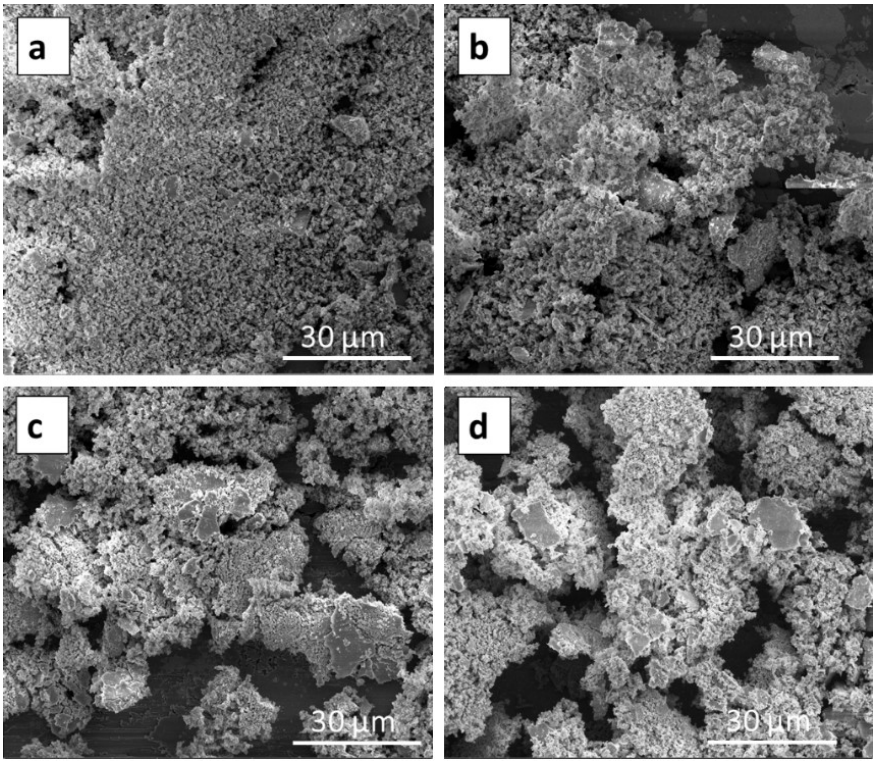

Fig. 6.10 Morphology of wear debris outside the wear track of (a) and (b) Ni-28WC, (c) and (d) Ni-30WCNi tested under 5 and 12 N, respectively.

6.3.4 Raman analysis of worn surfaces

Raman spectra were collected on the MML of the two coatings to identify the chemical phase compositions. For Ni-28WC, Raman analysis indicated that the oxidation of Ni and W started from early cycles, with the NiO and WO_3 peak detected at ~550, and 800 and 930 cm^{-1}, [150] respectively (see Fig. 6. 11a). Increasing sliding distance led to increasing amount of NiO and WO_3 phases (see Fig. 6. 11a). In addition, there was new tribochemical phase of $CoWO_4$ and/or $NiWO_4$ (Co- or Ni- tungstate) at ~890 cm^{-1} [150] started to form at 50 cycles (see Fig. 6. 11a). CoWO4 and $NiWO_4$ are very Raman active compounds, where a very thin layer of a few nanometer produces detectable peaks. No metal oxides were detected in the Raman spectra for the Ni-30WCNi tested under two loads of 5 and 12 N for initial cycles of 10 (see Fig. 6. 11b). As the sliding progressed, WC agglomerates oxidized to WO_3 due to deformation induced by sliding. Using Raman analysis, the MML developed on the Ni-30WCNi at 5 N was identified as containing NiO and WO_3. However, at higher load of 12 N, the MML contains the mechanically mixed

$CoWO_4$ and/or $NiWO_4$ tribochemical phase as well, as shown by the Raman spectra in Fig. 6. 11.b. Representative EDX spectra that is obtained from MMLs of composite coatings is shown in Fig. 6. 11c, where the Kα peak of oxygen and Lα peak of Ni and Co are centered at 0.52, 0.85 and 0.77keV, respectively. Elemental composition analysis of the MML revealed increased oxygen in the wear scar. Semi-quantitative analysis of the EDX relative intensities showed a very low amount of Co, indicating that the $NiWO_4$ is the major phase in the MML. However, another possible instance could be a relatively thin layer of highly Raman active Ni- and/or Co- tungstate being present at the surface that is detected by Raman spectroscopy. Whereas, a quite large interaction volume is encountered by EDX beam and X-rays are emitted from much larger depth, where Ni is the major element. It is worth to point out that Raman analysis of unworn WC-Co countersphere (not shown here) revealed no Raman active phase, except two peaks at 1350 and 1600 cm^{-1} which corresponds to WC.

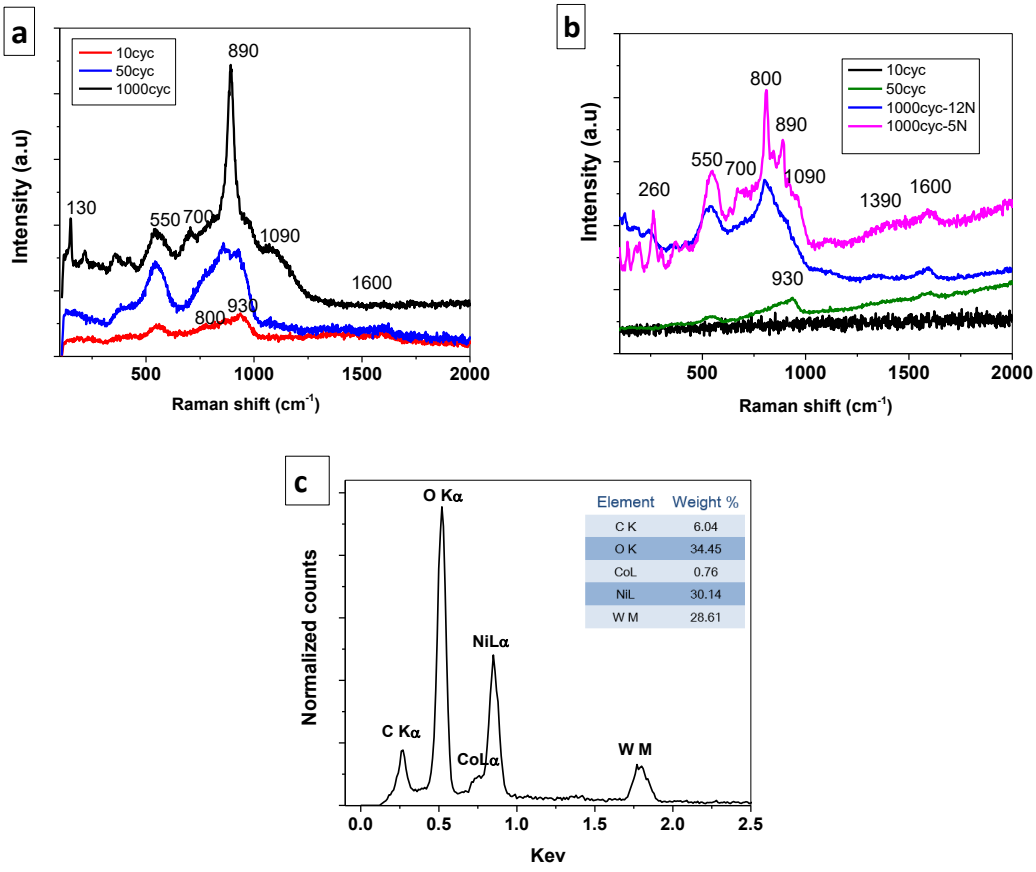

Fig. 6.11 Raman spectra of the MMLs obtained from (a) Ni-28WC and (b) Ni-30WCNi coatings, (c) a typical EDX spectra obtained from MML of composite coatings.

Figure 6.12 shows SEM images of the WC-Co counterfaces with normal load of 12 N and corresponding Raman spectra acquired on the counterfaces after sliding for 1000 cycles on the Ni-28WC and Ni-30WCNi coatings. Raman analysis showed that the ejected wear debris on the WC-Co counterface side is composed of NiO, WO_3, and $Co/NiWO_4$, which are the same tribochemical phases present on the wear track surfaces, as shown in Fig. 6. 11. Raman spectrum on plate-like debris found on the edge of counterface mating with Ni-30WCNi in Fig. 6. 12b showed that oxidation degree is less than the fine debris. SEM images showed that the counterface exhibited a wear flat and Raman spectroscopy analysis determined that there is no evidence of an oxide containing transfer film on the counterfaces.

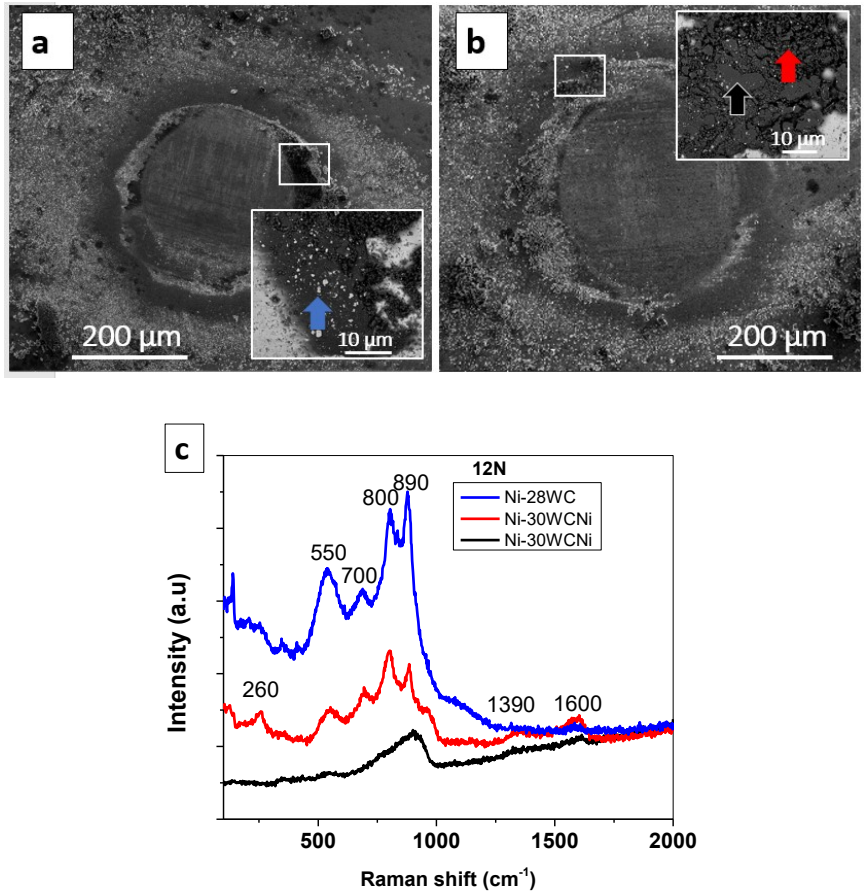

Fig. 6.12 SEM images of WC-Co counterfaces after 1000 cycles sliding on (a) Ni-28WC coating and (b) Ni-30WCNi, under 12 N, (c) Raman spectra of wear debris on the WC-Co counterfaces. The arrows in the SEM images indicate the location for each Raman spectra.

6.3.5 Subsurface microstructure and hardness

In order to see additional details on the near-surface MML, TEM observation and selective area electron diffraction (SAED) was performed on a cross-sectional thin foil on the surface of the wear tracks. Subsurface microstructure observation of the Ni-28WC and Ni-30WCNi wear tracks tested under 12 N was carried out through a FIB cut across MMLs, a typical feature developed for both coatings (see Fig. 6.13).

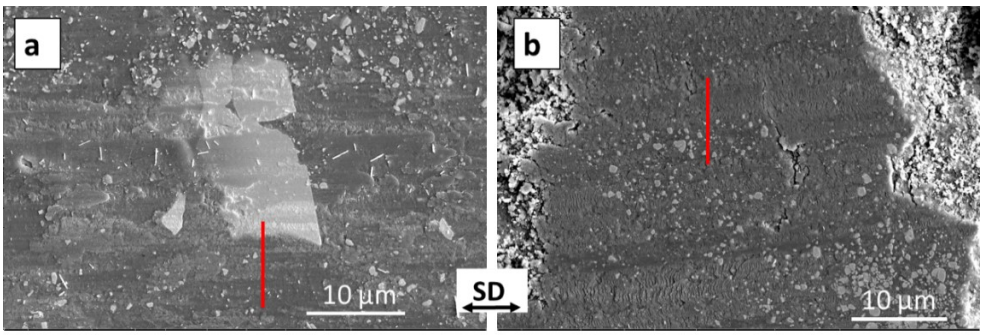

Fig. 6.13 Location of TEM foils obtained through FIB cutting on wear track of (a) Ni-28WC and (b) Ni-30WCNi after 1000 cycles of wear under 12 N.

For Ni-28WC, TEM images revealed an MML with uneven thickness (Fig. 6. 14a). MML was thicker (~2.4 µm) where it is supported by a relatively big WC particle. Using higher magnification image of the MML, fine WC can be seen which are distributed uniformly inside MML (Fig. 6. 14b). Underneath the MML, ultrafine grained and elongated grained Ni induced by plastic deformation was observed, where the modified layer was roughly 1 µm in thickness (Fig. 6. 14c). Upon closer investigation inside MML (Fig. 6. 14d), nanocrystalline structure was observed with grain size of 4 - 10 nm. SAED was performed on the MML and resulting ring patterns, indicating the nano-crystalline structure, was indexed. The d-spacing was compared with standard PDF card of NiO phase, which matched well to the d-spacing of the rings, indicating the presence of NiO in the nanocrystalline layer (Fig. 6. 14d).

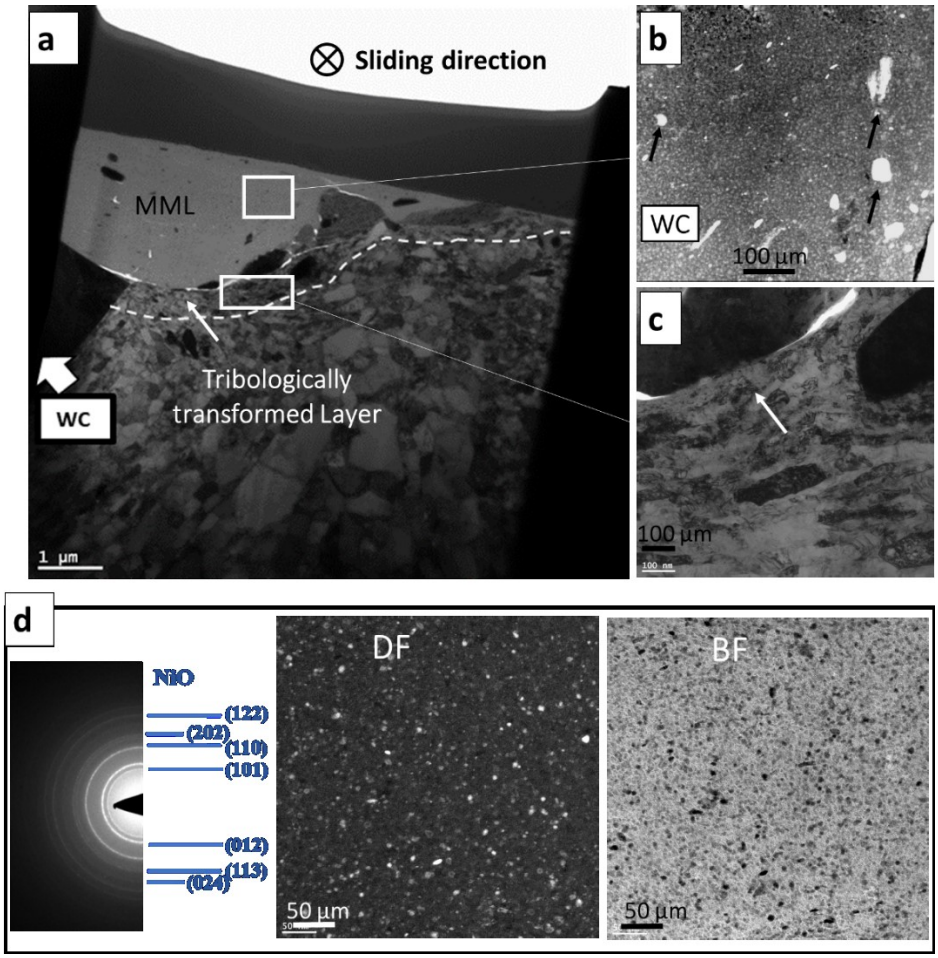

Fig. 6.14 (a) TEM images of Ni-28WC wear track surface cross-section (tested under 12 N), (b) upper inset shows high-angle annular dark-field (HAADF) image of WC distribution, (c) lower inset shows HAADF image of tribologically transformed layer at subsurface of wear track, (d) dark field and bright field of MML and SAED patterns of MML.

The MML thickness is relatively uniform across the worn surface for Ni-30WCNi coating (Fig. 6. 15a). WC fragments distributed inside MML, similar to the previous case (Fig. 6. 15a). Underneath the MML, on the right side of the thin foil, a relatively large Ni particle (Fig. 6. 15b). This contained WC fragments and its microstructure was found to be similar to original microstructure of coating. However, on the left side of the thin foil, sliding induced deformation zone, with ultra-fine grained (UFG) and elongated grains can be observed. Cracking can be observed nucleated and propagated inside the Ni particle, indicating large shear transferred to subsurface region. Similar to Ni-28WC, MML consisted of NiO as major phase. However, EDX

mapping and point analysis revealed some areas that were detected to be metallic Ni with significantly lower oxygen content compared to the surrounding areas (Fig. 6. 15c and d).

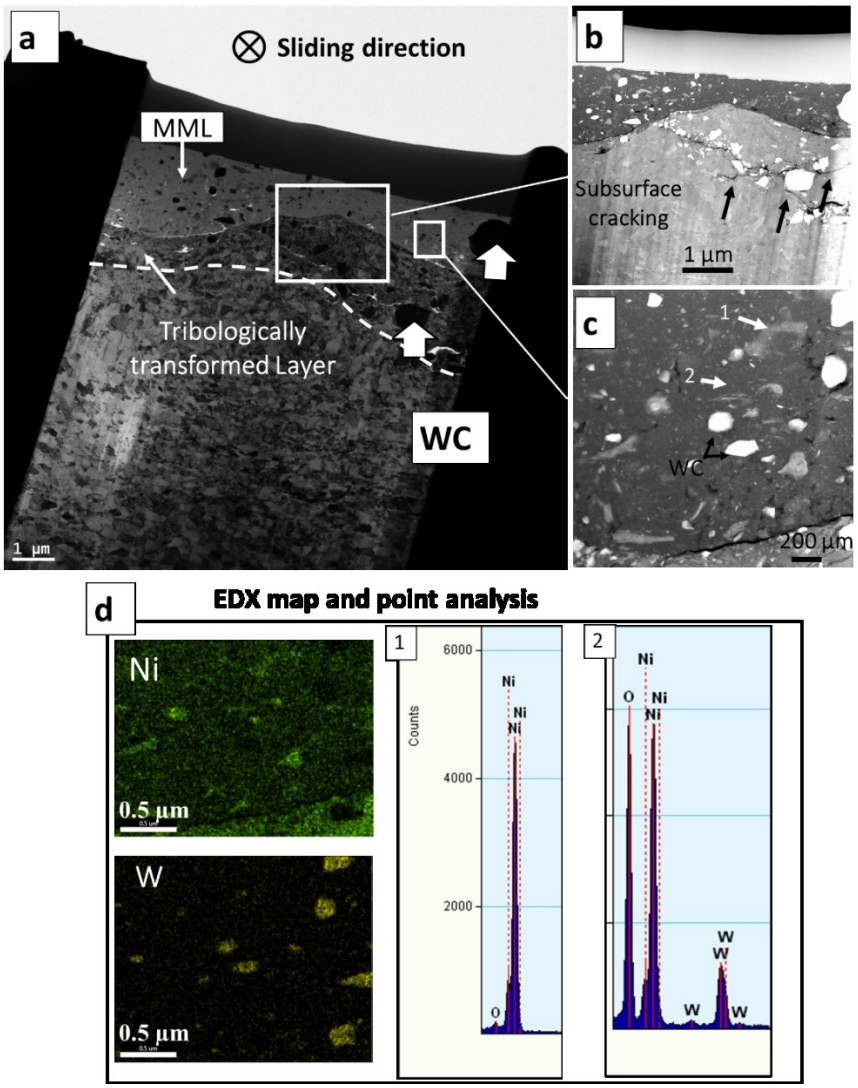

Fig. 6.15 (a) TEM images of Ni-30WCNi wear track surface cross-section (tested under 12 N), (b) upper inset shows HAADF image of tribologically transformed layer at subsurface of wear track, (c) lower inset shows HAADF image of WC distribution at MML, (d) EDX map of the region (c) and EDX point analysis of points 1 and 2 in (c).

Nanoindentation was performed on worn surfaces and on cross-section of worn surfaces. In order to identify the deformation degree in the subsurface region for Ni-28WC and Ni-30WCNi composites, nano-hardness profiles as a function of depth beneath the worn surface were obtained (Fig. 6. 16a and b). MML was only retained for some of the mechanical cross-sections. The

hardness values corresponding to top surface (depth zero) was extracted from top-surface nano-hardness measurements. For both coatings, the nano-hardness values on the worn surface were significantly higher than that of the unworn coatings. A large value of nano-hardness on the worn surface is due to the formation of MML. MMLs of Ni-28WC coatings was slightly harder than that of the Ni-30WCNi coatings. The hardness values showed a decreasing trend and stabilizes at some depths from the worn surface (Fig. 6. 16). These matched well with depths up to which the UFG layer (deformed zone) extended beneath the worn surfaces. For Ni-30WCNi, tested under both loads, hardness values reached the unworn value at depth of around 6 μm from the worn surface. Whereas, this was significantly lower (~3 μm) for Ni-28WC, indicating lower shear stresses transferred to the subsurface regions.

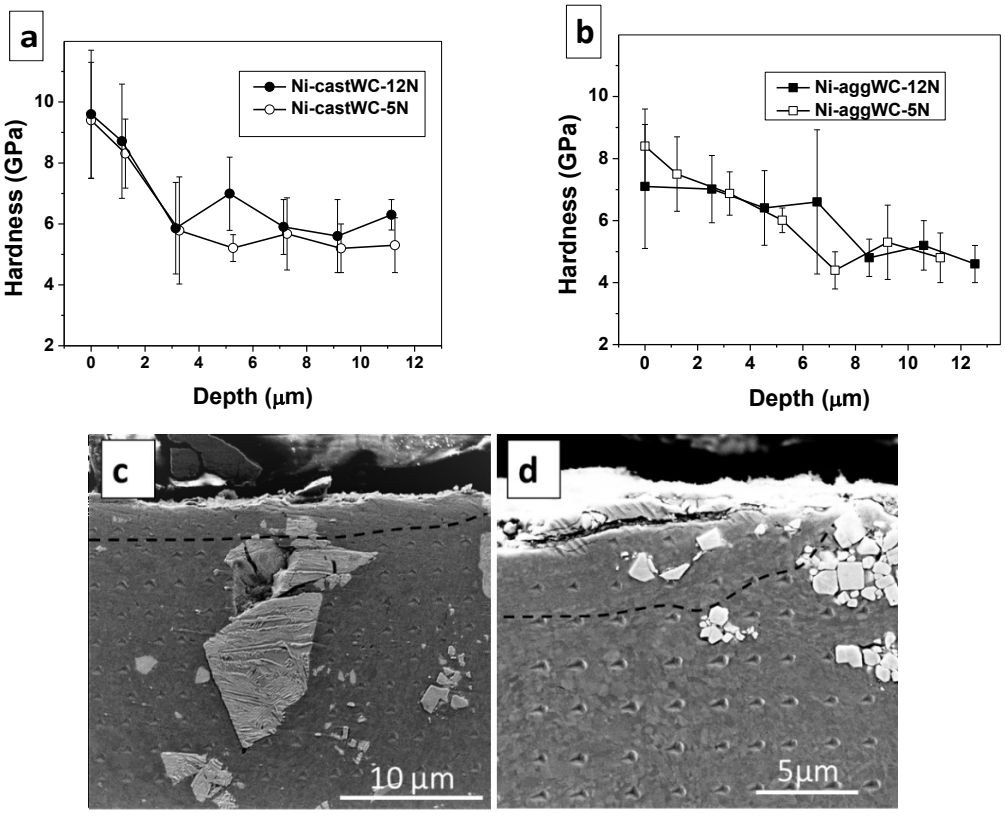

Fig. 6.16 Hardness of the MMLs and subsurface to worn surfaces of (a) Ni-28WC and (b) Ni-30WCNi coatings tested at 5 and 12 N. (c) and (d) SEM micrograph containing part of the nanoindentation matrix of Ni-28WC and Ni-30WCNi coatings, respectively, tested at 12 N. Dashed lines indicate sliding induced deformation layer.

6.4 Discussion

Deposition of MMCs with cold spray is becoming a viable process, with a wide range of coating systems studied including Ni-WC system. In order to retain high volume fractions of WC particles, researchers have turned to composite powders. Despite being commonplace, this could override tribological properties due to poor cohesive strength and/or poor morphology of ceramic particles. Therefore, for future tribological applications of cold sprayed MMCs, both process optimization and characterization of the tribological performance is required [58]. Two Ni-28WC and Ni–30WCNi coatings were cold sprayed using two different power types, namely cast WC and agglomerated WCNi, and then, subjected to dry sliding wear testing. Due to addition of WC, the hardness of the coatings was increased as compared to cold sprayed Ni coatings (345 ± 17HV1kg) tested in a previous study [145]. The addition of hard particles also densified the coatings. Lower MFPs between WC particles (8.5 ± 0.7 μm vs 31 ± 4 μm in Ni-30WCNi) and harder surface (431 ± 26 HV_{1kg} vs 390 ± 27 HV_{1kg} for Ni-30WCNi) for Ni-28WC coatings was observed. The morphology of WC particles was found to influence the friction and wear behavior of the coatings under the two tested loads, 5 and 12 N. CoF analysis combined with microstructural and chemical examination demonstrated that friction and wear behavior were controlled by the behavior of third bodies and the supporting role of WC particles, both of which was modified by the morphology of WC particles.

For Ni-30WCNi, adhesion of Ni to the counterface initiated upon sliding (Fig. 6. 7). Initial adhesion of coatings materials to countersphere led to pulling out of WC fragments (Fig. 6. 7). This could be due to decohesion of WC fragments along weak interfaces of porosities or Ni binder. De-bonding and pulling-out of WCNi particles from Ni matrix is another possible case. Adhesive wear created large wear debris (Fig. 6. 10), that were easier to eject from interface and contributed to high initial wear rates in Ni-30WCNi. This is supported by the observation of large debris at the ends of the wear tracks in initial cycles and high materials removal rates recorded. Some of the wear debris, generated at initial cycles at the contacting asperities may leave the tribological system and some may remain trapped between the mating surfaces and damage on both surfaces [151]. Higher load led to higher initial wear rate. Adhesive wear resistance of Ni-28WC was significantly enhanced due to harder surface provided by cast WC particles and lower MFP between them. Very less adhesive wear was observed on the worn surfaces of the Ni-28WC tested

under two loads. However, fine scratching marks was observed on both center and sides of the wear tracks (Fig. 6. 6). As some of WC fragments were observed on the surface and size of the abrasive marks implied, only fine WC particles were dislodged from surfaces (Fig. 6. 6). As reported by previous studies [147, 152], fine ceramic particles are more susceptible to be pulled out during the sliding process. Whereas, coarse particles are embedded deeply in the matrix and can be retained on the surface during wear test [147, 152]. Micro-ploughing in the direction of sliding along with light adhesion as the main wear initiation mechanism for Ni-28WC produced fine wear particle (Fig. 6. 6).

As shown by Raman spectroscopy (Fig. 6. 11a) and confirmed by the EDX analysis, for Ni-28WC coatings, oxidation of third-bodies started from early cycles. However, for Ni-30WCNi, longer cycles were needed for oxidation (Fig. 6. 11b). The rate of the oxidation is controlled by debris size and the density of surface defects. Easy adhesion and flow of materials in the Ni-30WCNi led to large wear particles with lower oxidation rate. Whereas, due to the harder surface in Ni-28WC, plastic deformation was localized in the interfacial region. This created dislocations and voids, which increased the rate of tribo-oxidation by providing routes for the presence of defects passage of oxygen ions [153]. The oxidation was also accelerated in small debris with higher relative surface area, which would increase the available surface energy [151, 153]. As sliding progressed, wear debris (metallic, oxide and carbides) were compacted between the sliding surfaces and developed progressively areas of wear-protective MMLs (Fig. 6. 8 and 9). Formation of MMLs has been frequently reported during sliding wear test of metallic and MMCs [130, 131]. Previous studies demonstrated that this not only reduced wear rate by recycling effect of wear debris, but also acted as hard protective layer for first bodies, since it consisted agglomeration of heavily deformed and oxidized wear debris [130, 131]. For the two coatings tested in this study, formation of MML was found to reduce the wear rate and caused a drop in CoF, as well. However, the rate of MML formation, its coverage on the surfaces, as well as its effectiveness in reducing wear and stabilizing of friction for the two coatings are influenced by the morphology of the WC particles. There are number of factors that favor the developing of MMLs and their stability. In Ni-30WCNi, large wear particles were easily ejected from interface. Those that stayed in the contact, behaved as in-situ elastic bodies and contributed to abrasive wear [154]. Whereas, for Ni-28WC, small debris were remained at interface, strain-hardened, fractured, and oxidized. The

adhesion force existed between small particles led to agglomeration and formation of protective MMLs to a higher coverage [131].

For both coatings studied here, the small WC fragments, with nano- to sub-micron size, were observed to be embedded into MMLs (Fig. 6. 8 and 9). These particles can be carried away when MML become unstable. In Ni-30WCNi coating, WC fragments are 0.3 - 1.3 µm size, smaller than "critical oxide thickness" (1-5 µm). Whereas, a multimodal distribution with a size ranges of 0.2 to 20 µm was established for Ni-28WC during cold spray deposition (Fig. 6. 9). Smaller particles are moved away when oxide layer is broken, whereas large WC particles stand exposed in the interface and reinforced metallic materials from severe wear damage (see Fig. 6. 17). No pulling out of coarse WC particles were observed, although they are only mechanically bonded to the matrix. Examination of cross-sections of the wear surfaces also revealed that MML thickness was higher (~2.4 µm), when it is supported by coarse WC particles (Fig. 6. 14a). It may imply that supporting effect of hard coarse particles to oxide film make it stable at higher thickness, i.e. increasing "oxide critical thickness". MMLs formed on Ni-28WC coatings were found to be more effective in reducing wear when compared to that formed on Ni-30WCNi coatings (see Fig. 6. 17).

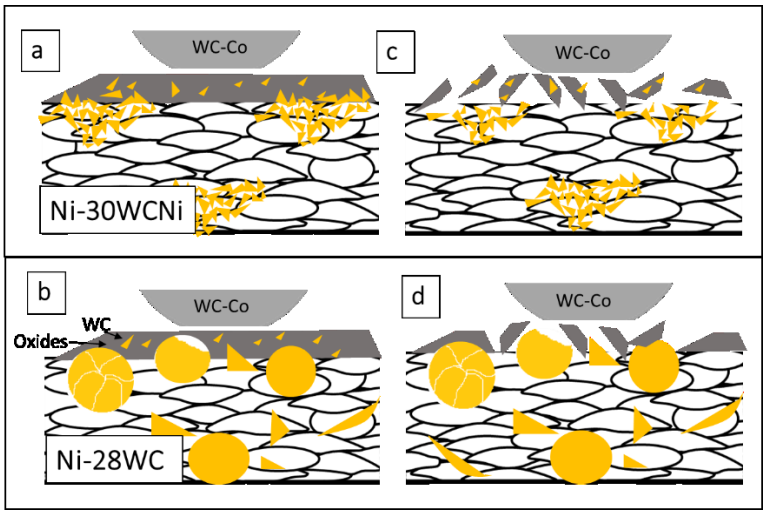

Fig. 6.17 A schematic showing MML development in the presence of agglomerated WCNi in (a) Ni-30WCNi and cast WC in (b) Ni-28WC; WC fragments are drawn by the oxide when it breaks up to form wear debris in Ni-30WCNi; large WC particles remain in place when the oxide breaks up in Ni-28WC.

For both coatings, as revealed by electron diffraction on the cross section of wear surfaces, NiO is dominating phase in the MML. Since it is less Raman active than Co/NiWO4 and WO_3 a weaker peak was obtained in Raman spectra. Chemical analysis of the MMLs on the worn surfaces was performed by Raman spectroscopy, as it showed for both coatings formation of tribochemical phases of WO_3 and Co/$NiWO_4$ (Fig. 6. 11). Previous studies [150, 155-157] reported formation of these phases during room and elevated temperature sliding of Ni-WC coatings. It is proposed that Co/$NiWO_4$ form due to interfacial mixing of Co/NiO and WO_3 during sliding. Raman analysis revealed that MML of Ni-28WC contained higher amount of Co/$NiWO_4$, whereas MML of Ni-30WCNi mainly consisted of NiO and WO_3. While for Ni-30WCNi, some regions inside MML with significantly low oxygen content was detected in the cross-section of wear tracks. This, along with large flakelike particles observed on the wear track (Fig. 6. 10) and counter-body (Fig. 6. 12), also implied that the particles didn't get sufficiently oxidized before they are dislodged from the sliding surfaces. Moreover, cracking was observed due to large shear stress transferred to subsurface regions, which imply low load-bearing capacity of both MMLs and subsurface. The intersection of these cracks led to detachment of wear particles by delamination process. The hard particles detached from MML, which were frequently observed in Ni-30WCNi tested under 5 N, acted as third-bodies abrasive particles which induced wear on sliding surfaces and resulted in increased wear rate and unstable CoF. Higher wear rate was recorded for Ni-30WCNi at 12 N. Although some cracks were observed on the MMLs surfaces and cross-sectional view of Ni-30WCNi at 12 N, however, smooth MMLs and significantly lower amount of wear debris along with a high initial wear rate inferred that most of the wear occurred during initial sliding cycles. At subsequent sliding cycles, the higher frictional heat generated under high load resulted in a temperature rise in the contacting regions, and hence, sintering the debris. Increasing normal load can promote mechanical mixing effects on entrapped particles, and then boost the oxidation process, as well.

6.5 Conclusion

The major conclusions resulting from the work presented in this paper are,

1- Ni-based composite coatings using cast WC exhibited a superior wear resistance when compared to that using agglomerated WC. A more stable CoF was attributed to rapid formation of stable MMLs on the worn surfaces of Ni-28WC coatings.
2- Cast WC particles, with lower MFPs between them in Ni-28WC, were more effective in resisting Ni against plastic deformation and adhesive wear.
3- The presence of relatively large WC particles in Ni-28WC, which were remained in coating during sliding, led to higher coverage of worn surfaces with more stable MMLs, with reducing shear stress transferred to the subsurface regions.
4- For both coatings, a nano-crystalline MML consisting of NiO, WO_3, $NiWO_4$ was observed on the worn surfaces. The presence of low oxygen regions inside MML in the Ni-30WCNi indicated its shorter sliding duration and lower stability.
5- Ni-28WC was wear resistance under the two tested loads. Whereas, higher wear rate for Ni-30WCNi at 12 N was attributed to intense adhesive wear in initial cycles.

Acknowledgments

The authors gratefully acknowledge the financial support from the Canadian Foundation for Innovation (CFI) project No. 8246 for the cold spray equipment, the CFI Leader's Opportunity Fund project No. 13029 for the tribometer and nanoindentation equipment, and the Natural Sciences and Engineering Research Council (NSERC) Strategic Grants Program for the operational funding of this project. Thanks, are also due to Tekna Inc for providing the Ni and spherical WC powders. The authors acknowledge administrative support from Drs. Phuong Vo, Eric Irissou and Jean-Gabriel Legoux and technical support from Mr. Jean Francois Alarie at the McGill Aerospace Materials and Alloy Design Center (MAMADC) cold spray facility at NRC-Boucherville.

Chapter 7

Erosive wear behavior of Cold-Sprayed Ni-WC composite coating

Sima Alidokht, Phuong Vo, Steve Yue, Richard R. Chromik

Adapted from a paper of the same title published in *Wear*, 2017. **376-377**: p. 566-577.

Abstract

The effect of WC on cold spray deposition and erosive wear performance of Ni-WC composite coatings was studied. WC and Ni powders were fed to the gun from separate hoppers and a blend of Ni-36vol.% WC was sprayed onto mild steel substrates. By using three different WC powder sizes, the effect of WC size on coating build-up and WC retention were tested. Using smaller size WC particle, higher retention of WC into coating was achieved. Using macro-indentation, a relationship between mechanical properties and content of WC was studied. Detailed microstructural analyses and wear loss measurements were conducted to study mechanism involved in solid particle erosion (SPE) of Ni and Ni-WC coatings. One of the Ni-WC coatings with highest WC retention (10.5vol.% WC) was selected for SPE studies. Both Ni and Ni-WC coatings exhibited ductile erosion. Higher erosion resistance of coatings under normal angle compared to oblique angle was related to the formation of a protective MML. It was found that 10.5vol.% WC content was too low to reinforce Ni against erosion under oblique angle. However, under a normal angle, the addition of 10.5vol.% WC deteriorated Ni erosion resistance, by preventing MML formation and the brittle fracture.

7.1. Introduction

Solid particle erosion (SPE) occurs when hard solid particles are entrained in the fluid and strike the surface. This type of material removal is a serious problem in many engineering systems,

including aircraft engines, steam and jet turbines, and pipelines [158, 159]. Erosion of compressor blades in the first stage of the aircraft engine is common, which is due to sand particles entrained in air. This can deteriorate aerodynamic performance and even structural integrity of blades [158]. Power-generating steam turbines are another example of engineering systems affected by erosive wear, where iron oxide scales from steel heaters are fragmented into approximately 100 μm particles and cause erosive damage of turbine blades and other components [159]. Many studies have been conducted to understand materials loss mechanisms during SPE and develop protective coatings to increase component lifetimes. In SPE, contact stress arises from the kinetic energy of particles, which is controlled by particle velocity, impact angle, and particles size. Particles kinetic energy is partially dissipated by plastic deformation and/or brittle fracture [158, 159]

SPE behavior of materials can be classified as ductile or brittle. Material removal by plastic deformation (ploughing or cutting) is the characteristics of ductile erosion; whereas brittle erosion of materials is characterized by crack initiation, propagation and intersection. The mechanisms by which materials are eroded depend on operational conditions and surface and erodent particles properties [2, 83]. The erosion rate dependence on the impact angle for ductile and brittle behavior is different. Ductile erosion behavior, such as for metals and polymers, presents maximum erosion rate at low angles of incidence, while for brittle materials, such as ceramics, a maximum of material loss is at a normal angle of incidence [2]. In real applications, erodent particles impinge surfaces at a wide range of angles. Therefore, neither metallic materials nor ceramic are the best choice for erosion resistant coatings [2, 83, 158, 159]. In order to decrease erosion damage, it is necessary to have a balance of high hardness and adequate fracture toughness. For this reason, more attention has been paid to metal matrix composites (MMCs), which consist of hard particles embedded in a tough metal binder, to control and minimize the wear. In this regard, in order to apply these coatings over components, a variety of techniques have been used in surface engineering including laser cladding and thermal spray processes as most widely employed [21, 110, 111]. Ni-based coatings are widely applied where wear resistance combined with oxidation or hot corrosion resistance is required [9, 109]. Previous studies showed that the wear resistance of Ni coatings can be greatly improved by incorporation of refractory carbides such as WC, WC-Co, TiC, and Cr_2C_3 into the metallic matrix [21, 110, 160].

Among the different coating deposition techniques, laser cladding has been widely employed to deposit Ni-based composite coating. Using laser cladding, although a very good adhesion of coating to the substrate as well as low porosity can be obtained [13, 39, 127-129], a non-homogenous distribution of reinforcing particles was reported, especially in the case of WC, which tends to precipitate and concentrate at the bottom of the coating [13, 39, 127]. Moreover, higher laser power is needed in order to obtain thicker coatings and higher concentration of ceramic particles. This results in unwanted chemical changes, formation of brittle phases and significant residual stress. Erosion behavior of Ni-WC coatings has not been widely reported. However, the presence of the brittle phases at interfaces is reported to provide preferential crack paths and increase wear rate [13, 39, 127].

Cold spray is a solid state thermal spray process where particles are accelerated in a de Laval nozzle to supersonic velocities (500–1200 m/s) in a gas stream and impact onto a substrate. Gas temperature is often much lower than the melting points of the particles. Besides, particles remain in solid state due to quite short contact time with the high-temperature gas. Hence, high-temperature-induced decomposition of carbides and/or other phase transformations that could be detrimental for tribological performance can be avoided. Furthermore, impact-induced high strains and the heat generated in this process may cause partial or complete recrystallization and evolution of ultra-fine microstructure [19, 20, 73]. Several studies were conducted to fabricate hard composite coatings by cold spray. It was found that pretreatment powder processing such as metal cladding on ceramic particles [78] and sintering [22] can help the retention of ceramic particles to the coating. However, achieving high content of ceramic particles using a blend of two powders still remains a challenge, which arises from non-deformability of hard ceramic particles. Little attention has been given in the literature to the mechanisms of hard particles retention to a coating and the effect of the cold spray and powder parameters. In the present study, cold spray deposition was utilized to fabricate Ni-WC composites. The cold spray behaviors of Ni and WC were studied using unmodified powders with no additional processing routes. The effect of WC and its size on coating formation, deposition efficiency, and hardness of Ni were investigated. For the two Ni and Ni-WC coatings, SPE tests were conducted and the role of WC on SPE behavior of coating was studied.

7.2. Experimental

7.2.1 Cold spray formation and Coating Characterization

Grit-blasted mild steel plates with thickness of 3 mm and roughness of 7.6 ± 0.6 µm were used as substrates. Commercially pure water atomized Ni (Novamet, Canada) and plasma spheroidized WC (Tekna, Canada) were used as feedstock powders (Fig. 7.1). Laser particle size analysis (Horiba, Japan) was used to measure feedstock powder size distribution. Three different particle sizes of WC, -45+15 (d_{50} = 40 µm), -38+25 (d_{50} = 30 µm), and -25+10 µm (d_{50} = 15 µm), were tested. Ni powders had particle size range of -10+4 µm (d_{50} = 7 µm).

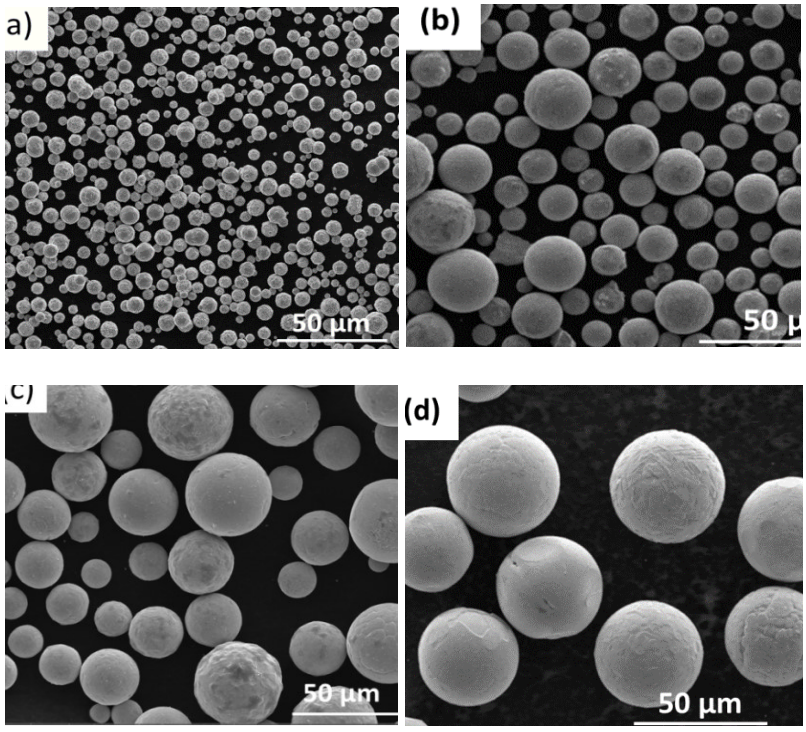

Fig. 7.1 Morphology and size distribution of the as-received powders: (a) Ni, (b) -25+10, (c) -38+25, and (d) -45+15 µm WC powder.

Cold spray was conducted using a PCS-1000 system (Plasma Giken, Japan) with nitrogen as the carrier gas. The cold spray unit utilized a de Laval nozzle made of WC-Co. Prior to entering the nozzle, the gas pressure was 4 MPa and temperature was 700°C. The stand-off distance between the substrate and nozzle exit was set at 40 mm, and the gun traverse speed at 30 mm/s.

The particle velocities were measured in a free-jet by a time-of-flight particle diagnostic ColdSprayMeter (Tecnar, Canada). The WC and Ni powders were fed to the gun from separate hoppers. The powder feeder systems were a custom install done by the gun manufacturer, Plasma Giken. By setting feed rates of Ni and WC on 1.25 and 0.5 rpm, respectively, a mixture of Ni-36vol.% WC was sprayed. The co-feeding system was used to avoid problems arising from the difficulty in admixing powder of differing densities and/or damage to powders due to mechanical mixing. Cold-sprayed coatings were cross-sectioned perpendicular to the gun traverse direction, mechanically ground, and polished using 9, 3 and 1 μm diamond pastes followed by 0.05μm colloidal silica. The morphology and microstructure of the initial powders and deposited coatings were observed by SEM (FEI, Quanta 600, USA). WC and porosity concentration within the coatings measured by image analysis of pixel count using ten random images of polished cross-sections taken with SEM. Deposition efficiency was calculated as the weight gain divided by the mass of powder sprayed, which is the product of feed rate and spray time. In order to obtain an average hardness value of the composite, a large load on a micro-hardness tester was used. Macro-indentation was performed on top polished surfaces. With 49 N, the diagonal of indent was 130-160 μm and many WC particles were encountered with indents.

7.2.2 Erosion test

SPE tests were carried out using a custom-built gas-blast erosion system based on the specifications of ASTM standard G76 [102]. Prior to erosion tests, top surfaces of coatings were mechanically ground, and polished using 9, 3 and 1 μm diamond pastes followed by 0.05 μm colloidal silica. Angular Al_2O_3 particles of 20-70 μm size (Fig. 7.2) were used as erodent particles. Hardness of the Al_2O_3 particles was measured by nano-indentation test performed using a Berkovich diamond tip with a Triboindenter system (Hysitron, Minneapolis). Back pressure of the abrasive blasting unit was adjusted in order to control particle velocity and its dependence on back pressure was tested using a double-disk time-of-flight technique. A particle velocity of 60 ± 6 m/s was obtained using 69 kPa air pressure in the nozzle. The particle feed rate was determined by altering the unit's shaker amplitude and the back pressure. The erosion test unit was turned on for a few minutes while the sample was shielded by a covered shutter, in order to stabilize the feed rate. Once feed rate was stabilized at 0.8 ± 0.1g/min, the test was started. The erodent powder was filled into the hopper and fed to a tungsten carbide nozzle with an inner diameter of 1.14mm and

a length of 36 mm. Working distance between the sample holder and the nozzle was kept constant at 20mm.

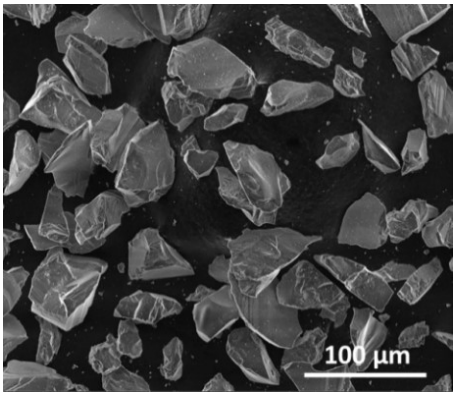

Fig. 7.2 Morphology of erodent Al_2O_3 particles.

The impact angle was adjusted by turning the sample holder at two different angles of impingement (30 and 90°). All erosion tests were performed at room temperature and 25% relative humidity until steady state erosion was reached. At least three repetitions were made per experimental condition to evaluate the experimental error of the measurement. Before and after the test, samples were cleaned in acetone, dried, and weighed using an analytical weight balance with an accuracy of 0.01 mg. Before weighing, Al_2O_3 particles were removed from the eroded surface by air blasting. The erosion rate was calculated by normalizing the measured weight loss by the mass of erodent particles causing weight loss (i.e., testing time×particle feed rate). The above procedure was repeated until erosion rate reached steady state erosion rate, a constant value independent of mass of erodent particles or erosion time. Steady-state erosion rates were converted into volume wear rate to take into account the different densities of the coating materials. Linear rule of mixture was used to calculate density of the coatings. In order to reveal erosive wear mechanisms, eroded surfaces and cross sections of wear scars were inspected using an SEM (FEI, Quanta 600, USA).

7.3 Results

7.3.1 Cold-sprayed coatings

Table 7.1 summarizes coatings' deposition efficiencies and thicknesses, WC in initial feedstock and in the coating, and porosity and micro-hardness of the coatings. Figure 7.3 shows micrographs of cross-sectioned Ni and Ni-WC composite coatings. Ni particles have been accelerated to an average velocity of 650 ± 125m/s (Table 7.2) and deposited onto mild steel substrate. 55% of sprayed Ni particles were recovered during coating to form a thick and relatively dense Ni coating with 1.40 ± 0.03 mm thickness and porosity of 3.8%. Adding WC into the initial mixture resulted in lower deposition efficiency, due to low retention of the hard WC phase. Feed rate of Ni particles was kept the same in both Ni and Ni-WC coatings; hence, the thickness reduction in Ni-WC sprayed coatings implies a decrease in deposition efficiency of Ni as WC was added to the initial feedstock. This can be due to WC fragments which avoid close contact between previously deposited and impacting Ni. Overall deposition efficiency and thickness of Ni-WC coating was greater using WC of -38+25 μm size than those using the two other size ranges. A reduction in deposition buildup of metallic phase with adding ceramic particles to initial feedstock has been reported in previous studies [65, 73]. However, in a few studies [66, 67], the positive effect of ceramic particles on coating growth was reported that might be related to roughening, cleaning, and activation effects of the ceramic particles.

Table 7.1 Characteristics of cold-sprayed coatings. Scatter bar on microhardness and thickness values indicate the standard deviation of 20 repeat measurements.

Sample designation	DE (%)	Thickness (mm)	WC in coatings (vol.%)	Porosity (%)	Micro-hardness(HV_5)
Ni	55 ± 3	1.40 ± 0.03	-	3.8 ± 0.5	368 ± 8
Ni-WC (-45+15 μm)	12 ± 4	0.56 ± 0.04	5.4 ± 0.7	0.9 ± 0.1	322 ± 11
Ni-WC (-38+25 μm)	22 ± 4	1.01 ± 0.01	10.5 ± 0.9	1.1 ± 0.2	378 ± 18
Ni-WC (-25+10 μm)	20 ± 5	0.93 ± 0.09	9.5 ± 0.5	1.7 ± 0.2	343 ± 16

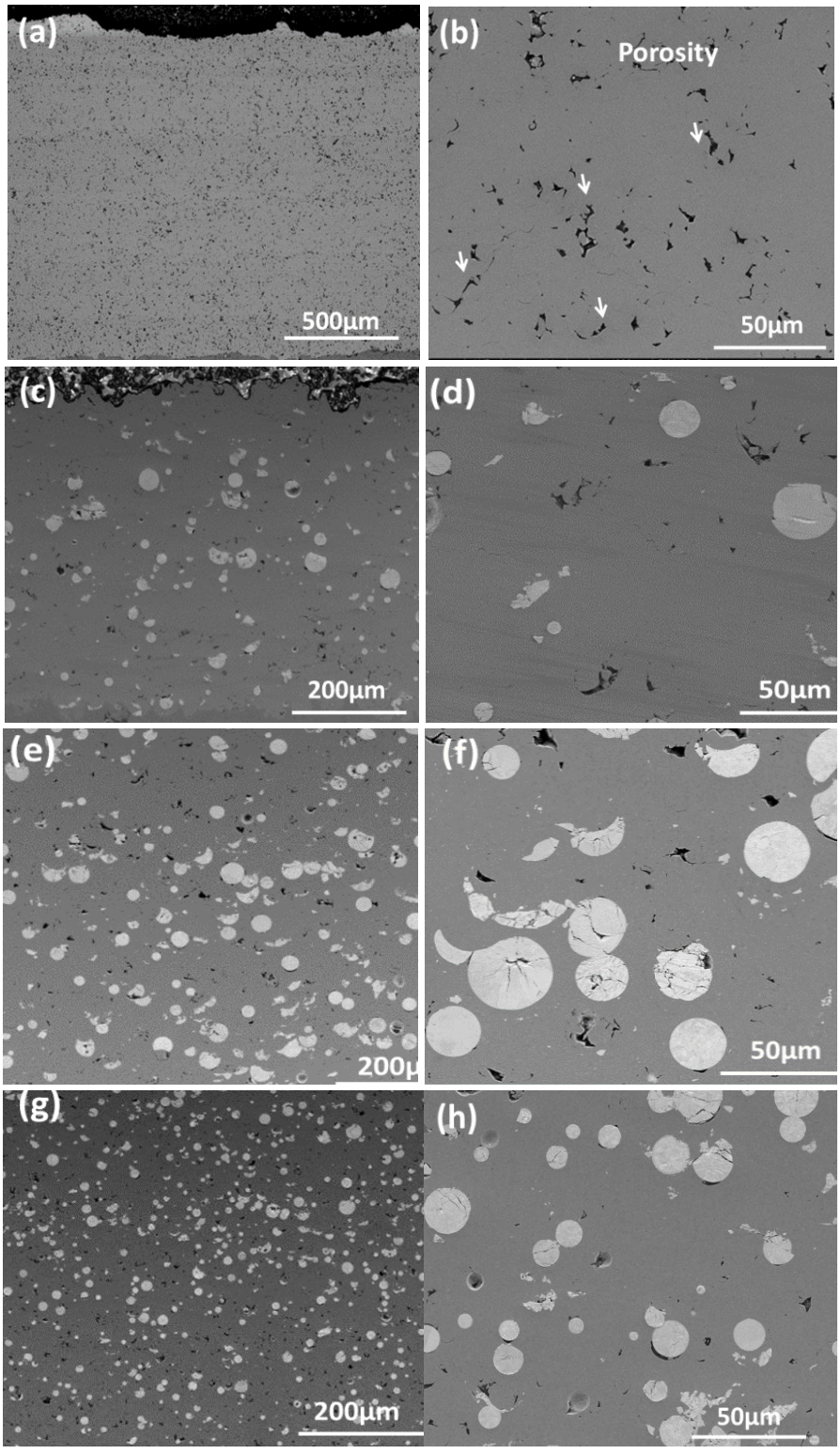

Fig. 7.3 SEM micrographs showing cross-section morphology of (a) Ni, (c) Ni-WC (45+15 µm), (e) Ni-WC (-38+25 µm) and (g) Ni-WC (-25+10 µm). (b), (d), (f), and (h) high magnification views of (a), (c), (e), and (g), respectively.

Table 7.2 Velocities of different particles in gas stream under tested spray condition.

Powder	Velocity (m/s)
Ni	650 ± 125
WC (-45+15 μm)	484 ± 78
WC (-38+25 μm)	520 ± 73
WC (-25+10 μm)	627 ± 135

Figs. 7.3c-h shows micrographs of cross-sectioned Ni-WC composite coatings. The particles in bright contrast correspond to WC particles and regions in dark contrast correspond to porosities. As can be seen, most of the retained WC particles are smaller particles (< 30 μm). As shown in a higher magnification view of the cross sections, some of the WC particles were cracked or fragmented upon impact. Comparing WC fractions in the coatings, the finer the WC particles, the higher velocity (Table 7.2) they can attain. However, even though too fine particles may achieve high acceleration velocity, they will eventually lose it afterward due to shock waves near the substrate [73]. This is the possible reason why, with WC of -25 μm size, WC retention to the coating wasn't improved. Similar results were reported by Koivuluoto *et al.* [73], where retention of Al_2O_3 to coating was higher using Al_2O_3 powder size of -45+22 than that of -90+45 μm. However, due to bow shock effect, smaller Al_2O_3 particles (-22+5 μm) resulted in coatings with lower amount of Al_2O_3 particles compared to a particles size of -45+22 μm.

As can be seen from the top-view image of the Ni-WC composites in Fig. 7.4, most of the WC particles bounced back after impacting the surface and left behind empty craters. A few particles penetrated deeply to the surface (see Fig. 7.4b). The ratio of embedded particles to empty craters was significantly lower than the actual WC concentration recovered in the coating (measured from polished cross-sections). This was probably because of high hardness of Ni and low velocity of dense and relatively large WC particles [135]. Therefore, during Ni-WC composite coating build up, WC particles were mainly entrapped in the coating by later-arriving Ni and WC particles, in which Ni particles deformed and surrounded WC particles [72]. There were also a large number of fine fragmented WC particles which can be observed on the top surface (Fig. 7.4c).

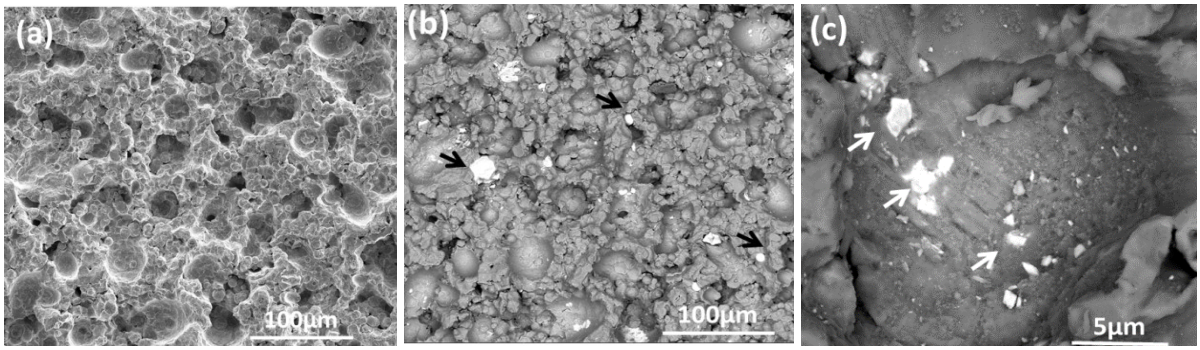

Fig. 7.4 SEM micrographs showing top-down morphology of the Ni-5.4vol.% WC coating, (a) secondary electron image showing empty craters, (b) Backscatter electron image showing adhered WC particles, and (c) high magnification view. Black arrows indicate WC particles adhered to the surface. White arrows indicate WC fragments.

Ni-WC composite coatings were less porous than Ni coating. Lower porosity of cold-sprayed Ni-WC composite coatings compared to Ni coating was due to continuous high-velocity impact of dense WC particles, which produced the tamping effect, and results in densification of deposited coatings. Micro-hardness tests were conducted on top surfaces of cold-sprayed Ni and Ni-WC coatings and the results were reported in Table 7.1. Higher hardness in the Ni-10.5vol.% WC composite coating is due to the relatively uniform dispersion of the hard WC particles and densification. However, hardness improvement is not significant, probably due to decreased bonding between Ni particles and fragmented/cracked WC particles. Ni-WC coatings using WC of -45+15 and -25+10 µm showed lower hardness than that of the Ni coating. This can be attributed to extensive fragmentation of WC and weak inter-splat bonding of Ni in Ni-5.4vol.% WC and higher porosity in Ni-9.5vol.% WC coating, respectively.

7.3.2 Solid particles erosion

7.3.2.1 Solid particles erosion rates

SPE tests were conducted on Ni and Ni-WC coatings with highest WC content (10.5vol.% WC). The erosion rates for Ni and Ni-WC composite coatings versus test duration were illustrated in Fig. 7.5. The volumetric steady-state wear loss was also presented in Fig. 7.6. At 30° impact angle, for Ni coating, the erosion rate was initially low, after which it increased and reached steady

state. For Ni-WC coating, erosion rate values did not change much with time. At normal angle, the erosion rate curves followed the same forms as reported in previous studies for ductile steels at 90°, in which steady state was approached after initial low erosion rate.

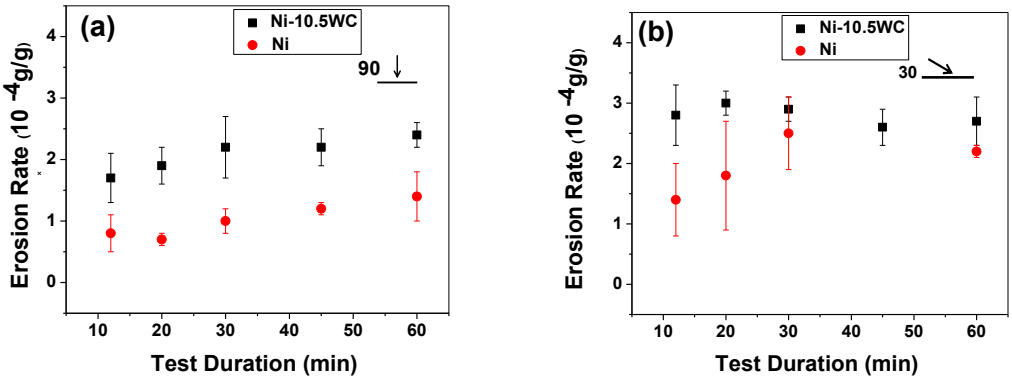

Fig. 7.5 Variation of erosion rate with erosion time for Ni and Ni-10.5vol.% WC coatings under (a) 90° and (b) 30° impact angle. Scatter bars indicate the standard deviation of 6 repeat measurements.

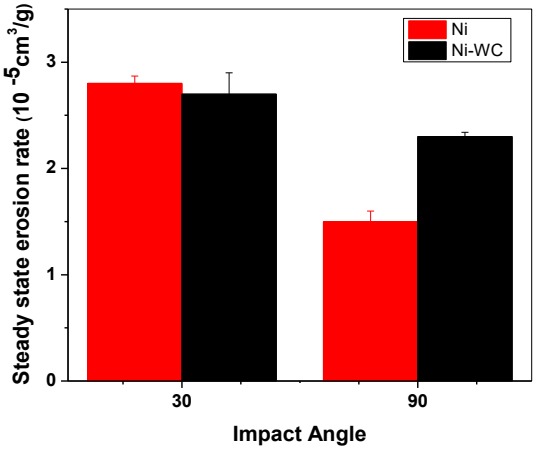

Fig. 7.6 Histogram illustrating the steady state volumetric erosion rate of Ni and Ni-10.5vol.% WC at different impact angles.

The steady-state erosion rates at two impact angles were compared in Fig. 7.6. For the Ni coating, the steady-state erosion rate at 30° was higher than that at 90°. This is characteristic of

ductile erosion, in which materials removal predominantly takes place by plastic deformation. Although Ni-WC coating exhibited ductile behavior as a function of impact angle, the difference in steady-state erosion rates at 30 and 90° was marginal, and therefore, it may not be conclusive in predicting the ductile or brittle angular dependence of erosion. As reported by Hutchings *et al.* [2] and Sundararajan and Roy [161], angular dependence of erosion is not a materials characteristic alone. It also depends on erosion conditions, and hence, the terms ductile and brittle should be used with caution. As depicted in Fig. 7.5a and b, although Ni-10.5vol.%WC is slightly harder than the Ni coating, its erosion resistance at 30° is initially lower. At longer erosion duration, steady state erosion rates for the two coatings approached the same value. Under normal impacts, for all test durations, Ni exhibited higher erosion resistance.

7.3.2.2 Worn surface analysis

To investigate the surface damage due to Al_2O_3 particles erosion, worn surfaces were analyzed by SEM. Micrographs were presented in Figs. 7.7 and 8, for 90 and 30° impact angles, respectively. For both coatings, under the two tested angles, worn surface morphologies exhibited materials removal by cutting and ploughing actions and also features associated with crater and lip formations. This implies characteristic features typical for ductile erosion, which is consistent with the angular dependence of erosion rates.

At normal impacts, it was found that at most of the craters, rather than cutting and scooping a chip out of the surface, the crater edge was pierced deep into surface and the displaced materials extruded (ploughing) and formed a lip (Fig. 7.7b and c). However, at oblique impact, the features associated with cutting and scooping chips out of the surface are dominating. It was found that although lips remained attached to the surface at the periphery of the scars and at some central region, most of them were detached under successive impacts of erodent particles, in the form of platelets. Moreover, deformation scratches (Fig. 7.7b and c), as indications of plastic deformations and materials removal, were detected at higher magnification. SEM micrographs revealed that fragmented Al_2O_3 particles were embedded into the surface (Fig. 7.7b). Embedded Al_2O_3 particles, which were more frequently imaged on 90° eroded surfaces than 30°, may impart a shielding effect against further material loss and contribute to the angular dependence of erosion rate. It was found that the ratio of erodent particles' hardness to target's hardness has a controlling effect on the

erosion performance of the materials. As reported by Hutchings [2], erodent particles of any size and shape, with hardness ratio of $H_{erodent}/H_{target}>2$, can cause plastic deformation and penetration of targets surfaces. Al_2O_3 particles, used as erodent in this study, have an average hardness of 13.4 ± 0.3 GPa, and the ratio of H_e/H_t is 3.8-4.2, approximately. This causes Al_2O_3 particles to penetrate and embed into the surface. The embedding of erodent particles has been also reported in previous studies [2, 111], where silica particles were embedded on eroded steels and Ni alloys.

In some of the craters, steps were observed (Fig. 7.7b) on the underside of the lips. Moreover, cracks (Fig. 7.7c) were observed passing into, and causing removal away of, the lips. Deformation shear bands, within which the deformation is localized at a high strain rate, are reported to cause cracking and assist detachment of lip material. Strain localization is believed to be due to thermal softening of the metal. The degree of thermal softening and localization of the shear stress is determined by thermo-mechanical properties of materials and hence, it is an important factor in controlling the erosion resistance [162-164]. Evidence of successive impacts and forging on extruded lips were also found which leads to flattening of the lips and causes platelet formation (Fig. 7.7c) and subsequent fracture [162, 163].

Similar eroded surface morphologies and removal mechanisms were observed in Ni-WC composite coatings. Upon impact of Al_2O_3 particles on WC particles, because of the very limited deformability of the latter, the kinetic energy of striking particles was mostly dissipated through crack initiation and propagation (Fig. 7.7d and f). Several types of cracking, which are analogous to those seen during indentation of brittle surfaces, were observed during erosion of brittle materials [165]. Radial and lateral cracking were observed on WC particles due to erodent particles impacts. A significant volume of material was detached from the surface when intersection existed among several lateral fractures.

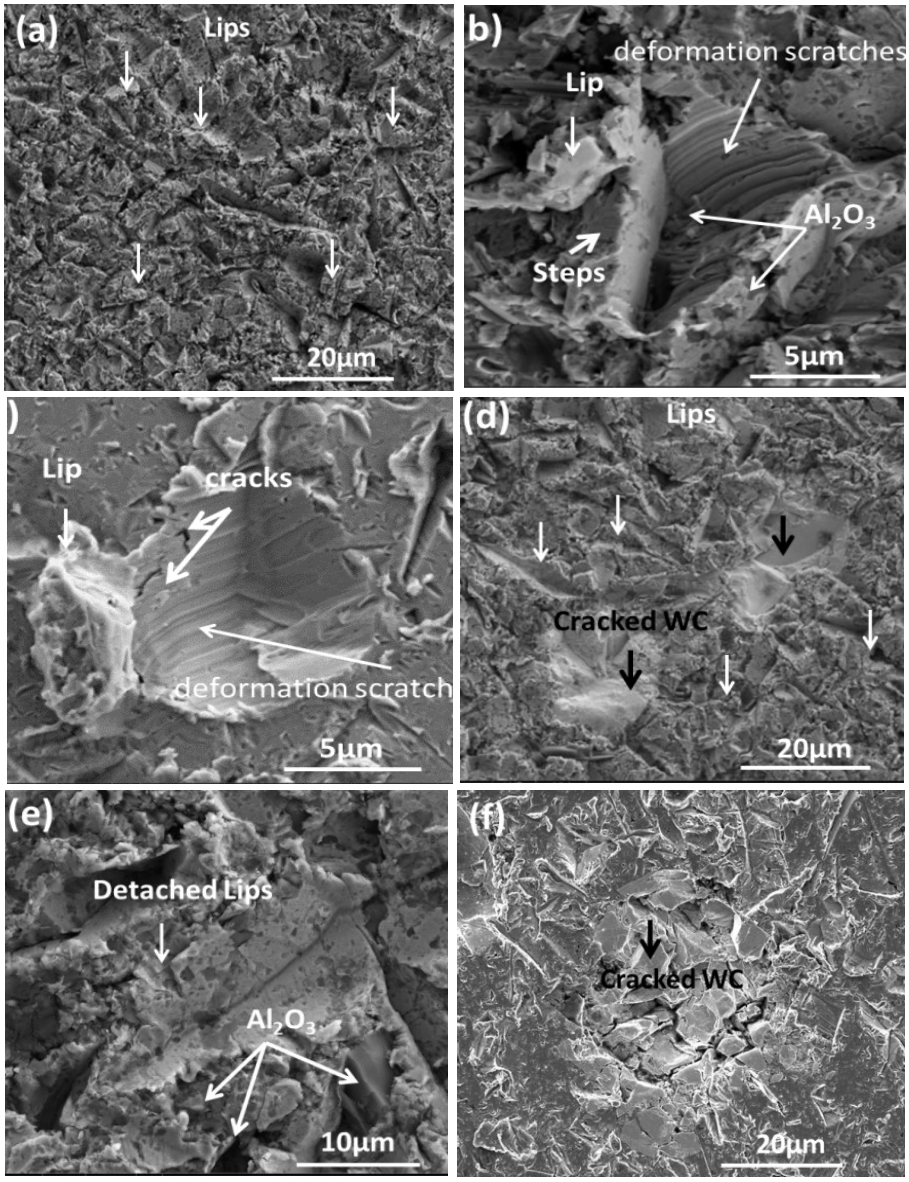

Fig. 7.7 SEM micrographs showing the eroded surface morphology of (a),(b), and (c) Ni, (d), (e), and (f) Ni-10.5vol.% WC coatings under 90˚ SPE impact angle.

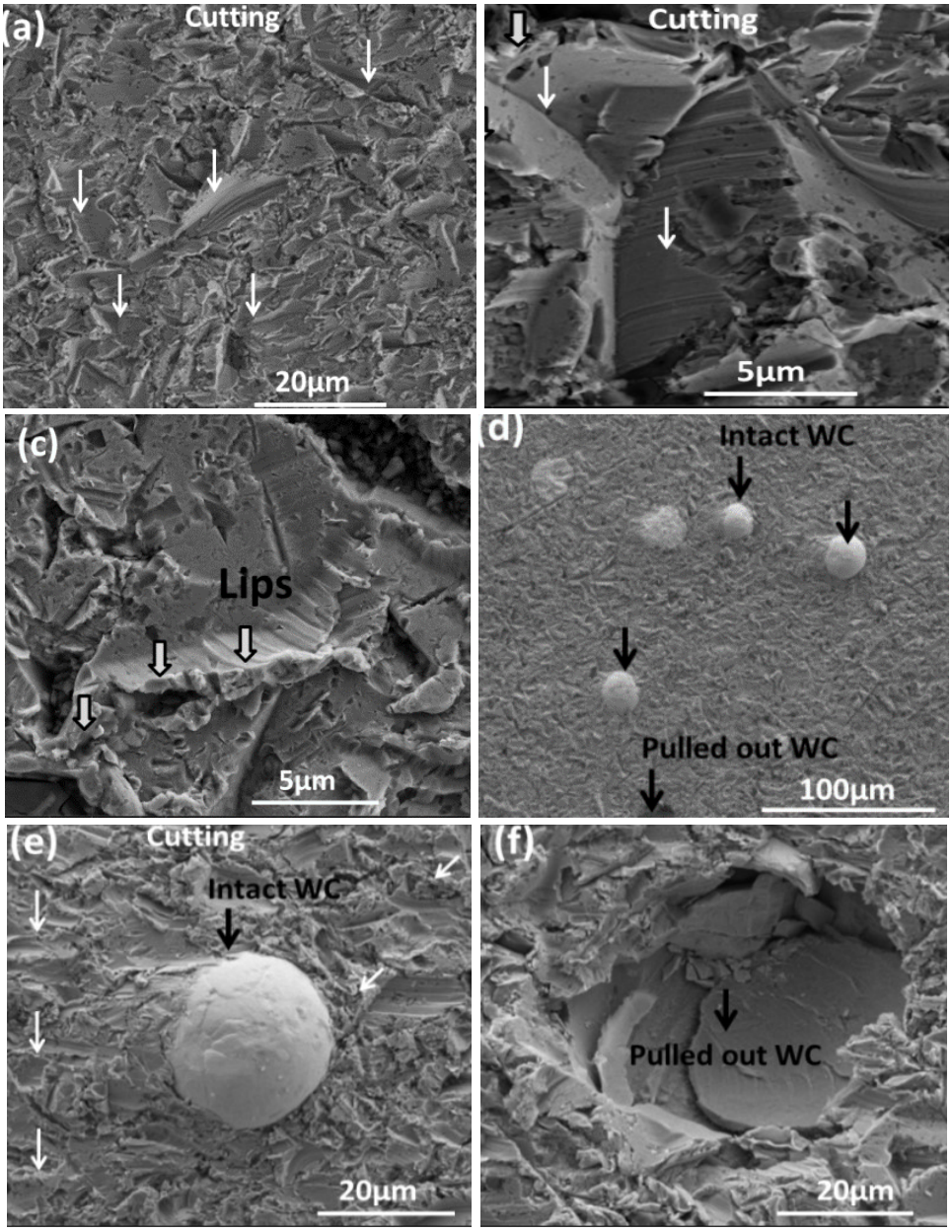

Fig. 7.8 SEM micrographs showing the eroded surface morphology of (a),(b), and (c)Ni, (d), (e), and (f) Ni-10.5vol.% WC coatings under 30° SPE impact angle. White arrows indicate cutting.

At oblique impact angles, lips were observed at the end of erodent particle exits (Fig. 7.8), whereas under normal incidence, lips were formed along the periphery of craters (Fig. 7.7). Most of the craters were oval shaped at oblique impact and pyramidal at normal impacts. The size of the craters was larger in the case of oblique impacts compared to those of normal impacts, suggesting higher erosion rates for oblique angle erosion. Similar erosion morphologies and removal

mechanisms were observed under oblique impacts of erodent particles. However, as mentioned before, micro-cutting dominated at oblique impacts while indentation induced plastic deformation and lip formation dominated at normal impacts. For the Ni-10.5vol.%WC composite coating, severe wear of Ni adjacent to WC particles was observed while WC particles remained intact. In fact, very limited evidence of cutting of WC was found. However, the removal of Ni matrix phase was followed by WC pull out.

7.3.2.3 Subsurface microstructural and deformation analysis

To study the microstructural evolution due to impact of erodent particles, cross sections of the erosion scars were examined using SEM. Figures 7.9 and 10 show the subsurface microstructures of Ni and Ni-10.5vol.% WC coatings after 60 min exposure to normal and oblique erosion, respectively. Erosion-induced microstructure consisted of a tribolayer or mechanically mixed layer (MML) and slightly relaxed microstructure due to dynamic recrystallization (DRX). MML appeared as islands, in which Al_2O_3 fragments and ultrafine grains (UFG) and large grains (LG) with lamellar structure were mixed (Figs. 7.9 and 10). Highly elongated grains with large aspect ratio were formed (Fig. 7.10b). At high magnification, shear bands were observed (Figs. 7.9 and 10). This suggests highly localized deformation [166]. Cracking was observed to follow the path of the shear band suggesting loose bonding along the shear band. The depth of the modified microstructure due to impacts varied in the range of 3–5 μm. Deformation localization and shear band formation were reported in previous studies. It was found that susceptibility to adiabatic shear can greatly influence the resistance to SPE [162-164]. As reported by Winter and Hutching [164], the higher erosion rate of Ti compared to mild steel, subjected to similar impacts, was attributed to greater localization of the deformation in Ti than in mild steel. Likewise, shear band and localized plastic deformation favor detachment of the formed lips in Ti, whereas in mild steel the lip remained attached to the surface. A significant amount of energy is needed to sever the lips in mild steel which makes less energy available for the formation of another lip.

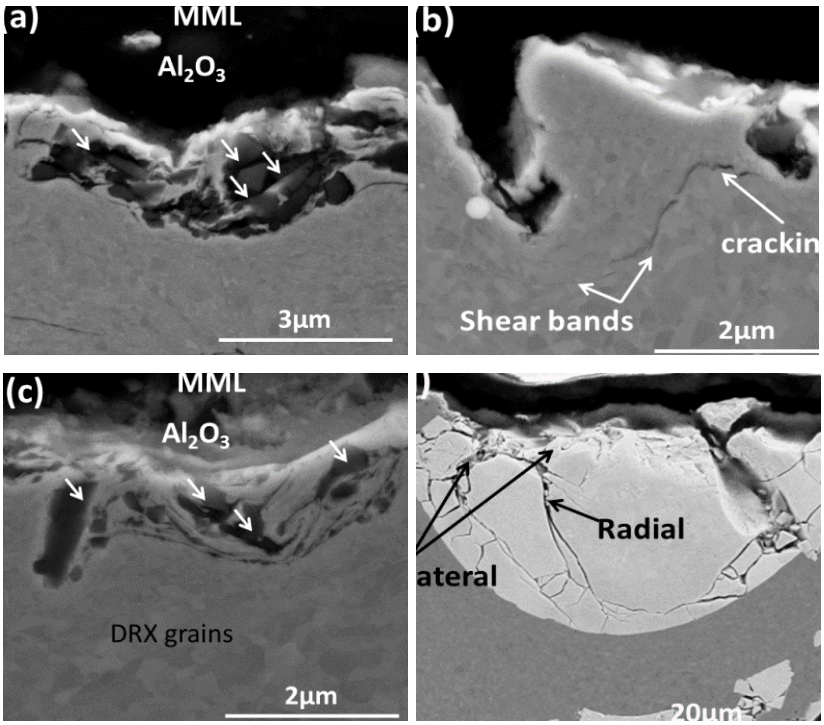

Fig. 7.9 SEM micrographs showing the sub-surface microstructure of (a) and (b) Ni, (c) and (d) Ni-10.5vol.% WC coatings under 90˚ SPE impact angle.

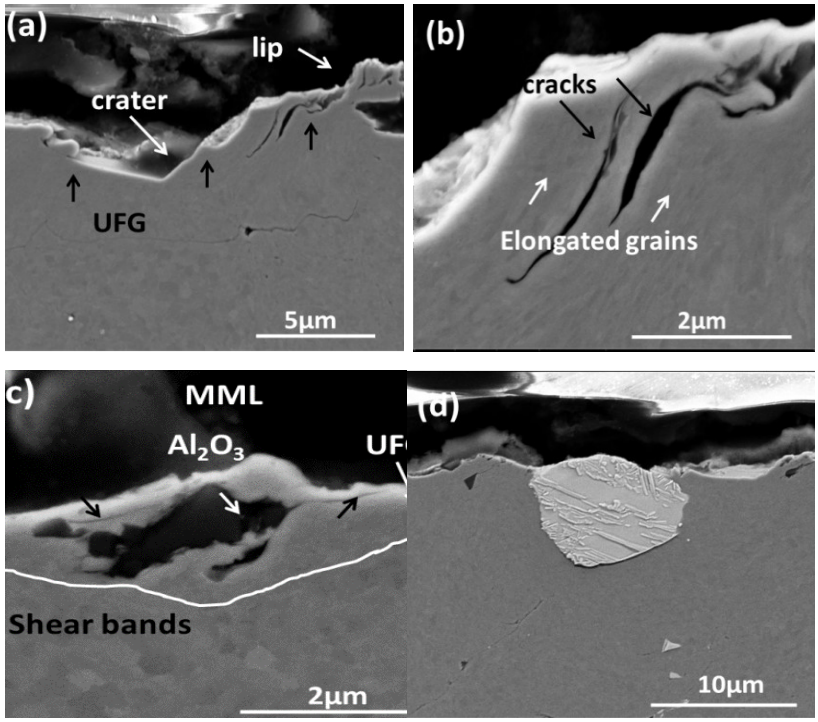

Fig. 7.10 SEM micrographs showing the sub-surface microstructure of (a) and (b) Ni, (c) and (d) Ni-10.5vol.% WC coatings under 30˚ SPE impact angle.

Similar subsurface morphologies and microstructures were observed in Ni-WC composite coating under normal impacts. However, presence of WC particles in Ni-WC hindered the formation of the MML at some regions of the surface where WC is present. The impingement of erodent particles on WC particles was associated with a number of cracks, which were analogous to those seen during indentation of brittle surfaces [165]. Radial and lateral cracking were observed on WC particles (Fig. 7.9d). There are two commonly accepted indentation mechanisms for fracture of brittle materials due to particles impact: 1-based on a purely elastic fracture, and 2-based on an elastic-plastic fracture [167]. These mechanisms depend on the size of impacting particles and contact radius. In the case of large rounded particles, circular cracks may propagate from the surface and form conical or Hertzian cracks. Significant volume of material is detached from the surface when intersection exists among several conical cracks. The latter mechanism, the elastic-plastic fracture, is applicable to smaller particles or particles attacking surface from sharp edge [165]. Large contact pressure created at the time of impact can form a plastic deformation zone. At a critical pressure, radial cracks develop and then can unify into half-penny cracking [165]. In order to relax strain mismatch between plastically deformed zone and elastically deformed regions, lateral cracking may occur upon unloading [167]. Intersecting lateral cracks led to material removal, as can be observed in Fig. 7.9d. Although it's practically difficult to distinguish the two WC failure mechanisms described above, the angular erodent particles used in this study should lead to a high contact pressure upon impact and the elastic-plastic mechanism more likely.

Similar to subsurface microstructure under normal impacts, shear localization features were observed in Ni and Ni-WC composite coatings under 30° impacts (Fig. 7.10). In contrast, however, in the cross-sectional microstructure of both coatings at 30° impacts, fewer events of MML formation were evidenced, although a mixture of UFG and LG with lamellar structure was observed.

7.4 Discussion

7.4.1 Cold spray deposition of Ni-WC coating and effect of WC size

Cold spray was used to fabricate Ni and Ni-WC composite coatings with three different WC size ranges. The concentration of WC in the sprayed coatings was lower than that of the feedstock for all three size ranges. WC, due to its nature as a hard-ceramic phase, does not deform upon impact on the substrate. Rather, they become embedded in the substrate and are entrapped by matrix particles. The size of the WC particles was found to affect their retention in the coating. The presence of WC was also found to significantly decrease the deposition of Ni compared to deposition of Ni alone.

In Ni-WC coatings, Ni undergoes plastic deformation and shear instability upon impact on WC particles, present in previously deposited coating. However, because of very limited deformability of WC, more elastic energy is stored in impacting Ni particles that would otherwise be accommodated partly by shear deformation of deposited Ni in Ni coatings. Stored elastic energy in impacting Ni on WC particles/fragments results in its rebound from the surfaces. A large number of retained fine WC fragments as well as a reduction in thickness with adding WC particles are consistent with the above explanation (Fig. 7.4 and Table 7.1). With coarse WC in the initial feedstock, a lower coating thickness was achieved compared to those with the finer WC particles (Table 7.1). Fragmentation of brittle ceramic particles upon impact during cold spray deposition has been reported by previous studies [68, 75]. It is generally found that fragmentation becomes more likely when the ceramic particle size or its impact velocity is increased [68, 75]. A lower amount of WC fragments on the cross section of coatings produced with lower size WC (Fig. 7.3) is consistent with the above explanation that fracture might be avoided by limiting the ceramic size. However, there is a limitation in using small sized powder for cold spraying due to the bow shock present close to substrate surface [73]. A strong erosion effect by ceramic powder, reported in previous studies [66], can be another reason which considerably reduces coating mass growth and deposition efficiency of the metal component with adding ceramic particles. However, this effect was mentioned to be dependent on the ceramic particles size.

In order to understand how particle size can affect WC recovery into the coating, we can consider the impact of WC on the coating surface. WC particles can impact any area of the coating surface, containing either WC particle or Ni (Fig. 7.11). During impact of WC on Ni splats (Fig. 7.11a and b), impact loading applied to Ni causes it to deform. The shear strength of Ni falls to values near zero once thermal softening dominates over strain hardening effects [50]. This leads

to shear instability at the interface [50, 51]. Impact is more elastic in nature if WC impacts on deposited WC (Fig. 7.11c and d). Eventually, after a part of the kinetic energy of the impacting WC particle was consumed by plastic deformation in the metallic part, ceramic particle cracking, and other inelastic events, the rest is stored as elastic energy and causes the WC particle to bounce off the surface (Fig. 7.11b and d) [72]. During cold spraying, there is a stream of powder targeting the surface over a very short time. Interaction between particles in cold spraying has not been widely studied yet. With assuming that there is interaction between particles, the capturing effect of next arriving particles can't be neglected (Fig. 7.11b and d) [72]. As reported in a similar study [26], in order to recover a ceramic particle to the coating, its rebounding momentum which is determined by its velocity, must be overcome by later-arriving particles (Fig. 7.11b and d). The total momentum of next coming WC and Ni particles required to trap WC into the coating is given by equation (7-1) [72],

$$\sum m_{WC} v_{WC} + \sum m_{Ni} v_{Ni} \geq m_r v_r \qquad (7\text{-}1)$$

Where, m_{WC} , m_{Ni} and v_{WC}, $v_{Ni}$are the mass and velocity of the later arriving WC and Ni particles, respectively, and m_r and v_r are the mass and velocity of the rebounding WC particle at the moment that it loses contact to the surface. The rebounding momentum ($m_r v_r$) of an impacting WC particle depends on its mass and rebounding velocity. The rebounding velocity (v_r) is related to impact velocity [168]. Studies have been conducted to relate the particle size and velocity of impact to rebounding velocity [72, 168]. Under ideal elastic impact, rebounding velocity equals impact velocity. However, in the case of the present study, as mentioned before, inelastic events such as plastic deformation and any adhesive interaction between particle and surface, leads to loss in kinetic energy. Likewise, rebounding velocity is lower than impact velocity [168]. Interestingly, when using a small size particle, on the left-hand side of Eq (7-1), the average velocity of WC particles in the gas stream is raised. This is confirmed by velocity measurement which revealed a significant increment in velocity (Table 7.2). On the other hand, using small size WC, the right-hand side of Eq (7-1), $m_r v_r$ is lower, because m strongly depends on particle radius ($m \sim r^3$). Although v_r is raised because of higher impact velocity (v_{WC}) in smaller size WC, it can be easily shown that the dependency of v_{WC}, and hence v_r, on particle radius is not as great as that of the mass (m_r) [72]. Less momentum is needed to entrap smaller size WC particle to coating, and hence, higher retention is expected, which is consistent with the results of this study. However,

using much smaller WC particle size of -25+10 µm didn't improve WC retention into coating. This can be due to the bow shock present close to substrate surface [73]. Other possible reason is higher stored elastic energy and rebounding velocity of very small particles. During cold spraying, fragmentation is one source of particles loss. However, formation of micro-cracks, although undesirable, uses part of the particle kinetic energy that would otherwise be stored as elastic energy and cause an increase in rebounding velocity. As mentioned before, smaller size ceramic particles are less prone to cracking and fragmentation [68, 75]. They rebound intact from surface with very high rebounding velocity. The hardness of composite coatings didn't improve significantly with adding WC particles. In order to obtain harder composite coating, higher retention of WC is required. Although higher WC concentration wasn't achieved in this study using cold spray at applied conditions, testing of processing parameters and initial feedstock are currently in progress to improve the efficiency of the process.

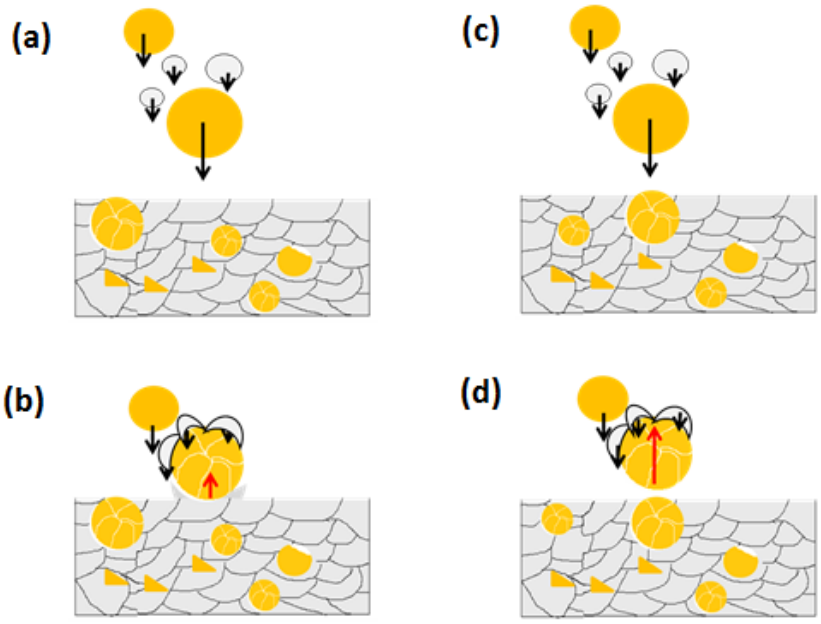

Fig. 7.11 A schematic graph showing how WC was retained into coating. Gray and orange spheres represents Ni and WC particles, respectively. WC particles impact an area of surface containing (a) Ni or (c) WC particle, (b) and (d) reboundig/capturing by later arriving particles after impact.

7.4.2 SPE of Ni and Ni-WC coating

The SPE behavior of Ni and Ni-10.5vol.% WC coatings were studied under 30 and 90° angle of impacts. Both coatings exhibited similar erosion resistance when subjected to SPE impinging at 30°; however, the Ni coating was more erosion resistant under normal impacts. For both coatings, the erosion rate is higher under oblique angle of impact which implies ductile erosion behavior. This was consistent with ductile features of materials removal and worn surface morphologies.

Dynamic indentation conditions were found to prevail during high strain rate deformation such as erosion. When hit by erodent particles, the material exhibits a net strain hardening capacity up to certain strain (critical strain), beyond which deformation becomes highly localized. Under such conditions, temperature rises in the target material, due to plastic deformation, thereby decreasing the flow stress [162, 163]. Critical strain represents the strain needed for lip formation, not its failure, and erosion rate involves materials deformation including lip formation and its fracture. However, the fracture of the lips is much easier than lip formation and requires less impact energy [163]. Sundararajan *et al.* [162, 169] analyzed strain localization during SPE on the basis of a constitutive flow equation of the material being eroded. They assumed an equation of the following form relating flow stress σ, plastic strain ε, and temperature T at a constant strain rate

$$\sigma = K\varepsilon^{n}(1 - BT) \qquad (7\text{-}2)$$

Where, K is the high strain rate strength coefficient and n is the strain hardening exponent. B is a constant characterizing the temperature dependence of the flow stress and B = 0.5/Tm for most metals [162, 169]. The critical strain (ε_c) for localization and hence lip formation was derived as,

$$\epsilon_c = \left(\frac{n\rho C_P}{KB}\right)^{\frac{1}{(n+1)}} \qquad (7\text{-}3)$$

Where, ρ and C_p are density and specific heat of the material being eroded, respectively [162, 169]. The model predicts the critical strain for onset of lip formation at which strain hardening is balanced by decreased flow stress due to thermal softening. It implies that the higher the critical strain, the lower the erosion rate, under an assumption of a constant strain rate. Later,

Sundararajan *et al.* [170] showed dependency of ε_c on strain rate. According to their studies, ε_c decreases as strain rate increases associated with higher impact velocities and/or using angular erodent particle. As mentioned before, the heat generated by plastic deformation is not dissipated away leading to an increase in the temperature of the eroding material. Thus, thermal diffusivity is an important factor, which is obtained as,

$$\alpha = \frac{k}{\rho C_P} \tag{7-4}$$

where, k is thermal conductivity of coating. Cold-sprayed Ni coatings tested in this study exhibit lower erosion resistance than Ni plating reported in previous studies [47, 171]. High density of defects and splat structure typical to cold-sprayed coatings can lower the thermal diffusivity and favor strain localization in cold-sprayed Ni coating leading to lip formation. Moreover, inter-splat boundaries provide preferential crack initiation and propagation path (Fig. 7.10a and b) and are main reason for inferior erosion resistance of cold sprayed Ni compared to Ni coating fabricated by other techniques.

The shear instabilities explained above can lead to formation of interfacial roll-ups and vortex-like features, as reported during cold-spraying [47]. As mentioned before, embedding of erodent particles was found to influence erosion behaviour. As shown in Fig. 7.9a and c, shear instabilities of target materials helped to capture erodent particles and mechanically interlock them into the coating. Continuous impact of erodent particles resulted in densification and compaction of the MML, a mixture of target materials lips, debris, and erodent particle fragments. Fragmentation of erodent particles upon impact was another factor which helped in developing the MML, assisted by kinetic energy loss. Under normal erosion, as explained above, shear instability caused strain localization to near-surface regions and led to lip extrusion. These lips were removed during subsequent impacts in the form of thin platelets. Detachment of the lips was assisted with cracks following the line of shear bands, or by the presence of a tensile stress and by necking [170].

At 90° impact angle, adding WC into Ni was found to deteriorate the erosion resistance of the coating. This is attributed to brittle cracking and fracture of WC, observed in worn surface and subsurface images, due to its very limited deformability. Moreover, the presence of the WC

particles inhibited erodent particles from being embedded into the surface and forming a MML, which protect the surface more effectively.

It was reported that under 30° impact angle erosion, the frictional force between erodent and target surfaces introduces very high shear stress which is high enough to exceed ϵ_c and form lips even during first impact. Lip removal was reported to be also easier in the case of oblique impact because of the higher resolved shear stress. Moreover, under oblique impact, the protruding lip is impacted from the side [163]. Rebounding erodent particles from the surface causes extra tensile stress on heavily deformed lips [163] as well and contributes to higher erosion rate under 30° impact angle compared to that under an angle of 90° for both coatings.

The higher resolved shear stress at 30° erosion provided enough shear stress to take eroding pieces away and the cutting depth was also shallow. Therefore, less embedding of erodent particles deep into the coating was expected [172]. Less evidence of the MML was found for both coatings at 30° erosion compared to normal erosion.

In erosion under 30° impact angle, both coatings had similar erosion rate. WC was found to resist the cutting action of the erodent particle due to its high hardness. However, the content of WC was very low to effectively protect Ni from being eroded. Strong interfacial bonding between Ni and WC is essential for the protecting effect of WC particles on the matrix [10]. In the absence of strong metallurgical bonding between cold-sprayed Ni and WC, WC particles were eroded away, before they got actually worn out.

7.5 Conclusion

Ni-WC composite coatings were fabricated by cold spray, and their erosive wear performance was studied and compared to a Ni coating. Three different WC size ranges were tested. It was found that WC particles were mostly retained in the coating by the help of later arriving particles. Using small size WC particles, less momentum has to be overcome to recover WC in the coating, which results in higher WC content. The presence of WC particles decreased deposition efficiency and also reduced the bonding between Ni particles.

Ni and Ni-10.5vol.% WC coatings exhibited ductile erosion behavior. The two coatings had similar erosive wear resistance at 30°, however, the erosion rate of the Ni-WC coating was higher at normal incidence angle. Cutting and plowing were the main wear mechanisms at 30° angle, whereas, Ni deformation localization and lip formation and WC fracture were observed at normal angle. Higher erosion resistance of both coatings at 90° compared to that at an angle impact 30° was attributed to the formation of a MML by embedment of the Al_2O_3 particles, which was less observed at 30°. The presence of the WC particles avoided the embedment of the Al_2O_3 particles and the MML formation, which contributed to the lower erosion resistance by adding WC particles. At 30°, WC particles were able to protect Ni from erosion at some regions of the surface; however, the content of WC was too low for significant improvement.

Acknowledgments

The authors gratefully acknowledge the financial support from the Canadian Foundation for Innovation (CFI) project No. 8246 for the cold spray equipment, the CFI Leader's Opportunity Fund project No. 13029 for the tribometer and nanoindentation equipment, and the Natural Sciences and Engineering Research Council (NSERC) Strategic Grants Program for the operational funding of this project. Thanks are also due to Tekna Inc. of Sherbrooke, QC for providing the Ni and spherical WC powders. The authors thank the Functional Coatings and Surface Engineering Laboratory (FCSEL) at Polytechnique Montréal and greatly acknowledge the assistance of Prof. Klemberg-Sapieha, Dr. Thomas Schmitt, and Jacques Lengaigne with the erosive wear testing.

Chapter 8

Influence of feedstock characteristics on solid particle erosion behavior of cold-sprayed Ni-WC composite coatings

Sima Alidokht, Jacques Lengaigne, Jolanta Sphieha, Steve Yue, Richard R. Chromik

This is a manuscript, intended to submit to a journal. In Chapter 7, the addition of a 10.5vol.% cast WC didn't correspond to a significant improvement in erosion resistance. Since, there was a limitation in cast WC retention into coatings, the Ni-WCNi coatings, in which a range of WC content was achieved using cold spray, were subjected to solid particle erosion testing. In addition, influence of Ni matrix hardness on SPE through two different Ni powder sizes were tested.

Abstract

Metal matrix composites (MMCs) of WC in Co or Ni matrixes are widely used due to a good combination of hardness and toughness, and good wear resistance. Previous studies showed that an optimum content of WC particles with tailored mechanical properties extend the life cycle of the MMCs. In this study, composite coatings of Ni with various WC content ranging between 10 to 55vol.% were cold sprayed using agglomerated WCNi powders and two size ranges Ni powders. Microstructural characterization, including deformed structure of Ni splats, as well as, retention and distribution of WC, was performed by scanning electron microscopy. Using micro-indentation, a relationship between coatings mechanical properties and Ni powder size and volume fraction of WC was studied. Coatings were subjected to ASTM standard G76 solid particle erosion at two 30 and 90° impact angles. Changes in erosive wear performance as a function of WC content was explained using the mean free path between the WCNi particles. It was found that the addition of below 30vol.% WC did not influence erosion behavior of composite coatings. Erosion occurred primarily by plastic deformation of Ni matrices and knocking-out of WC particles. Composite coatings using finer size Ni was more erosion resistant. Network distribution of highly compacted

WCNi particles in high concentration WC coatings led to a significant drop in erosion rates. This was assisted by a change in erosion mechanism from severe cutting and ploughing of Ni and WC dislodging to WCNi splats spalling, resulted from strain accumulation and propagation of cracks along WCNi interfaces.

8.1 Introduction

Solid particle erosion (SPE) is the wear of materials that occurs when hard solid particles are entrained in a fluid and impinge a surface. SPE is different from other types of erosion such as slurry and cavitation erosion, since it is involved with a series of independent but similar impact events where erodent particles hit the surface [158, 159]. In SPE, the materials are traditionally divided to ductile and brittle based on their response to wear. Ductile materials often exhibit maximum erosion rates at small impact angle, while for brittle materials, a high erosion damage is detected at normal angle of incidence [2, 83]. Recently much attention has been paid to metal matrix composite (MMC) coatings which combine hardness of hard ceramic particles with toughness of metallic binder to control and minimize erosion damage for a wide range of impact angles [9, 109].

Studies of Wang *et al* [8] an Kulu and Pihl [110] showed that the wear resistance of Ni coatings can be greatly improved by incorporation of refractory carbides such as WC, WC-Co, TiC, and Cr_2C_3 into the metallic matrices. Paul *et al* [173]conducted SPE testing using alumina erodent particles on high content Ni-WC laser clad surfaces with 75-92vol.% WC. Worn surface observation revealed that ductile erosion mechanisms followed by the removal of WC particulates from the matrix dominates the erosion damage. They found that erosion behavior of composite coatings was primarily governed by erodent particles velocity followed by their impact angle, whereas erosion does not much depend on the Ni-concentration in MMCs. Gee *et al* [174] and Hussainova *et al* [175] performed SPE on the WC-12Co hard metals, accumulation of plastic strain in WC, intergranular cracking, interphase debonding and micro-cracking of carbides was reported. In another study, Zhou *et al* [160] observed that the coatings of 35vol.% WC reinforced iron matrix showed the best erosion resistance under impact angle of 70°. They observed the worn surfaces with a characteristic of protruding of WC particles and sinking of the matrix, indicating preferential wear of matrices and a high resistance of WC particles against erosion damage, due to their higher

hardness compared to abrasive-silica erodent particle. With increasing WC content up to 35vol.%, erosion rates was reduced. However, further increase in WC content above 35vol.% led to rise in erosion rates of composites. The increase in erosion rates of composites for volume fraction above 35vol.% was linked to weak interfacial bonding at high WC contents, where the matrix between WC became too little or not existed, leading to WC contact with each other. The result is an increase in erosion damage, since the supporting effect of the matrix to WC particles through a good interface bond is essential for the protecting effect of WC particle [160]. This emphasize the importance of microstructural factors, i.e. spacing between reinforcement particles, their size, as well as their volume fractions. Although, the relationship between structure, matrix and hard particles, and wear parameters is critical as well.

Cold spray has been widely explored to deposit WC containing composites over the last decade due to its distinct advantages over traditional thermal spray processes. Cold spray is a solid-state process, in which oxidation, decomposition, and any other unwanted phase transformation of heat sensitive feedstock such as WC particles can be avoided due to its limited heat effects [20, 92, 93]. Erosion performance of cold sprayed WC-CoCr, Cr_3C_2-NiCr, and Al-Al_2O_3 coatings were tested in a previous study [176]. Friction stir processing (FSP) was used to improve the distribution of reinforcing particles within the matrix. It was found that reduction in the interparticle spacing led to less of the matrix alloy being exposed to the impinging particles, and hence, improved erosion resistance. However, to the current authors' knowledge, SPE wear performance of cold sprayed Ni-WC with various WC content, has not been conducted yet, and was therefore the main focus of the current study. Moreover, the influence of Ni matrix microstructure and hardness on SPE was tested using two size ranges Ni powders, referred to as Ni(7) and Ni(25). In a previous work by the authors, coatings of pure Ni(7) and Ni(7)-WCNi were cold sprayed and mechanisms of WCNi retention and Ni deformed microstructure evolution were discussed. This study was largely limited to a discussion of powder size effect on Ni coatings microstructure, as well as, SPE mechanisms of Ni and composite coatings.

8.2 Experimental

8.2.1 Cold sprayed Coatings Characterization

Feedstock powders for cold spray were commercially pure gas atomized Ni (H.C.Starck, Germany) referred to as Ni(25) and agglomerated and sintered WCNi (AMPERIT® 547, H.C.Starck, Munich, Germany) (Fig. 8.1). The Ni(25) and WCNi powders had particle size ranges of -35+15 (d_{50} = 25 µm) and -30+15 µm (d_{50} = 20 µm), respectively. Similar cold spray parameters such as the cold spray gun, deposition parameters and feeding system that are explained in a previous work for Ni(7) and Ni(7)-WCNi coatings, were used here. The only distinction was the gas preheat temperature that was selected 700 and 800 °C for the composite with Ni(7) and Ni(25) matrices, respectively. Pure Ni coatings was sprayed at gas preheat temperature of 700 °C.

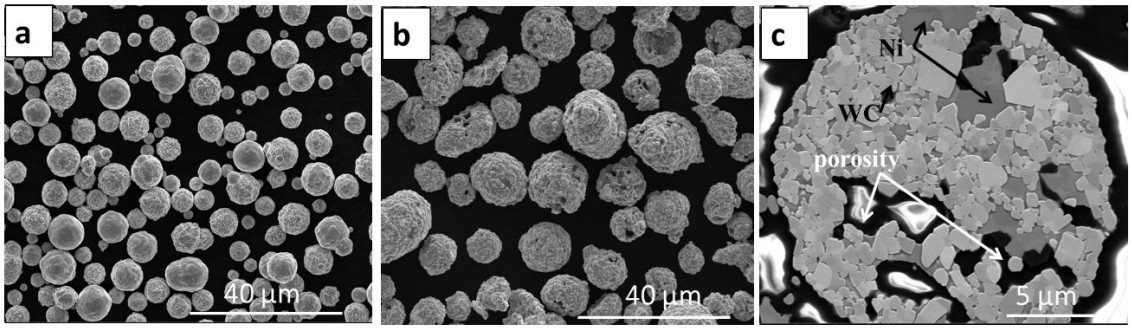

Fig. 8.1 Morphology of as-received powders: (a) Ni -35+15 (d_{50} = 25 µm), and (b) and (c) morphology and cross section of WCNi -35+15 (d_{50} = 20 µm), respectively.

Cold-sprayed coatings were cross-sectioned perpendicular to the gun traverse direction, mechanically ground, and polished using 9, 3 and 1 µm diamond pastes followed by 0.05 µm colloidal silica. The morphology and microstructure of the initial powders and deposited coatings were observed by scanning electron microscopy (SEM) (Quanta 600, FEI, Oregon, USA). The WC and porosity concentrations within the coatings were measured by image analysis of pixel count using ten random SEM images of polished cross-sections. To characterize mechanical properties of Ni powder and sprayed coatings, nano-hardness and micro-hardness testing were used. Nano-hardness testing was performed using a Berkovich diamond tip with a triboindenter system (TI 950, Hysitron, Minnesota, USA). The peak load, loading and unloading rate, and hold

time at peak loads are fixed as 5 mN, 200 μN/s and 2 s, respectively. To calculate hardness and elastic modulus, the indentation load-displacement data during indentation was analyzed using the Oliver and Pharr method [107]. Vickers micro-indentation (Clark CM-100AT, Clarke Instruments Ltd, Salisbury, UK) was performed on the top polished surfaces. To obtain an average hardness value of the composite, a large load of 1 kgf with a dwell time of 15 s on a micro-hardness tester was used.

8.2.2 Erosion test

SPE tests were carried out using a custom-built gas-blast erosion system based on the specifications of ASTM standard G76 [102]. Prior to erosion tests, top surfaces of coatings were mechanically ground, and polished using 9, 3 and 1 μm diamond pastes followed by 0.05μm colloidal silica. Angular Al_2O_3 particles of 20 to 70 μm size were used as erodent particles. Al_2O_3 particles have an average hardness of 13.47 ± 0.3 GPa. Back pressure of the abrasive blasting unit was adjusted in order to control particle velocity and its dependence on back pressure was tested using a double-disk time-of-flight technique. A particle velocity of 60 ± 6 m/s was obtained using 69 kPa air pressure in the nozzle. The particle feed rate was determined by altering the unit's shaker amplitude and the back pressure. The erosion test unit was turned on for a few minutes while the sample was shielded by a covered shutter, in order to stabilize the feed rate. Once feed rate was stabilized at 0.8 ± 0.1 g/min, the test was started. The erodent powder was filled into the hopper and fed to a tungsten carbide nozzle with an inner diameter of 1.14 mm and a length of 36mm. Working distance between the sample holder and the nozzle was kept constant at 20 mm.

The impact angle was adjusted by turning the sample holder at two different angles of impingement (30 and 90°). All erosion tests were performed at room temperature and 25% relative humidity. ASTM G76 standard recommends a 600 s test length (without piercing the coating) to establish the steady-state erosion rate. In this study, each test was performed for 1800 s (30 min) to better ensure steady state. At least three repetitions were made per experimental condition to evaluate the experimental error of the measurement. Before and after the test, samples were ultra-sonic cleaned in an acetone and ethanol for 5 minutes, dried, and scanned using a non-contact optical profilometer (Zygo instruments, USA) to obtain profiles of the wear tracks. The erosion rate was calculated by normalizing the measured volume loss by the mass of erodent particles

causing weight loss (i.e., testing time×particle feed rate). In order to reveal erosive wear mechanisms, eroded surfaces and cross sections of wear scars were inspected using an SEM (FEI, Quanta 600, USA).

8.3 Results

8.3.1 Coatings

Figure 8.2 shows micrographs of cross-sections and top surfaces of Ni coatings. Mechanically trapped particles, as well as deformed particles, were observed for finer Ni(7) particles (Fig. 8.2c). However, for Ni(25) particles, highly flattened particles (see Fig. 8.2d) were consistent with slightly lower porosity of 1.3± 0.4 %, as compared to 3.8 ± 0.5 % for Ni(7) coatings. Ni(7) coatings displayed a higher micro-hardness (345 ± 17HV_1) than the Ni(25) coatings (215 ± 15 HV_1), even though it was more porous. Figures 8.3a and b show ECC images of cross-sectioned Ni coatings. A non-uniform microstructure was observed for both coatings. Near particle interfaces, grains are ultra-fine, while the central region of particles contain a relatively coarse structure. This is reported in previous studies and related to an inhomogeneous plastic deformation field in cold spray, where particle/particle interfaces experience ultra-high strains, strain rates and adiabatic shear instability [113, 116]. The grain structures of both Ni powders revealed relatively large grain sizes of 1 to 10 μm (not shown here). Whereas, for Ni(7) coating, near particle interfaces, cell structures with average size of 280 - 360 nm were observed, which is due to dislocation re-arrangement [116]; for Ni(25) coating, cells were significantly coarser with grain size of 5 - 7 μm. Nevertheless, at some interfacial regions, a fine microstructure of 300 - 400 nm was observed. Nano-indentation was used to measure hardness of Ni coatings. The representative load-displacement curves are given in Fig. 8.3c. The average nano-hardness of 3.4 ± 0.3 GPa for Ni(25) coating was measured, while for Ni(7) coating it was significantly higher (4.8 ± 0.7 GPa). The relatively coarser microstructure in the Ni(25) coating (Fig. 8.3b) led to a lower hardness compared to that of the Ni(7) coating.

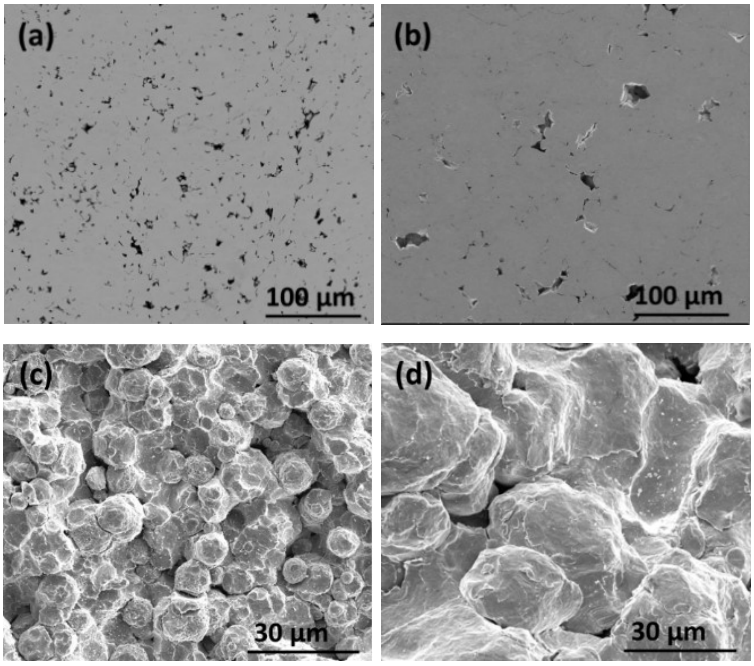

Fig. 8.2 Cross-section morphology (a) and (b) and top-down morphology (c) and (d) of the Ni(7) coating and Ni(25) coating, respectively.

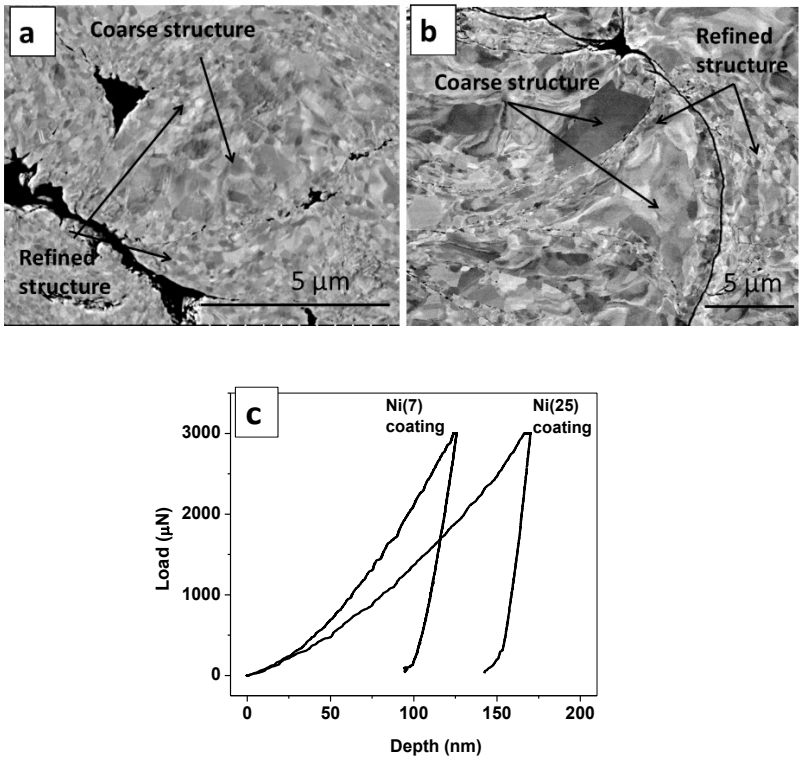

Fig. 8.3 ECC imaging of (a) Ni(7) and (b) Ni(25) coatings, (c) representative load-displacement curves typically obtained from the specified coatings.

Ni-WCNi composite coatings properties including porosity and mean free paths (MFPs) between WC particles are listed in Table 8.1. Figure 8.4 shows micrographs of cross-sectioned Ni-WCNi composite coatings. Similar microstructure in terms of the WCNi splats morphologies and MFP between WCNi particles (see Table 8.1) was obtained. Ni(7)-WCNi coatings were slightly more porous than Ni(25)-WCNi coatings at a given WC content. Retention of WC into coatings and microhardness of coatings are illustrated in Fig. 8.5a and b, respectively, where they are compared to those for Ni(7)-WCNi coatings. WCNi particles retention mechanism in Ni(7)-WCNi coatings was discussed in detail in the previous work [146]. The results showed that using coarser Ni particles did not change the WC recovery to coating. The retention of WC into the coatings was similar to that of Ni(25)-WCNi. For both composite systems, WC content was close to that of the initial feedstock composition, except above 60vol.% WC in initial feedstock, in which higher retention was obtained for Ni(25)-WCNi coatings. Using Ni(25) as matrix, 63vol.% WC in feedstock powder yielded in 55vol.% WC in coating. To obtain similar WC content, a higher WC percentage, around 76vol.%, was needed, when spraying using Ni(7).

Table 8.1 Characteristics of cold-sprayed Ni and Ni-WCNi coatings.

Sample designation 'Matrix-WC vol.% WCNi'	Porosity (%)	MFP (μm)
Ni(25)	1.3 ± 0.4	-
Ni(25)-18WCNi	1.0 ± 0.3	39 ± 4
Ni(25)-26WCNi	0.4 ± 0.2	29 ± 4
Ni(25)-39WCNi	0.4 ± 0.1	19.0 ± 1.2
Ni(25)-55WCNi	0.5 ± 0.4	14.5 ± 2.5
Ni(7)	3.8 ± 0.5	-
Ni(7)-13WCNi	1.9 ± 0.2	36 ± 5
Ni(7)-30WCNi	0.5 ± 0.2	31 ± 3
Ni(7)-43WCNi	0.4 ± 0.1	22 ± 4
Ni(7)-54WCNi	0.9 ± 0.2	18 ± 3

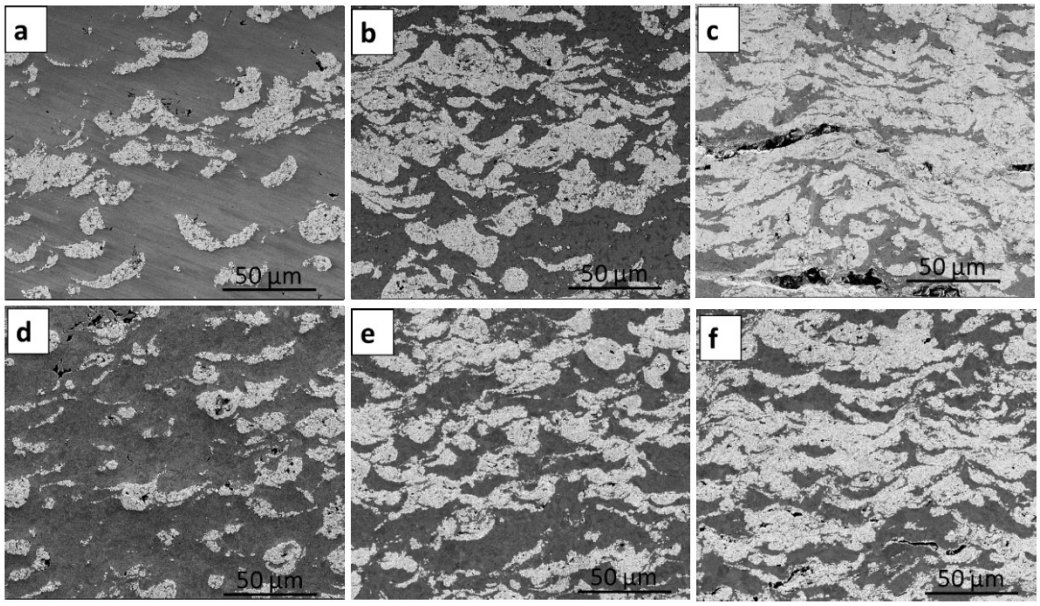

Fig. 8.4 Cross-section morphology of (a) Ni(7)-13WCNi, (b) Ni(7)-43WCNi and (c) Ni(7)-54WCNi coatings. (d) Ni(25)-18WCNi, (e) Ni(25)-40WCNi and (f) Ni(25)-55WCNi coatings

Micro-hardness testing showed that incorporation of below 20vol.% WC into Ni did not improve the hardness of the Ni-WCNi coatings compared to the Ni coatings. As the WC content in the coating increased further, the micro-hardness increased. This was related to reduced MFPs between WCNi particles, which acted as load bearing in high content WC coatings [27, 76]. Moreover, addition of hard particles reduced the porosity and enhanced the density of the coatings, contributing to higher hardness. Moreover, higher compaction of WCNi particles, and hence improved cohesion between WC fragments and Ni binder, was achieved as higher WC contents were sprayed (see high magnification images in Fig. 8.6). Addition of WC to the coating did not change the microstructure of Ni coatings and their nano-hardness. The Ni(25)-WCNi coatings showed a lower hardness when compared to Ni(7)-WCNi coatings for a given WC content, despite being slightly denser. The lower hardness of the Ni(25)-WCNi coatings was due to the presence of the softer Ni(25) matrix.

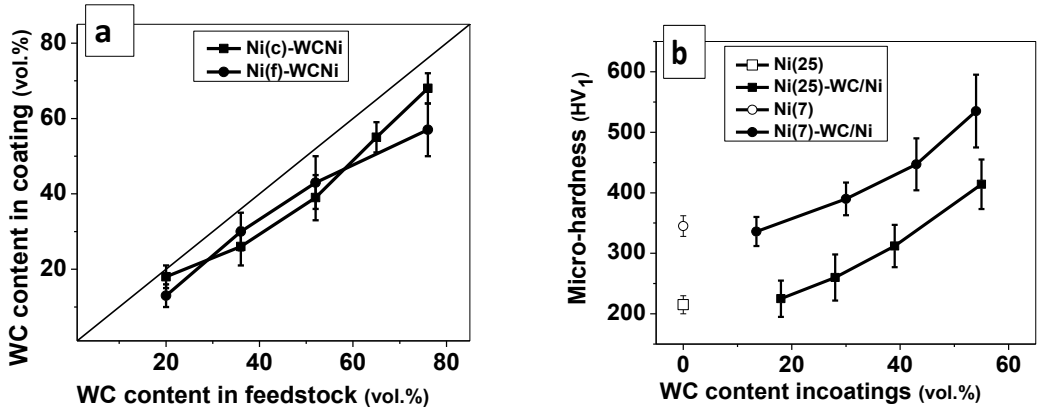

Fig. 8.5 (a) WC content in the coating versus WC content in the feedstock powder, (b) Vickers micro-hardness versus WC content in the coating. Scatter bar on microhardness values indicate the standard deviation of 20 repeat measurements.

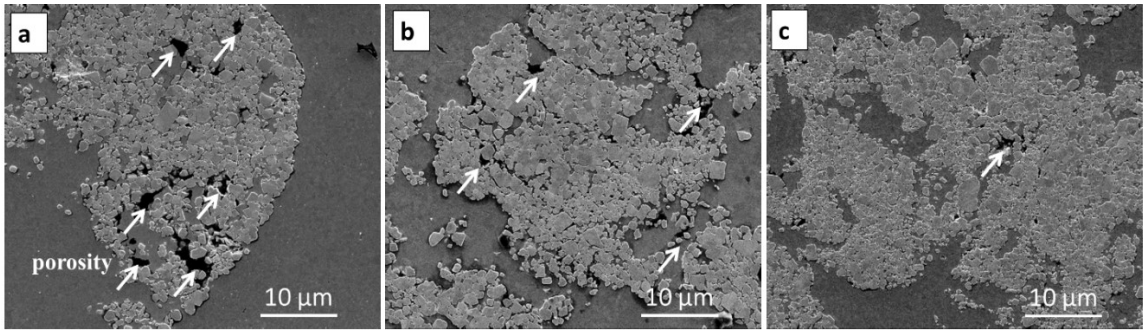

Fig. 8.6 High magnification SEM micrographs of WCNi particles in (a) Ni-13WCNi, (b) Ni-43WCNi, and (c) Ni-54WCNi coatings.

8.3.2 Solid Particle Erosion rates

SPE tests were conducted on Ni and Ni-WCNi coatings. The volumetric erosion rates for Ni and composite coatings versus WC content in coatings were illustrated in Fig. 8.7. Erosion rates of Ni(7) was lower, by a factor around 35 and 48% at 30 and 90° impact angles, respectively, as compared to Ni(25) coatings. At 30° impact angle, as shown in Fig. 8.7, erosion rate did not change much with addition of WCNi particles up to 30vol.%WC. Erosion rates of Ni(25)-WCNi were higher than those recorded for Ni(7)-WCNi coatings at a given WC content. Addition of around 40 and 55vol.% in Ni(7) and 55vol.% in Ni(25) led to significant drop (80-85%) in erosion rates, where the erosion rates of the two composite systems approached around the same values. Under

normal impacts, addition of WCNi into Ni(25) was found to slightly decrease the erosion damage, only around 20% and it was independent of WC content. For Ni(7)-WCNi coatings, no notable change of erosion rates was detected by incorporation of hard phase tested at normal impacts.

For both Ni coatings, the erosion rate at 30° was higher than that at 90°, indicating ductile erosion, in which materials removal predominantly takes place by plastic deformation. Similar characteristic of ductile erosion was recorded for Ni-WCNi composite coatings up to 30vol.% WC in coatings. While for Ni-WCNi composite coatings with WC fill ratios of 40 and 55vol.%, erosion rates at 90° was slightly higher than that at 30°. This was specified as brittle angular dependence of erosion, in which crack formation and propagation is the dominant materials removal mechanism [2, 83].

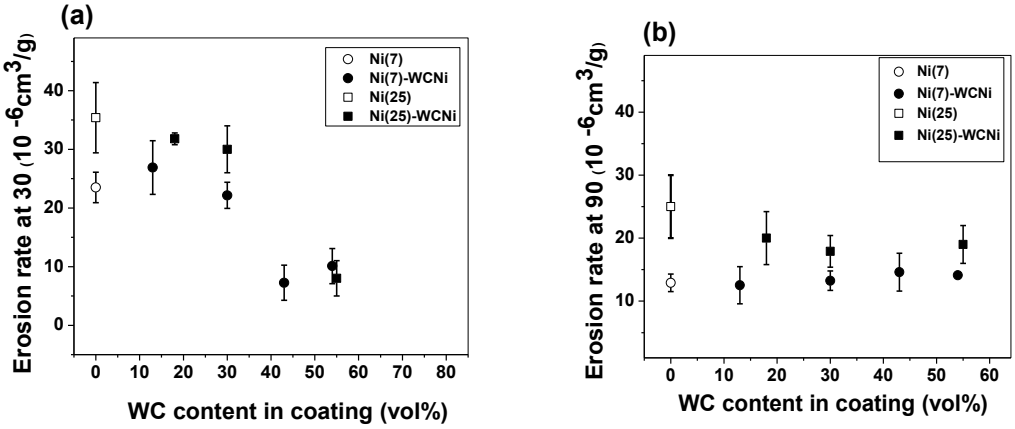

Fig. 8.7 Variation of erosion rate with WC vol.% tested at (a) 30° and (b) 90° impact angle. Scatter bars indicate the standard deviation of 6 repeat measurements.

8.3.3 Worn surface morphologies

8.3.3.1 Worn surfaces of Ni coatings-subsurface

SPE behavior of Ni(7) was reported in an earlier work [177]. In this study, SPE of Ni(25) was compared to that of Ni(7). Micrographs of Ni worn surfaces are presented in Figs. 8.8, for 90 and 30° impact angles. For both coatings, at 30° angles, worn surface morphologies exhibited materials removal by cutting and ploughing actions. At normal impacts, features associated with

crater and lip formations was observed on the worn surfaces. Similar results were stated in previous studies on SPE of metallic materials, where the material removal is mainly due to the micro-cutting and ploughing action of the erodent particle at a low impact angle. Whereas, lip formation, strain hardening of lips and subsequent fracture of these lips in the form of thin platelets are active material removal modes under normal attack [178, 179].

Analysis of subsurface microstructure of Ni(7) in the previous work [177] revealed formation of shear bands, within which the deformation is localized at a high strain rates. It was found that detachment of the lips was assisted with cracks following the line of shear bands, or by the presence of a tensile stress and by necking [170]. Moreover, embedding of erodent particles into Ni worn surfaces was observed, more frequently imaged on 90°, along with shear-induced interfacial roll-ups and vortex-like features of Ni coating, led to formation of an MML [177]. MML featured a shielding effect against severe erosion loss and contributed to better erosion resistance at 90° when compared to that at 30° [177]. More severe wear for Ni(25) was consistent with higher erosion rate, at some regions where deep craters was formed. Subsurface analysis of Ni(25) (Fig. 8.8c and f) revealed embedding of Alumina particles, more frequently noted under normal angle of incidence, similar to Ni(7) coatings. The features on the worn surfaces for both coatings implied characteristic features typical for ductile erosion, which is consistent with the angular dependence of erosion rates.

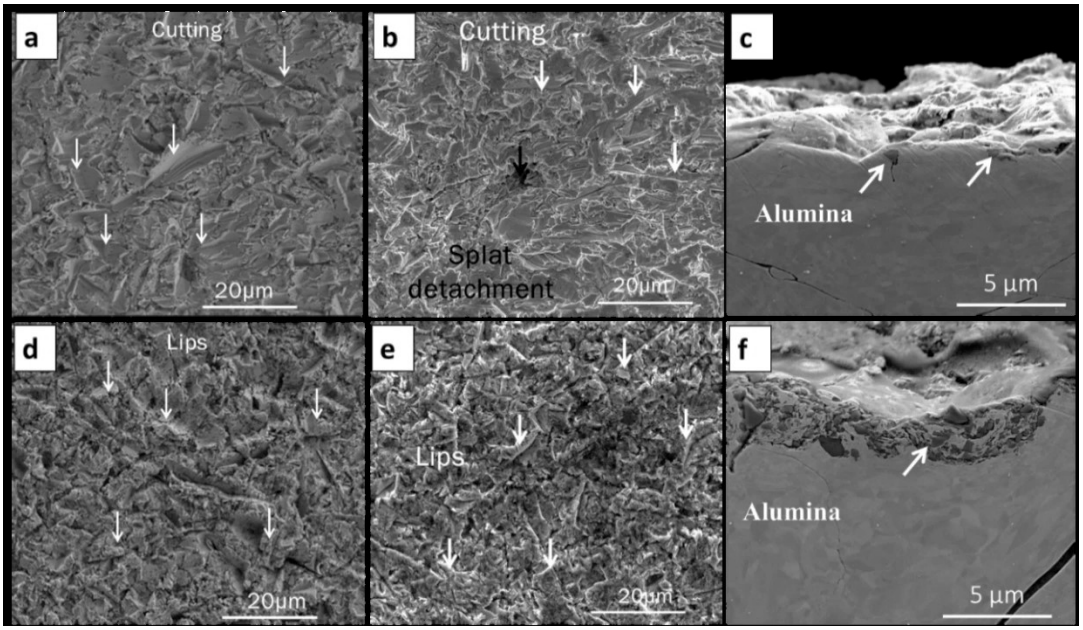

Fig. 8.8 SEM micrographs of worn surfaces of (a) Ni(7), (b) Ni(25), and (c) subsurface of worn Ni(25) coatings after 30min erosion test at 30° impact angle, (d) Ni(7), (e) Ni(25), and (f) subsurface of worn Ni(25) coatings after 30min erosion test at 90° impact angle.

8.3.3.2 Worn surfaces of composite coatings

To investigate the surface damage on the composite coatings due to Al_2O_3 particles erosion, worn surfaces were analyzed by SEM. Worn surface morphologies were obtained on the regions of wear scar with highest impingement of erodent particles after 30min exposure to 30 and 90° impact angle erosion. Similar observations were obtained on Ni erosion features that were recorded for pure Ni coatings. However, due to substantial number of impact events and combined mode of erosion mechanism (i.e. ductile and brittle), it is difficult to determine the prevailing mechanism. For this reason, the "halo" regions on worn surfaces, where there were only a few impact events, was analyzed. Figure 8.9 shows the surface morphology on the halo regions of wear scars for Ni(7)-WCNi coatings at 30° impact angles. From the micrographs, it is evident that Ni was preferentially worn away due to its lower hardness. The WCNi particles were subjected to erosion damages too. However, type of damage was found to shift from knocking-out of WC fragments from surface at low content WC to combined dislodgment and micro-cracking of WC fragments for high content WC composites (Fig. 8.9). Similar behavior was recorded for WCNi particles in Ni(25)-WCNi coatings (not shown here), where less damage on WCNi particles were recorded at

higher content WC coatings. This implies that densification and improved cohesion between WC fragments/Ni binder, may have contribution to improved erosion resistance, in addition to WC content itself. Figure 8.10 shows the surface morphology on the halo regions of wear scars for Ni(7)-WCNi coatings at 90° impact angles. From the micrographs, lips formation for Ni matrices was observed. At low WC concentrations, WCNi particles behaved ductile, as evidenced by the indentation marks of erodent particles on their worn surfaces. However, cracking of WC particles was more frequently noted with increasing WC contents (Fig. 8.10). Similar observations were made for WCNi particles in Ni(25)-WCNi coatings under normal impacts.

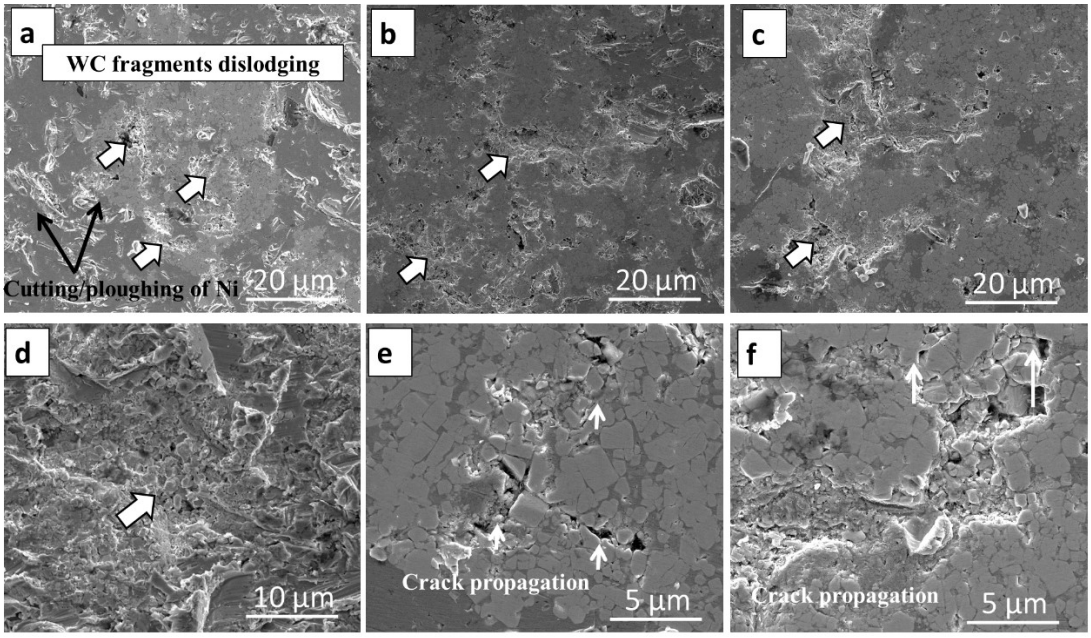

Fig. 8.9 SEM micrographs of worn surfaces of (a) Ni(7)-13WCNi, (b) Ni(7)-43WCNi, and (c) Ni(7)-54WCNi coatings after 30 min erosion test at 30° impact angle, (d), (e), and (f) are high magnification views of (a), (b), and (c) respectively.

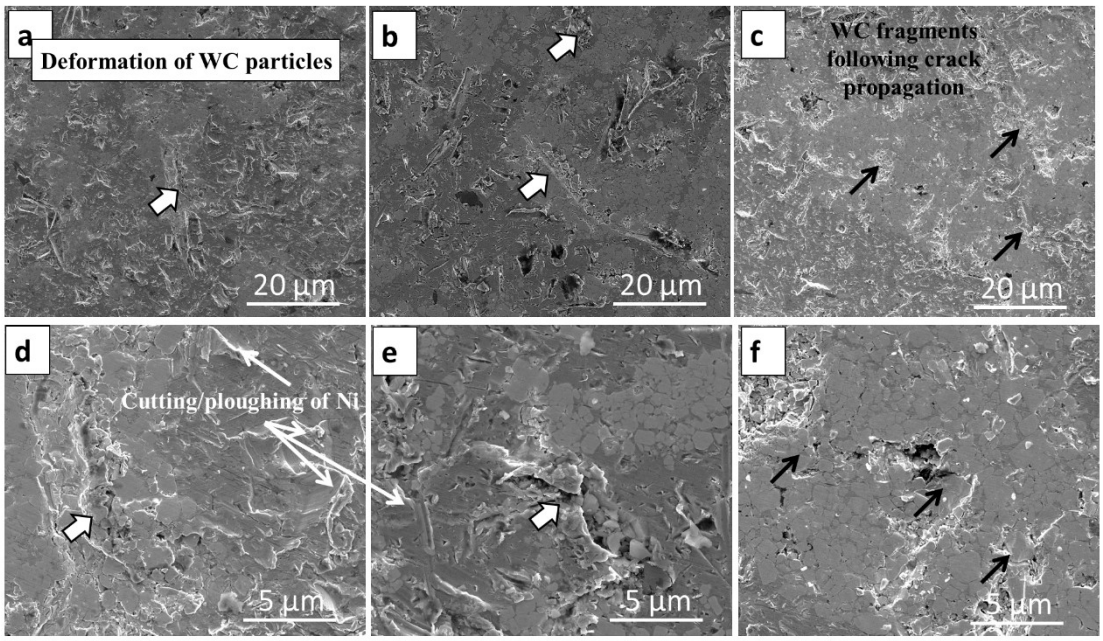

Fig. 8.10 SEM micrographs of worn surfaces of (a) Ni(7)-13WCNi, (b) Ni(7)-43WCNi, and (c) Ni(7)-54WCNi coatings after 30 min erosion tested at 90° impact angle, (d), (e), and (f) are high magnification views of (a), (b), and (c) respectively.

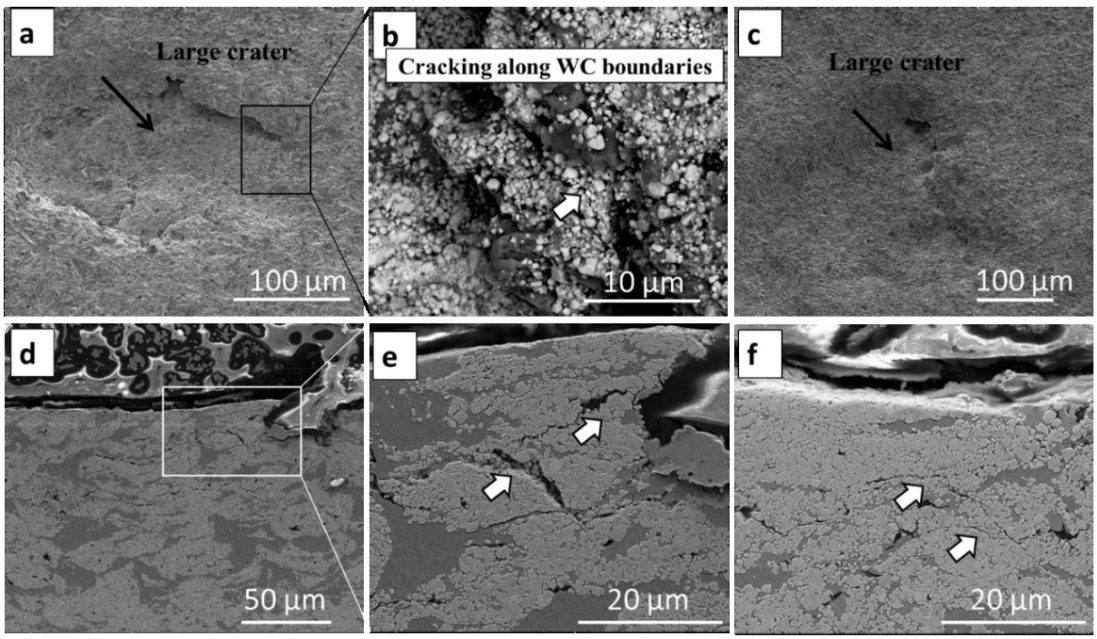

Fig. 8.11 SEM micrographs of worn surfaces of (a) Ni(7)-54WCNi, (c) Ni(25)-55WCNi, (b) BSE high magnification view of (a), subsurface microstructure of Ni(7)-54WCNi tested at (d) 30°, (f) 90° impact angles. (e) high magnification view of (d).

Another interesting observation was the presence of a few deep and large craters (Fig. 8.11a and c) for both Ni(7)-54WCNi and Ni(25)-55WCNi coatings, noted at both angles. It is postulated that removal of large patches of materials, following subsurface crack propagation, was the reason of the slight increase in erosion rates at both angles. Subsurface images of Ni(7)-54WCNi worn surfaces revealed crack propagation along WCNi boundaries (Fig. 8.11d and f).

8.4 Discussion

Ni-WCNi composite coatings were cold-sprayed using two different size distribution of Ni powders. WC retention and their distribution and morphologies were not influenced by the size of Ni powders, except when high WC contents were sprayed, in which slightly higher WC content was recovered to Ni(25) matrix. It was found that at higher initial content, WCNi particles were more densified upon impact, suggesting an improvement in cohesion of these particles. Lower MFPs between WCNi particles, besides improved cohesion between WC and Ni binder, yielded in harder surfaces, as WC content in the coatings was increased.

Ni(25) particles underwent more severe plastic deformation compared to Ni(7) particles during spraying. Previous studies showed that shear instability in smaller metallic particles can be hindered because of higher cooling rates during impact and intensified strain-rate hardening [52]. Another possible reason could be the higher amounts of surface contaminations in smaller size particles, such as oxide shells, which can have a negative effect on bonding [52]. Ni(25) coating featured a coarser microstructure compared to Ni(7) coating. This may be explained by a higher driving energy for restoration mechanisms in highly deformed Ni(25) particles during cold-spraying, where the initial increase in dislocation density at some regions is dynamically restored. Whereas, for finer size Ni(7), the extent of plastic deformation is significantly lower, and thus, there is insufficient energy to activate restoration mechanisms. Another possible reason can be the lower dissipation rate of gas heat transferred to Ni(25) particles during cold-spraying, which means the deposited particles spend more time at higher temperature and can undergo restoration more readily. Micro- and nano-hardness testing showed Ni(25) coatings were softer than Ni(7) coatings, due to coarser microstructure, despite being slightly less porous. Addition of WCNi particles to Ni matrix densified the coatings for both composite systems, however, it didn't influence microstructure of Ni matrices. Nano-hardness testing on Ni matrices of composite coatings gave

similar values that were obtained from pure Ni coatings. On a larger scale indentation, micro-hardness of composite coatings having WC content above 20vol.% was enhanced. Ni(7) and Ni(7)-WCNi coatings were harder than Ni(25) and Ni(25)-WCNi coatings at a given WC content, due to refined microstructure.

Ni and Ni-WCNi coatings were subjected to SPE tests. It was found that Ni(7) coatings were more wear resistant when compared to Ni(25) coatings, under both impact angles. Examination of cross sections and surfaces of eroded Ni coatings suggested that the erosion occurs through ductile mechanisms. Higher resistance to plastic deformation and cutting action of erodent particles in Ni(7) coatings led to lower erosion rates. The same mechanisms were maintained for Ni matrices in Ni-WCNi composite coatings. In fact, no considerable influence on Ni matrices erosion was recorded when WC was added. This could be due to weak bonding between Ni and WCNi particles in cold-sprayed coatings, where WCNi bonded to matrix by mechanical interlocking. Other crucial factor that must be considered is the homogeneity of the material with respect to the contact area of the abrasive particles. In erosive wear, the influence of the reinforcement contents is highly dependent on the wear conditions. The "scale of individual contacts" [2] has a key effect on the erosion behavior of the metal matrix composites. A large contact area of the abrasive particles compared to the scale of the material microstructure defines material as homogeneous and vice versa, small contact area of the erodent particles when compared to the scale of microstructure lead to inhomogeneous wear behaviour of the material [2].

Previous studies reported that when a heterogeneous composite is subjected to wear, the binder phase will preferentially wear, and eventually the hard particles will fall out of the matrix, unless strong bonding between matrix and reinforcement particles prevent reinforcement dislodging too easily from the matrix [8, 110, 160, 173-175]. In this study, the erodent particles were angular with the size from 20 to 70 μm; however, sharp grooving edges of the particles are much smaller. SPE of Ni-WCNi composite coating can be defined as heterogeneous, when the "scale of individual contacts" is concerned, i.e. smaller contact area than microstructure scales of the composite coatings, MFPs between WCNi particles in the present case. Considering the scale effect, the erosion performance of the coatings can depend mainly on one of the three factors: matrix, WCNi reinforcements or WCNi/Ni interfaces, i.e., which one is the "weakest link" in the

structure concerning wear. Likewise, erosion of reinforcements, WCNi particles, is controlled by cohesion of WC fragments to Ni binder.

At 30° impact angle, erosion rates measurements and examination of the cross sections and surfaces of eroded coating showed that up to 30vol.% WC additions to Ni did not influence its wear performance. Ni-WCNi coatings displayed a significantly lower erosion rates than the predicted values by a mechanism-independent averaging law (see Fig. 8.7a). This is due to weak mechanical bonding of WCNi particles to Ni matrices as well as porosities which were remained inside WCNi particles at low content WC coatings. A high concentration of WC of above 40vol.% was needed for a drop-in erosion rates for both composite systems, assisted by a mechanism change from ductile erosion of matrix and knocking-out of WC fragments to intergranular crack propagation (see Fig. 8.9, 10 and 11). This is due to plastic strain accumulation, where linking between WC particles prevent crack arresting by Ni plastic deformation. Erosion rates of Ni(7)-40 and 55WCNi coatings were close to that measured for Ni(25)-55WCNi, despite different Ni matrices, which supports the view that erosion rate was controlled by the subsurface cracking of WCNi particles network.

Under normal impact angle, high concentration of agglomerated WCNi particles didn't deteriorate erosion performance of the coatings much despite being a brittle phase. This is due to voids were present between WC particles. This, along with porosity inside the powders and Ni binder between WC agglomerates, provide ductility. When subjected to erosive wear, compaction and deformation of WCNi particles near the contact area occurred through slipping and rotation of WC particles along the Ni binder. However, a high degree of compaction, achieved in high concentration of agglomerated WCNi particles, caused crack propagation due to strain accumulation.

8.5 Conclusion

Two size ranges of Ni, -10+4 (d_{50} = 7 μm) and -35+15 (d_{50} = 25 μm) were sprayed alone and mixed with WC and WCNi powders. SPE wear performance of Ni and Ni-WCNi coatings was studied. The size of Ni particles did not change the WC recovery to coating and the concentration of WC in sprayed Ni-WCNi coatings was similar, and close to that of the initial feedstock for both Ni powders. It was found that Ni-WCNi coatings can be tailored to contain 18-70vol.% WC and display a varied hardness ranging between 225 to 550 HV_1. Higher concentration

of WCNi in initial feedstock led to more compaction of WCNi particles in coatings. At low WC contents, erosion performance was controlled by Ni matrices and WC knocking-out from surface. Whereas, high concentration of WCNi particles aided in erosion resistance for low angles, due to improved resistance to dislodging and improved cohesion bonding. For high WC concentration coatings, due to linking between WC particles, the crack propagation was not arrested by Ni deformation, which led to slight increase in erosion rate. Under normal impact angle, high concentration of agglomerated WCNi particles didn't deteriorate erosion performance of the coatings much despite being a brittle phase.

Acknowledgments

The authors gratefully acknowledge the financial support from the Canadian Foundation for Innovation (CFI) project No. 8246 for the cold spray equipment, the CFI Leader's Opportunity Fund project No. 13029 for the tribometer and nanoindentation equipment, and the Natural Sciences and Engineering Research Council (NSERC) Strategic Grants Program for the operational funding of this project. Thanks, are also due to Tekna Inc for providing the Ni and spherical WC powders. The authors acknowledge administrative support from Drs. Phuong Vo, Eric Irissou and Jean-Gabriel Legoux and technical support from Mr. Jean Francois Alarie at the McGill Aerospace Materials and Alloy Design Center (MAMADC) cold spray facility at NRC-Boucherville.

Chapter 9

Global discussion

Since Chapters 5 – 8 were prepared as separate manuscripts, there are some comparisons among those that needed to be discussed. Therefore, a global discussion is provided here to cover those variations that were not discussed at the time the manuscripts were prepared.

9.1 Cold spray deposition

In this thesis, influence of feedstock powders morphology and size distribution on the WC retention to coatings, their microstructure and mechanical properties, mainly hardness and wear properties are tested. In this section, a brief description of the WC retention, coatings microstructure and hardness are provided. In Fig. 9.1, the composite coatings are categorized to 4 groups, based on the morphology of WC and size of the Ni matrix powder, i.e., Ni(7)-cast WC, Ni(25)-cast WC, Ni(7)-WCNi, and Ni(25)-WCNi. In addition, three size ranges of the cast WC, i.e. WC(40), WC(30), and WC(15), were tested.

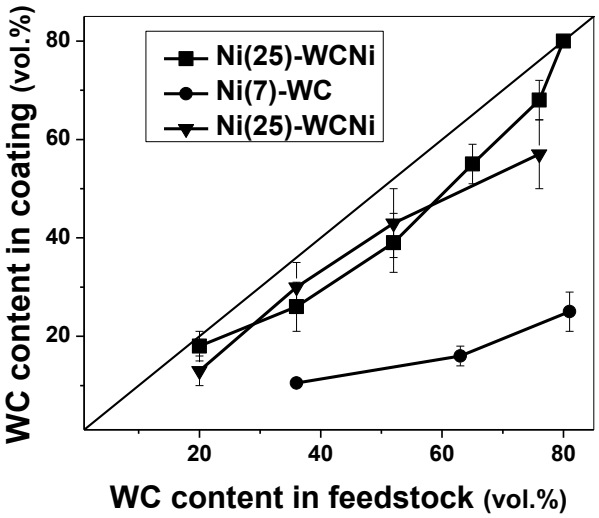

Fig. 9.1 Vickers micro-hardness of coatings versus WC content for Ni and composite coatings.

Comparison of cast WC content in the feedstock and coatings indicates that smaller cast WC particle recovered more into coating. For the ceramic to be retained, two mechanisms are mentioned in the literature, i.e. embedding into pre-deposited metal particles, or so-called "burial" mechanism by which rebounding ceramic particles are trapped by later-arriving particles [71, 72]. For burial" mechanism, it is reported that less momentum is needed to entrap smaller size particle to coating, and hence, higher retention is expected [72]. For this to occur, it requires the interaction between particles. Whereas, in most studies of cold spray, the impacts are believed to be isolated [19, 50, 52], although there are some studies on the interaction between particles [71, 72], influencing the ceramic particles retention. Considering embedding mechanism, finer size ceramic particles was found to be more prone to embed into substrate. This was attributed to their higher velocities attained in gas stream in the previous studies [54, 65, 66]. Although, one should consider the kinetic energy of particles instead ($1/2\ mv^2$), which is converted to plastic deformation of matrix, causing a crater and leading to particle attachment to surface. For the WC particles tested in the present thesis, coarser particles impact the surface with larger kinetic energy, although less recovering to coating. Two other factors may be involved here. First, for spherical powder to embed, the sphere must cause a crater with a depth greater than its radius and be enveloped by displaced material to prevent its rebound [121]. Therefore, for coarser particles a larger crater is required to embed the particles, i.e. a higher penetration depth. This requires the plastic deformation of the surface extended to greater depth, which was not realized although the kinetic energy of the particles was raised. The second factor that should be considered is the fragmentation of ceramic particles, which is intensified in coarser particles. Fragmentation uses the kinetic energy of article that would otherwise contribute to plastic deformation of surface and hence, retention of ceramic particles. Smaller WC particles (d_{50} = 30 μm) were recovered more than WC (d_{50} = 40 μm), due to combination of the factors mentioned above. Using much smaller size (d_{50} = 15 μm) was not effective in further improving the retention, probably due to decreased kinetic energy of the particles. Increasing WC content in feedstock led to coatings with higher fill ratio of WC, where higher fragmentation ratio was recorded due to increased ceramic particles collisions.

Comparison of cast WC and WCNi content in coatings (see Fig. 9.1) indicates that significant improvement in ceramic retention was achieved using agglomerated WC powders. This is due to enhanced ductility of WC particles provided by the porous structure, as well as the Ni

binder. Upon impact, WCNi particles undergo pseudo-plastic deformation [22] in which WC fragments are slipped along metallic binder and porosities and rearranged to form a near splat-type morphology. Moreover, the pores are closed. This led to a significant improvement in WC recovery to coating, being close to that in initial feedstock. However, with increasing the WC particles to feedstock, although the coating composition is still retained, deposition efficiency is decreased. This is due to transition in surface hardness, when spraying high concentration WC feedstock, on which WCNi particles were heavily deformed and flattened in coating. This along with high concentration of WC on the surface caused a harder surface. When impacting a WCNi particle on such that surface, after consuming a part of the kinetic energy of particle was consumed by plastic deformation, the rest was stored as elastic energy and causes the particle to bounce off the surface. Whereas, with Ni addition in initial feedstock, shear deformation is accommodated partly by metallic particles. This leads to partial compaction of porous particles near the impact area, with upper part still being porous. Upon impact of particles on such a WCNi layer during coating buildup, deformation of the top surface of the underlying coating and the bottom portion of impacting particle occurs. This results in an improvement in deposition efficiency.

Comparison of the WC content in coatings sprayed using two Ni particle sizes (see Fig. 9.1) indicates that the size and deposition efficiency of Ni particles do not change the WC recovery to coating. Although Ni(25) coatings featured lower hardness, it did not correspond to an improvement in cast WC particles retention into Ni(25) coating. While cast WC particles retention to Ni(7) was slightly more. This could be due to rougher top surface of the Ni(7) coating, which could help with inter-mechanical trapping of incoming WC particles.

The hardness values of the composite coatings are influenced by WC type, content, distribution, as well as hardness of the matrix and porosity of coatings (see Fig. 9.2). Higher WC content in coating led to harder composites, due to the reduced mean free path between WC particles and the densification of coatings. Comparing the micro-hardness values of the composite coatings with same Ni matrix and similar WC content revealed that cast WC particles produced harder coatings when compared to WCNi particles. Lower MFP between WC fragments as well as, higher hardness of cast WC compared to WCNi are the possible reasons. A significantly harder Ni and composite coating are deposited using finer size Ni powders, due to finer microstructure developed during cold spraying.

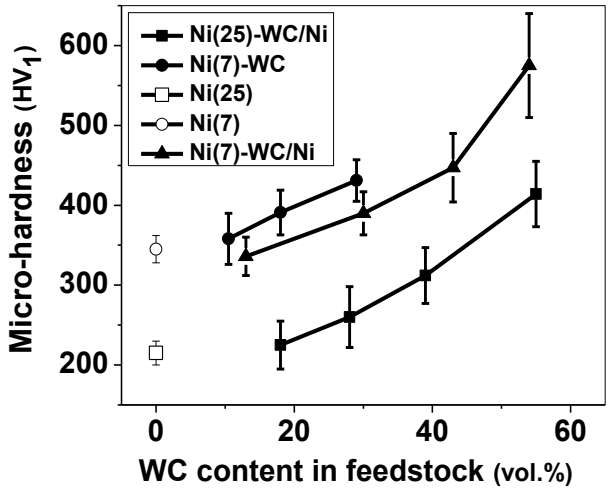

Fig. 9.2 Vickers micro-hardness of coatings versus WC content for Ni and composite coatings. Scatter bars indicate the standard deviation of 20 repeat measurements.

9.2 Influence of WC on sliding wear

Sliding wear tests were performed on the Ni(7), Ni(7)-10.5 and 28 WC and Ni(7)-30 WCNi coatings. Part of chapter 5 was to examine the sliding wear performance of a Ni(7) and Ni(7)-10.5vol.% cast WC composite coatings, where the role of WC particle on third body behaviour including morphology, chemistry, dynamics, as well as microstructure was observed. Chapter 6 was devoted to the influence of WC morphology, i.e. cast WC versus agglomerated WCNi, on sliding wear behavior of composite coating under two loads, i.e. 5 and 12 N, using similar fill ratio of WC particles incorporated to the Ni(7) matrix.

Figure 9.3 illustrates the CoF versus number of cycles for cold-sprayed coatings. The wear rates at the end of 1000 cycles tests were calculated and presented in Fig. 9.4. The results indicated that the addition of 10.5vol.% WC stabilized the friction (Fig. 9.3a) and decreased wear rate by a factor of seven (see Fig. 9.4). With further adding of WC particles, a shift in steady-state CoF value from 0.70 and 0.71 for Ni and Ni-10.5WC, respectively, to lower value of 0.67 was recorded for Ni-28WC coating. No wear was recorded for Ni-28WC coating after 1000 cycles. Comparison of WC morphology (cast WC versus agglomerated WCNi particles) on sliding wear behavior indicated that cast WC was more effective in stabilizing CoF and improving wear resistance.

Although addition of 30vol.% WC in Ni-30WCNi caused a drop in CoF to 0.61 at 5 N, friction behavior of Ni-30WCNi coatings was considerably less stable than that of composites reinforced with cast WC. However, with increasing applied load to 12 N, CoF was stabilized for Ni-30WCNi coating and its average value was close to that of Ni-28WC. At both tested loads, Ni-28WC was wear resistant after 1000 cycles sliding test, whereas Ni-30WCNi showed a wear rate similar to that recorded for Ni-10.5WC at 5 N, with significantly lower WC content. Increasing the load from 5 to 12 N, mean wear rates of Ni-WCNi increased by a factor of 5.

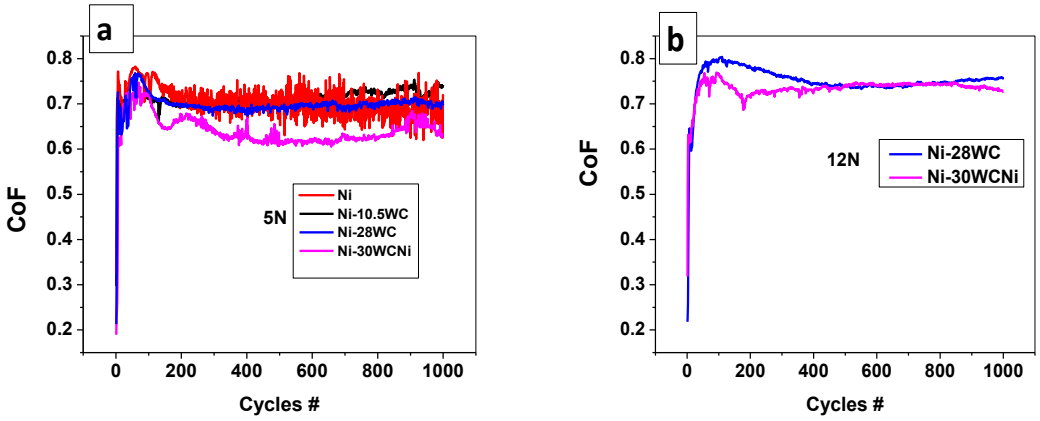

Fig. 9.3 Representative CoF versus sliding distance for cold sprayed Ni, Ni-10.5WC, Ni-28WC and Ni-30WCNi coatings at 5 (a) and (b) 12 N.

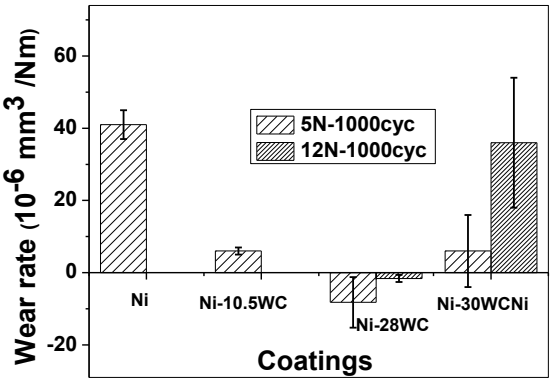

Fig. 9.4 Volumetric wear rate plotted for cold sprayed Ni, Ni-10.5WC, Ni-28WC and Ni-30WCNi coatings. Scatter bars indicate the standard deviation of 5 repeat measurements.

Significant plastic flow and adhesive wear were observed for both Ni and Ni-10.5WC coatings for initial cycles. For the Ni-10.5WC composite, Ni was preferentially worn early in the test and squeezed onto WC particles. This led to an earlier formation of a protective MML, consisting of compacted Ni wear particles rich in oxygen, WC fine fragments, and tribochemical phases of NiO, WO_3, and $NiWO_4$. Whereas, for the Ni coating, an adhesive wear mechanism persisted longer and the MML formed later in the test. At higher cycles, the coverage of the MML on the worn surface was lower for pure Ni than the Ni-10.5WC composite coating (Fig. 9.5). Very little adhesive wear was recorded in initial cycles for Ni-28WC tested under both loads. Fine WC fragments which were fragmented upon impact, pulled out during sliding and caused fine abrasive groove, and acted as initial source of debris formation. Moreover, oxidation of surface was initiated at initial cycles. This is followed by a formation of a protective oxide layer, where oxidized metallic debris and WC fragments were compacted to form MMLs. In this case, around 85% of surface was covered with MML, which was significantly higher than Ni and Ni-10.5WC coatings (Fig. 9.5).

Ni-30WCNi coatings initial wear rate was similar to those recorded for Ni, indicating lower effectiveness of WCNi particles in resisting surface against plastic deformation and adhesive wear. This is followed by a transition to oxidative wear and formation of MMLs, where MMLs coverage

ratio was significantly lower than that observed in Ni-28WC (Fig. 9.5). Another distinct feature that was noted from worn surface morphology is the dynamic of third-bodies, where unstable MMLs in the case of both Ni and Ni-30WCNi coatings lead to abrasive wear debris. This, in turn, led to grooving marks in the direction of sliding, as well as, causing fluctuation in CoF (Fig. 9.3). Effectiveness of cast WC in stabilizing CoF and reducing wear rates was preserved at high load of 12 N as well (Fig. 9.3), where the Ni-28 WC exhibited an stable CoF and no wear at the end of 1000 cycles sliding test (Fig. 9.4). In contrary, although increasing load stabilized CoF and led to formation an smoother surface for Ni-30WCNi coating, it didn't correspond to a lower wear rates (Fig. 9.3 and 4). Lower wear debris can be observed on the surface of Ni-30WCNi tested at 12 N, yet the coverage of surface with MML was still low (Fig. 9.5 and 6).

The wear rate of counter-spheres was linked to stability of MMLs and dynamic of third-bodies, where WC-Co balls mating with Ni and Ni-30WCNi were worn more, due to cracking of MML and presence of hard oxidized/carbide debris in the contact. Whereas, lower wear rate was recorded for WC–Co ball mating with Ni-28WC coating (Fig. 9.7).

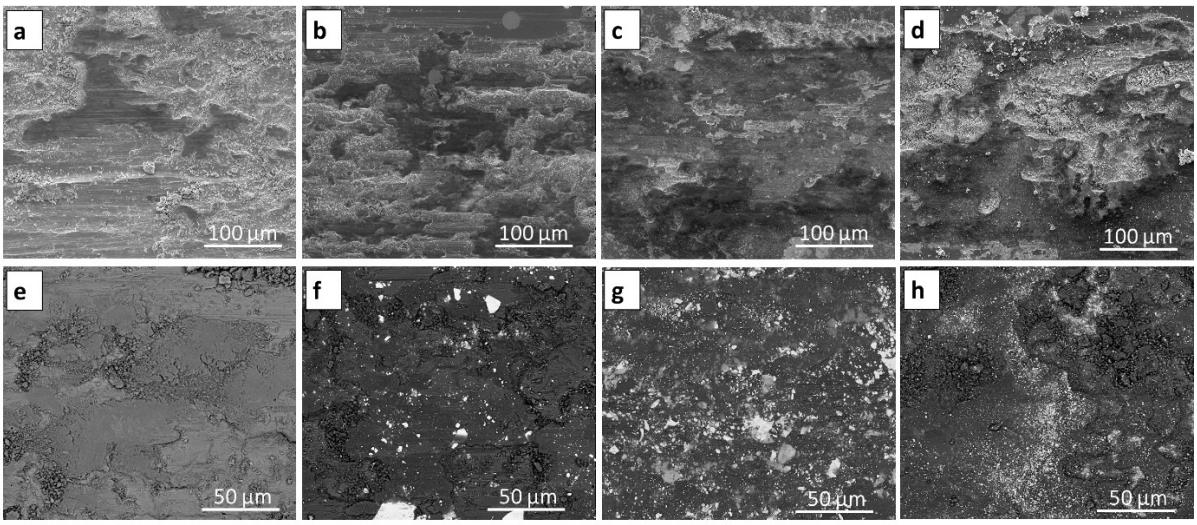

Fig. 9.5 Wear track topography of (a) Ni, (b)Ni-10.5WC, (c) Ni-28WC and (d) Ni-30WCNi after 1000cycles sliding at 5 N, (e), (f), (g) and (h) high magnification BSE images of (a), (b), (c) and (d), respectively.

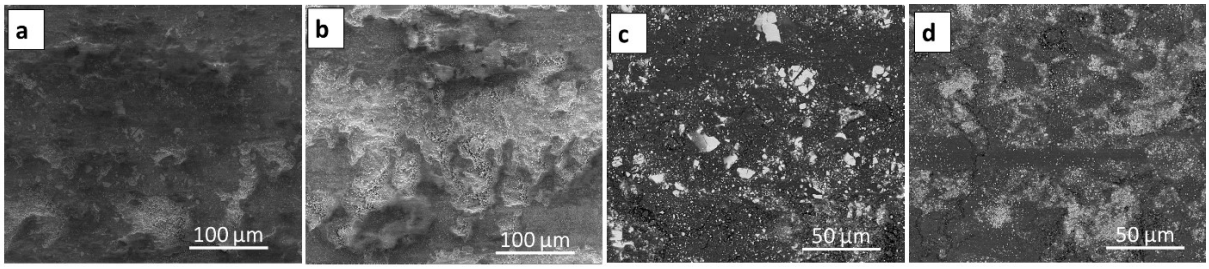

Fig. 9.6 Wear track topography of (a) Ni-28WC (b) Ni-30WCNi after 1000cycles sliding under 12 N, (c) and (d) high magnification BSE images of (a) and (b), respectively.

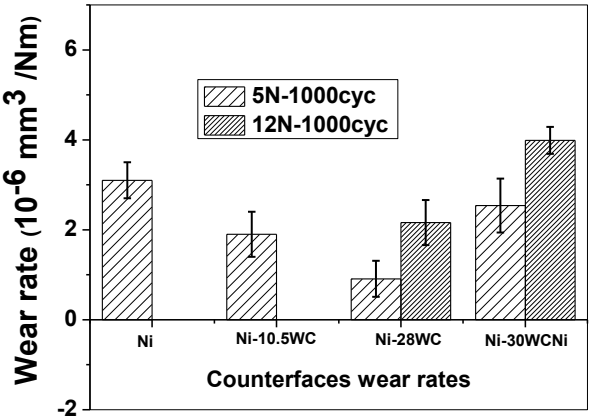

Fig. 9.7 Volumetric wear rate plotted for counter-spheres mating with Ni, Ni-10.5WC, Ni-28WC and Ni-30WCNi coatings. Scatter bars indicate the standard deviation of 5 repeat measurements.

Nano-indentation testing performed inside wear tracks on the MML, as well as, on the cross-section of worn surfaces, indicated that MMLs developed on the surfaces during sliding is significantly harder than that of unworn surfaces. While, oxidation and plastic deformation induced defects enhanced hardness of MML in Ni coating (6.2 ± 0.7GPa versus 4.6 ± 1.0), the presence of WC fragments in MML of composite coating led to significantly higher hardness (around 9.4 ± 1.9 GPa for Ni-28 coating and 8.4 ± 1.2 and 7.1 ± 2.0 GPa for Ni-30WCNi teste at 5 and 12 N, respectively). Microstructural analysis of worn subsurface indicated nucleation and propagation of cracking inside MML for Ni coating, which is attributed to the shear stresses transferred to the subsurface regions. Whereas, fewer cracking was noted for MML of Ni-10.5WC coating. No cracking was observed for Ni-28WC with nano-crystalline microstructure obtained

from high-resolution TEM images and SAD pattern. However, the cross-section microstructure of Ni-30WCNi worn surface showed cracking in the subsurface regions, indicating low load-bearing capacity of both MMLs and subsurface.

9.3 Influence of WC on erosive wear

In Chapter 7, Ni(7) and Ni-10.5vol.% cast WC coatings were subjected to SPE wear testing. In Chapter 8, the influence of WC content, as well as, Ni matrix hardness, on the erosion resistance of Ni-WCNi coatings was tested.

During SPE, the contact area of the erodent particles (a few microns) is smaller than the scale of microstructure, MFPs between WC particles, which lead to inhomogeneous wear behaviour of the materials on the surface. A ductile erosion behavior for Ni matrix was observed, where the material removal is mainly due to micro-cutting and ploughing action of the erodent particle at a low impact angle, and lip formation, strain hardening of lips and subsequent fracture of these lips in the form of thin platelets under normal attack. Ni(7) coating was more erosion resistant than Ni(25) coating under both impact angles tested. This was due to higher resistance to plastic deformation and cutting action of erodent particles in Ni(7) coatings. For both coatings, localized plastic deformation caused by impact of erodent particles was observed near surfaces, which assisted in materials removal in the form of cutting/ploughing or lips formation. Moreover, embedding of alumina particles into Ni matrix led to a shielding effect against severe erosion damage, which was more frequently observed under normal angle of impact. Similar mechanisms of erosive wear were maintained for Ni matrices in Ni-WCNi composite coatings. In fact, no considerable influence on Ni matrices erosion was recorded when WC was added.

Addition of 10.5vol.% cast WC particles did not correspond to an improvement in erosion resistance at 30° impact angle, although it led to an increase in erosion damage under normal. For Ni-30WC coatings, at low angle of attack, the Ni matrix was preferentially worn away. This is followed by WC dislodging from surface when the support of Ni matrix no longer exists. A high fill ratio of WC was required to reinforce Ni against erosion damage, which was not realized with cast WC content. A maximum of 28vol.% WC was recovered to coating using cast WC. For this reason, no further erosion testing was performed on the composite coatings with cast WC. Instead,

Ni(7)-WCNi coatings with WC content ranging from 13-55vol.% was subjected to SPE testing. Moreover, to examine the influence of matrix hardness on erosion resistance, SPE tests was performed on Ni(25)-WCNi and compared to that of Ni(7)-WCNi coatings.

At low angle of attack, addition of WCNi particles, below 40vol.% WC contents, did not improve erosion resistance of Ni-WCNi coatings. Composite coatings with Ni(7) as matrix were more erosion resistant when comparing with Ni(25)-WCNi, with a difference in magnitude similar to those recorded for pure Ni coatings. This indicates that the erosion behavior is controlled by Ni matrices in low WC fill ratio. The WCNi particles were subjected to erosion damages too, however, similar morphology and compactness was obtained in the two Ni(7)-WCNi and Ni(25)-WCNi with similar fill ratio. Knocking-out of WC fragments was observed in coatings with below 40vol.% WC contents.

A significant reduction in erosion rates was recorded with incorporation of 40vol.% WC into coating, which was assisted by a mechanism change from knocking-out of WC fragments at low content WC to combined dislodgment and micro-cracking of WC fragments for high content WC composites. This was due to higher compaction of WCNi particles, due to transition in hardness of surface during cold spraying of high WC concentration feedstock. Moreover, a network distribution of highly compacted WCNi particles in high concentration WC coatings led to a significant resistance again dislodging from surface, although it led to propagation of cracks along WCNi interfaces due to strain accumulation.

Chapter 10

Concluding remarks

10.1 Global conclusions

Ni-WC composite coatings were fabricated by cold spray using dual feeding system. The influence of WC particles morphology in the forms of cast and agglomerated, cast WC particles size and Ni particles size on the coatings deposition was tested. It was found that WCNi particles was recovered more, with being close to that in initial feedstock, compared to cast WC particles, sprayed at the identical condition. This was linked to the morphology of WCNi particles, where slipping of WC particles along Ni binder and porosities as well as densification of particles helped with retention of particles. Smaller size cast WC was more effective in recovering them to coating, considering either of embedding and burial mechanisms. However, lack of ductility in cast WC particles led to significant loss during cold spraying when compared to WCNi particles. The presence of WC particles also influenced Ni deposition behavior, led to lower partial deposition efficiency of Ni particles. Yet the pinging effect of WC particles densified Ni coatings.

Reciprocating sliding wear tests revealed an improvement in sliding wear resistance of composite coatings by incorporation of WC into the Ni matrix. The improvement in sliding wear resistance in composite coatings was linked to the providing resistance to Ni against plastic deformation and adhesive wear in initial cycles and, at longer cycles, to formation of a stable and cohesive MML on top of the wear tracks. Higher WC content was more effective, due to lower MFP between WC particles, leading to higher coverage ratio of a protective MML. Chemical and microstructural analysis of MML revealed that it consisted of nano-crystalline tribochemical phases of NiO, $NiWO_4$ and WO_3, as well as, WC fragments. It was found that coarser WC particles in coating facilitated the fast development of MML, as well as, improving its stability. While the presence of Fine fragmented WC particles in MML increased its hardness and contributed to superior wear resistance of composite.

Reciprocating sliding wear behaviour of Ni-28WC and Ni-30WCNi coatings in dry air exhibited contrasts due to the change in morphology of WC reinforcements. The Ni-28WC with multi-modal size distribution of WC particles and significantly lower MFPs between them exhibited lower wear damage when compared to Ni-30WCNi coating. It was found that cast WC particles more effectively minimized adhesive wear and helped to develop protective mechanically mixed layers (MMLs) more rapidly. Subsurface microstructure and chemical analysis of MMLs suggested higher oxidation and more stable MMLs in Ni-28WC, with lower depths of deformation zones extended beneath the MML and fewer number of cracking. The higher durability in MML of Ni-28WC was linked to the load supporting effect of harder subsurface. Moreover, coarser WC particles in Ni-28WC, relative to the thickness of MML, were retained in the matrix and not removed along with the oxide, and hence, substantially reduced the time for which the Ni matrix was in contact with the countersphere.

The single erosive wear events were localized to either Ni or WC particles, due to smaller erodent particles compared to the scale of composite microstructure and/or weak interfacial bonding. The local material response to the external wear event differs locally. Top-down and cross-section view of wear scars of Ni coating revealed characteristics of ductile erosion features, i.e. cutting and ploughing at low angle of impact, and lip formation, its embrittlement and fracture in the form of chips at normal impact. Ni coatings sprayed using finer size particles were more erosive wear resistant than coatings deposited using coarser size, at both impact angles, due to harder surface. At low angle of attack, cast WC particles remained intact against the damages caused by erodent particles, due to their high hardness. However, WC retention was limited to 28vol.%, even when feedstocks containing high concentration WC were sprayed. The WCNi particles erosive behavior varied depending on their content and porosity and distribution, as well as, erodent particles impact angle. A network distribution of WCNi particles, where highly dense and flattened WCNi particles were interconnected, assisted a mechanism change from dislodging of WC fragments from surface to propagation of cracking. This led to a significant improvement in erosion resistance in both Ni(7)-WCNi and Ni(25)-WCNi coatings with WC content above 40vol.%.

10.2 Contributions to original knowledge

1. The feasibility of Ni-WC cold spray deposition using unmodified spherical WC powders with no additional processing routes was tested for the first time. Effect of cast WC particles size distribution on their cold spray behavior and retention into coating was explored. Composite coatings containing 10 to 28vol.% WC with micro-hardness ranging between 225 to 550 HV_1 were fabricated.
2. Ni-WCNi composite coatings were cold sprayed using agglomerated WCNi powders, where composite coatings were tailored to contain 18-70vol.% WC and display a varied hardness ranging between 225 to 550 HV_1.
3. Deposition mechanism and lower retention of cast WC compared to agglomerated WCNi powders, that could have practical and financial significance for high-pressure cold spray industries, were discussed for the first time.
4. The significance of WC morphology in friction and wear of cold spray coatings was explored and discussed for the first time.
5. For the first time, third body approach was applied extensively to describe sliding wear behavior of cold sprayed WC coatings, where morphology, phase/chemical composition, microstructure, and mechanical property of third body were linked to friction and wear.
6. For the first time, cold sprayed WC composite coating was subjected to solid particles erosion wear at two impact angles, where effect of coatings structure mainly WC content and Ni matrix properties on erosion damage mechanisms was discussed.

10.3 Suggested future work

1- For deposition of ceramic by cold spray, it has been demonstrated that using a metallic coating on ceramic particles could improve retention of ceramic particles. This approach can be used to spray Ni clad WC powders, which are available in the market. However, the metallic coating thickness is critical factor to be considered. It needed to be thick enough to accommodate impact energy of ceramic particle efficiently by plastic deformation without getting detached from core.

2- The possible interaction of metallic and ceramic particles near substrate during cold spray and its contribution in ceramic particles retention into coating can be investigated using modeling.

3- For the sliding wear tests, two composite coatings containing 10.5 and 28vol.% cast WC was tested. That permitted an observation on the influence of cast WC content on friction and wear. Influence of WC content as well as, Ni matrices mechanical properties on sliding wear performance of Ni-WCNi are other interesting topics to explore.

4- Oxygen-free environments such as inert atmosphere or vacuum can be used to perform sliding wear to better understand the contribution of several factors in friction and wear, such as reinforcing effect of WC particles, the role of oxygen and oxidized third-bodies, etc. Additionally, water vapor could be incorporated in testing chamber at varying relative humidity, to explore its effect on third bodies evolution and friction and wear response of composite coatings.

5- In this thesis, the erosive wear condition mainly the type of erodent particles and its size distribution and morphology, erodent particles velocity and their feeding rate was kept constant. An erosion map for cold sprayed composite coatings can be constructed with varying those parameters. Moreover, more detailed and systematic approach can be employed to investigate the cohesive bond strength of cold sprayed composite coatings and their influence on erosive wear behavior.

References

[1] B. Bhushan, *Principles and Applications of Tribology*, Second ed. John Wiley & Sons, 2013.

[2] I. Hutchings and P. Shipway, *Tribology Friction and Wear of Engineering Materials*, Second ed. Butterworth-Heinemann, 1992.

[3] K. Holmberg and A. Erdemir, "Influence of tribology on global energy consumption, costs and emissions," *Friction,* vol. 5, no. 3, pp. 263-284, 2017.

[4] K. Holmberg and A. Matthews, *Coatings Tribology: Properties, Mechanisms, Techniques and Applications in Surface Engineering*, Second ed. Elsevier, 2009.

[5] K. H. a. A. Erdemir, "Global Impact of Friction on Energy Consumption, Economy and Environment " *FME Transactions* vol. 43, no. 3, pp. 181-185, 2015.

[6] K. Holmberg, P. Andersson, N.-O. Nylund, K. Mäkelä, and A. Erdemir, "Global energy consumption due to friction in trucks and buses," *Tribology International,* vol. 78, pp. 94-114, 2014.

[7] I. M. Hutchings, "Tribological properties of metal matrix composites," *Materials Science and Technology,* vol. 10, no. 6, pp. 513-517, 1994.

[8] H. Wang, W. M. Xia, and Y. S. Jin, "A study on abrasive resistance of Ni-based coatings with a WC hard phase," *Wear,* vol. 195, no. 1-2, pp. 47-52, 1996.

[9] P. L. Hurricks, "Some Aspects of Metallurgy and Wear Resistance of Surface Coatings," *Wear,* vol. 22, no. 3, pp. 291-320, 1972.

[10] L. M. Berger, P. Ettmayer, P. Vuoristo, T. Mantyla, and W. Kunert, " Microstructure and properties of WC-10%Co-4% Cr spray powders and coatings: Part 1. Powder characterization," *Journal of Thermal Spray Technology,* vol. 10, no. 2, pp. 311-325, 2001.

[11] S. Houdkova, F. Zahalka, M. Kasparova, and L. M. Berger, "Comparative Study of Thermally Sprayed Coatings Under Different Types of Wear Conditions for Hard Chromium Replacement," *Tribology Letters,* vol. 43, no. 2, pp. 139-154, 2011.

[12] M. J. Tobar, C. Álvarez, J. M. Amado, G. Rodríguez, and A. Yáñez, "Morphology and characterization of laser clad composite NiCrBSi–WC coatings on stainless steel," *Surface and Coatings Technology,* vol. 200, no. 22-23, pp. 6313-6317, 2006.

[13] K. Van Acker, D. Vanhoyweghen, R. Persoons, and J. Vangrunderbeek, "Influence of tungsten carbide particle size and distribution on the wear resistance of laser clad WC/Ni coatings," *Wear,* vol. 258, no. 1-4, pp. 194-202, 2005.

[14] C. J. Li, A. Ohmori, and Y. Harada, "Effect of powder structure on the structure of thermally sprayed WC-Co coatings," *Journal of Materials Science,* vol. 31, no. 3, pp. 785-794, 1996.

[15] H. L. D. Lovelock, "Powder/processing/structure relationships in WC-Co thermal spray coatings: A review of the published literature," *Journal of Thermal Spray Technology,* vol. 7, no. 3, pp. 357-373, 1998.

[16] J. H. Yuan, Y. C. Zhu, X. B. Zheng, H. Ji, and T. Yang, "Fabrication and evaluation of atmospheric plasma spraying WC-Co-Cu-MoS2 composite coatings," *Journal of Alloys and Compounds,* vol. 509, no. 5, pp. 2576-2581, 2011.

[17] D. A. Stewart, P. H. Shipway, and D. G. McCartney, "Abrasive wear behaviour of conventional and nanocomposite HVOF-sprayed WC-Co coatings," *Wear,* vol. 225, no. 1, pp. 789-798, 1999.

[18] P. Suresh Babu, B. Basu, and G. Sundararajan, "Processing–structure–property correlation and decarburization phenomenon in detonation sprayed WC–12Co coatings," *Acta Materialia,* vol. 56, no. 18, pp. 5012-5026, 2008.
[19] A. Papyrin, *Cold Spray Technology*, illustrated ed. Amsterdam ; London : Elsevier, 2007.
[20] V. K. Champagne, *The cold spray materials deposition process : fundamentals and applications*. Cambridge : Woodhead ; Boca Raton : CRC Press, 2007.
[21] J. Wang and J. Villafuerte, "A Novel Method to Spray Tungsten Carbide Using Low Pressure Cold Spray Technology," *Processing and Properties of Advanced Ceramics and Composites,* vol. 203, pp. 161-168, 2009.
[22] C. J. Li, G. J. Yang, P. H. Gao, J. Ma, Y. Y. Wang, and C. X. Li, "Characterization of nanostructured WC-Co deposited by cold spraying," *Journal of Thermal Spray Technology,* vol. 16, no. 5-6, pp. 1011-1020, 2007.
[23] R. S. Lima, J. Karthikeyan, C. M. Kay, J. Lindemann, and C. C. Berndt, "Microstructural characteristics of cold-sprayed nanostructured WC-Co coatings," *Thin Solid Films,* vol. 416, no. 1-2, pp. 129-135, 2002.
[24] P. H. Gao, Y. G. Li, C. J. Li, G. J. Yang, and C. X. Li, "Influence of Powder Porous Structure on the Deposition Behavior of Cold-Sprayed WC-12Co Coatings," *Journal of Thermal Spray Technology,* vol. 17, no. 5-6, pp. 742-749, 2008.
[25] M. Couto, S. Dosta, M. Torrell, J. Fernandez, and J. M. Guilemany, "Cold spray deposition of WC-17 and 12Co cermets onto aluminum," *Surface & Coatings Technology,* vol. 235, pp. 54-61, 2013.
[26] H. J. Kim, C. H. Lee, and S. Y. Hwang, "Fabrication of WC-Co coatings by cold spray deposition," *Surface & Coatings Technology,* vol. 191, no. 2-3, pp. 335-340, 2005.
[27] D. Lioma, N. Sacks, and I. Botef, "Cold gas dynamic spraying of WC-Ni cemented carbide coatings," *International Journal of Refractory Metals & Hard Materials,* vol. 49, pp. 365-373, 2015.
[28] W. D. R. Callister, David G., *Materials science and engineering : an introduction*, 2 ed. John Wiley & Sons, Incorporated 2001.
[29] C. P. Bergmann and J. Vicenzi, *Protection against Erosive Wear Using Thermal Sprayed Cermet: A Review*. Springer Berlin Heidelberg,, 2011, pp. 1-82.
[30] C. S. M. Alexander Evans, Andreas Mortensen, *Introduction, In: Metal Matrix Composites in Industry: An Introduction and a Survey, Volume 1*, illustrated, reprint ed. Springer Science & Business Media, 2003.
[31] K. K. C. Nikhilesh Chawla, *Introduction, In: Metal Matrix Composites*, 2, illustrated ed. Springer New York, 2013.
[32] S. A. Alidokht, V. N. V. Munagala, and R. R. Chromik, "Role of Third Bodies in Friction and Wear of Cold-Sprayed Ti and Ti–TiC Composite Coatings," *Tribology Letters,* vol. 65, no. 3, 2017.
[33] H. O. Pierson, *Handbook of refractory carbides and nitrides : properties, characteristics, processing, and applications*. Westwood, N.J.: Noyes Publications, 1996.
[34] S. T. Oyama, *The Chemistry of Transition Metal Carbides and Nitrides*, illustrated ed. Glasgow: Springer Science & Business Media, 1996.
[35] A. S. Kurlov and A. I. Gusev, "Tungsten carbides and W-C phase diagram," *Inorganic Materials,* vol. 42, no. 2, pp. 121-127, 2006.

[36] J. D. Yijie Wu, Zepeng Lv, Shengfu Zhang, Xuewei Lv and Chenguang Bai, "A Review of the Preparation Methods of WC powders, In: TMS 2018 147th Annual Meeting & Exhibition Supplemental Proceedings," Pittsburgh, PA USA, 2018.
[37] Teknaplasma. (2018). Available: http://www.tekna.com/our-icp-technology
[38] W. Su, Y. Sun, J. Feng, J. Liu, and J. Ruan, "Influences of the preparation methods of WC–Co powders on the sintering and microstructure of coarse grained WC–8Co hardmetals," *International Journal of Refractory Metals and Hard Materials,* vol. 48, pp. 369-375, 2015.
[39] M. R. Fernandez, A. Garcia, J. M. Cuetos, R. Gonzalez, A. Noriega, and M. Cadenas, "Effect of actual WC content on the reciprocating wear of a laser cladding NiCrBSi alloy reinforced with WC," *Wear,* vol. 324, pp. 80-89, 2015.
[40] A. G. Grigoryants *et al.*, "Laser surfacing of nickel-based composite war-resisting coatings reinforced with tungsten carbide," *Welding International,* vol. 31, no. 1, pp. 52-57, 2016.
[41] J. R. Davis, *Introduction to Thermal Spray* (In: Handbook of Thermal Spray Technology). ASM International and the Thermal Spray Society, 2004.
[42] S. S. Herbert Herman, and Robert McCune, "Thermal spray Current status and future trends," *MRS Bulletin,* vol. 25, no. 7, pp. 17-25, 2000.
[43] S.-K. P. a. Y.-J. K. Jae-Sang Baik, "A Numerical Study on Gas Phase Dynamics of High-Velocity Oxygen Fuel Thermal Spray," *Japanese Journal of Applied Physics,* vol. 47, no. 8, pp. 6907–6909, 2008.
[44] B. Wielage *et al.*, "Development and trends in HVOF spraying technology," *Surface and Coatings Technology,* vol. 201, no. 5, pp. 2032-2037, 2006.
[45] P. H. S. D.A Stewart, D.G McCartney, "Microstructural evolution in thermally sprayed WC–Co coatings: comparison between nanocomposite and conventional starting powders," *Acta Materialia,* vol. 48, no. 7, pp. 1593-1604, 2000.
[46] S. Kuroda, M. Watanabe, K. Kim, and H. Katanoda, "Current Status and Future Prospects of Warm Spray Technology," *Journal of Thermal Spray Technology,* vol. 20, no. 4, pp. 653-676, 2011.
[47] M. Grujicic, J. R. Saylor, D. E. Beasley, W. S. DeRosset, and D. Helfritch, "Computational analysis of the interfacial bonding between feed-powder particles and the substrate in the cold-gas dynamic-spray process," *Applied Surface Science,* vol. 219, no. 3-4, pp. 211-227, 2003.
[48] S. B. S. K. T. S. S. Harminder Singh, "Cold spray technology: future of coating deposition processes," *Frattura ed Integrità Strutturale (Fracture and Structural Integrity), ,* vol. 22, no. 22, pp. 69-84, , 2012.
[49] A. Moridi, S. M. Hassani-Gangaraj, M. Guagliano, and M. Dao, "Cold spray coating: review of material systems and future perspectives," *Surface Engineering,* vol. 30, no. 6, pp. 369-395, 2014.
[50] H. Assadi, F. Gärtner, T. Stoltenhoff, and H. Kreye, "Bonding mechanism in cold gas spraying," *Acta Materialia,* vol. 51, no. 15, pp. 4379-4394, 2003.
[51] M. Grujicic, C. L. Zhao, W. S. DeRosset, and D. Helfritch, "Adiabatic shear instability based mechanism for particles/substrate bonding in the cold-gas dynamic-spray process," *Materials & Design,* vol. 25, no. 8, pp. 681-688, 2004.
[52] T. Schmidt, F. Gärtner, H. Assadi, and H. Kreye, "Development of a generalized parameter window for cold spray deposition," *Acta Materialia,* vol. 54, no. 3, pp. 729-742, 2006.

[53] B. Jodoin, L. Ajdelsztajn, E. Sansoucy, A. Zuniga, P. Richer, and E. J. Lavernia, "Effect of particle size, morphology, and hardness on cold gas dynamic sprayed aluminum alloy coatings," *Surface & Coatings Technology,* vol. 201, no. 6, pp. 3422-3429, 2006.
[54] H. Koivuluoto and P. Vuoristo, "Effect of Powder Type and Composition on Structure and Mechanical Properties of Cu + Al_2O_3 Coatings Prepared by using Low-Pressure Cold Spray Process," *Journal of Thermal Spray Technology,* vol. 19, no. 5, pp. 1081-1092, 2010.
[55] C. Borchers, F. Gartner, T. Stoltenhoff, and H. Kreye, "Microstructural bonding features of cold sprayed face centered cubic metals," *Journal of Applied Physics,* vol. 96, no. 8, pp. 4288-4292, 2004.
[56] K. Kim, M. Watanabe, J. Kawakita, and S. Kuroda, "Grain refinement in a single titanium powder particle impacted at high velocity," *Scripta Materialia,* vol. 59, no. 7, pp. 768-771, 2008.
[57] Y. Zou, W. Qin, E. Irissou, J. G. Legoux, S. Yue, and J. A. Szpunar, "Dynamic recrystallization in the particle/particle interfacial region of cold-sprayed nickel coating: Electron backscatter diffraction characterization," *Scripta Materialia,* vol. 61, no. 9, pp. 899-902, 2009.
[58] S. A. A. R. R. Chromik, J. M. Shockley, Y. Zhang, *Tribological Coatings Prepared by Cold Spray, In: Cold-Spray Coatings Recent Trends and Future perspectives, Pasquale Cavaliere*. Springer 2017.
[59] V. Shukla, G. S. Elliott, and B. H. Kear, "Nanopowder deposition by supersonic rectangular jet impingement," *Journal of Thermal Spray Technology,* vol. 9, no. 3, pp. 394-398, 2000.
[60] G. L. Eesley, A. Elmoursi, and N. Patel, "Thermal properties of kinetic spray Al-SiC metal-matrix composite," *Journal of Materials Research,* vol. 18, no. 4, pp. 855-860, 2003.
[61] H. Y. Lee, Y. H. Yu, Y. C. Lee, Y. P. Hong, and K. H. Ko, "Cold spray of SiC and Al_2O_3 with soft metal incorporation: A technical contribution," *Journal of Thermal Spray Technology,* vol. 13, no. 2, pp. 184-189, 2004.
[62] S. R. Bakshi, V. Singh, K. Balani, D. G. McCartney, S. Seal, and A. Agarwal, "Carbon nanotube reinforced aluminum composite coating via cold spraying," *Surface & Coatings Technology,* vol. 202, no. 21, pp. 5162-5169, 2008.
[63] I. Smid, A. E. Segall, P. Walia, G. Aggarwal, T. J. Eden, and J. K. Potter, "Cold-Sprayed Ni-hBN Self-Lubricating Coatings," *Tribology Transactions,* vol. 55, no. 5, pp. 599-605, 2012.
[64] L. M. Stark, I. Smid, A. E. Segall, T. J. Eden, and J. Potter, "Self-Lubricating Cold-Sprayed Coatings Utilizing Microscale Nickel-Encapsulated Hexagonal Boron Nitride," *Tribology Transactions,* vol. 55, no. 5, pp. 624-630, 2012.
[65] A. Sova, V. Kosarev, A. Papyrin, and I. Smurov, "Effect of Ceramic Particle Velocity on Cold Spray Deposition of Metal-Ceramic Coatings," *Journal of Thermal Spray Technology,* vol. 20, no. 1-2, pp. 285-291, 2011.
[66] A. Sova, A. Papyrin, and I. Smurov, "Influence of Ceramic Powder Size on Process of Cermet Coating Formation by Cold Spray," *Journal of Thermal Spray Technology,* vol. 18, no. 4, pp. 633-641, 2009.
[67] E. Irissou, J. G. Legoux, B. Arsenault, and C. Moreau, "Investigation of Al- Al_2O_3 cold spray coating formation and properties," *Journal of Thermal Spray Technology,* vol. 16, no. 5-6, pp. 661-668, 2007.

[68] E. Sansoucy, P. Marcoux, L. Ajdelsztajn, and B. Jodoin, "Properties of SiC-reinforced aluminum alloy coatings produced by the cold gas dynamic spraying process," *Surface & Coatings Technology,* vol. 202, no. 16, pp. 3988-3996, 2008.
[69] K. Spencer, D. M. Fabijanic, and M. X. Zhang, "The use of Al- Al_2O_3 cold spray coatings to improve the surface properties of magnesium alloys," *Surface & Coatings Technology,* vol. 204, no. 3, pp. 336-344, 2009.
[70] M. Yu, W. Y. Li, X. K. Suo, and H. L. Liao, "Effects of gas temperature and ceramic particle content on microstructure and microhardness of cold sprayed SiCp/Al 5056 composite coatings," *Surface & Coatings Technology,* vol. 220, pp. 102-106, 2013.
[71] J. M. Shockley, S. Descartes, P. Vo, E. Irissou, and R. R. Chromik, "The influence of Al_2O_3 particle morphology on the coating formation and dry sliding wear behavior of cold sprayed Al- Al_2O_3 composites," *Surface & Coatings Technology,* vol. 270, pp. 324-333, 2015.
[72] P. C. King, S. H. Zahiri, and M. Z. Jahedi, "Rare earth/metal composite formation by cold spray," *Journal of Thermal Spray Technology,* vol. 17, no. 2, pp. 221-227, 2008.
[73] H. Koivuluoto and P. Vuoristo, "Effect of Ceramic Particles on Properties of Cold-Sprayed Ni-20Cr+ Al_2O_3 Coatings," *Journal of Thermal Spray Technology,* vol. 18, no. 4, pp. 555-562, 2009.
[74] O. Meydanoglu, B. Jodoin, and E. S. Kayali, "Microstructure, mechanical properties and corrosion performance of 7075 Al matrix ceramic particle reinforced composite coatings produced by the cold gas dynamic spraying process," *Surface & Coatings Technology,* vol. 235, pp. 108-116, 2013.
[75] F. Sevillano, P. Poza, C. J. Munez, S. Vezzu, S. Rech, and A. Trentin, "Cold-Sprayed Ni-Al_2O_3 Coatings for Applications in Power Generation Industry," *Journal of Thermal Spray Technology,* vol. 22, no. 5, pp. 772-782, 2013.
[76] N. M. Melendez and A. G. McDonald, "Development of WC-based metal matrix composite coatings using low-pressure cold gas dynamic spraying," *Surface & Coatings Technology,* vol. 214, pp. 101-109, 2013.
[77] H. Na, G. Bae, S. Shin, S. Kumar, H. Kim, and C. Lee, "Advanced deposition characteristics of kinetic sprayed bronze/diamond composite by tailoring feedstock properties," *Composites Science and Technology,* vol. 69, no. 3-4, pp. 463-468, 2009.
[78] C. Feng *et al.*, "B_4C/Ni Composite Coatings Prepared by Cold Spray of Blended or CVD-Coated Powders," *Journal of Thermal Spray Technology,* vol. 21, no. 3-4, pp. 561-570, 2012.
[79] D. T. F. P. Bowden, *The Friction and Lubrication of Solids*, illustrated, reprint, revised ed. ed. Clarendon Press, 2001.
[80] R. R. Chromik, H. W. Strauss, and T. W. Scharf, "Materials Phenomena Revealed by In Situ Tribometry," *Jom,* vol. 64, no. 1, pp. 35-43, 2012.
[81] J. R. Davis, *Metals Handbook Desk Edition*. ASM International, 1998.
[82] K. G. Budinski, *Guide to Friction, Wear, and Erosion Testing*, illustrated ed. ASTM International, 2007.
[83] I. Finnie, "Some Reflections on the Past and Future of Erosion," *Wear,* vol. 186, no. 1, pp. 1-10, 1995.
[84] A. Ghabchi, "Wear Resistant Carbide-Based Thermal Sprayed Coatings: Process, Properties, Mechanical Degradation and Wear," Doctor of Philosophy, Stony Brook University, New York, USA, 2001.

[85] F. H. Stott, J. Glascott, and G. C. Wood, "Models for the Generation of Oxides during Sliding Wear," *Proceedings of the Royal Society of London Series a-Mathematical Physical and Engineering Sciences,* vol. 402, no. 1822, pp. 167-186, 1985.
[86] J. Glascott, F. H. Stott, and G. C. Wood, "The Effectiveness of Oxides in Reducing Sliding Wear of Alloys," *Oxidation of Metals,* vol. 24, no. 3-4, pp. 99-114, 1985.
[87] M. Godet, "The third-body approach A mechanical view of wear," *Wear,* vol. 100, no. 1-3, pp. 437-452, 1984.
[88] Y. Berthier, M. Godet, and M. Brendle, "Velocity Accommodation in Friction," *Tribology Transactions,* vol. 32, no. 4, pp. 490-496, 1989.
[89] M. Couto, S. Dosta, J. Fernández, and J. M. Guilemany, "Comparison of the Mechanical and Electrochemical Properties of WC-25Co Coatings Obtained by High Velocity Oxy-Fuel and Cold Gas Spraying," *Journal of Thermal Spray Technology,* vol. 23, no. 8, pp. 1251-1258, 2014.
[90] M. Couto, S. Dosta, and J. M. Guilemany, "Comparison of the mechanical and electrochemical properties of WC-17 and 12Co coatings onto Al7075-T6 obtained by high velocity oxy-fuel and cold gas spraying," *Surface and Coatings Technology,* vol. 268, pp. 180-189, 2015.
[91] S. Dosta, M. Couto, and J. M. Guilemany, "Cold spray deposition of a WC-25Co cermet onto Al7075-T6 and carbon steel substrates," *Acta Materialia,* vol. 61, no. 2, pp. 643-652, 2013.
[92] G.-C. Ji, H.-T. Wang, X. Chen, X.-B. Bai, Z.-X. Dong, and F.-G. Yang, "Characterization of cold-sprayed multimodal WC-12Co coating," *Surface and Coatings Technology,* vol. 235, pp. 536-543, 2013.
[93] H.-T. Wang, X. Chen, X.-B. Bai, G.-C. Ji, Z.-X. Dong, and D.-L. Yi, "Microstructure and properties of cold sprayed multimodal WC–17Co deposits," *International Journal of Refractory Metals and Hard Materials,* vol. 45, pp. 196-203, 2014.
[94] N. M. Melendez, V. V. Narulkar, G. A. Fisher, and A. G. McDonald, "Effect of reinforcing particles on the wear rate of low-pressure cold-sprayed WC-based MMC coatings," *Wear,* vol. 306, no. 1-2, pp. 185-195, 2013.
[95] B. Venkataraman and G. Sundararajan, "Correlation between the characteristics of the mechanically mixed layer and wear behaviour of aluminium, Al-7075 alloy and Al-MMCs," *Wear,* vol. 245, no. 1-2, pp. 22-38, 2000.
[96] J. M. Shockley *et al.*, "In situ tribometry of cold-sprayed Al- Al_2O_3 composite coatings," *Surface & Coatings Technology,* vol. 215, pp. 350-356, 2013.
[97] H. Fukanuma, N. Ohno, B. Sun, and R. Z. Huang, "In-flight particle velocity measurements with DPV-2000 in cold spray," *Surface & Coatings Technology,* vol. 201, no. 5, pp. 1935-1941, 2006.
[98] R. Chakrabarty and J. Song, "Effect of Impact Angle on Ceramic Deposition Behavior in Composite Cold Spray: A Finite-Element Study," *Journal of Thermal Spray Technology,* vol. 26, no. 7, pp. 1434-1444, 2017.
[99] R. C. Dykhuizen and M. F. Smith, "Gas dynamic principles of cold spray," *Journal of Thermal Spray Technology,* vol. 7, no. 2, pp. 205-212, 1998.
[100] P. H. Gao, C. J. Li, G. J. Yang, Y. G. Li, and C. X. Li, "Influence of substrate hardness transition on built-up of nanostructured WC-12Co by cold spraying," *Applied Surface Science,* vol. 256, no. 7, pp. 2263-2268, 2010.

[101] B. C. Ng, B. A. Simkin, and M. A. Crimp, "Electron channeling contrast imaging of dislocation structures in deformed stoichiometric NiAl," *Materials Science and Engineering a-Structural Materials Properties Microstructure and Processing,* vol. 240, pp. 150-156, 1997.
[102] *ASTM-G76, Standard Test Method for Conducting Erosion Tests by Solid Particle Impingement Using Gas Jets*, 2007.
[103] E. Bousser, "Solid particle erosion mechanisms of protective coatings for aerospace applications," Du Diplôme de Philosophiæ Doctor, Université de Montréal, École Polytechnique de Montréal, Montreal, Canada, 2013.
[104] A. W. Ruff and L. K. Ives, "Measurement of solid particle velocity in erosive wear," *Wear,* vol. 35, no. 1, pp. 195-199, 1975.
[105] Renishaw. (2018). *Raman software: control*. Available: http://www.renishaw.com/en/raman-software-control--25908
[106] A. C. Fischer-Cripps, *Nanoindentation, Mechanical engineering series*. Springer, 2002.
[107] W. C. Oliver and G. M. Pharr, "An Improved Technique for Determining Hardness and Elastic-Modulus Using Load and Displacement Sensing Indentation Experiments," *Journal of Materials Research,* vol. 7, no. 6, pp. 1564-1583, 1992.
[108] *Hysitron TI 950 Triboindenter User Manual Revision 9.3.0314* Hysitron Incorporated 2014.
[109] J. M. Miguel, J. M. Guilemany, and S. Vizcaino, "Tribological study of NiCrBSi coating obtained by different processes," *Tribology International,* vol. 36, no. 3, pp. 181-187, 2003.
[110] P. Kulu and T. Pihl, "Selection criteria for wear resistant powder coatings under extreme erosive wear conditions," *Journal of Thermal Spray Technology,* vol. 11, no. 4, pp. 517-522, 2002.
[111] M. R. Ramesh, S. Prakash, S. K. Nath, P. K. Sapra, and B. Venkataraman, "Solid particle erosion of HVOF sprayed WC-Co/NiCrFeSiB coatings," *Wear,* vol. 269, no. 3-4, pp. 197-205, 2010.
[112] M. Yu, X. K. Suo, W. Y. Li, Y. Y. Wang, and H. L. Liao, "Microstructure, mechanical property and wear performance of cold sprayed A15056/SiCp composite coatings: Effect of reinforcement content," *Applied Surface Science,* vol. 289, pp. 188-196, 2014.
[113] Y. Zou, D. Goldbaum, J. A. Szpunar, and S. Yue, "Microstructure and nanohardness of cold-sprayed coatings: Electron backscattered diffraction and nanoindentation studies," *Scripta Materialia,* vol. 62, no. 6, pp. 395-398, 2010.
[114] X. K. Suo, Q. L. Suo, W. Y. Li, M. P. Planche, and H. L. Liao, "Effects of SiC Volume Fraction and Particle Size on the Deposition Behavior and Mechanical Properties of Cold-Sprayed AZ91D/SiCp Composite Coatings," *Journal of Thermal Spray Technology,* vol. 23, no. 1-2, pp. 91-97, 2014.
[115] T. Schmidt *et al.*, "From Particle Acceleration to Impact and Bonding in Cold Spraying," *Journal of Thermal Spray Technology,* vol. 18, no. 5-6, pp. 794-808, 2009.
[116] C. Borchers, F. Gartner, T. Stoltenhoff, H. Assadi, and H. Kreye, "Microstructural and macroscopic properties of cold sprayed copper coatings," *Journal of Applied Physics,* vol. 93, no. 12, pp. 10064-10070, 2003.
[117] L. E. Murr, C. S. Niou, S. Pappu, J. M. Rivas, and S. A. Quinones, "Leds in Ultra-High Strain-Rate Deformation," *Physica Status Solidi a-Applied Research,* vol. 149, no. 1, pp. 253-274, 1995.

[118] B. Bay, N. Hansen, D. A. Hughes, and D. Kuhlmann-Wilsdorf, "Overview no. 96 evolution of f.c.c. deformation structures in polyslip," *Acta Metallurgica et Materialia,* vol. 40, no. 2, pp. 205-219, 1992.
[119] H. Burt, J. P. Dennison, and B. Wilshire, "Friction stress measurements during creep of Nimonic 105," *Metal Science,* vol. 13, no. 5, pp. 295-300, 1979.
[120] D. Goldbaum *et al.*, "Mechanical behavior of Ti cold spray coatings determined by a multi-scale indentation method," *Materials Science and Engineering a-Structural Materials Properties Microstructure and Processing,* vol. 530, pp. 253-265, 2011.
[121] H. Getu, J. K. Spelt, and M. Papini, "Conditions leading to the embedding of angular and spherical particles during the solid particle erosion of polymers," *Wear,* vol. 292, pp. 159-168, 2012.
[122] B. Daneshian and H. Assadi, "Impact Behavior of Intrinsically Brittle Nanoparticles: A Molecular Dynamics Perspective," *Journal of Thermal Spray Technology,* vol. 23, no. 3, pp. 541-550, 2014.
[123] E. W. Andrews and K. S. Kim, "Threshold conditions for dynamic fragmentation of ceramic particles," *Mechanics of Materials,* vol. 29, no. 3-4, pp. 161-180, 1998.
[124] A. S. M. Ang, C. C. Berndt, and P. Cheang, "Deposition effects of WC particle size on cold sprayed WC-Co coatings," *Surface & Coatings Technology,* vol. 205, no. 10, pp. 3260-3267, 2011.
[125] L. M. Berger *et al.*, "Microstructure and properties of HVOF-sprayed chromium alloyed WC-Co and WC-Ni coatings," *Surface & Coatings Technology,* vol. 202, no. 18, pp. 4417-4421, 2008.
[126] Y. P. Kathuria, "Some aspects of laser surface cladding in the turbine industry," *Surface & Coatings Technology,* vol. 132, no. 2-3, pp. 262-269, 2000.
[127] P. Wu, H. M. Du, X. L. Chen, Z. Q. Li, H. L. Bai, and E. Y. Jiang, "Influence of WC particle behavior on the wear resistance properties of Ni-WC composite coatings," *Wear,* vol. 257, no. 1-2, pp. 142-147, 2004.
[128] C. Guo, J. S. Zhou, J. M. Chen, J. R. Zhao, Y. J. Yu, and H. D. Zhou, "High temperature wear resistance of laser cladding NiCrBSi and NiCrBSi/WC-Ni composite coatings," *Wear,* vol. 270, no. 7-8, pp. 492-498, 2011.
[129] J. S. Xu, X. C. Zhang, F. Z. Xuan, Z. D. Wang, and S. T. Tu, "Microstructure and Sliding Wear Resistance of Laser Cladded WC/Ni Composite Coatings with Different Contents of WC Particle," *Journal of Materials Engineering and Performance,* vol. 21, no. 9, pp. 1904-1911, 2012.
[130] J. R. Jiang, F. H. Stott, and M. M. Stack, "The role of triboparticulates in dry sliding wear," *Tribology International,* vol. 31, no. 5, pp. 245-256, 1998.
[131] J. R. Jiang, F. H. Stott, and M. M. Stack, "Some Frictional Features Associated with the Sliding Wear of the Nickel-Base Alloy N80a at Temperatures to 250C," *Wear,* vol. 176, no. 2, pp. 185-194, 1994.
[132] R. Gonzalez, M. Cadenas, R. Fernandez, J. L. Cortizo, and E. Rodriguez, "Wear behaviour of flame sprayed NiCrBSi coating remelted by flame or by laser," *Wear,* vol. 262, no. 3-4, pp. 301-307, 2007.
[133] V. K. Champagne, "The Repair of Magnesium Rotorcraft Components by Cold Spray," *Journal of Failure Analysis and Prevention,* vol. 8, no. 2, pp. 164-175, 2008.
[134] J. Villafuerte, *Modern Cold Spray: Materials, Process, and Applications*. Springer International Publishing, 2015.

[135] X. T. Luo and C. J. Li, "Large sized cubic BN reinforced nanocomposite with improved abrasive wear resistance deposited by cold spray," *Materials & Design,* vol. 83, pp. 249-256, 2015.
[136] R. B. Waterhouse, "The role of adhesion and delamination in the fretting wear of metallic materials," *Wear,* vol. 45, no. 3, pp. 355-364, 1977.
[137] K. I. Triantou, D. I. Pantelis, V. Guipont, and M. Jeandin, "Microstructure and tribological behavior of copper and composite copper plus alumina cold sprayed coatings for various alumina contents," *Wear,* vol. 336, pp. 96-107, 2015.
[138] N. Kang, P. Coddet, H. L. Liao, and C. Coddet, "The effect of heat treatment on microstructure and tensile properties of cold spray Zr base metal glass/Cu composite," *Surface & Coatings Technology,* vol. 280, pp. 64-71, 2015.
[139] K. L. Johnson, *Contact Mechanics*. Cambridge: Cambridge University Press, 1985.
[140] T. W. Clyne and P. J. Withers, *An Introduction to Metal Matrix Composites*. Cambridge University Press, 1993.
[141] G. G. Zhao, Y. B. Zhou, and H. J. Zhang, "Sliding wear behaviors of electrodeposited Ni composite coatings containing micrometer and nanometer Cr particles," *Transactions of Nonferrous Metals Society of China,* vol. 19, no. 2, pp. 319-323, 2009.
[142] M. Shafiei and A. T. Alpas, "Friction and wear mechanisms of nanocrystalline nickel in ambient and inert atmospheres," *Metallurgical and Materials Transactions a-Physical Metallurgy and Materials Science,* vol. 38a, no. 7, pp. 1621-1631, 2007.
[143] J. R. Davis, *Corrosion of Weldments*. ASM International, 2006.
[144] S. Yin, E. J. Ekoi, T. L. Lupton, D. P. Dowling, and R. Lupoi, "Cold spraying of WC-Co-Ni coatings using porous WC-17Co powders: Formation mechanism, microstructure characterization and tribological performance," *Materials & Design,* vol. 126, pp. 305-313, 2017.
[145] S. A. Alidokht, P. Manimunda, P. Vo, S. Yue, and R. R. Chromik, "Cold spray deposition of a Ni-WC composite coating and its dry sliding wear behavior," *Surface & Coatings Technology,* vol. 308, pp. 424-434, 2016.
[146] S. A. Alidokht, P. Vo, S. Yue, and R. R. Chromik, "Cold Spray Deposition of Ni and WC-Reinforced Ni Matrix Composite Coatings," *Journal of Thermal Spray Technology,* vol. 26, no. 8, pp. 1908-1921, 2017.
[147] C. C. Degnan, P. H. Shipway, and J. V. Wood, "Elevated temperature sliding wear behaviour of TiC-reinforced steel matrix composites," *Wear,* vol. 251, pp. 1444-1451, 2001.
[148] M. Vardavoulias, "The role of hard second phases in the mild oxidational wear mechanism of high-speed steel-based materials," *Wear,* vol. 173, no. 1, pp. 105-114, 1994.
[149] T. F. J. Quinn, "Oxidational Wear," *Wear,* vol. 18, no. 5, pp. 413-419, 1971.
[150] G. Bolelli, L. M. Berger, M. Bonetti, and L. Lusvarghi, "Comparative study of the dry sliding wear behaviour of HVOF-sprayed WC-(W,Cr)(2)C-Ni and WC-CoCr hardmetal coatings," *Wear,* vol. 309, no. 1-2, pp. 96-111, 2014.
[151] G. Straffelini, *Wear Mechanism, In: Friction and Wear Methodologies for Design and Control*. Switzerland: Springer International Publishing, 2015.
[152] S. Mahdavi and F. Akhlaghi, "Effect of the SiC particle size on the dry sliding wear behavior of SiC and SiC–Gr-reinforced Al6061 composites," *Journal of Materials Science,* journal article vol. 46, no. 24, pp. 7883-7890, 2011.

[153] I. A. Inman, S. Datta, H. L. Du, J. S. Burnell-Gray, and Q. Luo, "Microscopy of glazed layers formed during high temperature sliding wear at 750 degrees C," *Wear,* vol. 254, no. 5-6, pp. 461-467, 2003.
[154] H. Heshmat, "The Rheology and Hydrodynamics of Dry Powder Lubrication," *Tribology Transactions,* vol. 34, no. 3, pp. 433-439, 1991.
[155] M. W. L.M. Berger, S. Saaro, "Comparison of self-mated hardmetal coatings under dry sliding conditions up to 600◦C," *Wear* vol. 266, pp. 406–416, 2009.
[156] S. S. L.M. Berger, T. Naumann, M.Kasparova, F. Zahalka, "Microstructure and Properties of HVOF-Sprayed WC-(W,Cr)2C-Ni Coatings," *Journal of Thermal Spray Technology,* vol. 17(3) pp. 395–403, 2008.
[157] A. W. Z. Weng, X. Wu, Y. Wang, Z. Yang, "Wear resistance of diode laser-clad Ni/WC composite coatings at different temperatures," *Surface and Coatings Technology,* vol. 304, pp. 283-292, 2016.
[158] W. T. A.J.D. Schell, M.L. Lasonde, G. Hein, M. Klein, M. Mendez, "Erosion durability improvement of the T64 engine for military helicopters. Paper presented at the " presented at the American Helicopter Society 60th Annual Forum Baltimore, MD, Baltimore, MD, 2004.
[159] *ASM handbook. Volume 18, Friction, lubrication, and wear technology*, 1992.
[160] R. Zhou, Y. H. Jiang, and D. H. Lu, "The effect of volume fraction of WC particles on erosion resistance of WC reinforced iron matrix surface composites," *Wear,* vol. 255, pp. 134-138, 2003.
[161] G. Sundararajan and M. Roy, "Solid particle erosion behaviour of metallic materials at room and elevated temperatures," *Tribology International,* vol. 30, no. 5, pp. 339-359, 1997.
[162] G. Sundararajan and P. G. Shewmon, "A New Model for the Erosion of Metals at Normal Incidence," *Wear,* vol. 84, no. 2, pp. 237-258, 1983.
[163] G. Sundararajan, "A Comprehensive Model for the Solid Particle Erosion of Ductile Materials," *Wear,* vol. 149, no. 1-2, pp. 111-127, 1991.
[164] R. E. Winter and I. M. Hutchings, "The role of adiabatic shear in solid particle erosion," *Wear,* vol. 34, no. 2, pp. 141-148, 1975.
[165] J. R. Zhou and S. Bahadur, "Sem Studies of Material Damage in Alumina Ceramics by Angular Single and Multiple Particle Impacts," *Wear,* vol. 162, pp. 285-295, 1993.
[166] Y. B. Xu, J. H. Zhang, Y. L. Bai, and M. A. Meyers, "Shear localization in dynamic deformation: Microstructural evolution," *Metallurgical and Materials Transactions a-Physical Metallurgy and Materials Science,* vol. 39a, no. 4, pp. 811-843, 2008.
[167] R. F. Cook and G. M. Pharr, "Direct Observation and Analysis of Indentation Cracking in Glasses and Ceramics," *Journal of the American Ceramic Society,* vol. 73, no. 4, pp. 787-817, 1990.
[168] I. M. Hutchings, "Strain Rate Effects in Microparticle Impact," *Journal of Physics D-Applied Physics,* vol. 10, no. 14, pp. 179-184, 1977.
[169] G. Sundararajan, "The nature op plastic deformation during single impact and its relevance to solid particle erosion," Doctor of Philosophy The Ohio State University, Columbus, OH, USA, 1981.
[170] G. Sundararajan, "An Analysis of the Localization of Deformation and Weight-Loss during Single-Particle Normal Impact," *Wear,* vol. 84, no. 2, pp. 217-235, 1983.

[171] F. Cai, X. Huang, Q. Yang, and D. Nagy, "Effect of Microstructure on the Solid Particle Erosion Properties of Ni Plating," *Journal of Materials Engineering and Performance,* vol. 18, no. 3, pp. 305-311, 2009.
[172] H. Y. Teng, C. H. Hsu, S. C. Chiu, and D. C. Wen, "Erosion behavior of CA-15 tempered martensitic stainless steel," *Materials Transactions,* vol. 44, no. 7, pp. 1480-1487, 2003.
[173] C. P. Paul, S. K. Mishra, P. Tiwari, and L. M. Kukreja, "Solid-Particle Erosion Behaviour of WC/Ni Composite Clad layers with Different Contents of WC Particles," *Optics and Laser Technology,* vol. 50, pp. 155-162, 2013.
[174] M. G. Gee, C. Phatak, and R. Darling, "Determination of wear mechanisms by stepwise erosion and stereological analysis," *Wear,* vol. 258, no. 1-4, pp. 412-425, 2005.
[175] I. Hussainova, M. Antonov, and A. Zikin, "Erosive wear of advanced composites based on WC," *Tribology International,* vol. 46, no. 1, pp. 254-260, 2012.
[176] T. Peat, A. Galloway, A. Toumpis, P. McNutt, and N. Iqbal, "The erosion performance of cold spray deposited metal matrix composite coatings with subsequent friction stir processing," *Applied Surface Science,* vol. 396, pp. 1635-1648, 2017.
[177] S. A. Alidokht, P. Vo, S. Yue, and R. R. Chromik, "Erosive wear behavior of Cold-Sprayed Ni-WC composite coating," *Wear,* vol. 376, pp. 566-577, 2017.
[178] A. S. Praveen, J. Sarangan, S. Suresh, and J. S. Subramanian, "Erosion wear behaviour of plasma sprayed NiCrSiB/ Al_2O_3 composite coating," *International Journal of Refractory Metals & Hard Materials,* vol. 52, pp. 209-218, 2015.
[179] Z. Hongwei, D. Xiaohui, and C. Shuguang, "Solid particle erosion-wear behaviour of Cr3C2–NiCr coating on Ni-based superalloy," *Advances in Mechanical Engineering,* vol. 9, no. 3, pp. 1-9, 2017.